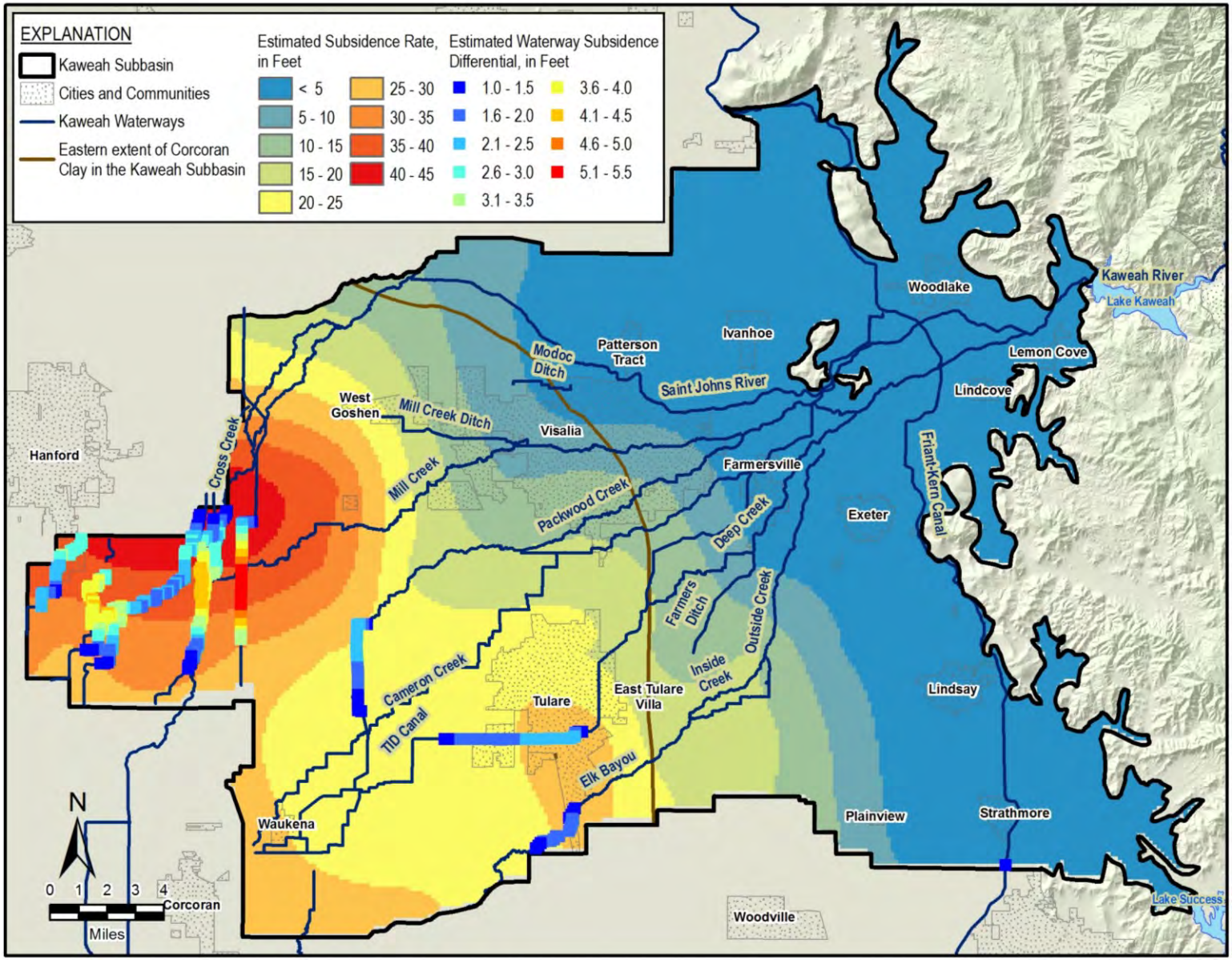

Figure 26. Estimated 2020 to 2070 Subsidence Impacts to Conveyance Infrastructure when Groundwater Levels Stabilize at Minimum Thresholds

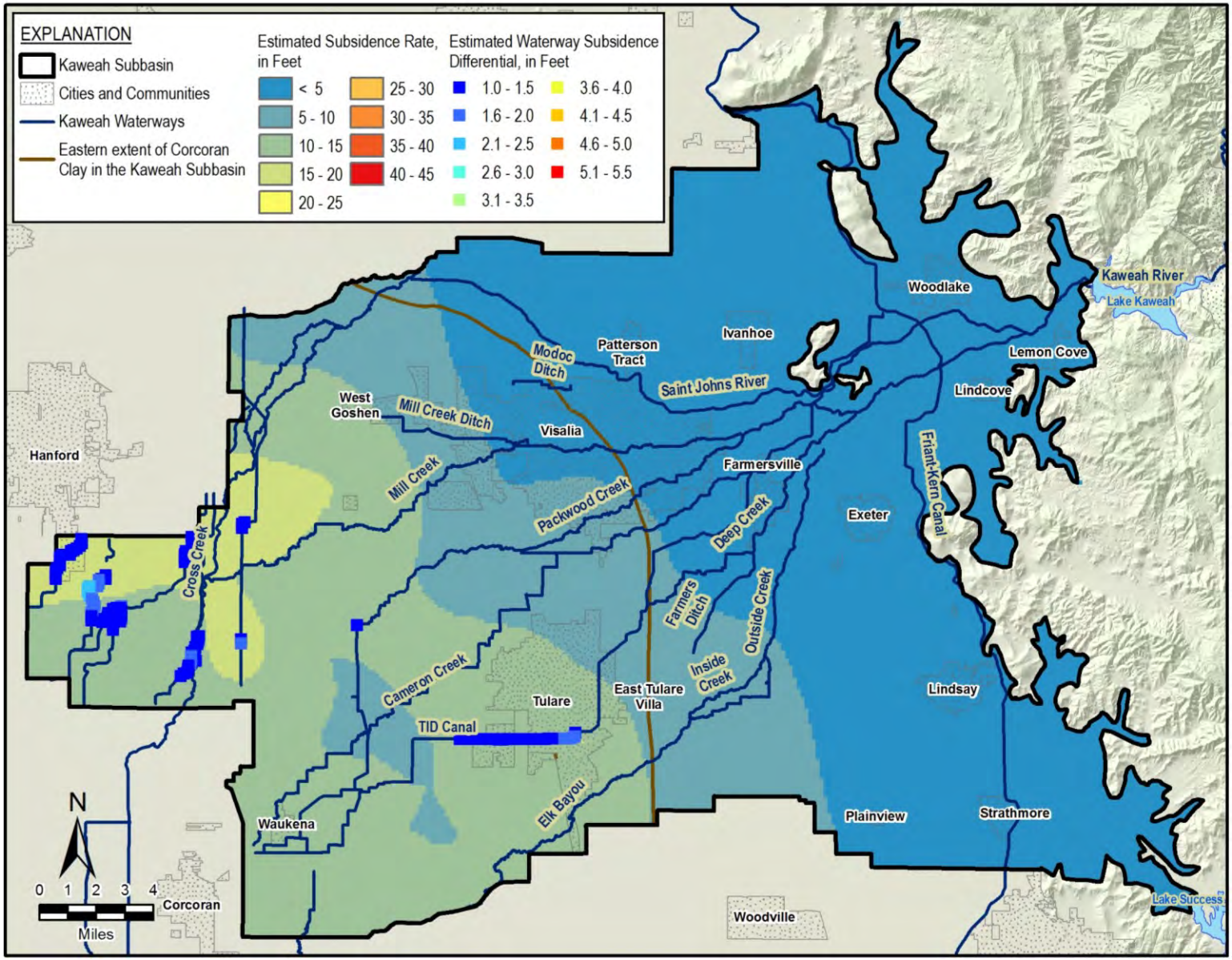

Figure 27. Estimated 2020 to 2040 Subsidence Impacts to Conveyance Infrastructure when Groundwater Levels Stabilize at Measurable Objectives

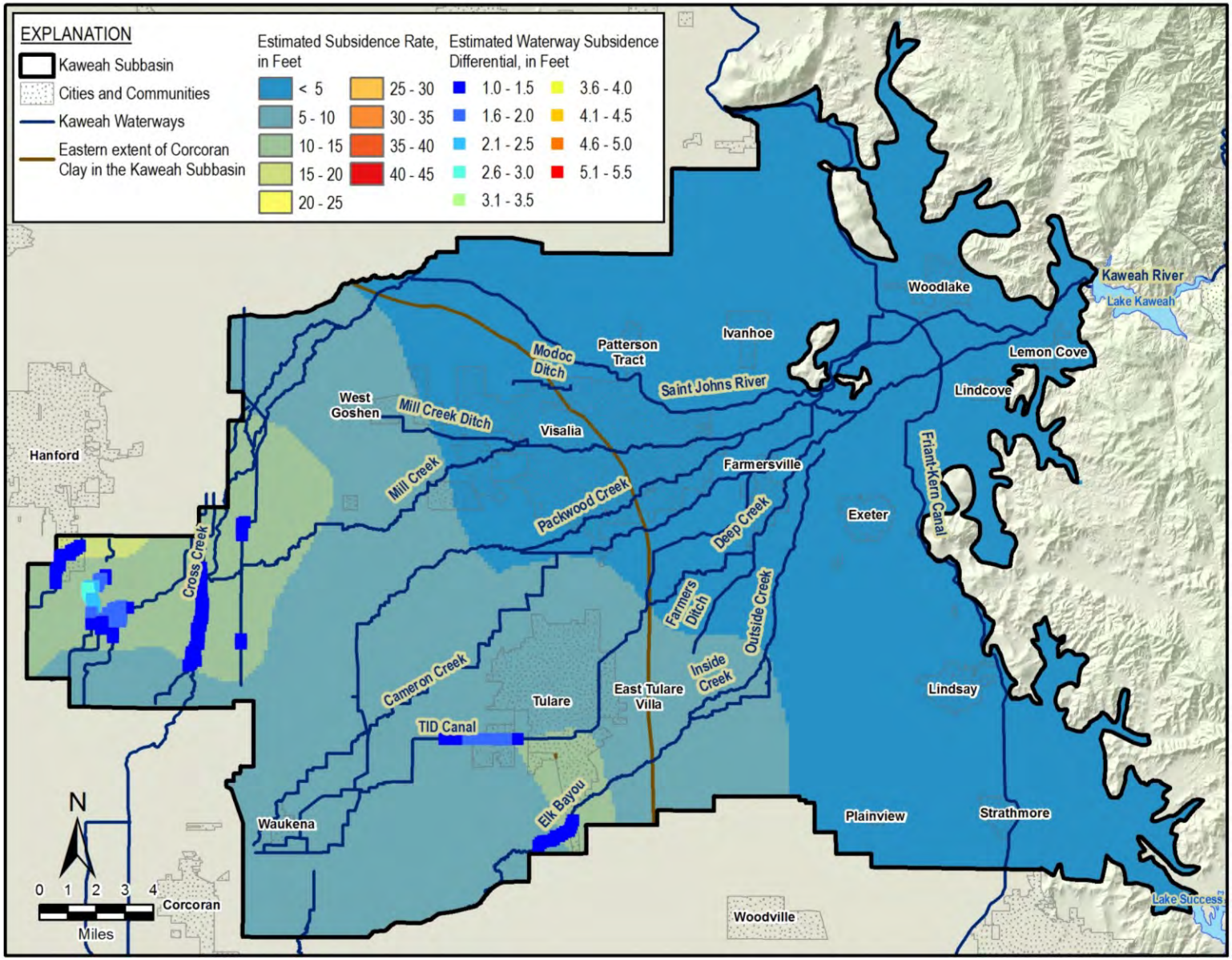

Figure 28. Estimated 2040 to 2070 Subsidence Impacts to Conveyance Infrastructure when Groundwater Levels Stabilize at Measurable Objectives

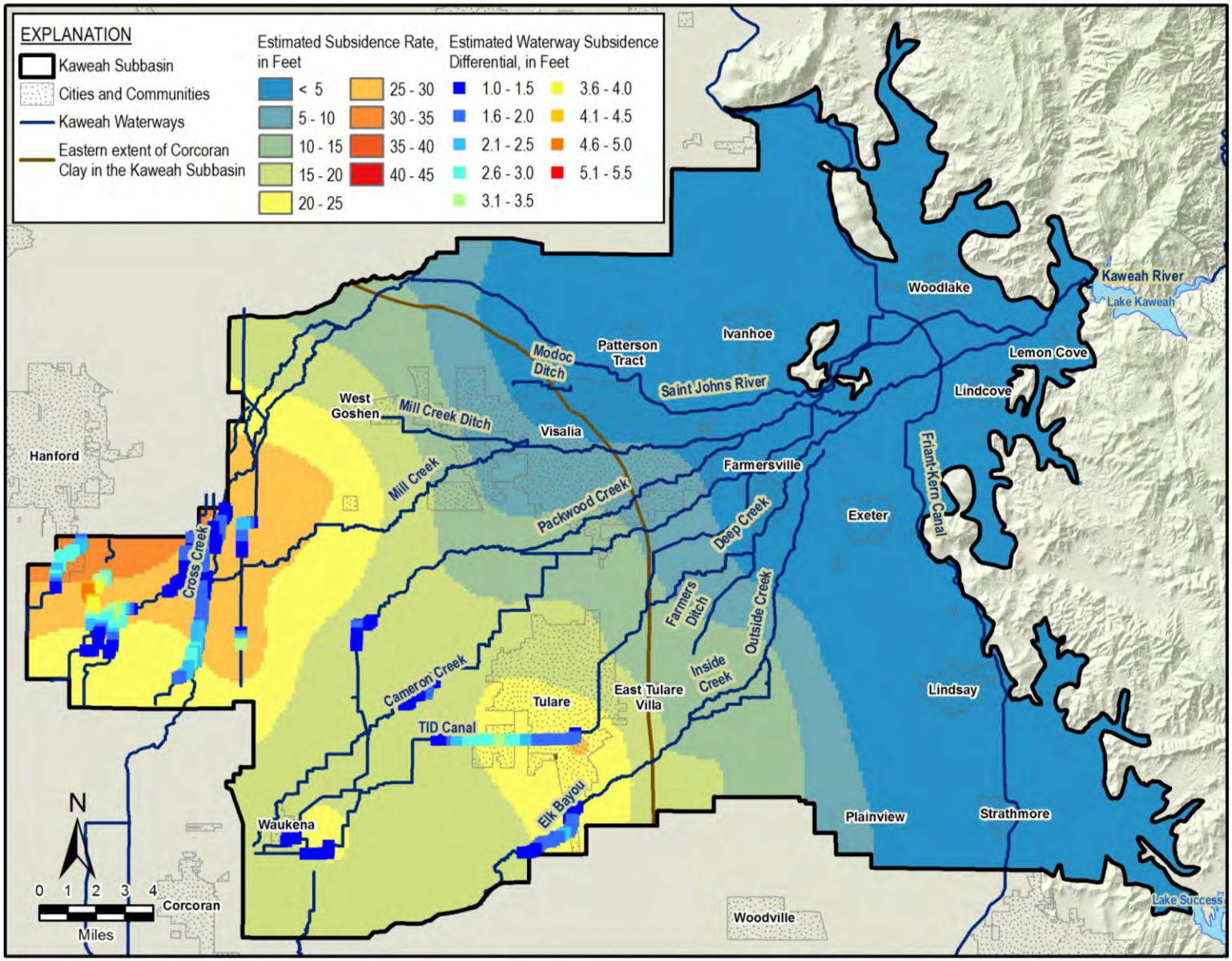

Figure 29. Estimated 2020 to 2070 Subsidence Impacts to Conveyance Infrastructure when Groundwater Levels Stabilize at Measurable Objectives

3 REFERENCES

California Department of Water Resources (DWR), 2022. Letter to Eric Osterling RE: Incomplete Determination of the 2020 Groundwater Sustainability Plans Submitted for the San Joaquin Valley – Kaweah Subbasin.

California Department of Water Resources InSAR data. https://gis.water.ca.gov/arcgisimg/rest/services/SAR

California Department of Water Resources GIS. https://gis.water.ca.gov/arcgis/rest/services/Elevation/Vertical_Displacement_SJV_DWR_1949_to_2005/MapServer/0

Faunt, C.C., ed., 2009, Groundwater Availability of the Central Valley Aquifer, California: U.S. Geological Survey Professional Paper 1766, 225 p.

Helm, D. C. (1975). One-dimensional simulation of aquifer system compaction near Pixley, California: 1. Constant parameters. Water Resources Research, 11(3), 465–478. https://doi.org/10.1029/WR011i003p00465

Lees, M., Knight, R., & Smith, R. 2022. Development and Application of a 1-D Compaction Model to Understand 65 Years of Subsidence in the San Joaquin Valley. Water Resources Research, https://agupubs.onlinelibrary.wiley.com/doi/10.1029/2021WR031390

Appendix 7A

Hydrogeologic Framework of Selected Areas of the Kaweah Subbasin Region in Tulare and Kings Counties, California

3. Recommendations

Recommendations provided to the Greater Kaweah, East Kaweah, and Mid-Kaweah Groundwater Sustainability Agencies in this section are based on the interpretation and understanding gained from the addition of the AEM data to existing information and from discussions with the representatives of the GSA's and water districts about their management challenges.

3.1 **Additional AEM Mapping** - If it is determined that greater fidelity is necessary in terms of groundwater flow, aquifer sustainability, volumes, and water in storage estimates, depletion to streams, well interference, groundwater withdrawal, and other management considerations, it is recommended that areas of closely spaced lines or "block-flights" be collected to develop more-detailed frameworks. The current 5 km line spacing between flight lines could be reduced to a 250 m to 400 m flight line spacing for greater detail on the natural system.

3.2 **Update the Water Table map** - The groundwater data used in the analyses presented in this report used the CA-DWR Fall 2017 water table map. Additional water level measurement locations would improve the water table map. This may be available after the delivery of this report.

3.3 **Siting new test holes and production wells** – The AEM framework maps and profiles provided in this report provide insight on the relationship between current test holes and production groundwater wells. At the time of this report, the currently available lithology and geophysical log data for the Kaweah Subbasin area were used in building the framework maps and profiles. It is recommended that the results from this report be used to site new test holes and monitoring wells. Often test holes are sited based on previous work that is regional in nature or for local projects of small size. By utilizing the maps in this report new drilling locations can be sited in optimal locations. Consideration for the areas that have been identified as confined to semi-confined aquifers is a good place to start doing this work. These wells need to be screened in discreet zones in order to understand the potentiometric surfaces from each zone. These wells should also be spaced geographically for water level/potentiometric head measurements as well as water quality sampling. Small screened intervals would allow for age dating the water for improved understanding of recharge, time of travel along flow paths and groundwater-surface water interaction.

The location of new water supply wells for communities can also use the AEM results in this report to guide development of new water supply wells. Planners should locate wells in areas of greatest saturated thickness with the least potential for non-point source pollution.

3.4 **Aquifer testing and borehole logging** - Aquifer tests are recommended to improve estimates of aquifer characteristics. A robust aquifer characterization program is highly recommended at the state, county, and smaller municipal levels. Aquifer tests can be designed based on the results of AEM surveys and existing production wells could be used in conjunction with three or more installed water level observation wells (which can be used as monitoring wells for levels and water quality sampling after the test).

Additional test holes with detailed, functional, and well calibrated geophysical logging for aquifer characteristics are highly recommended. Most of the borehole geophysical logs provided for this investigation were well calibrated. However, there were also quite a few that demonstrate that additional calibrated and verified geophysical logs would be useful in the Kaweah Subbasin.

Examples of additional logging would be flow meter logs and geophysical logs including gamma, neutron, electrical, and induction logs. Detailed aquifer characteristics can be accomplished with nuclear magnetic resonance logging (NMR). This is a quick and effective way to characterize porosity and water content, estimates of permeability, mobile/bound water fraction, and pore-size distributions with depth. NMR logs compare well with the aquifer tests in our experience and are very cost effective when compared to traditional aquifer tests.

3.5 **Recharge Zones** - The Kaweah Subbasin hydrogeologic framework in this report provides areas of recharge, that are widely spatially distributed, from the ground surface to the groundwater aquifers. Block flights of AEM data acquisition can provide the most detailed information for understanding recharge throughout the block flight areas. It is, again, recommended that additional AEM data be collected and interpreted utilizing closely-spaced flight lines using an AEM system that has near-surface resolution in the reconnaissance line flight areas. It is further recommended that future work integrate new soils maps with the results of this study to provide details on soil permeability, slope, and water retention to provide a more complete understanding of the transport of water from the land surface to the groundwater aquifers.

4. Deliverables

In summary, the following are included as deliverables:

- Raw EM Mag data as ASCII *.xyz
- SCI inversion as ASCII *.xyz
- Borehole databases as ASCII *.xyz
- Interpretations as ASCII *.xyz
- Raw Data Files - SkyTEM files *.geo, *skb, *.lin
- ESRI ArcView grid files – surface, topo, etc.
- 3D fence diagrams of the lithological interpretation

KMZs for AsFlown, Retained, Recharge, and Interpretation results

Table of Contents

1 Introduction 1
1.1 Purpose of Current Project 1
1.2 Background 4
1.3 Description of the Kaweah Subbasin AEM Project Area 4
2 Project Area Hydrogeology 6
2.1 Geologic Setting 6
2.1.1 Physiography and Regional Geologic Setting 6
2.1.2 Surficial Geology 7
2.1.3 Tertiary Geology 10
2.1.4 Pre-Tertiary Geology 12
2.2 Kaweah Subbasin AEM Survey Area Hydrogeologic Characteristics 12
2.2.1 Groundwater in the Kaweah Subbasin Area 13
2.2.2 Aquifer Characteristics 16
2.2.3 Connectivity to Surface Water and to Other Aquifers 18
2.2.4 Water Quality 18
3 Additional Background Information 21
3.1 Borehole Data 21
4 Geophysical Methodology, Acquisition and Processing 23
4.1 Geophysical Methodology 23
4.2 Flight Planning/Utility Mapping 24
4.3 AEM Survey Instrumentation 25
4.4 Data Acquisition 27
4.4.1 System Flight Parameters 29
4.4.2 Primary Field Compensation 37
4.4.3 Automatic Processing 37
4.4.4 Manual Processing and Laterally-Constrained Inversions 37
4.4.5 Power Line Noise Intensity (PLNI) 40
4.4.6 Magnetic Field Data 43
4.5 Spatially-Constrained Inversion 44
5 AEM Results and Interpretation 49
5.1 Interpretive Process – Merge AEM Flight Lines, Construct DEM 49

5.1.1 Merge AEM Flight Lines and Databases from Different Flights 49
5.1.2 Construct the Project Digital Elevation Model 50
5.2 Create Interpretative 2D Profiles 51
5.3 Comparison of Borehole Logs and the AEM Inversion Results 64
5.4 Create Interpretative Surface Grids 69
5.5 Comparison of 2018 SkyTEM 312 with 2015 SkyTEM 508 AEM Inversion Results 76
5.6 Resistivity-Lithology Relationship 81
5.7 Hydrogeological Framework of the Kaweah Subbasin AEM Survey Area 97
5.8 Recharge Areas within the Kaweah Subbasin AEM Survey Area 101
5.9 Key AEM Findings 109
5.9.1 Boreholes 109
5.9.2 Digitizing Interpreted Geological Contacts 109
5.9.3 Comparing the 2018 Kaweah 312 AEM Results with the 2015 Tulare 508 AEM Results . 109
5.9.4 Resistivity/Lithology Relationship 109
5.9.5 Hydrogeological Framework of the Kaweah Subbasin AEM Survey Area 109
5.9.6 Estimation of Aquifer Volume and Water in Storage in the Kaweah Subbasin AEM Survey Area 110
5.9.7 Potential Recharge Zones within the Kaweah Subbasin AEM Survey Area 110
5.10 Recommendations 111
5.10.1 Additional AEM Mapping 111
5.10.2 Update the Water Table map 111
5.10.3 Siting new test holes and production wells 111
5.10.4 Aquifer testing and borehole logging 112
5.10.5 Recharge Zones 112
6 Description of Data Delivered 113
6.1 Tables Describing Included Data Files 113
6.2 Description of Included Google Earth KMZ Data and Profiles 119
6.2.1 Included README for the Kaweah Subbasin AEM Interpretation KMZ 119
7 References 122
Appendix 1. 2D Profiles and Surfaces
Appendix 2. 3D Images
Appendix 3. Data Deliverables

List of Figures

Figure 1-1. Map showing locations of Eastern Kaweah GSA, Greater Kaweah GSA, and Mid-Kaweah GSA 2

Figure 1-2. The Kaweah Subbasin AEM survey area showing main highways passing through the area (99, 43, 65, 198). 3

Figure 1-3. Map of major river basins with streams within the Kaweah Subbasin AEM survey area in relation to the AEM flight lines 5

Figure 2-1. Surface geologic map of the Kaweah Subbasin AEM survey area in relation to the AEM flight lines 8

Figure 2-2. Map showing highly generalized regional groundwater elevations around the project area, 2017. 14

Figure 2-3. Graph showing groundwater fluctuations at USGS groundwater recorder 364200119420003 near Fresno, not far from the project area 16

Figure 2-4. Map showing concentrations of total dissolved solids in groundwater samples in Kings and Tulare Counties, California 19

Figure 2-5. Map showing concentrations of nitrate in groundwater samples in Kings and Tulare Counties, California 20

Figure 3-1. Locations of the boreholes near the Kaweah Subbasin AEM survey area 21

Figure 4-1. Schematic of an airborne electromagnetic survey, modified from Carney et al. (2015a) 23

Figure 4-2. A) Example of a dB/dt sounding curve. B) Corresponding inverted model values. C) Corresponding resistivity earth model. 24

Figure 4-3. SkyTEM304M frame, including instrumentation locations and X and Y axes. Distances are in meters. Instrumentation locations listed in Table 4-1 26

Figure 4-4. Photo of the SkyTEM312 system in suspension beneath the helicopter... 26

Figure 4-5. Kaweah Subbasin AEM flight lines grouped by acquisition date 28

Figure 4-6. Map of the system height recorded during the Kaweah Subbasin AEM survey 31

Figure 4-7. Map of the ground speed recorded during the Kaweah Subbasin AEM survey 32

Figure 4-8. Map of the X-angle tilt recorded during the Kaweah Subbasin AEM survey 33

Figure 4-9. Map of the Y-angle tilt recorded during the Kaweah Subbasin AEM survey 34

Figure 4-10. Plot of the 210 Hz LM waveform for the SkyTEM312 system recorded during the Kaweah Subbasin AEM survey 35

Figure 4-11. Plot of the 30 Hz HM waveform for the SkyTEM312 system recorded during the Kaweah Subbasin AEM survey 36

Figure 4-12. Example locations of electromagnetic coupling with pipelines or power lines 38

Figure 4-13. A) Example of AEM data affected by electromagnetic coupling in the Aarhus Workbench editor. The top group of lines is the unedited data with the Low Moment on top and the High Moment on the bottom. The bottom group shows the same data after editing. 39

Figure 4-14. A) Example of laterally-Constrained inversion results where AEM data affected by coupling with pipelines and power lines were not removed. B) Inversion results where AEM data affected by coupling were removed. 40

Figure 4-15. Power Line Noise Intensity (PLNI) map of the Kaweah Subbasin AEM project area. 41

Figure 4-16. Locations of inverted data (blue lines) along the AEM flight lines (red lines) in the Kaweah Subbasin AEM survey area. 42

Figure 4-17. Residual magnetic Total Field intensity data for the Kaweah Subbasin AEM survey area corrected for diurnal drift, with the International Geomagnetic Reference Field (IGRF) removed 43

Figure 4-18. An example of an AEM profile illustrating increasing model layer thicknesses with depth. . 46

Figure 4-19. Data/model residual histogram for the Kaweah Subbasin SCI inversion results 47

Figure 4-20. Map of data residuals for the Kaweah Subbasin 312 SCI inversion results 48

Figure 5-1. Map of the Digital Elevation Model for the Kaweah Subbasin AEM survey area 50

Figure 5-2. Google Earth image of Kaweah Subbasin AEM flight lines and the six Fugro West (2007) cross-sections 53

Figure 5-3. Cross-section A-A' from Plate 14 of Fugro West (2007) 54

Figure 5-4. 3D fence diagram of the six cross-sections A-F from Fugro West (2007), modified with the boreholes and resistivity logs removed and different coloring applied to the E-Clay and the basement material 55

Figure 5-5. 2D profile of inverted resistivity data from Kaweah Subbasin AEM flight line L200300, located across the northern extent of the AEM survey area 56

Figure 5-6. Illustration of the development sequence of stratigraphic cycles on an alluvial fan 57

Figure 5-7. 2D profile of inverted resistivity data from Kaweah Subbasin AEM flight line L200401, located southeast of L200300 58

Figure 5-8. 2D profile of inverted resistivity data from Kaweah Subbasin AEM flight line L200200, located north of L200300 59

Figure 5-9. Inversion results for Kaweah Subbasin AEM flight line L100901 60

Figure 5-10. 2D profile of inverted resistivity data from Kaweah Subbasin east-west AEM flight line L2001001, located on the western side of the AEM survey area 62

Figure 5-11. 2D profile of inverted resistivity data from Kaweah Subbasin AEM north-south flight line L100600, located on the western side of the AEM survey area 63

Figure 5-12. Comparison of borehole resistivity and lithology logs and AEM flight line L100200 65

Figure 5-13. Comparison of borehole resistivity and lithology logs and AEM flight line L101202 66

Figure 5-14. Comparison of borehole resistivity and lithology logs and AEM flight line L101702 67

Figure 5-15. Comparison of borehole resistivity and lithology logs and AEM flight line L200300 68

Figure 5-16. Map of the water table elevation during the fall of 2017 (CA-DWR, 2018a) within and surrounding the Kaweah Subbasin AEM survey area 70

Figure 5-17. Map of the top elevation of the Corcoran Clay within the 2018 Kaweah Subbasin AEM survey area 71

Figure 5-18. Map of the depth to the top of the Corcoran Clay within the 2018 Kaweah Subbasin AEM survey area 72

Figure 5-19. Map of the thickness of the Corcoran Clay within the 2018 Kaweah Subbasin AEM survey area 73

Figure 5-20. Map of the top elevation of the basement rock within the 2018 Kaweah Subbasin AEM survey area 74

Figure 5-21. Map of the depth to the top of the basement rock within the 2018 Kaweah Subbasin AEM survey area 75

Figure 5-22. Comparison of 2018 SkyTEM 312 and the 2015 SkyTEM 508 AEM inversion results for 2018 AEM flight line L100400 and 2015 flight line 100401 77

Figure 5-23. Comparison of 2018 SkyTEM 312 and the 2015 SkyTEM 508 AEM inversion results for 2018 AEM flight line L100600 and 2015 flight line 100601 78

Figure 5-24. Comparison of 2018 SkyTEM 312 and the 2015 SkyTEM 508 AEM inversion results for 2018 AEM flight line L101501 and 2015 flight line 100501 79

Figure 5-25. Comparison of 2018 SkyTEM 312 and the 2015 SkyTEM 508 AEM inversion results for 2018 AEM flight line L200701 and 2015 flight line 100401. 80

Figure 5-26. Table 2 from Knight et al. (2018) delineating a resistivity to lithology relationship for unsaturated and saturated sediments above and below the water table in the Tulare, CA area 81

Figure 5-27. Plot displaying the resistivities by major lithological material color categories 81

Figure 5-28. Lithological interpretation of Kaweah Subbasin AEM flight line L200300 83

Figure 5-29. Lithological interpretation of Kaweah Subbasin AEM flight line L200401 84

Figure 5-30. Lithological interpretation of Kaweah Subbasin AEM flight line L200200 85

Figure 5-31. Lithological interpretation of Kaweah Subbasin AEM flight line L2001001 86

Figure 5-32. Lithological interpretation of Kaweah Subbasin AEM flight line L100600 87

Figure 5-33. 3D lithologic interpretative fence diagram of the Kaweah Subbasin AEM inverted earth models, looking north 88

Figure 5-34. 3D lithologic interpretative fence diagram of the Kaweah Subbasin AEM inverted earth models, looking south 89

Figure 5-35. 3D lithologic interpretative fence diagram of the Kaweah Subbasin AEM inverted earth models, looking east 90

Figure 5-36. 3D lithologic interpretative fence diagram of the Kaweah Subbasin AEM inverted earth models, looking north. The top and bottom extents of the Corcoran Clay are indicated on the western side in blue 91

Figure 5-37. This is the same 3D fence diagram view as in Figure 5-36 except the top and bottom extents of the Corcoran Clay are highlighted with a transparent grey color instead of blue 92

Figure 5-38. 3D lithologic interpretative fence diagram of the Kaweah Subbasin AEM inverted earth models, looking north, along with the Fugro West (2007) cross-sections, A-F 93

Figure 5-39. 3D lithologic interpretative fence diagram of the Kaweah Subbasin AEM inverted earth models, looking north, along with the Fugro West (2007) cross-sections, A-F 94

Figure 5-40. 3D lithologic interpretative fence diagram of the Kaweah Subbasin AEM inverted earth models, looking southwest, along with the eastern/northern ends of the Fugro West (2007) A, B, and F cross-sections 95

Figure 5-41. 3D lithologic interpretative fence diagram of the Kaweah Subbasin AEM inverted earth models, looking southeast, along with the Fugro West (2007) cross-sections 96

Figure 5-42. Lithological interpretation of Kaweah Subbasin AEM flight line L201100 99

Figure 5-43. Lithological interpretation of Kaweah Subbasin AEM flight line L101202 100

Figure 5-44. USGS *Map of distribution of coarse-grained deposits for the upper 50 ft for part of the Central Valley* (Faunt et al., 2009) 102

Figure 5-45. Map of "current and proposed" (as of 2007) Recharge Basins in the Kaweah Delta Water Conservation District (modified from Plate 10 in Fugro West, 2007) 103

Figure 5-46. Google Earth image of areas of potential recharge showing coarse-grained material with resistivities >25 ohm-m for the depth range 0 m – 3 m or 0 ft – 10 ft 104

Figure 5-47. Google Earth image of areas of potential recharge showing coarse-grained material with resistivities >25 ohm-m for the depth range 6 m – 10 m or 20 ft – 31 ft 105

Figure 5-48. Google Earth image of areas of potential recharge showing coarse-grained material with resistivities >25 ohm-m for the depth range 13 m – 17 m or 43 ft – 56 ft 106

Figure 5-49. Google Earth image of areas of potential recharge showing coarse-grained material with resistivities >25 ohm-m for the depth range 26 m – 31 m or 85 ft to 100 ft 107

Figure 5-50. Google Earth image of "current and proposed" (as of 2007) Recharge Basins in the Kaweah Delta Water Conservation District (modified from Plate 10 in Fugro West, 2007) plus first layer (0 m – 3 m or 0-10 ft) of AEM earth model for resistivities >25 ohm-m 108

Figure 6-1. Example Google Earth image for the Kaweah Subbasin Interpretation kmz 121

List of Tables

Table 2-1. Table of generalized geologic formations in the project area. 9

Table 2-2. Summary information for Quaternary and Tertiary aquifer units within the area 11

Table 2-3. Summary of generalized aquifer-test data in or near the Kaweah Subbasin project area..... 17

Table 4-1. Positions of instruments on the SkyTEM312 frame, using the center of the frame as the origin, in meters 27

Table 4-2. Positions of corners of the SkyTEM312 transmitter coil, using the center of the frame as the origin in meters 27

Table 4-3. Location of DGPS and magnetic field base station instruments at the Mefford Airport..... 27

Table 4-4. Kaweah Subbasin AEM flight line production by flight..... 29

Table 4-5. Thickness and depth to bottom (in meters and feet) for each layer in the Spatially Constrained inversion (SCI) AEM earth models for the SkyTEM312..... 45

Table 5-1. Combination of SkyTEM 312 flight lines within the Kaweah Subbasin AEM survey area 49

Table 6-1. Raw SkyTEM data files 114

Table 6-2. Channel name, description, and units for Kaweah_EM312_MAG.xyz with EM, magnetic, DGPS, Inclinometer, altitude, and associated data 114

Table 6-3. Channel name, description, and units for Kaweah_AEM_SCI_Inv_v1.xyz with EM inversion results..... 115

Table 6-4. Files containing borehole information 116

Table 6-5. Channel name, description, and units for borehole collar files 116

Table 6-6. Channel name description and units for Lithology borehole data 116

Table 6-7. Channel name description and units for E-Logs borehole data..... 116

Table 6-8. Channel name, description, and units for the interpretation results file Kaweah_InterpSurfaces_v1.xyz 117

Table 6-9. Files containing ESRI ArcView Binary Grids *.flt (NAD 83 UTM 11 North, meters) 118

List of Abbreviations

1D	One-dimensional
2D	Two-dimensional
3D	Three-dimensional
$A*m^2$	Ampere meter squared
AEM	Airborne Electromagnetic
AGF	Aqua Geo Frameworks, LLC
ASCII	American Standard Code for Information Interchange
Bgl/Bgs	Below Ground Level/Below Ground Surface
Ca	Calcium
CA-DWR	California Department of Water Resources
CV	Central Valley of California
CVA	Central Valley Aquifer
CVP	Central Valley Project
dB/dt	Change in amplitude of magnetic field with time
DEM	Digital Elevation Model
DOI	Depth of Investigation
DGPS	Differential global positioning system
em, EM	Electromagnetic
EPA	U.S. Environmental Projection Agency
ft	Feet
Fm, FM	Formation
GIS	Geographic Information System
gpm	Gallons per minute
gr	granitic rocks
GSA	Groundwater Sustainability Agency
HEM	Helicopter Electromagnetic
Hz	Hertz (cycles per second)
IGRF	International Geomagnetic Reference Field
KDWCD	Kaweah Delta Water Conservation District
Km/km	Kilometers
KMZ/kmz	Keyhole Markup language Zipped file
$\mathbf{K_r}$	Horizontal hydraulic conductivity
Lm^{-1}	Liters per minute
m	Meters
m	Undifferentiated metamorphic rocks of pre-Cretaceous age
MCL	Maximum contamination level
ms	metamorphic rocks
md^{-1}	Meters per day
m^2d^{-1}	Meters squared per day
MAG	Magnetic (data); Magnetometer (instrument)
MCG	Minimum curvature gridding
md	Meters per day
m^2d^{-1}	Meters squared per day
mg/L	Milligrams per liter
NAD83	North American Datum of 1983
NAVD88	North American Vertical Datum of 1988

NMR	Nuclear Magnetic Resonance
NWIS	Natinal Water Information System
OM	Geosoft Oasis montaj
Ohm-m	Ohm per meter
PDF	Portable Document Format
PFC	Primary Field Compensation
PLNI	Power Line Noise Intensity
PLSS	Public Land Survey System
Q	Quaternary
QA/QC	Quality Assurance and Quality Control
Qa	Quaternary alluvium
Qb	Quaternary younger and older alluvium, flood-basin deposits, sand dunes
Qc	Quaternary continental deposits
Qf	Quaternary younger and older alluvium, flood-basin deposits, sand dunes
Ql	Quaternary lake Tulare Lake Bed
Qls	Holocene landside deposits
Qm	Quaternary Modesto Formation
QTt	Tertiary Tulare Formation
Rx	Receiver
S	Storativity
Sy	Specific yield
SCI	Spatially-Constrained Inversion
SJV	San Joaquin Valley
STD	Standard Deviation
Te	Miocene Etchegoin Formation
TEM	Transient Electromagnetic
TDEM	Time-Domain Electromagnetic
TDS	Total dissolved solids
Tm	Tertiary marine to nonmarine sediments
Tsj	Tertiary San Joaquin Valley Formation
Tx	Transmitter
ub	ultra basic ophiolites
USGS	United States Geological Survey
UTM	Universal Transverse Mercator
V/m^2	Volts per meter squared

1 Introduction

1.1 Purpose of Current Project

The East Kaweah Groundwater Sustainability Agency (GSA), the Greater Kaweah GSA, and the Mid-Kaweah GSA desire an improved understanding of the hydrogeologic framework in their management areas (Figure 1-1). Groundwater and surface water sustainability, groundwater recharge including storage facilities, water quality and surface water supply are some of the top reasons for using the information from the AEM survey. Characterization of the bedrock and its topography including any geologic structural control are of interest as well including mapping any high Total Dissolved Solids (TDS) at depth.

An airborne electromagnetic (AEM) survey was selected, and designed (Figure 1-2), to assist in the development of a 3D hydrogeologic framework of the project areas and to suggest future work to enhance groundwater management activities. The SkyTEM 312 would be utilized to conduct this investigation (Figure 1-2) to provide higher resolution at depth in the southeastern San Joaquin Valley near the foothills of the Sierra Nevada mountains. As a quality control measure and to provide the clients with greater understanding of the use of AEM, part of one flight line was to be flown over part of one flight line from the 2015 Tulare AEM investigation (Knight et al., 2018) and the results compared. The Tulare AEM survey utilized a SkyTEM 508 system which images somewhat deeper than the SkyTEM 312. The SkyTEM 508 is no longer available.

The survey design involves flying a total of approximately 800-line kilometers. The flight lines are arranged in a “reconnaissance”-style layout with about 3-5 km (2.5-3 miles) between flight lines. The proposed survey areas include water wells considered “active” by the California Department of Water Resources (CA-DWR) and the reconnaissance flight lines represent transects that connect points of good well control through regions that address one or more of the key issues. The specific design of this survey seeks to address the Project Goals with a layout of AEM lines that strikes a balance between line density, cost efficiency, logistical constraints, and geologic control.

Maps, 2D profiles, and other 3D images of the aquifer materials, their relationship to current test holes and production groundwater wells, and of estimated potential recharge areas along the flight lines are desired.

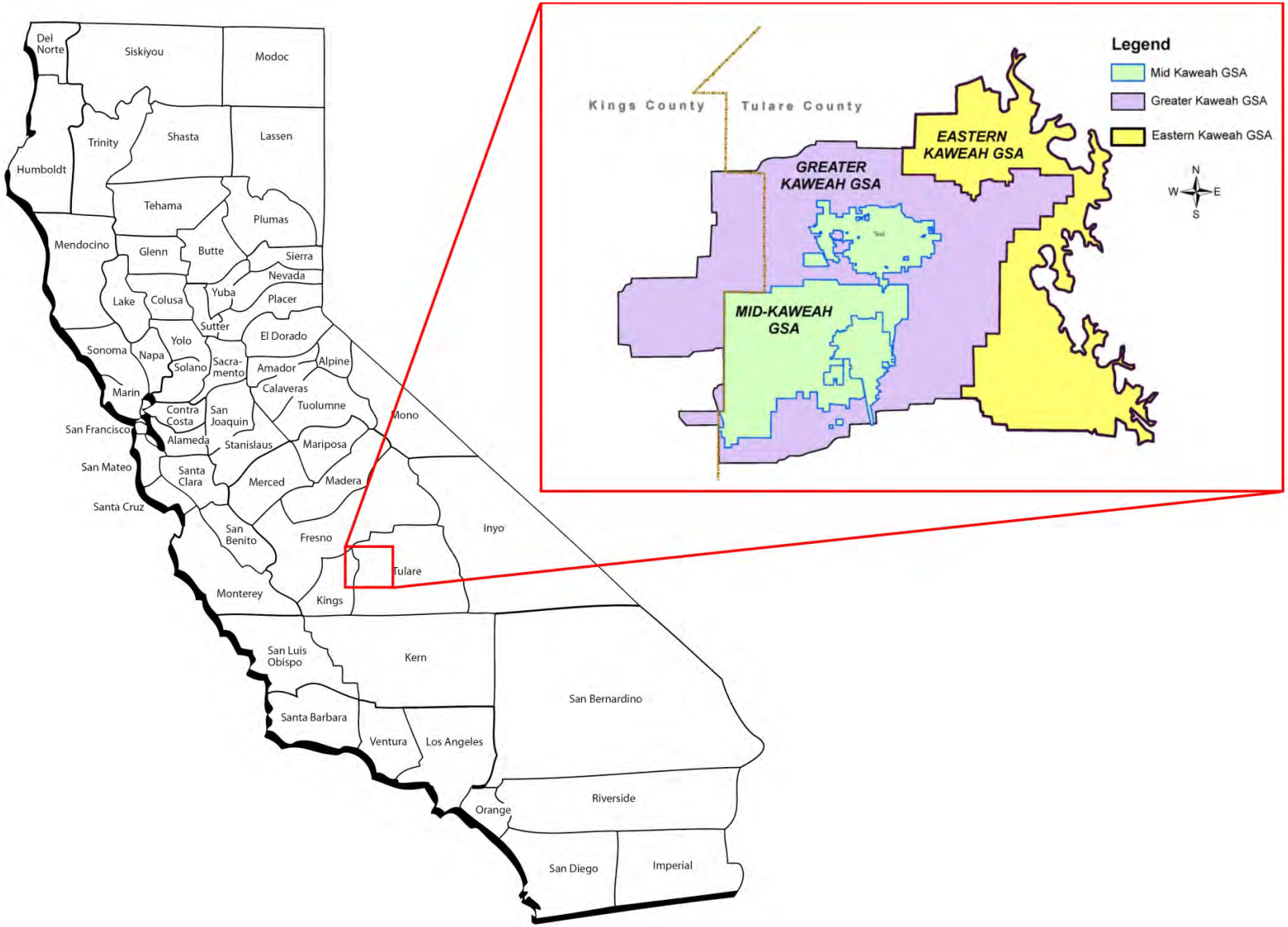

Figure 1-1. Map showing locations of Eastern Kaweah GSA, Greater Kaweah GSA, and Mid-Kaweah GSA (modified from http://tulareid.org/1st-qtr-2016-newsletter.pdf).

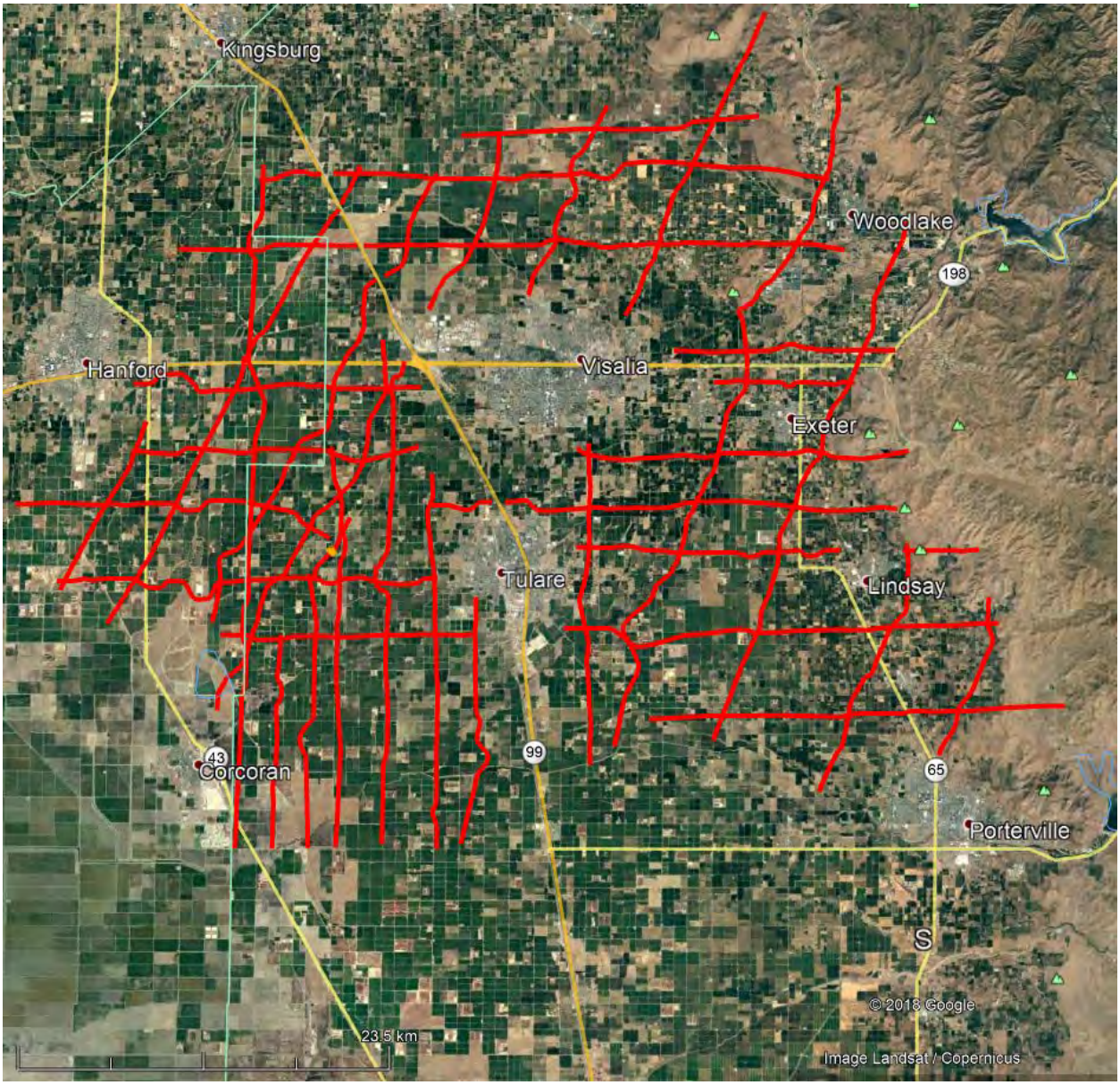

Figure 1-2. Google Earth image of the Kaweah Subbasin AEM survey area showing main highways passing through the area (99, 43, 65, 198). The red lines are the "as-flown" SkyTEM312 flight lines.

1.2 Background

Use of AEM technology to map and evaluate groundwater resources has gained momentum over the last 20 years in the United States and abroad. The State of California and others have been implementing AEM for water resources management over the last few years with projects across the state in a variety of geologic settings (Asch et al., 2017; Asch et al., 2018). In recent years, Stanford University has coordinated efforts between various local and state agencies and Aqua Geo Frameworks, LLC (AGF) in support of several projects designed to characterize the hydrogeology at various locations across the state. For purposes of this pilot project, Mid-Kaweah, East Kaweah GSA, Greater Kaweah GSA, and Stanford University are cooperating with AGF to complete this AEM investigation. This pilot project will not only provide information on the hydrogeologic framework of the Kaweah Subbasin area but will also provide experience for all partners in design and application of AEM surveys as well as educate the partners on the expectations on the nature of the results from these types of surveys. Mid-Kaweah GSA is the managing agency for this work and entered into contract with AGF on October 2, 2018.

1.3 Description of the Kaweah Subbasin AEM Project Area

The area of interest in the Kaweah Subbasin AEM survey area is located in the southeastern San Joaquin Valley in California and encompass approximately 3,672 km^2 (1,386 square miles) (Figure 1-2). The AEM survey area lie within parts of two counties: Kings and Tulare. Precipitation and irrigation runoff within the survey area feed into the Kaweah River and its distributaries including St. Johns Creek, Deep Creek, Packwood Creek, Mill Creek, and Cottonwood Creek (Figure 1-3). Water is also delivered through irrigation systems. The area has a groundwater supply within the interbedded clays, sands, and gravels of the unconsolidated alluvial materials that cover the area. Groundwater flow is towards the center of the San Joaquin Valley. The land use is a combination of irrigated agriculture and municipal. Irrigation comes from groundwater wells and surface water supplies.

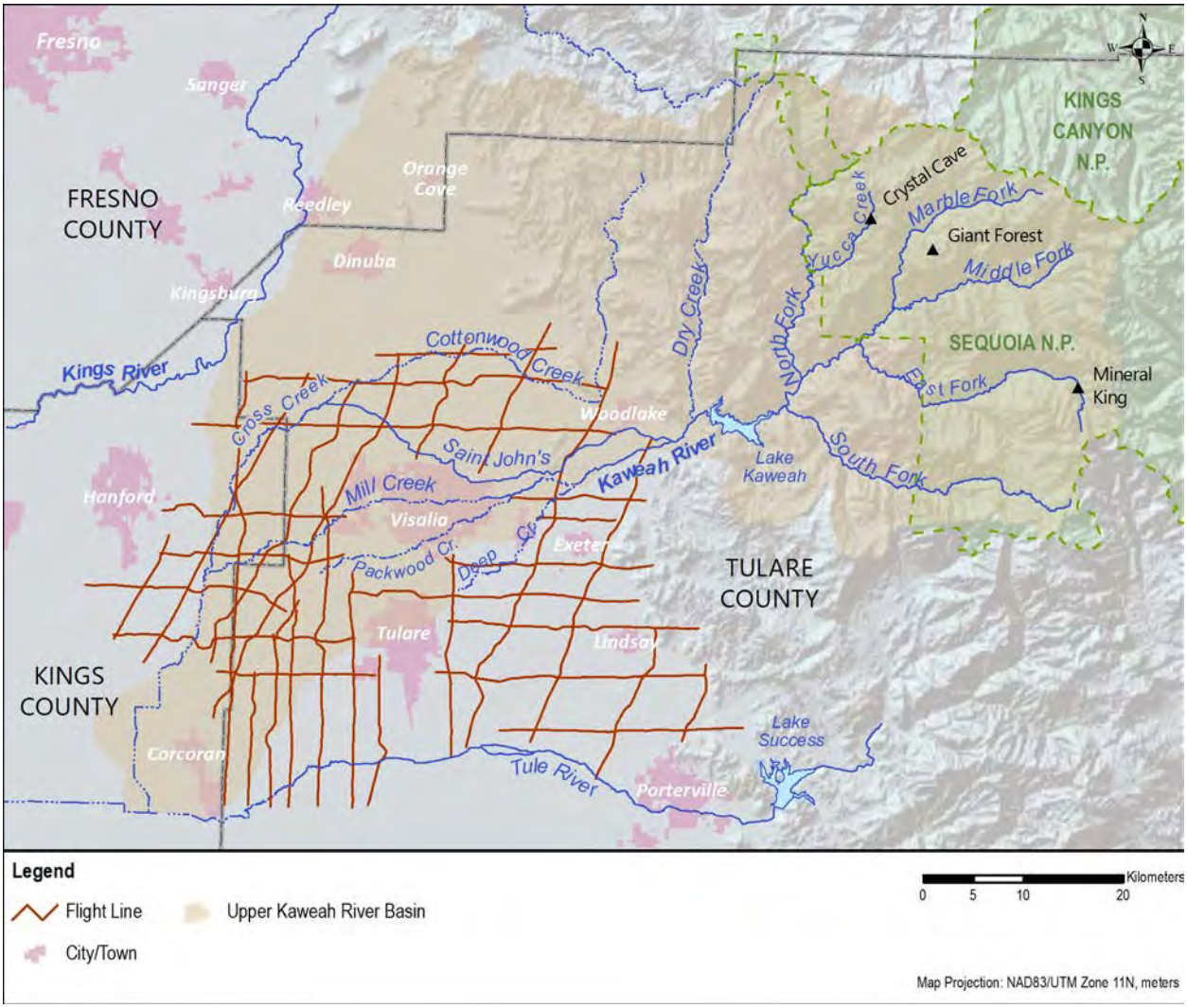

Figure 1-3. Map of major river basins with streams within the Kaweah Subbasin AEM survey area in relation to the AEM flight lines (brown); (modified from https://en.wikipedia.org/wiki/Kaweah_River#/media/File:Kaweah_river_basin.png)

2 Project Area Hydrogeology

The AEM survey's objective was to map the geology and related hydrogeology of Quaternary and Tertiary deposits and the primary underlying bedrock that serves as a groundwater confining unit. Background geology and hydrogeology in and around the project area are discussed in more detail in reports by Page (1983, 1986), Bartow (1991), Planert and Williams (1995), Galloway (1999), California Department of Water Resources (CA-DWR) (2003, 2014), Johnson and Belitz (2014), White (2016), and Kaweah Delta Water Conservation District (KDWCD) (2018), among others. The following narratives are based primarily on the findings from these reports.

2.1 Geologic Setting

The project area lies on the southeastern edge of the San Joaquin Valley (SJV) portion of California's Central Valley. Here, the SJV abuts the foothills of the Sierra Nevada Mountains where the geology largely is granitic and marine to nonmarine deposits (CA-DWR, 2014). Much of the geologic character of the project area is dominated by the Sierra Nevada Mountains to the east, in addition to fluvial outwash from the mountains in the form of undifferentiated alluvial and colluvial fan deposits that occupy the SJV and much of the incised valleys of the uplands. The Quaternary alluvial fans of Holocene age in the SJV, overlie continental deposits—Plio-Pleistocene and Pliocene marine and nonmarine deposits that together can be thousands of meters in thickness.

2.1.1 Physiography and Regional Geologic Setting

As mentioned in the Section 1 above, AEM data were collected over the project area. The approximately 3,672 km^2 (1,386 square miles) Kaweah Subbasin AEM project area mostly lies in the 1,803 km^2 (696 square miles) Kaweah Groundwater Basin (GU 5-22.11)—Kings and Tulare Counties, California (CA-DWR, 2003; Johnson and Belitz, 2014)—but small portions extend into adjacent groundwater units not discussed in this report. The project area also contains several large to small cities. U.S. Census Bureau (2018) reports the 2010 population of the largest cities in the project area, by population, as: Visalia (124,442), Tulare (59,278), Porterville (54,165), Hanford (53,967), Corcoran (24,813), Lemoore (24,531), Exeter (10,334), Lindsay (11,768), and Woodlake (7,279). Smaller communities, such as Goshen (2010 population 3,006) can be found throughout the project area.

Galloway (1999) reports the SJV, which includes the project area, is one of the world's most productive agricultural regions. Furthermore, the SJV receives streamflow from larger systems such as the Kaweah River, and the Kings and Kern Rivers, which lie outside the project area and are not shown on the maps. Over many millennia, these and smaller streams, which terminated at topographically low closed basins or sinks, deposited a network of alluvial fans along the eastern side of the SJV (Galloway, 1999).

The SJV is filled with marine sediments overlain by continental deposits such as clay, silt, sand, fluvial, and lacustrine deposits. The SJV is at its widest (about 55 miles or 89 km, Davis et al., 1964) where the project area is located within the valley.

Surficial geology (Figure 2-1) in and around the AEM survey area typically ranges from slightly to moderately tilted or folded Tertiary to early Quaternary deposits (Davis et al., 1964). The topography varies from deeply incised foothills to the east, where the relief can be as great as 152 m or 498 ft, to less than 3 m or 10 ft in the Tulare Lake bed to the west. Much of the Pliocene, Pleistocene, and Holocene age arkosic material was derived from the Sierra Nevada just east of the project area. CA-DWR (2003) reports this arkosic material is divided into three stratigraphic units—continental deposits, older alluvium, and younger alluvium. The continental deposits are deeply weathered, poorly to highly permeable Pliocene and Pleistocene deposits. Older alluvium makes up the major aquifer in the Kaweah Subbasin and overlies the continental deposits. These deposits are moderately to highly permeable. The younger alluvium consists of moderately to highly permeable arkosic beds consisting of sand and silty sand (CA-DWR, 2003).

Basement geology, some of which outcrops in the AEM field area and is traversed by several of the AEM reconnaissance flight lines, consists of Mesozoic granitic units and ultramafic rocks, chiefly Mesozoic, including the Kings-Kaweah ophiolite mélange.

Figure 2-1 presents the local geology in the Kaweah Subbasin AEM survey area.

2.1.2 Surficial Geology

The surficial geology of the project area, presented in Figure 2-1, is a complex assortment of Tertiary to early Quaternary deposits (Davis et al., 1964; Matthews and Burnett, 1965). Quaternary basin (***Qb***) and fan (***Qf***) deposits comprise the primary material around the Visalia area (approximately mid-center of project area). The ***Qf*** sediments generally are coarsest near the upper parts of the alluvial fans valleyward and finer toward the Valley's trough (Barow et al, 1998).

Plio-Pleistocene continental deposits (***Qc*)** primarily consisting of the Tulare Formation (***QTt***; Page, 1983) and Upper Pliocene San Joaquin Formation (***Tsj***; Page, 1983) underlie the **Qb**/**Qf** deposits (Table 2-1). The Mesozoic granitic rocks (**gr**), and overlying ***ub*** ophiolites in spots, primarily serve as both the basement complex and crop out as the primary deposits of the Sierra Nevada. About 5 km to the southwest of the project area, the Tulare Lake Bed (***Ql***) forms a large flatland that under natural conditions was poorly drained (Davis et al., 1964). The ***Ql*** is named for the Tulare Lake that covered much of the region in the Pleistocene (Planert and Williams, 1995).

The Sierra Nevada are the predominant topographic feature in the area. However, at the project area, the SJV is the primary surficial feature. On the eastern side of the SJV, the ***QTt*** conformably overlies the ***Tsj*** (Page, 1986). These two formations, in turn, generally overlie Tertiary marine deposits described below. Page (1986) discusses the ***QTt*** and ***Tsj*** Formations in more detail than what is presented in this report. The following discussions of the two formations are based largely on his work.

The ***QTt*** generally consists of continental beds of poorly consolidated sandstone, siltstone, and conglomerate (Matthews and Burnett, 1965). The ***QTt*** thins from west to east where it eventually becomes indistinguishable with other continental rocks (Hilton et al., 1963). Near the southwest corner of the project area the thickness of the ***QTt*** can exceed 1,000 m (Page, 1986).

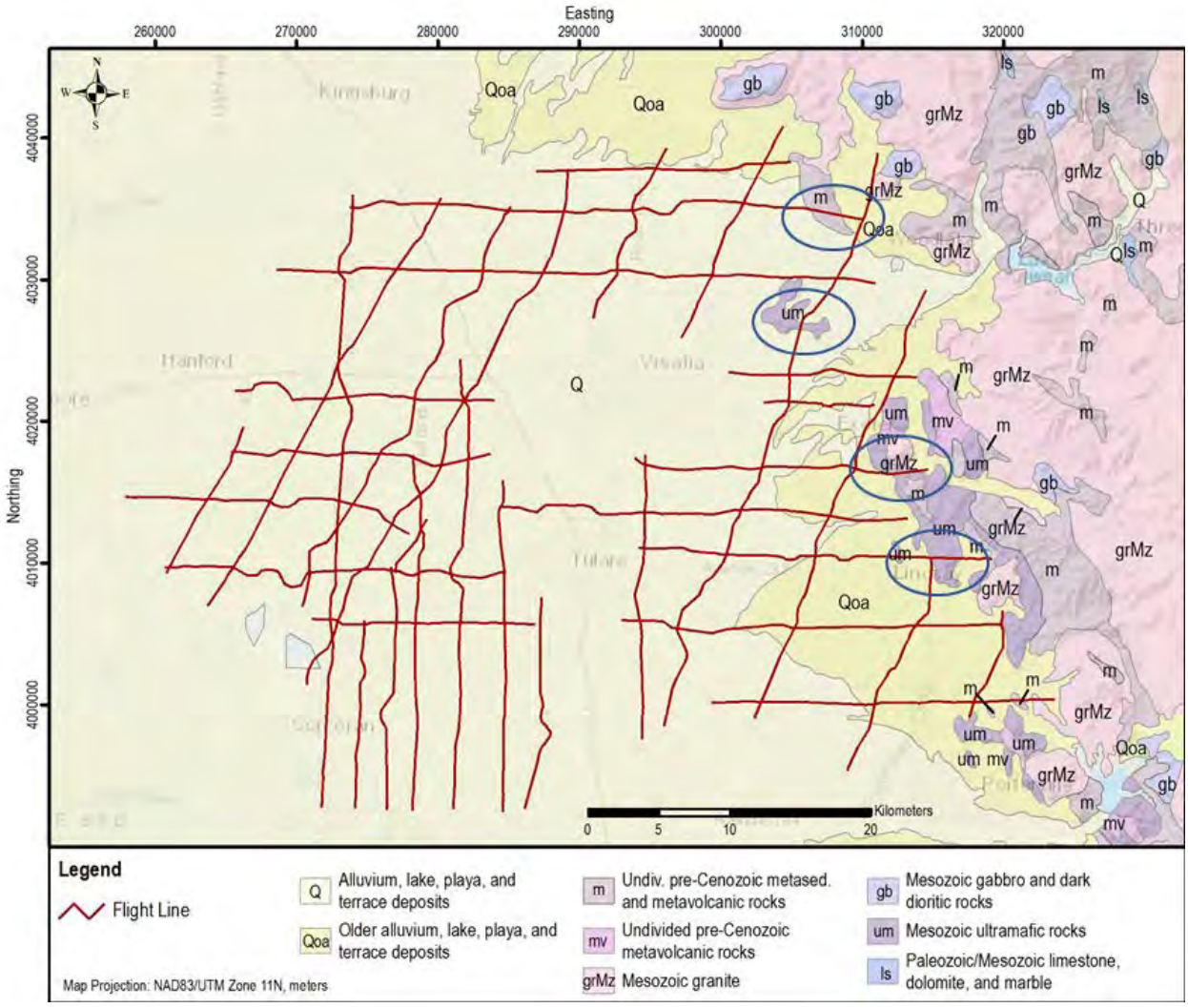

Figure 2-1. Surface geologic map of the Kaweah Subbasin AEM survey area in relation to the AEM flight lines. (modified from California Geological Survey, 2010). The areas circled represent locations where the AEM flight lines crossed pre-Tertiary metavolcanics geology.

Table 2-1. Table of generalized geologic formations in the project area.

Age		Unit/ Formation	Description[1] [symbols in parentheses after Matthews and Burnett (1965); ***QTt***, ***Tsj***, and ***Te*** (Page, 1983)]
Cenozoic	Holocene	Alluvium	(Younger) - (***Qf***, ***Qb***) Aerially extensive. Include younger alluvium, flood-basin deposits, and sand dunes. Heterogeneous clean well-sorted sand and gravel deposited by perennial stream such as the Kaweah. Coarse sand and gravel interbedded with finer grained poorly sorted material deposited during floods. Permeability generally high. Maximum thickness about 20 m.
			(Older) - (***Qf***, ***Qb***) Aerially extensive. Include older alluvium, lacustrine, march, and basin deposits, as well as terrace and major alluvial fans. Older alluvium makes up a majority of the aquifer in the project area. Deposits range from poorly sorted fine-grained material to lenses of coarser grained sand and gravel that represent buried channels of minor streams. Coarser grained than underlying Continental deposits. Generally, less permeable than younger alluvial fans. Maximum thickness[2] ~100 m.
	Plio-Pleistocene	Continental deposits	(***Qc***): Unconsolidated deposits that yield about 10 percent of groundwater to wells. Derived from eastern sources (e.g., Sierra Nevada). Consist of silt, clay, sandy clay, clayey and silty sand, sand, and gravel.[3]
		Tulare Formation	(***QTt***): Heterogeneous mix of continental rocks of poorly consolidated sandstone, siltstone, and conglomerate. Interfingers with the Turlock Lake Formation north and west in the valley. Maximum thickness of ***QTt*** can be over 1,000 m. ***QTt*** contains Page's (1986) very low permeable "Modified E Clay" of which the Corcoran Clay Member is associated. Modified E Clay thins easterly to 0 m.
	Pliocene	San Joaquin Formation	(***Tsj***): Marine and nonmarine sedimentary rock. Fine-grained silty sandstone, silt and clay.
	Tertiary	Continental and Marine deposits	(***Tm***) Deep Miocene and Pliocene deposits in the San Joaquin Valley. Metamorphosed shale, sandstone, limestone, and chert, intruded by great masses of granodiorite and related igneous rocks. Might include the Etchegoin Formation[3]. Deposits of clay, claystone, silt, sand, sandstone, and some conglomerate. Maximum thickness[4] more than 3,000 m. Not shown in Matthews and Burnett (1965).
Mesozoic	Pre-Tertiary[2]	Marine and Nonmarine	(***ub***, ***m***) Mesozoic ultrabasic intrusive rocks—ophiolites, serpentine, etc.; locally including talc, schist, etc. Undifferentiated metamorphic rocks of pre-Cretaceous age. Includes Jurassic age metamorphosed marine limestones and dolomites.
		Intrusives	(***gr***, ***ms***) Massive undifferentiated granites, granodiorites, and related granitic rocks. Unnamed pre-Cretaceous metasedimentary rocks primarily composed of schists, quartzite, slate, and marble. Generally, serve as basement complex.

[1]Modified from Davis et al., 1964; Matthews and Burnett, 1965; Page and LeBlanc, 1969; Muir, 1977; Page, 1983; California Department of Water Resources, 2003.

[2]Matthews and Burnett, 1965; Page, 1986.
[3]Page, 1983.
[4]Includes continental and marine sedimentary rocks of Cretaceous age (Muir, 1977).

The ***QTt*** contains the Corcoran Clay Member, a diatomaceous laterally extensive clay that is part of the extensively mapped lacustrine "*modified E Clay*" (Page, 1986; hereinafter the E Clay). Page (1986) and the Kaweah Delta Water Conservation District (2015) report the eastern boundary of the E Clay, that part within the project area, lies in or near Visalia. Here, the E Clay thickens from 0 m near Visalia to over 18 m near the southwest corner of Tulare County. The E Clay thickens to around 49 m beneath the Tulare Lake Bed (Page, 1986). Note, some reports (e.g., cross sections in KDWCD, 2015) indicate the E Clay could be within the younger Pleistocene and Holocene sediments. For this report, usage will be Plio-Pleistocene as described in Page (1986).

Woodring et al. (1940) described the base of the ***QTt*** as a layer just above the upper *Mya* zone of the ***Tsj***. The "upper *Mya* zone refers to the uppermost strata in which the burrowing pelecypod, or clam, *Mya* occurs in the San Joaquin Formation" (Page, 1983, p. 7). Where present, the *Mya* zone and folded strata have been used to mark the contact of the ***QTt*** in the subsurface. Moreover, "this base marks a change from a dominantly marine environment [***Tsj***] to a continental environment [***QTt***] of lakes, swamps, and streams" (Page, 1983, p. 7).

The partly continental and partly marine ***Tsj*** generally consists of fine-grained silty sandstone, sit and clay (Matthews and Burnett, 1965; Page, 1986). The ***Tsj*** has different sediment types, but much of the formation contains silt and silty sandstone. In the Kettleman Hills area (approximately 25 miles or 40 km southwest of the project area), the formation contains a basal conglomerate (Page, 1986). Moreover, the ***Tsj*** is the youngest formation in the SJV of marine origin (Page, 1986). No documentation has been found to show that the basal conglomerate extends to the project area.

2.1.3 Tertiary Geology

This section and the next section of this report give only brief overviews of the Tertiary and Pre-Tertiary deposits in and around the project area. Bartow (1991) goes into substantial detail regarding the sedimentary sequences of the San Joaquin Valley.

Tertiary geology within and adjacent to the project area is a complex sequence of marine to nonmarine sediments (***Tm***) (Table 2-2). Tertiary sediments composed of "metamorphosed shale, sandstone, limestone, and chert, intruded by great masses of granodiorite and related igneous rocks" (Davis et al., 1964, p. 11) and found at depth. Tertiary deposits include marine rocks and deposits of Miocene and Pliocene age and primarily consist of sand, clay, silt, sandstone, shale, mudstone, and siltstone (Page, 1986). Table 2-2 describes the primary Tertiary sediments in the project area. Wells yield little to no water, but form the eastern boundary to the groundwater basin (Muir, 1977).

Page (1983) reports the Miocene age Etchegoin Formation (***Te***) underlies the ***Tsj***. The transgression of the ***Te*** over the older Miocene enabled the creation of basin-ward alluvial fans and deltas from abundant coarse detritus coming out of the rising Sierra Nevada (Bartow, 1991).

Table 2-2. Summary information for Quaternary and Tertiary aquifer units within the area. Included in this table are the geologic system hosting the aquifer, generalized aquifer thickness, and a general discussion regarding the aquifer framework, groundwater flow system characteristics, and aquifer parameters.

System	Series	Hydrologic unit	Maximum thickness, ft.
Quaternary	Holocene to Plio-Pleistocene	Aquifer in undifferentiated Central Valley alluvial deposits	Generally, less than 328 ft or 100 m
Undifferentiated sand and gravel units in younger and older alluvium (alluvial fans) and paleo-valley systems. Younger alluvium is highly permeable beneath river channels, poorly permeable beneath flood plains. Yields small to moderate quantities of water to wells. Older alluvium serves as primary aquifer. Yields to wells are small to large. Kaweah River stream-aquifer systems can be intermixed with flood deposits. Hydraulic head is typically unconfined. Locally or regionally hydraulically connected to underlying Plio-Pleistocene deposits. Recharge is principally from influx from adjacent near mountain boundaries, leakage from surface-water canals, and local precipitation. Surface-water canal leakage can be rapid if the source area is primarily sand and gravel. Typical wells capable of yielding between 20 and 3,434 gpm (76 and 13,000 Lm^{-1}). Horizontal hydraulic conductivity values can exceed 140 md^{-1}.			
Quaternary	Plio-Pleistocene	Aquifer in Tulare Formation	Can exceed 3,281 ft or 1,000 m
Tulare Formation... Aquifer underlies much of the southern part of California's Central Valley (San Joaquin Valley). Interfingers with the Turlock Lake Formation at depth in the Central Valley to the north and west. Lies at considerable depth in the Fresno area so few wells tap the aquifer (Muir, 1977). Considered unconfined except where the Corcoran Clay Member, or "E-clay" exists. Well yields variable; wells capable of producing up over 2,906 gpm (11,000 $Lmin^{-1}$), but vary greatly by location. Horizontal hydraulic conductivity values for deposits within or near the project area not determined from aquifer tests.			
Tertiary	Pliocene	Aquifer in the San Joaquin Formation	
Generally, not a source of groundwater due to depths and saline concentrations. Saturated thickness varies by location. Thins easterly.			

2.1.4 Pre-Tertiary Geology

Pre-Tertiary age rocks in the project area include granitic (***gr***) and metamorphic rocks (***ms***) that crop out along the eastern flank of the Central Valley (Matthews and Burnett, 1965; Page, 1986) and nonmarine and marine sediments such as ophiolites (***ub***, ***m***) in the Central Valley. The Sierra Nevada Mountains form the eastern side of the valley and "is the eroded edge of a huge tilted block of crystalline rock that also partially defines the base of the valley sediments" (Planert and Williams, 1995, p. B16). The uplift that formed the Sierra Nevada likely occurred during the Late Jurassic to Late Cretaceous (Planert and Williams, 1995). These basement intrusives create the eastern boundary of the groundwater basin. Moreover, the upthrust of the Sierra Nevada tilted the younger Tertiary and pre-Tertiary continental and marine rocks and deposits in the SJV.

2.2 Kaweah Subbasin AEM Survey Area Hydrogeologic Characteristics

The primary hydraulic features in the project area are related to the major streams, the Kaweah and Tule Rivers, whose headwaters are in the Sierra Nevada Mountains, and several large surface-water canals. The Kaweah and Tule River Basins are closed in the sense that the Kaweah River flows westerly from its reservoir at Lake Kaweah to McKay Point where water is equally diverted into two rivers—Lower Kaweah and St. Johns (KDWCD, 2018). The Lower Kaweah breaks into four lesser natural and manmade dendritic distributaries on the alluvial fan—Cameron, Deep, Mills, and Packwood Creeks. Additional creeks bring water and sediment into the valley (e.g., Yokohl Creek). However, KDWCD (2015) reports the Kaweah River is a primary surface-water source in the area for groundwater recharge. Highest peak monthly outflows at the Terminal Dam (Kaweah Lake) since January 2010 generally occurred during the March to July time frame—sometimes during a single month or for four or five month stretches (CA-DWR, 2018a). Since January 2010, the average monthly peak outflow from Success Dam was about 4.1×10^7 m^3, whereas the greatest was about 2.4×10^8 m^3.

The Tule River flows along the bottom of the project area. Its primary reservoir just outside the project area is Lake Success. From Success Dam, the Tule River flows southwest then northwesterly through the southern edge of Porterville, CA. Similar to Lake Kaweah, the highest peak monthly outflows since January 2010 generally occurred during the January to July time frame—sometimes during a single month or for four or five month stretches (CA-DWR, 2018b). Since January 2010, the average monthly peak outflow from Success Dam was about 1.2×10^7 m^3, whereas the greatest was 1.2×10^8 m^3.

Two prominent canals in the project area—the Friant-Kern Canal and the Lakeland Canal—serve various water districts in and around the project area. The 245-km long cement lined Friant-Kern Canal traverses the eastern portion of the project area and augments the Kaweah River supply, where it either percolates or offsets groundwater extraction (KDWCD, 2015, 2018).

KDWCD, the surface water conservation district in the project area, takes some water from the Friant-Kern canal (Central Valley Project [CVP]). KDWCD (2017) reports that the Kaweah River, in normal years, reaches its highest stage in May or early June—as seen above in discussion from the Kaweah Lake—with an average annual runoff of 5.6×10^8 m^3. Besides the Kaweah River, water enters the district to infiltrate

into the groundwater by way of canals from the Kings River and smaller streams (e.g., Dry and Yokohl Creeks). Water also is imported from the CVP, with a total surface-water supply for 2017 of 1.48 x 10^9 m^3 (KDWCD, 2017).

McKay Point serves as a significant geographical feature in the KDWCD. Here, the Kaweah River equally divides into the St. Johns River and Lower Kaweah River. Then, within the KDWCD, water from these two rivers branches divide into both natural and manmade distributaries forming the Kaweah Delta (KDWCD, 2017).

2.2.1 Groundwater in the Kaweah Subbasin Area

Under natural conditions groundwater moves from recharge areas at the foothills of the Sierra Nevada southwest toward the valley trough—from an unconfined system to a confined system (Page, 1986). This water resupplies the ***Qf*** which serves as the major aquifer in the area (Galloway, 1999). Moreover, groundwater supplies all municipal and industrial water use within the KDWCD, which mostly encompasses the project area (KDWCD, 2018). Although groundwater supplies all municipal and industrial use wells, resupplying the groundwater under non-natural conditions is now completed with myriad diversions from irrigation and supply canals (e.g., Friant Kern Canal, Lakeland Canal, others outside project area: Homeland Canal, Liberty Mile Canal, Blakeley Canal; Goose Creek Canal) in the project area that supply recharge water to the system.

The shallow, unconfined or partially-confined ***Qf*** aquifers occur throughout much of the valley. Galloway (1999) reports these shallow unconfined aquifers are particularly important near the margins of the valley and near the toes of younger alluvial fans. As mentioned above, under natural conditions water infiltration through stream channels near the valley margins was the primary means to replenish groundwater supplies. Runoff from streams emitting out of the Sierra Nevada provided most recharge for valley aquifers. Infiltration and seepage from streams and lakes on the valley floor also recharged the aquifer, but to a much lesser extent. Galloway (1999) reports that in 1999, the natural recharge replenishment mechanism of the aquifer systems remained relatively the same. However, Galloway (1999) noted that even in 1999 that more water was being discharged (pumped) from the aquifer system than was being recharged, resulting in land subsidence in some areas.

Generally, groundwater in the ***Qf*** is under unconfined conditions. Groundwater in the ***QTt***, however, can be unconfined, semi-confined, or confined. Where found within the ***QTt***, the E Clay; as well as other clay layers (e.g. A and C Clays), act as a confining or semi-confining unit. Therefore, these can be a substantial hydrogeologic unit within the ***QTt***. Planert and Williams (1995) report that recent studies suggest vertically and horizontally scattered clay lenses exist throughout the ***QTt*** rather than a single clay unit. Page and LeBlanc (1969) report three confined aquifers due to the clay below the A, below the C, and below the E clay layer. Generally hydraulic head decreases with increasing depth so the clays allow for a slow vertical passage of groundwater.

Groundwater-level elevations in the form of water-table maps provide guidance to direction of groundwater flow. The groundwater elevation in the project area is generalized and shown in Figure 2-2.

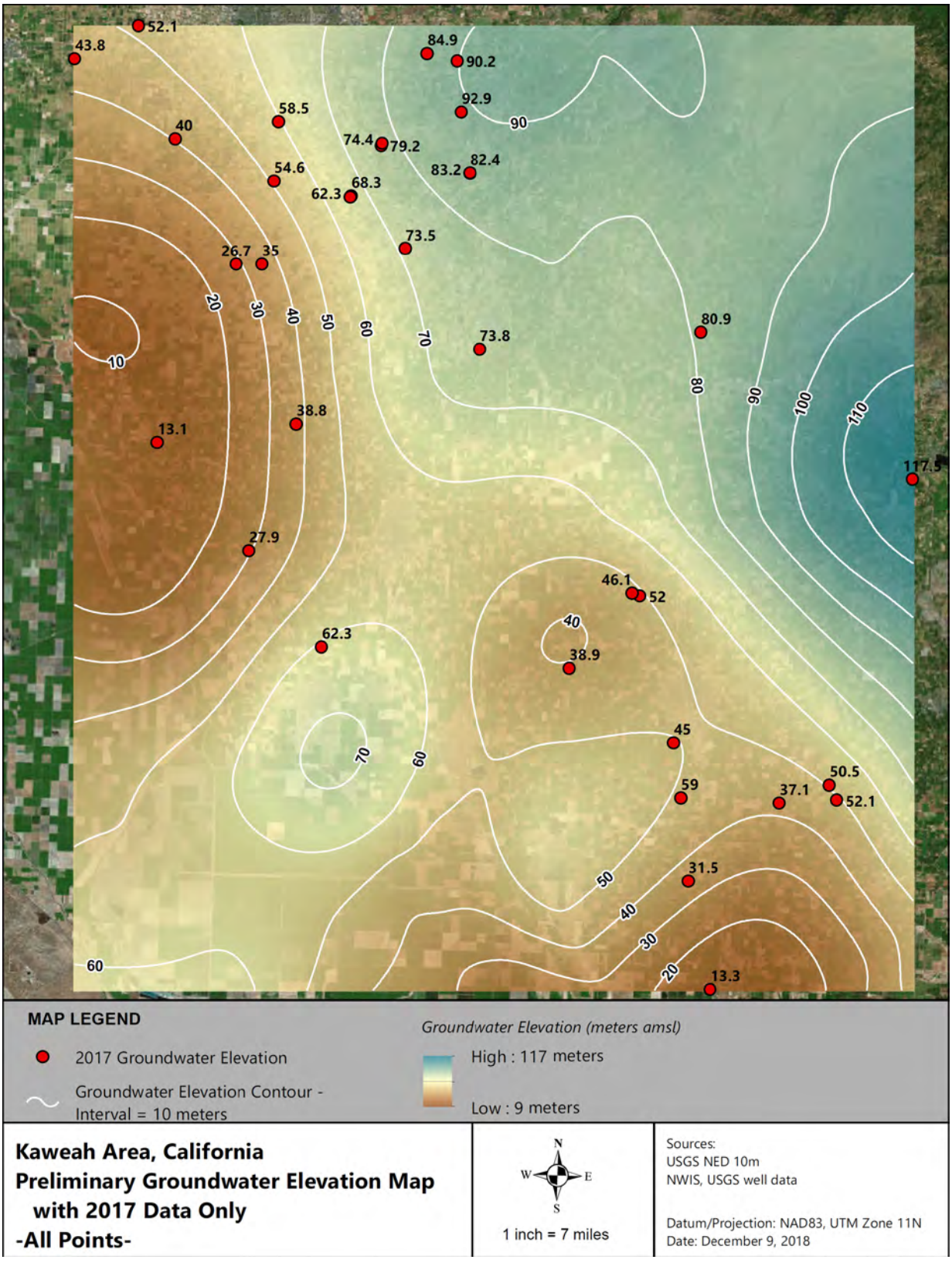

Figure 2-2. Map showing highly generalized regional groundwater elevations around the project area, 2017. Data from USGS, 2018.

Depths to groundwater below ground surface (bgs) vary greatly with topography. Groundwater levels in the upland areas typically are (1) under unconfined and (2) have depths to water that generally are less than 3 to 15 m (10 to 50 ft) bgs. Generally, groundwater levels in the ***Qb/Qf*** is unconfined. Within the ***QTt***, groundwater conditions generally are semi-confined to confined where the E Clay is present.

Regional maps showing the configuration of the water table (Figure 2-2) indicate groundwater flow from east to west. The U.S. Geological Survey's (USGS) National Water Information System (NWIS) was used to access the most recent water levels since 1970 per well from 495 wells with depths greater than 23 ft or 7 m in Tulare and Kings Counties, California. These data were used to determine general groundwater indications in and around the project area. Wells less than 7 m (23 ft) deep were excluded due to a large number of them (about 180) in the center of the valley. Data from the 495 wells indicate a general pattern of shallowest in the east (near the Sierra Nevada foothills) to deepest in the west (near the center of the valley). Spring 2017 groundwater-levels from 34 of these same wells were looked at and 16 of the 34 water levels were in close proximity (within 15 km or 9 miles) of the project area. Most (69 percent, or 11 of 16) of the wells had water levels were greater than 98 ft (30 m) below the land surface. However, aerial placement of the wells did not facilitate groundwater flow paths. However, in 2017 KDWCD (2017) measured 236 wells in and around their district. They compared 201 of these measurements 2016 water levels. KDWCD comparisons show an overall combined 2016 to 2017 water-level change in their district of 0.85 m or 2.8 ft.

KDWCD (2017) spring 2017 groundwater elevation map, similar to long term data from the NWIS, show groundwater gradients generally slope from east to west (Figure 2-2). The highest groundwater elevations were found just west of McKay Point, whereas the lowest were found in areas in and around Hanford and Corcoran, California. Note, most water levels in and around Corcoran are semi-confined to confined by the E Clay, while those water levels east of Visalia and onto McKay Point are generally unconfined. Although the KDWCD groundwater contour map was computer generated, the map is more than sufficient to show a generalized groundwater gradient of east to west. Similarly, spring 2018 groundwater level data (CA-DWR, 2018a) also show water levels were shallowest at the foothills of the Sierra Nevada (< 6 m or 20 ft bgs). Further, towards the middle of the valley, water levels ranged from 30 to 100 m (98 ft to 328 ft) bgs.

Temporally, USGS site 364200119420003 shows quite a variation in dates when groundwater levels generally reached pre-stress levels (USGS, 2018). At this site, pumpage of nearby wells occurred toward the end of August in 2015, but much of the first half of 2016, and as late as March and May in 2017 and 2018, respectively (Figure 2-3). Pumpage from large volume production wells during irrigation season stresses the aquifer. The magnitude of stress from pumpage and any corresponding groundwater-level decline is dependent on many factors—e.g., characteristics of the aquifer, the amount and timing of rainfall, land use, and density of high-volume wells stressing the aquifer. Consequently, pumpage of high capacity wells during drought conditions would cause groundwater levels to decline more than during times when precipitation is timely and plentiful. Recovery of groundwater levels during the non-irrigation season also is more difficult during drought. The amount of recovery is dependent on the amount and source of recharge available. Copious amounts of precipitation or leakage from surface-

water canals can help groundwater levels recover to or exceed pre-stress groundwater levels; whereas drought conditions can dampen recovery of groundwater levels.

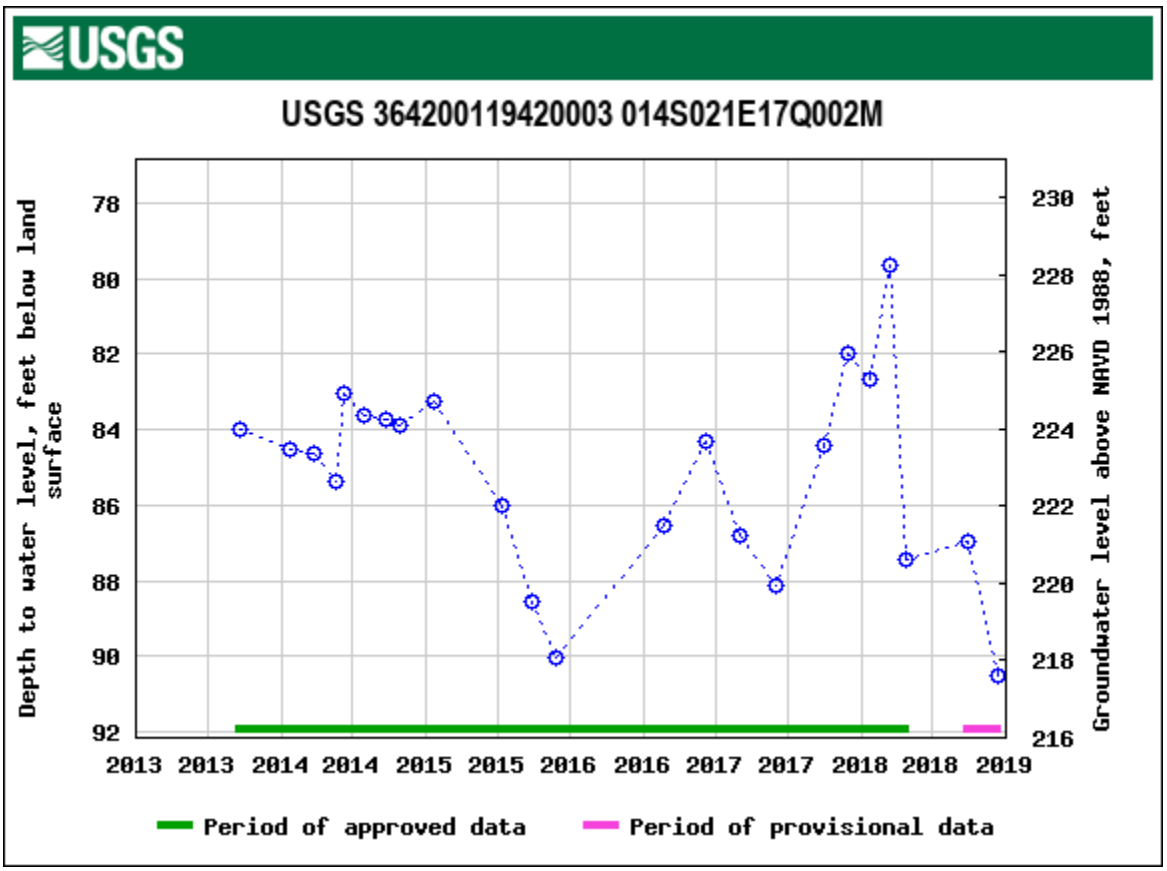

Figure 2-3. Graph showing groundwater fluctuations at USGS groundwater recorder 364200119420003 near Fresno, not far from the project area (USGS, 2018).

2.2.2 Aquifer Characteristics

Aquifer characteristics of the project area were compiled from localized or large regional studies. Aquifer tests (constant discharge, slug, or permeameter) performed in or near (within 31 miles or 50 km) of the project area, help characterize the aquifer(s). However, discussions on aquifer tests are point source tests and should not be construed as representing an aquifer as a whole. Point-source tests can be qualitatively used to represent regional systems when viewed with certain caveats (e.g., difference in scale—local vs. regional, difference in sediment, and difference in aquifer thickness). Keeping scale in mind, all discussion of aquifer tests herein are local tests used to represent a regional system. Consequently, these values are reported as regional generalities and not meant to qualitatively represent any place other than where the aquifer tests were performed.

Aquifer tests conducted in or near the project area and available to the public are limited. There appear to have been numerous aquifer tests during the 1950s in and around Fresno (about 25 miles of 40 Km north-northwest of the project area); however, this report consolidates these tests into those described in references in Page and LaBlanc (1969) (Table 2-3).

Table 2-3. Summary of generalized aquifer-test data in or near the project area (--, not reported or not applicable; UTLF, Upper Turlock Lake Formation; LTLF, Lower Turlock Lake Formation; SJV, San Joaquin Valley; JID, James Irrigation District]

Researcher(s)	Year published	Location	K_r (md^{-1})	T (m^2d^{-1})	*Sy*	*S*
USGS and Nolte[a]	1957	Fresno, California	0 to 143	650 to 2,000	0.2 to 0.36	--
White	2016	Visalia, California	--	232[b]	--	--
		UTLF	13.586	253	--	--
		LTLF	0.336	2.558	--	--
Schmidt[c]	2004	Well C-81 K Basin	--	596 to 907	--	--
Driscoll[d]	1986	SJV, northern part JID	--	1,320 to 1,580	--	--
Driscoll[e]	1986	SJV, southern part JID	--	1,060	--	--
City of San Joaquin	2003	Well No. 5	--	485	--	--
USGS[f]	1954	19S/18E-35E1	--	1,240 to 1,860	--	--
		20S/19E-25Q1	3	870	--	$3x10^{-4}$
		20S/22E-10H2	--	323	--	--
		23S/25E-17Q2	--	186	--	$1x10^{-5}$
		24S/22E-28A2	--	559 to 808	--	$5x10^{-4}$
		24S/25E036J1	--	186	--	--

[a] Referenced in Page and LeBlanc, 1969
[b] Determined using constant-head permeameter testing (White, 2016).
[c] Referenced in Provost & Pritchard Consulting Group, 2015, Appendix F; not found in references
[d] Compilation of regional specific capacity values of pump tests across San Joaquin Valley
[e] Likely in unconfined aquifer above the E Clay
[f] McClelland, 1962

Horizontal hydraulic conductivity (***K_r***) values in ***Qf*** sediments ranged from 0 to 143 md^{-1}. Consequently, this indicates a large heterogeneity in the ***Qf*** deposits. Transmissivity values depend on the K_r and saturated thickness. The volume of water that moves through an aquifer would depend on the groundwater gradient at the site.

Specific yield (***Sy***) can be related closely to, but is less than an aquifers total porosity Bear (1979). Specific Yield is an estimate of the percentage of water in an aquifer that will drain under gravity (Heath, 1983). Specific Yield values in ***Qaf*** deposits were reported by references in Page and LeBlanc (1969) as 0.2 to 0.36.

2.2.3 Connectivity to Surface Water and to Other Aquifers

Groundwater connectivity to surface-water systems in the project area is complex due to the numerous surface-water features that recharge the groundwater system.

2.2.4 Water Quality

Concentrations of total dissolved solids (TDS) above 1,500 milligrams per liter (mg/L) can affect the bulk resistivity values impacting the interpretations of the geological materials. Therefore, TDS data from 107 wells in the USGS NWIS (USGS, 2018) were used to determine TDS concentrations in the Kaweah Subbasin AEM project area. Almost all wells showed TDS concentrations less than the 1,500 mg/L threshold. Those that did have samples greater than 1,500 mg/L were west of the flight area (Figure 2-4), in the Tulare Lake Bed area. As a result, groundwater samples collected from wells throughout the Kaweah Subbasin AEM project area show most TDS concentrations were less than the 1,500 mg/L threshold and; therefore, water quality in the project area likely did not affect interpretation of bulk resistivity values.

Nitrate as nitrogen concentrations in water samples in Kings and Tulare Counties were downloaded from USGS NWIS (USGS, 2018). Data indicate 138 samples from 1979 to 2015 ranged from non-detectable to 100 mg/L (Figure 2-5). About two-thirds of the concentrations (68%, 94 of 138 samples) were less than the U.S. Environmental Protection Area (EPA) Maximum Contaminant Level (MCL) of 10 mg/L. Moreover, samples exceeding 10 mg/L generally were scattered throughout the project area.

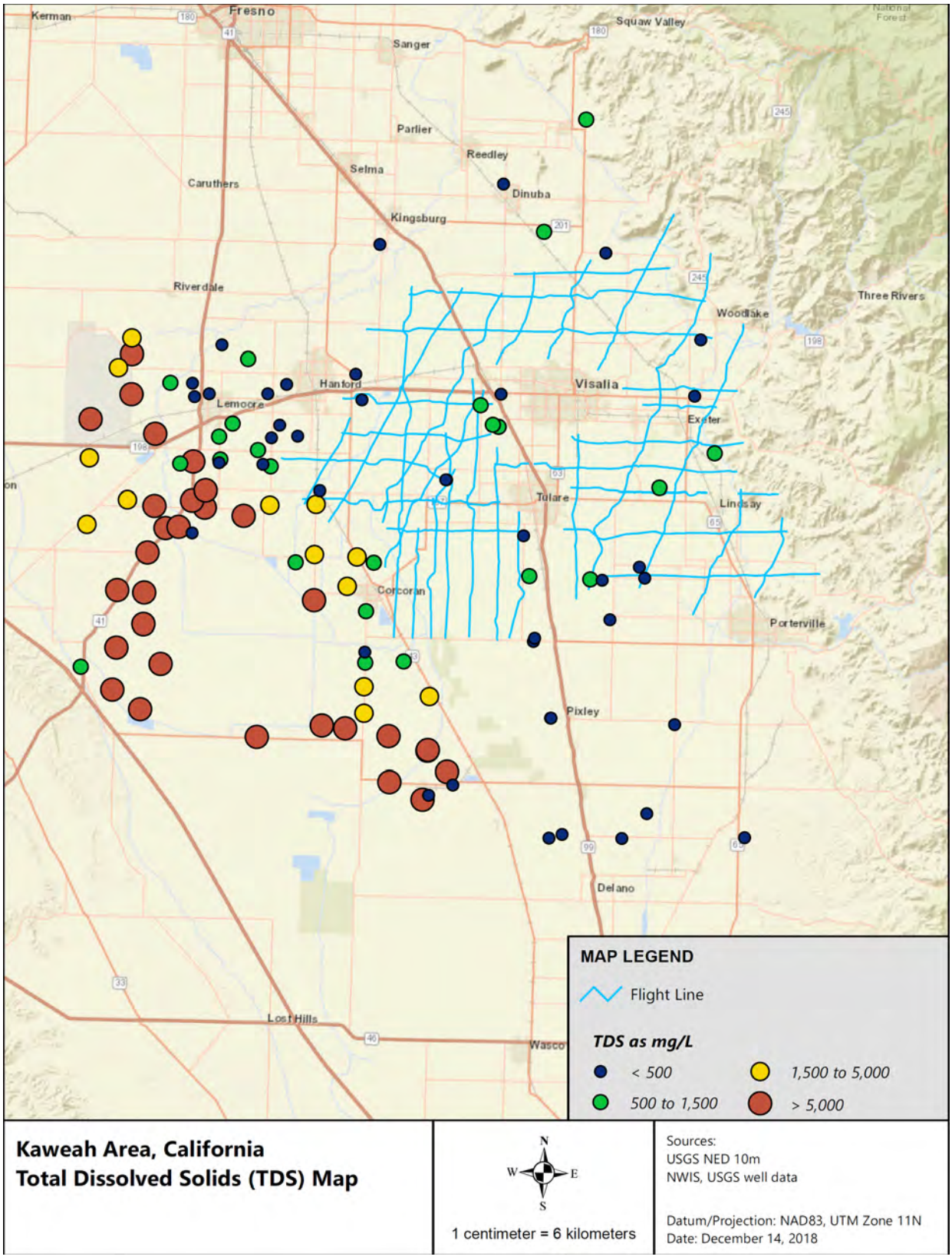

Figure 2-4. Map showing concentrations of total dissolved solids in groundwater samples in Kings and Tulare Counties, California. (USGS, 2018)

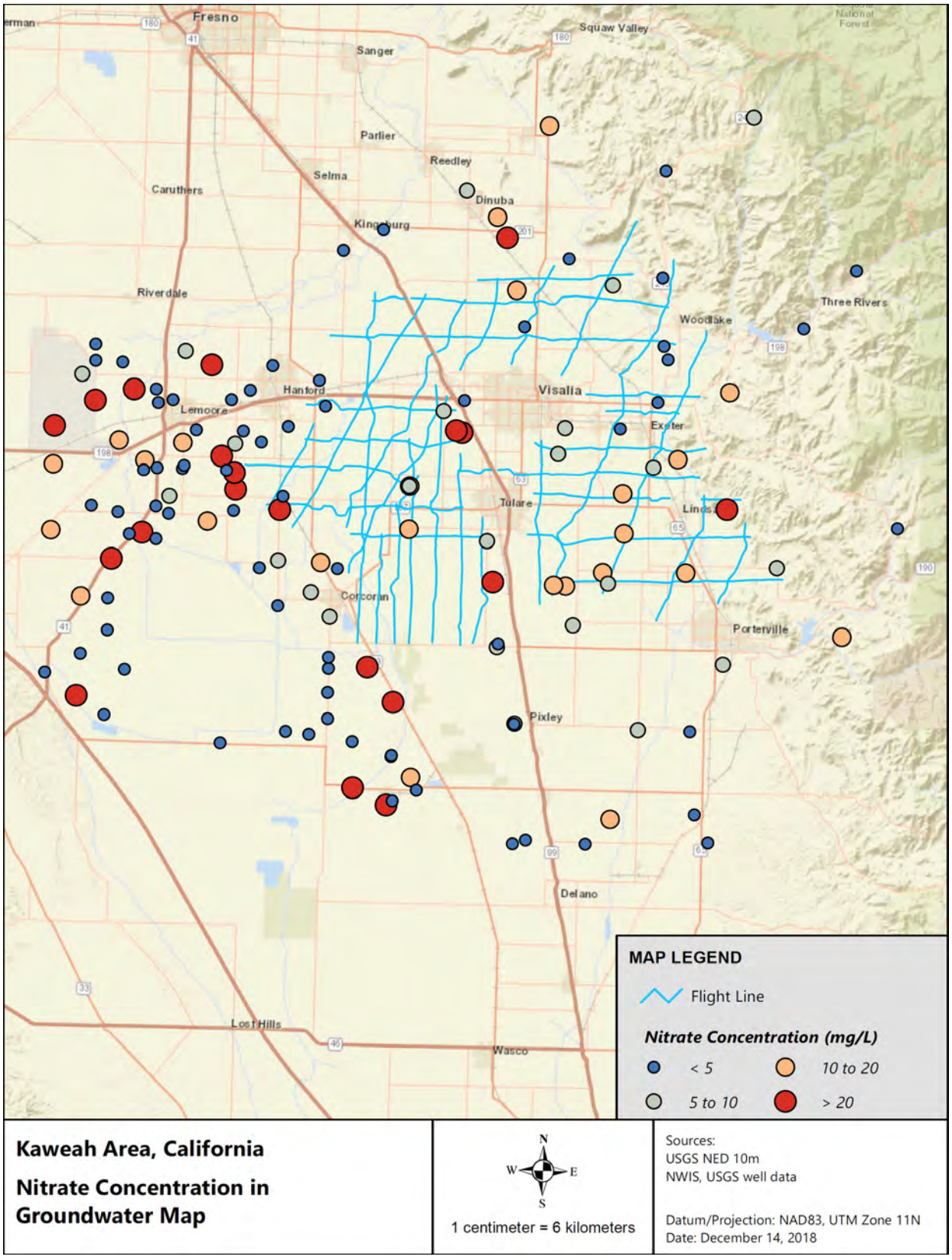

Figure 2-5. Map showing concentrations of nitrate in groundwater samples in Kings and Tulare Counties, California. (USGS, 2018)

3 Additional Background Information

Various sources of background information were used to interpret the AEM data, which is discussed in Section 5.

3.1 Borehole Data

Borehole data for this project consisted of a combination of lithologic and downhole geophysical logs. The borehole information was gathered by GEI Consultants under a separate contract with Stanford University. The borehole logs were first provided on November 2, 2018.

The locations of the boreholes utilized in the Kaweah Subbasin AEM survey analysis are indicated in Figure 3-1. A total of 440 holes contained lithology information and 52 holes contained geophysical information within the Kaweah Subbasin AEM survey area.

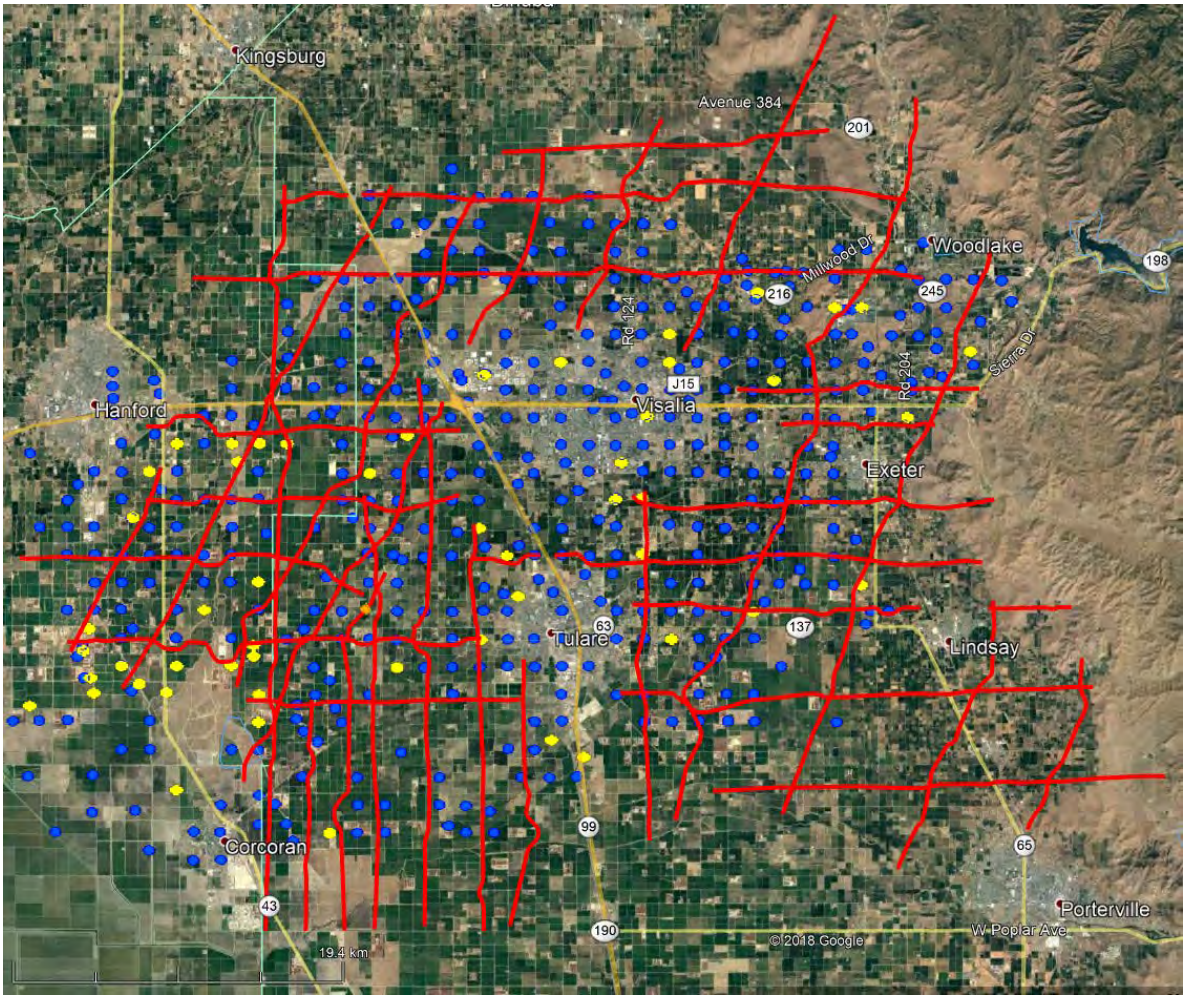

Figure 3-1. Locations of the boreholes near the Kaweah Subbasin AEM survey area. Blue circles represent boreholes with lithology information and yellow circles are borehole locations with geophysical information. AEM flight lines are in red.

Part of the AEM inversion analysis is also an analysis of the borehole logs. As noted in Section 3 there were 440 lithological logs made available. Of these, the mean bottom depth of the lithology logs was 110 m (361 ft) with a standard deviation of 89 m (292 ft) and maximum bottom depth of 738 m (2,420 ft). Of the 52 resistivity logs made available, the average bottom of borehole depth of the resistivity logs was 337 m (1,106 ft) with a standard deviation of 352 m (1,155 ft) and a maximum bottom depth was 1,634 m (6,226 ft), much deeper than the AEM is imaging. There is discussion coming below on the comparison of the borehole resistivity logs and the AEM inversion results in Section 5.3.

Since, typically, resistivity logs are of various vintages and acquired by various staff with differing equipment, a critical examination of the absolute values of the resistivity needs to include an awareness of errors in calibration and in the proper operation of the equipment. There is a long-standing issue with using geophysical logs as ground truths when comparing to AEM inversions that are well calibrated using modern techniques. Throughout much of the geophysical logging world at the time it was acquired, the relative deflections of the resistivity measurements were all that was required or expected from a geophysical log. Operators were seldom trained in the proper operation of a calibrated sonde or in the ability to recognize high contact resistance of a cable head. This has led to many geophysical logs that are potentially uncalibrated. Note that these logs still have scientific merit in their ability to relatively indicate an increase or a decrease in the formation resistivity. The logs used herein are for qualitative comparison to the AEM because detailed calibration and corrections would need to be carried out for the resistivity values in some of the logs to be directly used as numerical constraints in the inversion of the AEM data (Ley-Cooper and Davis, 2010).

4 Geophysical Methodology, Acquisition and Processing

4.1 Geophysical Methodology

Airborne Transient Electromagnetic (TEM) or airborne Time-Domain Electromagnetic (TDEM), or generally AEM, investigations provide characterization of electrical properties of earth materials from the land surface downward using electromagnetic induction. Figure 4-1 gives a conceptual illustration of the airborne TEM method.

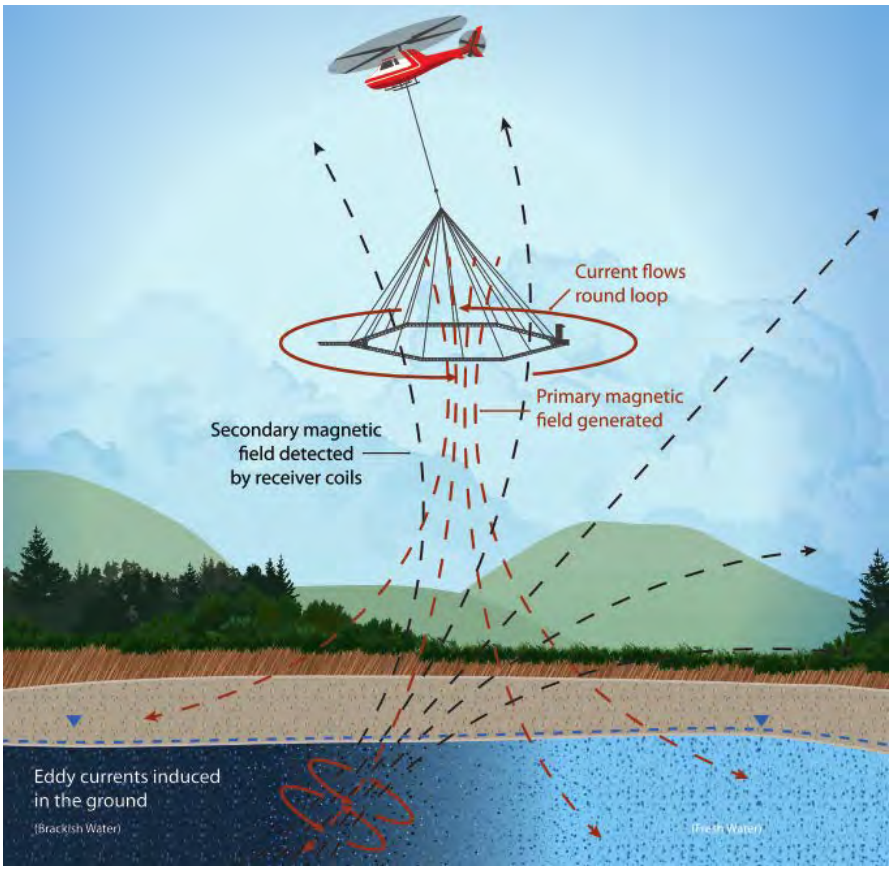

Figure 4-1: Schematic of an airborne electromagnetic survey, modified from Carney et al. (2015).

To collect TEM data, an electrical current is sent through a large loop of wire consisting of multiple turns which generates an electromagnetic (EM) field. This is called the transmitter (Tx) coil. After the EM field produced by the Tx coil is stable, it is switched off as abruptly as possible. The EM field dissipates and decays with time, traveling deeper and spreading wider into the subsurface. The rate of dissipation is dependent on the electrical properties of the subsurface (controlled by the material composition of the geology including the amount of mineralogical clay, the water content, the presence of dissolved solids, the metallic mineralization, and the percentage of void space). At the moment of turnoff, a secondary EM field, which also begins to decay, is generated within the subsurface. The decaying secondary EM field generates a current in a receiver (Rx) coil, per Ampere's Law. This current is measured at several different moments in time (each moment being within a time band called a "gate"). From the induced current, the time rate of decay of the magnetic field, B, is determined (dB/dt). When compiled in time,

these measurements constitute a “sounding” at that location. Each TEM measurement produces an EM sounding at one point on the surface.

The sounding curves are numerically inverted to produce a model of subsurface resistivity as a function of depth. Inversion relates the measured geophysical data to probable physical earth properties. Figure 4-2 shows an example of a dual-moment TEM dB/dt sounding curve and the corresponding inverted electrical resistivity model.

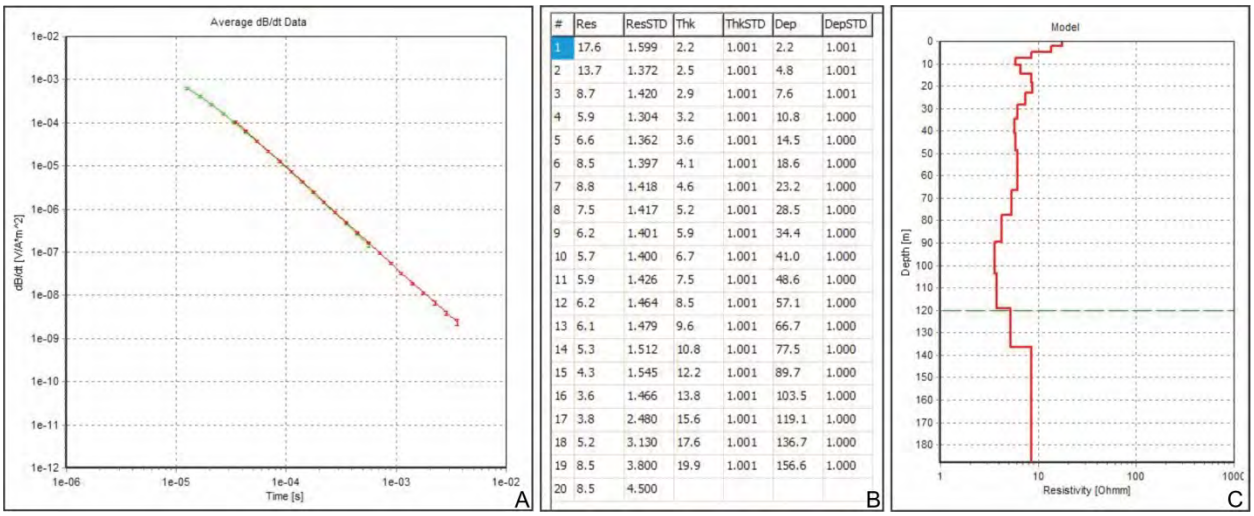

Figure 4-2: A) Example of a dB/dt sounding curve. B) Corresponding inverted model values. C) Corresponding resistivity earth model.

4.2 Flight Planning/Utility Mapping

The primary source of noise in geophysical electromagnetic surveys are other electromagnetic devices that are part of typical municipal utility infrastructure. These include, for example, power lines, railroads, pipelines, and water pumps. Prior to AEM data acquisition in the Kaweah Subbasin, three types of utilities (pipelines, railroads, and power lines) were located.

The locations of the flight lines were converted from a regularly spaced grid to one with flight lines optimized in order to avoid electromagnetic coupling with the previously mentioned utilities. This was done by moving along each flight line in Google Earth to inspect the path for visible power lines, radio towers, railroads, highways and roads, confined feeding operations and buildings, and any other obstructions that needed to be avoided during flight. The paths of the flight lines were also modified so as to fly closer to known borehole locations.

At the conclusion of the design process, the Kaweah Sub-Basin AEM flight lines were arranged into reconnaissance flight lines approximately 44 km in length (27 miles) at their longest and approximately 4 km (2.5 miles) at their shortest. The reconnaissance flight lines were separated by about approximately 4 to 5 km2 or (2.5 to 3 miles). (Figure 1-2 and Figure 4-5).

4.3 AEM Survey Instrumentation

AEM data were acquired using the SkyTEM312 (312) airborne electromagnetic system (SkyTem Airborne Surveys Worldwide, 2018). The 312 is a rigid frame, dual-magnetic moment (Low and High) TEM system. The area of the 312 Tx coil is 342 m^2. A peak current of six (6) amps is passed through two (2) turns of wire in the Tx for Low Moment measurements and a peak current of 110 amps is passed through the twelve (12) turns of wire for High Moment measurements. This results in peak Tx Low and High magnetic moments of ~4,100 Ampere-meter-squared ($A*m^2$) and ~450,000 $A*m^2$, respectively.

The SkyTEM312 system utilizes an offset Rx positioned slightly behind the Tx resulting in a 'null' position which is a location where the intensity of the primary field from the system transmitter is minimized. This is desirable as to minimize the amplitude of the primary field at the Rx to maximize the sensitivity of the Rx to the secondary fields. The 312 multi-turn Rx vertical (Z) coil has an effective area of 105 m^2. In addition to the Tx and Rx that constitute the TEM instrument, the 312 is also equipped with a Total Field magnetometer (MAG) and data acquisition systems for both instruments. The 312 also includes two each of laser altimeters, inclinometers/tilt meters, and differential global positioning system (DGPS) receivers. Positional data from the frame mounted DGPS receivers are recorded by the AEM data acquisition system. The magnetometer includes a third DGPS receiver whose positional data is recorded by the magnetometer data acquisition system. Figure 4-3 gives a simple illustration of the 312 frame and instrument locations. The image is viewed along the +z axis looking at the horizontal x-y plane. The axes for the image are labeled with distance in meters. The magnetometer is located on a boom off the front of the frame (right side of image). The Tx coil is located around the octagonal frame and the Rx Coil is located at the back of the frame (left side of image).

The coordinate system used by the 312 defines the +x direction as the direction of flight, the +y direction is defined 90 degrees to the right and the +z direction is downward. The center of the transmitter loop, mounted to the octagonal SkyTEM frame is used as the origin in reference to instrumentation positions. Table 4-1 lists the positions of the instruments and Table 4-2 lists the corners of the transmitter loop.

The DGPS and magnetometer mounted on the frame of the 312 require the use of base stations, which are located on the ground and are positioned in an area with low cultural noise. In this case these instruments were located at the Mefford Field Airport, south of Tulare, California. Data from the magnetometer and DGPS base stations were downloaded each day after the end of the day's AEM flights. The DGPS and magnetometer base stations were placed at the Universal Transverse Mercator (UTM) coordinate system Zone 10 North (Table 4-3). The horizontal geodetic reference used is North American Datum of 1983 (NAD83 in meters). All elevations are from USGS's National Elevation Dataset, referenced to the North American Vertical Datum of 1988; with meters as the unit of measurement.

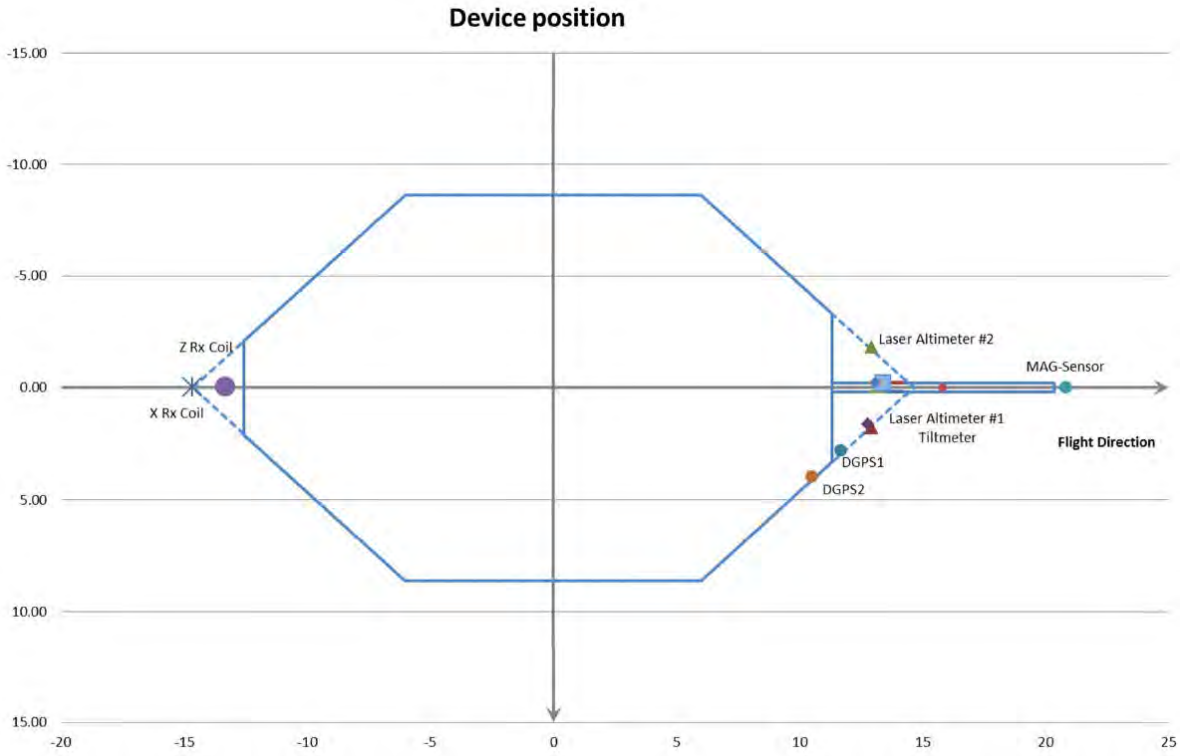

Figure 4-3: SkyTEM304M/312 frame, including instrumentation locations and X and Y axes. Distances are in meters. Instrumentation locations listed in Table 4-1.

Figure 4-4: Photos of the SkyTEM312 system in suspension beneath the helicopter.

For this project, the 312 was flown at an average speed of 55 mi/hr (89.0 kilometers/hr) at an average flight height of 39.6 m (130 ft) above the land surface, using the sling-load cargo system of a Eurocopter AS350 helicopter. Figure 4-4 displays a couple of images of the 312 in operation.

Table 4-1: Positions of instruments on the SkyTEM312 frame, using the center of the frame as the origin, in meters.

	DGPS 1	DGPS 2	Inclinometer 1	Inclinometer 2	Altimeter 1	Altimeter 2	Magnetic Sensor	Rx Coil
X	11.68	10.51	12.79	12.79	12.94	12.94	20.50	-13.25
Y	2.79	3.95	1.64	1.64	1.79	-1.79	0.00	0.00
Z	-0.16	-0.16	-0.12	-0.12	-0.12	-0.12	-.56	-2.00

Table 4-2: Positions of corners of the SkyTEM312 transmitter coil, using the center of the frame as the origin, in meters.

Tx Corners	1	2	3	4	5	6	7	8
X	-12.55	-6.03	6.03	11.34	11.34	6.03	-6.03	-12.55
Y	-2.10	-8.63	-8.63	-3.31	3.31	8.63	8.63	2.10

Table 4-3: Location of DGPS and magnetic field base station instruments at the Mefford Airport.

Instrument	Easting (m)	Northing (m)	UTM Zone
Magnetometer Base Station	290424	4003813	11 N
DGPS Base Station	290424	4003813	11 N

4.4 Data Acquisition

All SkyTEM systems are calibrated to a ground test site in Lyngby, Denmark prior to being used for production work (HydroGeophysics Group Aarhus University, 2010; HydroGeophysics Group Aarhus University, 2011; Foged et al., 2013). The calibration process involves acquiring data with the system hovering at different altitudes, from 5 m to 50 m (16 ft to 164 ft), over the Lyngby site. Acquired data are processed and a scale factor (time and amplitude) is applied so that the inversion process produces the model that approximates the known geology at Lyngby.

For these surveys, installation of the navigational instruments in the helicopter and assembly of the SkyTEM312 system commenced at the Mefford Airport. Calibration test flights were flown to ensure that the equipment was operating within technical specifications. Survey set-up procedures included measurement of the transmitter waveforms, verification that the receiver was properly located in a null position, and verification that all positioning instruments were functioning properly. A high-altitude test, used to verify system performance, was flown prior to the beginning of the survey's production flights. In the field, quality control of the operational parameters for the EM and magnetic field sensors including current levels, positioning sensor dropouts, acquisition speed, and system orientation were conducted with proprietary SkyTEM software following each flight.

Approximately 821.1 line-kilometers (506.9 line-miles) were acquired by the SkyTEM312 over the Kaweah Subbasin AEM survey area on November 9 - 12, 2018. The field at the Mefford Airport was used for landing and refueling between production flights. A data acquisition map is presented in Figure 4-5 with the flight lines grouped by acquisition date and Table 4-4 lists the acquisition dates, flights, and amount acquired on each day.

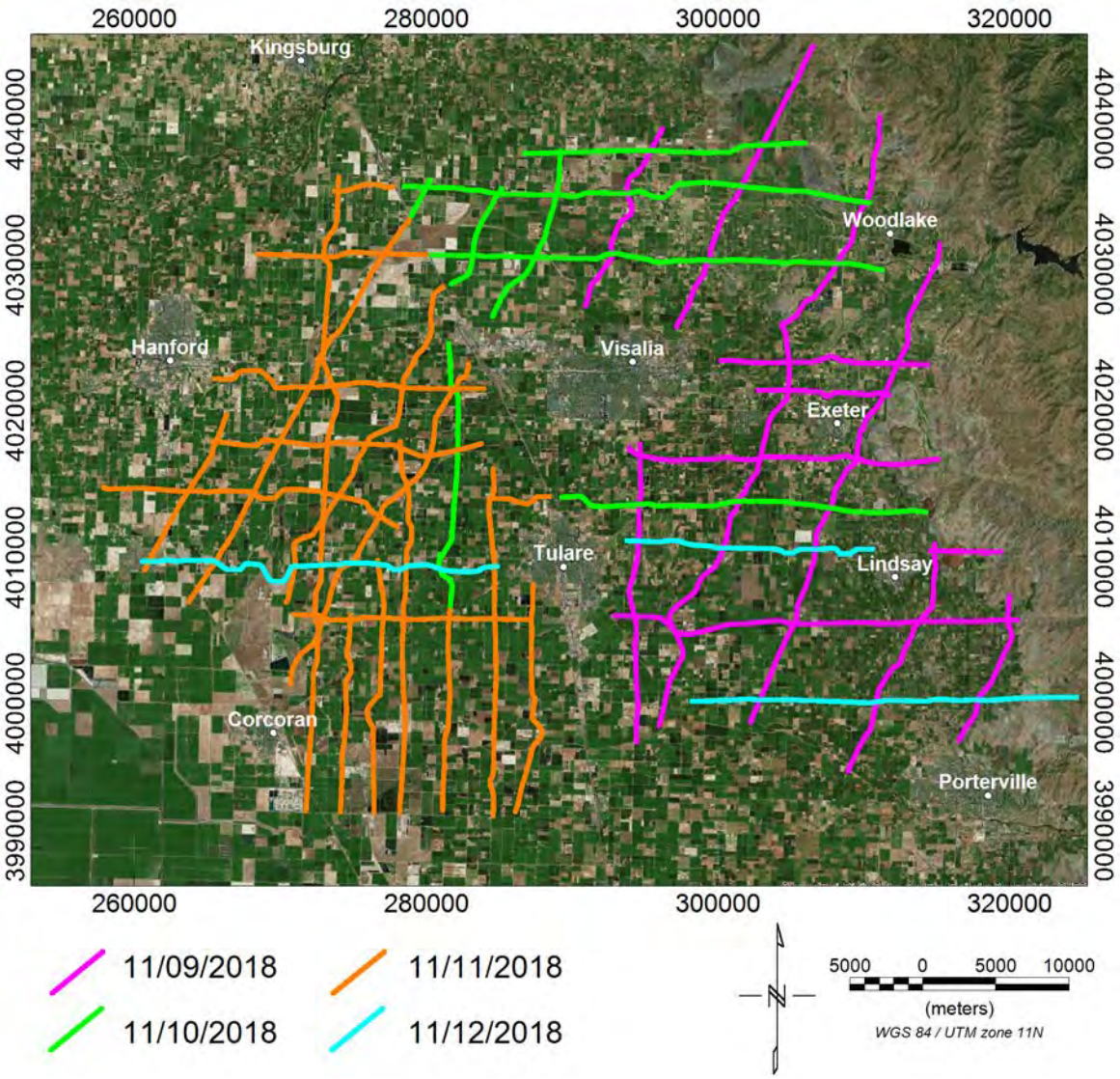

Figure 4-5: Kaweah Subbasin AEM flight lines grouped by acquisition date.

Table 4-4. Kaweah Subbasin AEM flight line production by flight.

Date	Flight	Distance (km)
09-November-18	1109FL1	163.7
09-November-18	1109FL2	83.4
10-November-18	1110FL1	152.3
11-November-18	1111FL2	179.5
11-November-18	1111FL1	166.5
12-November-18	1112FL1	75.7
Total	**6**	**821.1**

4.4.1 System Flight Parameters

4.4.1.1 Flight Height

The system height was specified at 30-35 meters AGL; however, due to safety and other judgments by the pilot the flight heights will deviate. The goal is to maintain a height as low as possible in the window from 25 to 50 m AGL. In the Kaweah Subbasin AEM data set the average height was 39.6 m AGL with a minimum of 18.3 m AGL and a maximum of 120.0 m AGL. The maximum flight heights were encountered over large powerlines. Those data contaminated by the power lines will be removed from the dataset before inversion due to EM coupling and will not impact the final product. A map of the flight height throughout the survey area is presented in Figure 4-6.

4.4.1.2 Flight Speed

Speed determines the distance between ground samples. However, there is a tradeoff between the cost of the survey and the speed of the system related to the foot print of the system. In many surveys, the specified speed is 100 km/hr. The critical factor in the flight speed is to maintain a speed where the system is as level as possible. This may require that the pilot speed up in the downwind direction or slowdown in the up-wind direction. The pilot uses the readout display of the system tilt angles to help maintain this speed. A map of the flight speeds of the Kaweah Subbasin AEM survey is presented in Figure 4-7. The average ground speed of the survey was 89.0 km/hr with a minimum ground speed of 0.4 km/hr and a maximum ground speed of 117.9 km/hr.

4.4.1.3 System Angles

System angles are critical to ensure that quality data are submitted to the inversion. The system's Tx initial current at time-off of 0.0 sec is the image of the size of the loop on the surface. If the system is tilted, that image will be less than the original size of the TX. Inversion algorithms can account for ±10 degrees of angle in calculating the effective Tx size. To this end, it is important to keep the Tx frame within ±10 degrees. The position of the Rx is also impacted by the angle of the system and any deviation from perpendicular has an impact by including off perpendicular components. As noted, algorithms can account for ±10 degrees in the Rx angle. Both the X-Angle (in the direction of flight) and the Y-Angle (perpendicular to the direction of flight) were checked during the Kaweah Subbasin AEM survey. When the system is flown over obstacles or while turning around at the end of a line, the angles can be higher

than the ±10 degrees. These flight line edges are typically cut out of the survey data set prior to inversion. Figure 4-8 and Figure 4-9 are plots of the X-angle and the Y-angle tilts, respectively. During the Kaweah Subbasin AEM survey, both angles were within acceptable ranges. The X-angle averaged approximately -0.9 degrees with a minimum of -20.3 degrees and a maximum of 25.90 degrees. The Y-angle tilt averaged about -0.1 degrees with a minimum of –24.7 degrees and a maximum of 25.6 degrees. Maximum and minimum tilts occurred around infrastructure and will not impact the data as much of that area will be removed during the decoupling processing

4.4.1.4 Transmitter Current

The SkyTEM system utilizes a dual-moment system (High (HM) and Low (LM)) and two different Tx currents and waveforms. These waveforms are recorded before and after the survey to ensure that no changes have occurred during the survey. Figure 4-10 and Figure 4-11 are plots of the recorded low moment (LM) and the high moment (HM) Tx waveforms for the SkyTEM312 system, respectively. The LM Tx source is used to highlight the very near surface geology and the HM current source is used to get more electromagnetic power at depth to characterize the deeper geologic units

The current should be stable throughout the survey, but changes in the temperature can impact the resistance of the Tx wire and circuit by either increasing or lowering the peak current output. The peak current is recorded during acquisition of each sounding and is used to adjust the Tx waveform in the inversion. For the Kaweah Subbasin AEM survey with the 312 system, the LM mean current was 5.95 amp with a minimum current of 5.94 amp and a maximum current of 5.96 amp. For the 312 HM, the mean current was 111.3 amp with a minimum current of 107.3 amp and a maximum current of 114.7 amp. All system moments show stability in the current and provided no problems in the inversions.

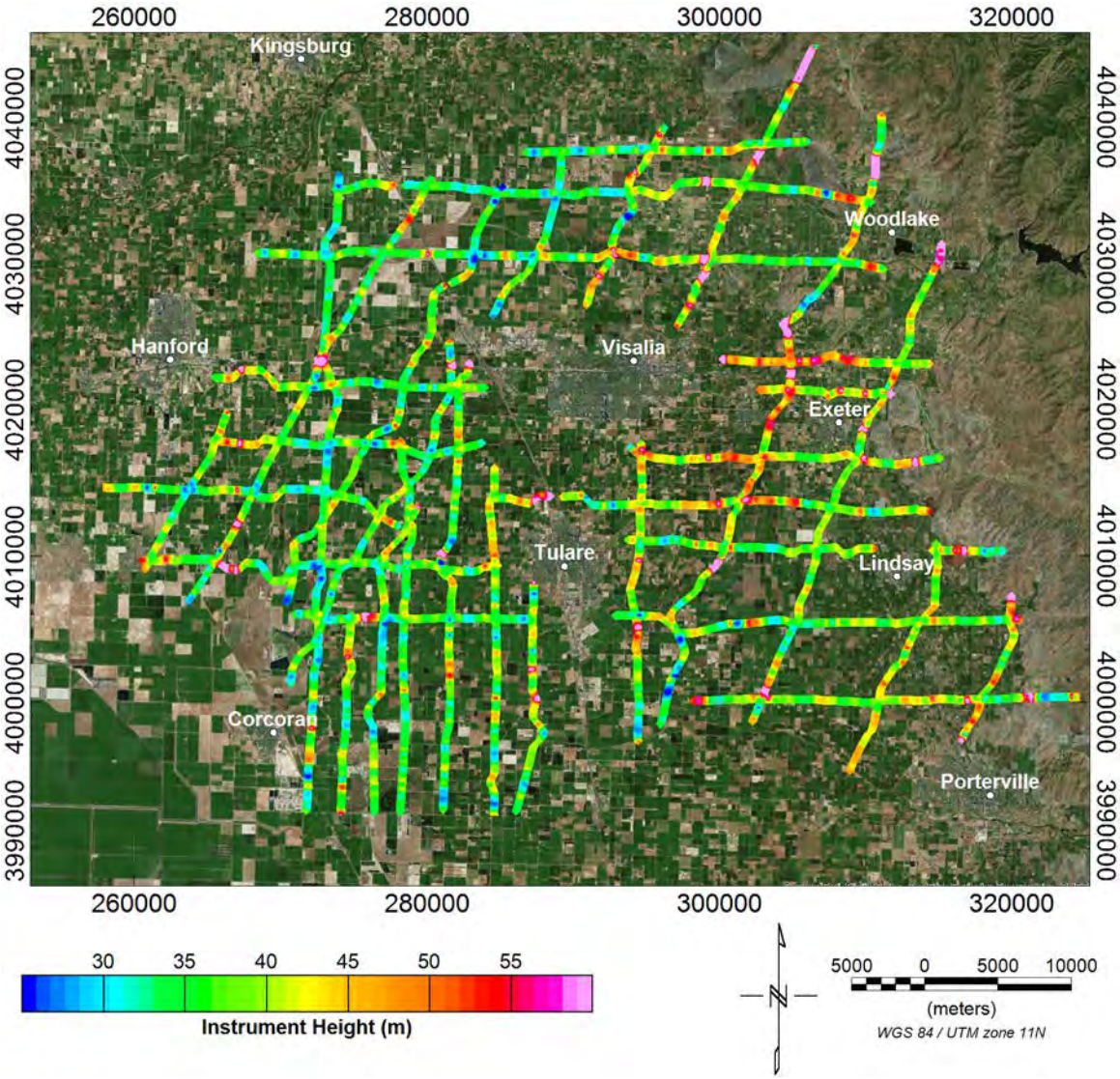

Figure 4-6. Map of the system height recorded during the Kaweah Subbasin AEM survey.

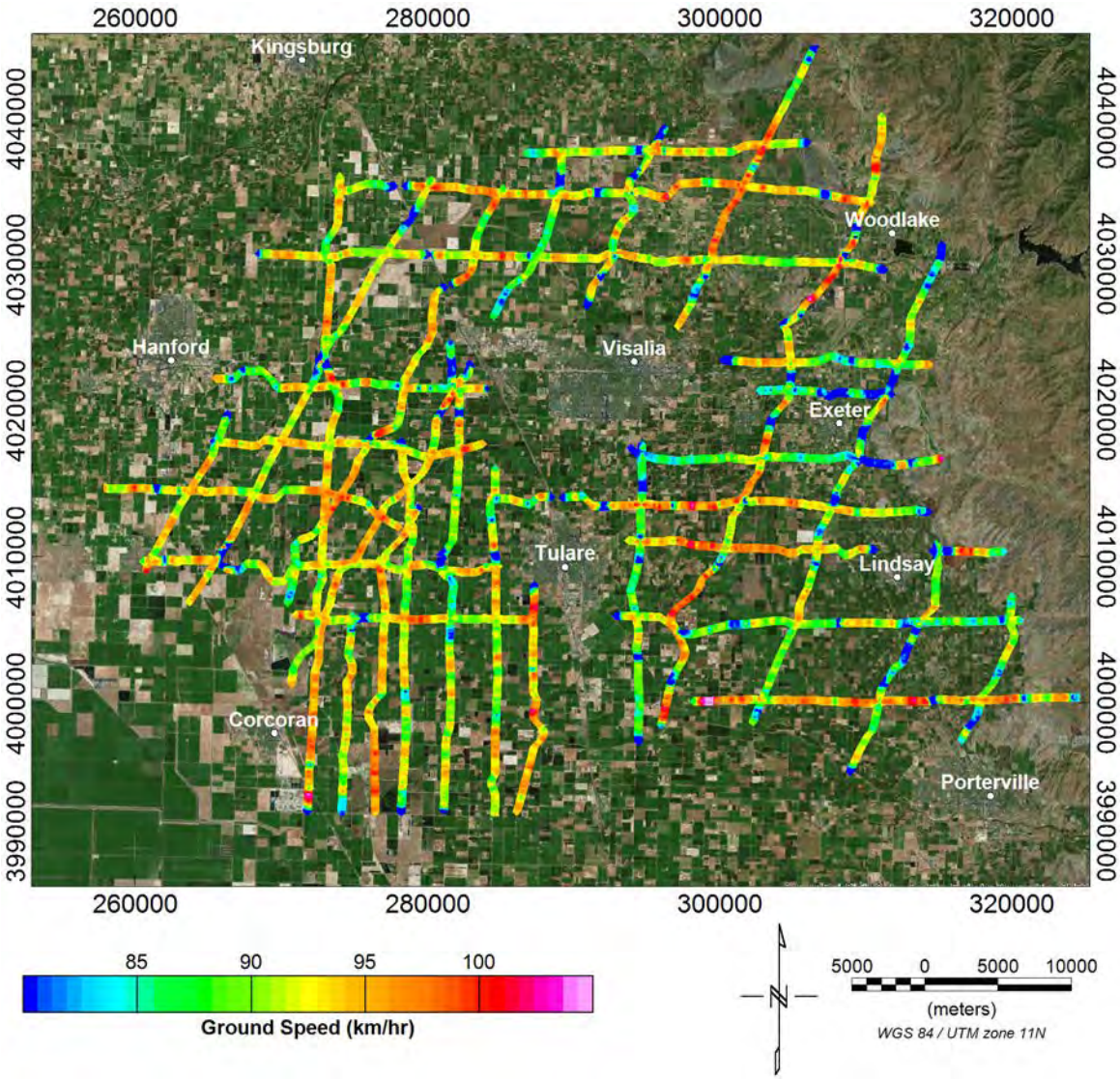

Figure 4-7. Map of the ground speed recorded during the Kaweah Subbasin AEM survey.

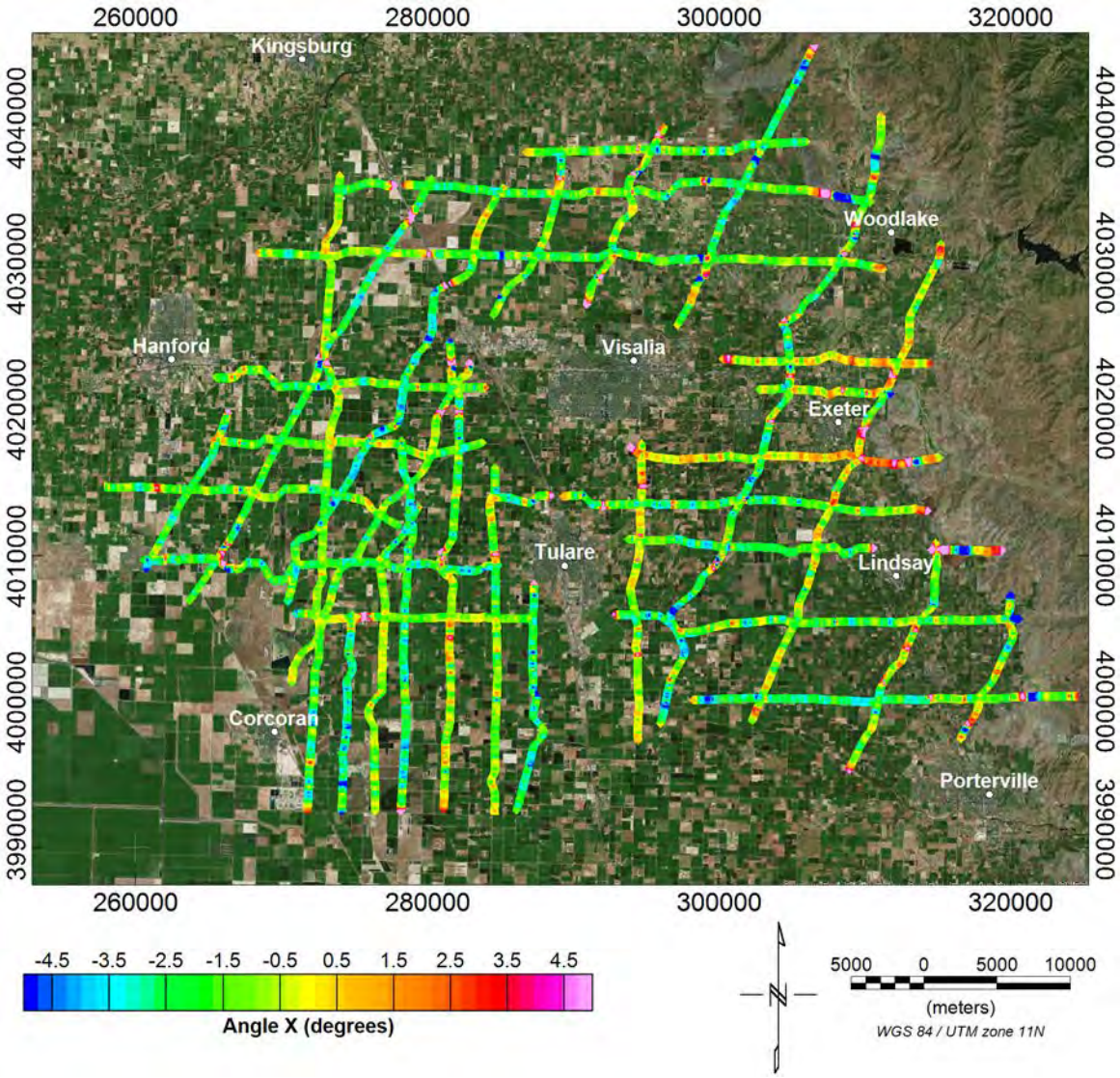

Figure 4-8. Map of the X-angle tilt recorded during the Kaweah Subbasin AEM survey.

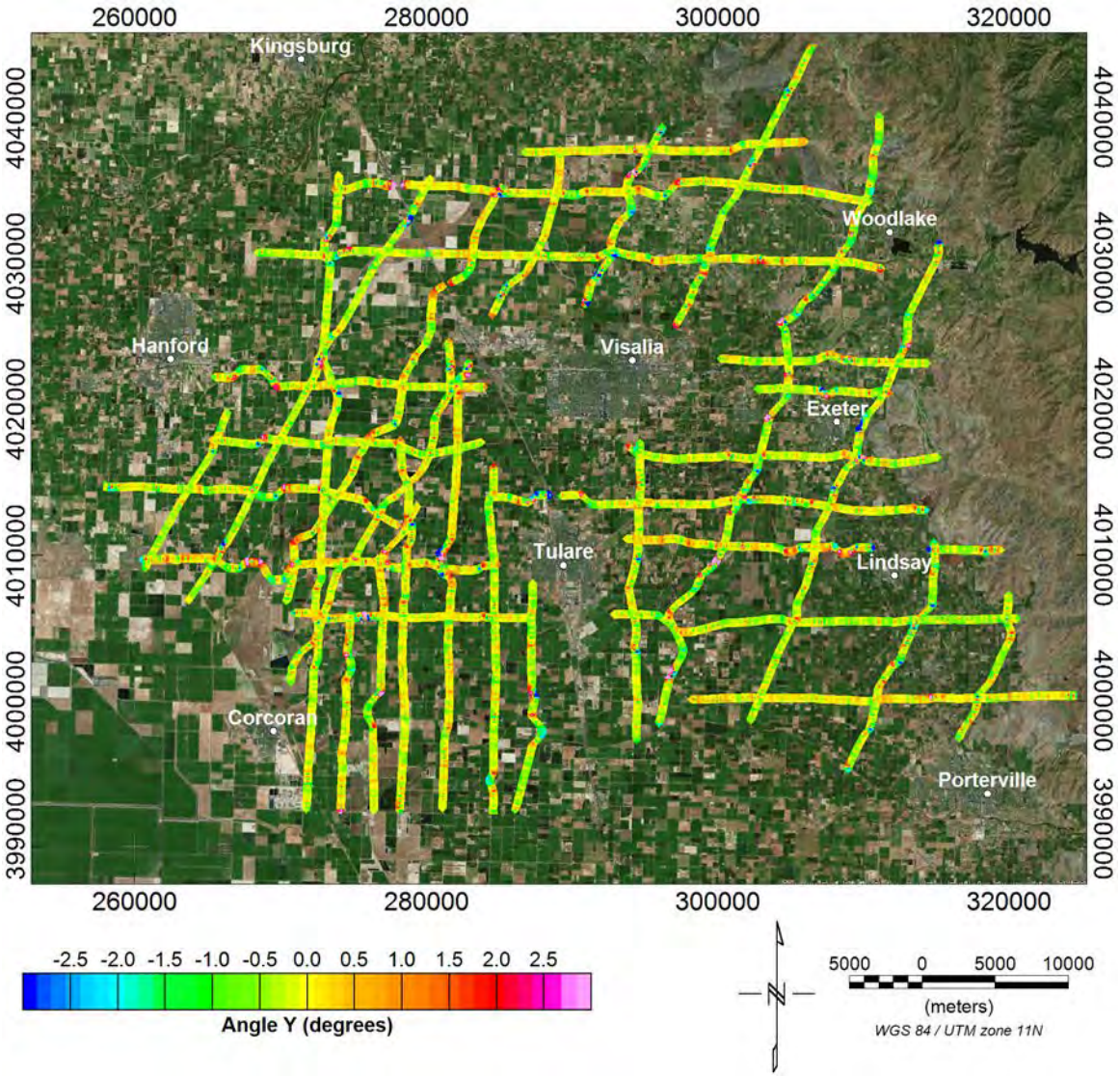

Figure 4-9. Map of the Y-angle tilt recorded during the Kaweah Subbasin AEM survey.

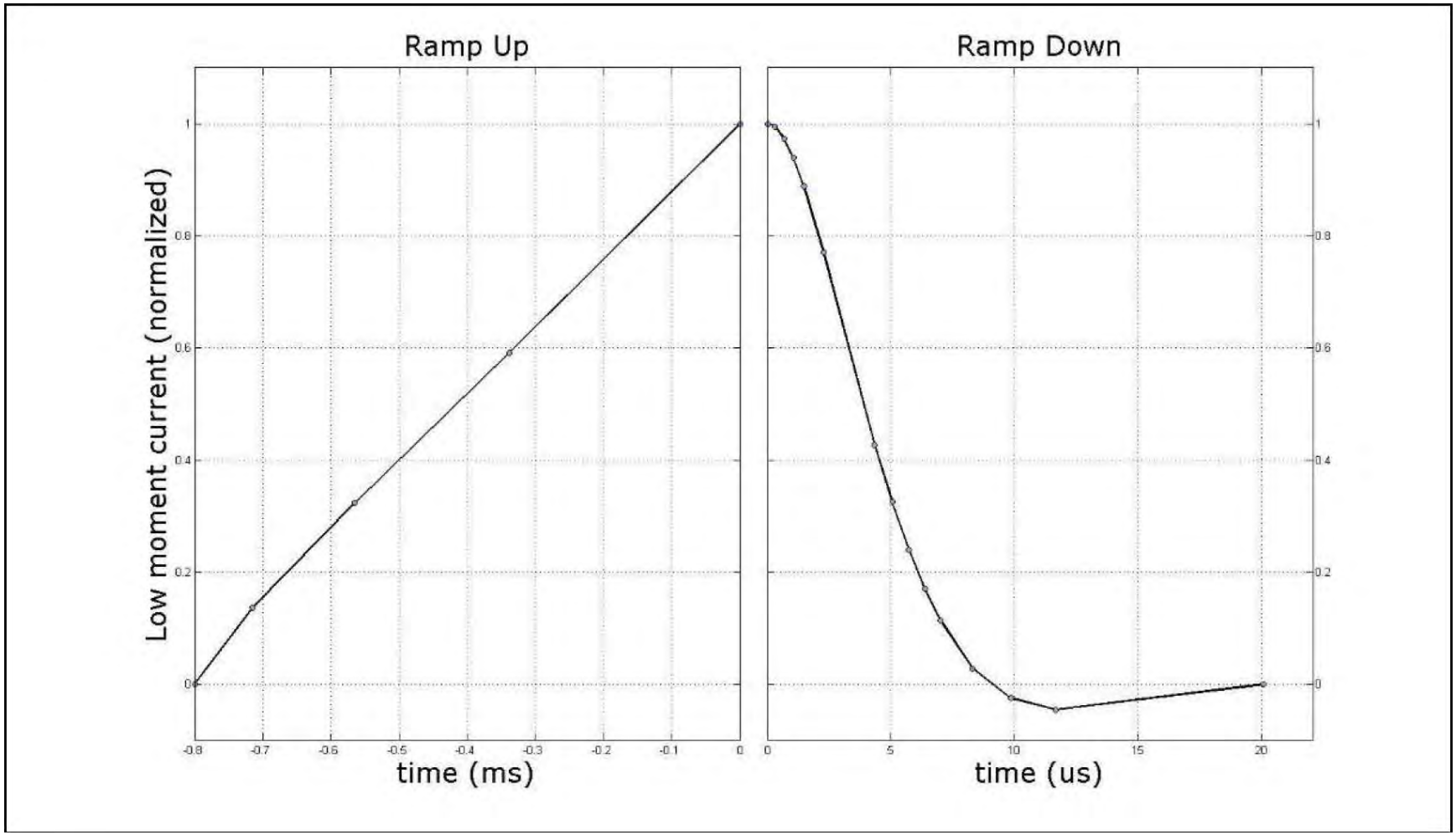

Figure 4-10. Plot of the 210 Hz LM waveform for the SkyTEM312 system recorded during the Kaweah Subbasin AEM survey. Current ramp up is on the left and the ramp down to turn off is on the right. The current is normalized. Note the different x-axis scales between the left and right sides of the figure.

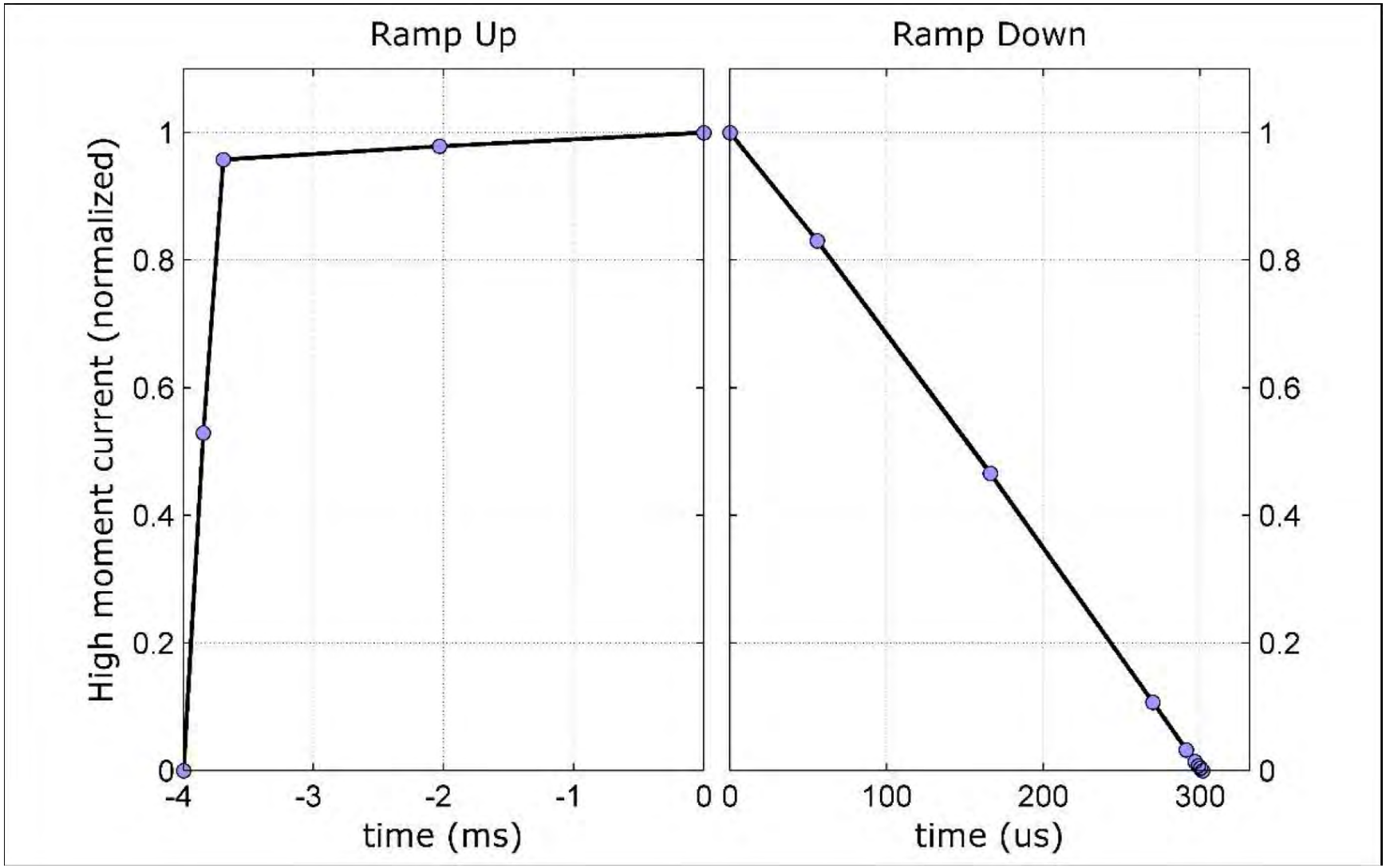

Figure 4-11. Plot of the 30 Hz HM waveform for the SkyTEM312 system recorded during the Kaweah Subbasin AEM survey. Current ramp up is on the left and the ramp down to turn off is on the right. The current is normalized. Note the different x-axis scales between the left and right sides of the figure.

4.4.2 Primary Field Compensation

A standard SkyTEM data acquisition procedure involves review of acquired raw data by SkyTEM in Denmark for Primary Field Compensation (PFC) prior to continued data processing by AGF (Schamper et al., 2014). The primary field of the transmitter affects the recorded early time gates, which in the case of the Low Moment, are helpful in resolving the near surface resistivity structure of the ground. The Low Moment uses a saw tooth waveform which is calculated and then used in the PFC correction to correct the early time gates.

4.4.3 Automatic Processing

The AEM data collected by the 312 were processed using Aarhus Workbench version 5.8.3 (at Aarhus Geosoftware (https://www.aarhusgeosoftware.dk/workbench-overview)) described in HydroGeophysics Group, Aarhus University (2011).

Automatic processing algorithms provided within the Workbench program are initially applied to the AEM data. DGPS locations were filtered using a stepwise, second-order polynomial filter of nine seconds with a beat time of 0.5 seconds, based on flight acquisition parameters. The AEM data are corrected for tilt deviations from level and so filters were also applied to both of the tilt meter readings with a median filter of three seconds and an average filter of two seconds. The altitude data were corrected using a series of two polynomial filters. The lengths of both eighth-order polynomial filters were set to 15 seconds with shift lengths of six (6) seconds. The lower and upper thresholds were 1 and 100 meters, respectively.

Trapezoidal spatial averaging filters were next applied to the AEM data. The times used to define the trapezoidal filters for the Low Moment were $1.0x10^{-5}$ sec, $1.0x10^{-4}$ sec, and $1.0x10^{-3}$ sec with widths of 4, 7, and 18 seconds. The times used to define the trapezoid for the High Moment were $1.0x10^{-4}$ sec, $1.0x10^{-3}$ sec, and $1.0x10^{-2}$ sec with widths of 10, 20, and 36 seconds. The trapezoid sounding distance was set to 1.0 seconds and the left/right setting, which requires the trapezoid to be complete on both sides, was turned on. The spike factor and minimum number of gates were both set to 25 percent for both soundings. Lastly, the locations of the averaged soundings were synchronized between the two moments.

4.4.4 Manual Processing and Laterally-Constrained Inversions

After the implementation of the automatic filtering, the AEM data were manually examined using a sliding two-minute time window. The data were examined for possible electromagnetic coupling with surface and buried utilities and metal, as well as for late time-gate noise. Data affected by these were removed. Examples of locating areas of EM coupling with pipelines or power lines and recognizing and removing coupled AEM data in Aarhus Workbench are shown in Figure 4-12 and Figure 4-13, respectively. Examples of two inversions, one without EM coupling and the other with EM coupling, are shown in Figure 4-14. Areas were also cut out where the system height was flown greater than 60 m (200 feet) above the ground surface which caused a decrease in the signal level.

The AEM data were then inverted using a Laterally-Constrained Inversion (LCI) algorithm (HydroGeophysics Group Aarhus University, 2011). The profile and depth slices were examined, and any remaining electromagnetic couplings were masked out of the data set.

After final processing, 626.2 line-km (386.5 line-miles) of 312 data were retained for the final inversions for the Kaweah Subbasin AEM survey area. This amounts to a data retention of 76.3% for the 312 data set. These high rates are the result of careful flight line planning and design.

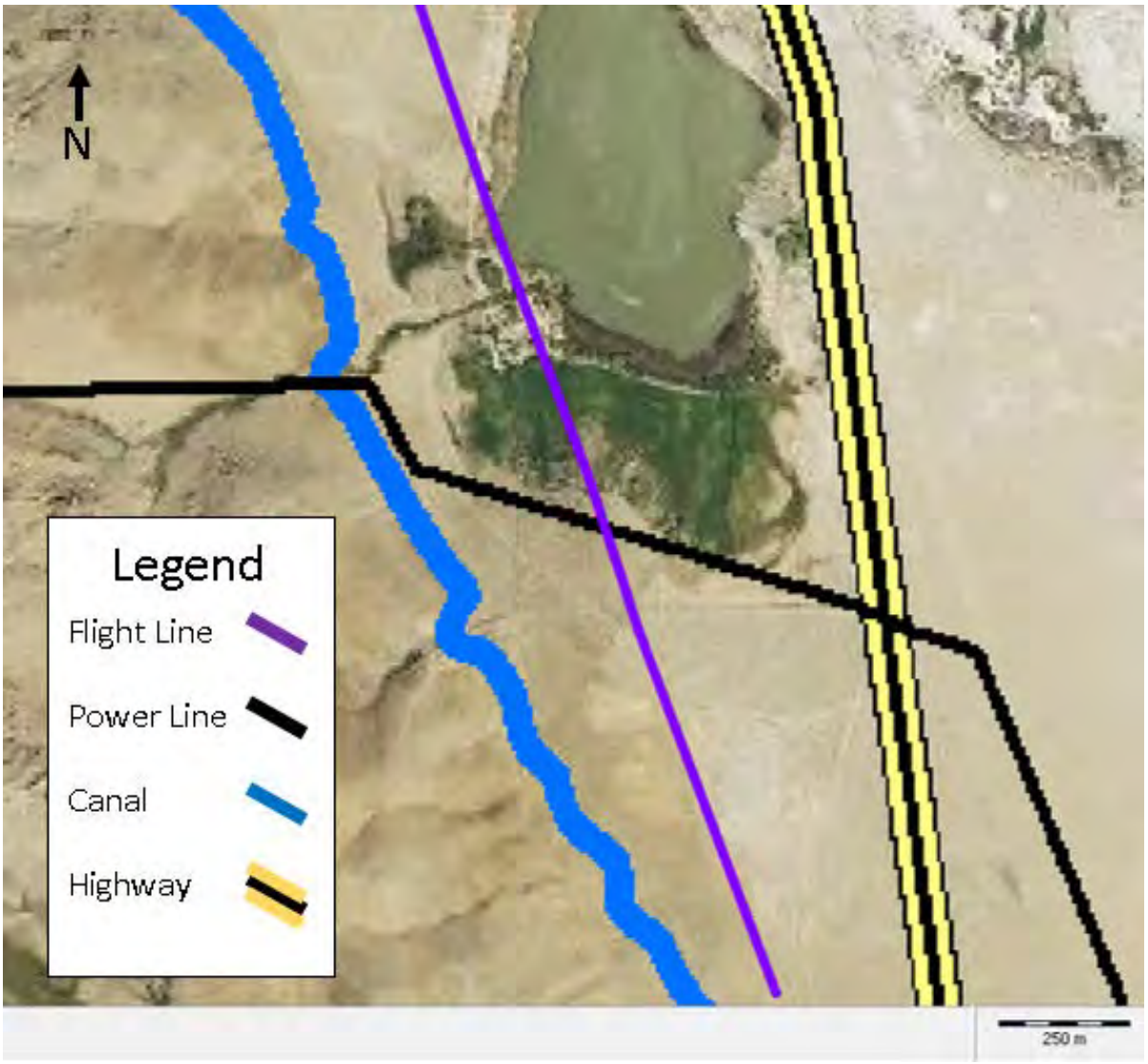

Figure 4-12. Example locations of electromagnetic coupling with pipelines or power lines.

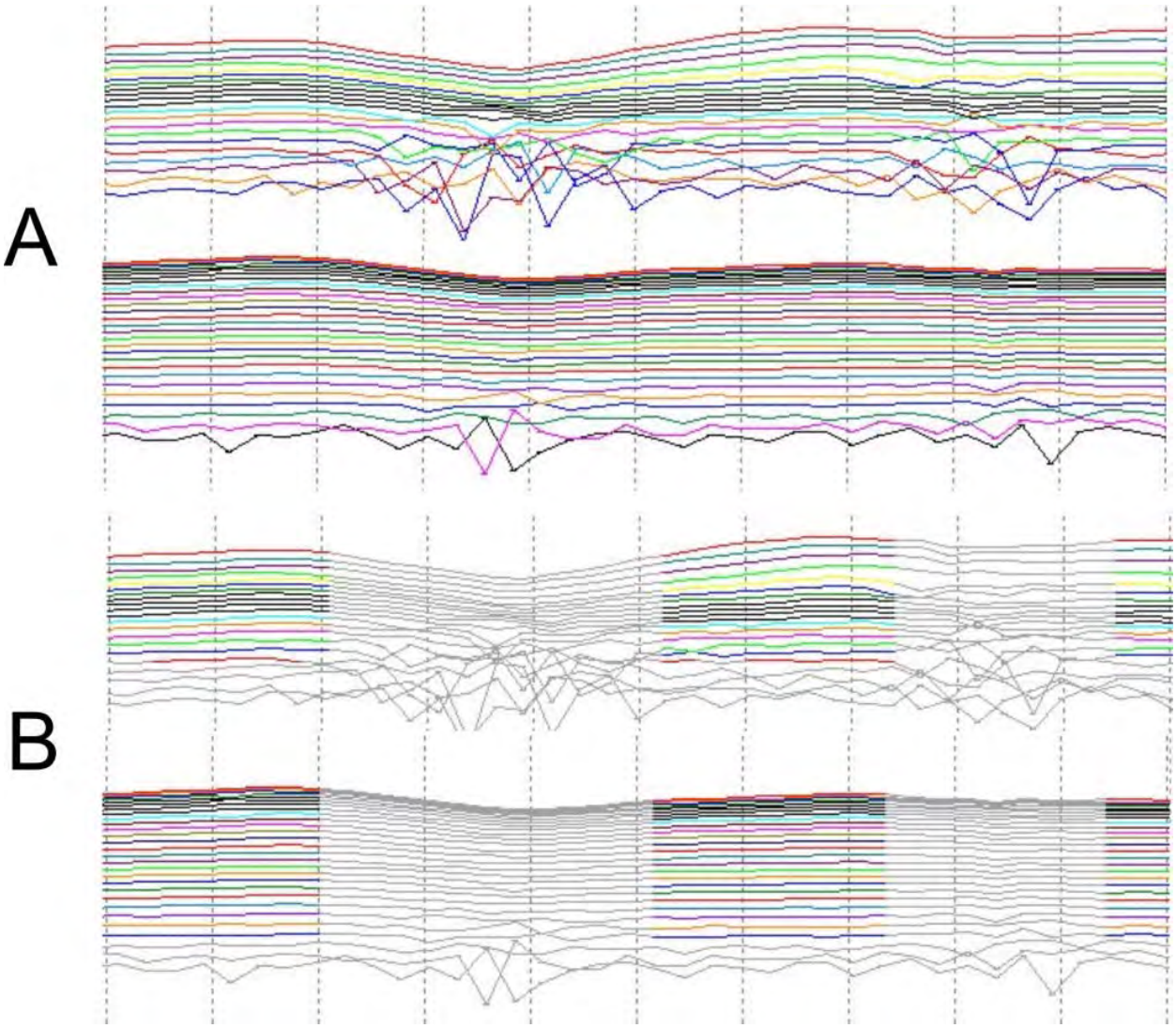

Figure 4-13. A) Example of AEM data affected by electromagnetic coupling in the Aarhus Workbench editor. The top group of lines is the unedited data with the Low Moment on top and the High Moment on the bottom. The bottom group shows the same data after editing.

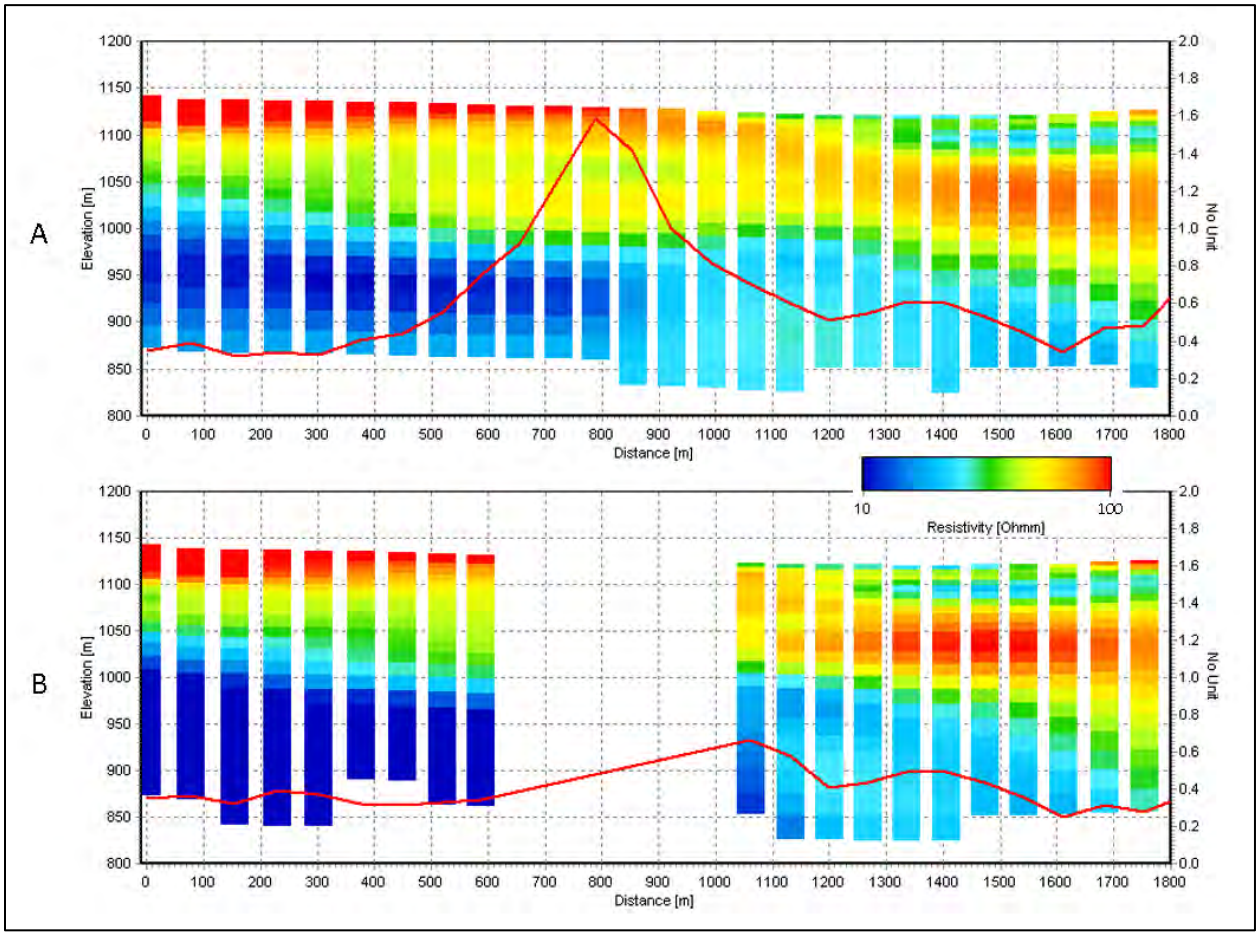

Figure 4-14. A) Example of Laterally-Constrained inversion results where AEM data affected by coupling with pipelines and power lines were not removed. B) Inversion results where AEM data affected by coupling were removed.

4.4.5 Power Line Noise Intensity (PLNI)

The Power Line Noise Intensity (PLNI) channel assists in identifying possible sources of noise from power lines. Pipelines, unless they are cathodically-protected, are not mapped by the PLNI. The PLNI is produced by performing a spectral frequency content analysis on the raw received Z-component SkyTEM data. For every Low Moment data block, a Fourier Transform (FT) is performed on the latest usable time gate data. The FT is evaluated at the local power line transmission frequency (60 Hz) yielding the amplitude spectral density of the local power line noise. The PLNI data for the Kaweah Subbasin AEM survey are presented in Figure 4-15. The Kaweah Subbasin AEM-flight lines with blue colors representing data retained for inversion and red lines representing 312 data removed due to infrastructure and late time noise are presented in Figure 4-16.

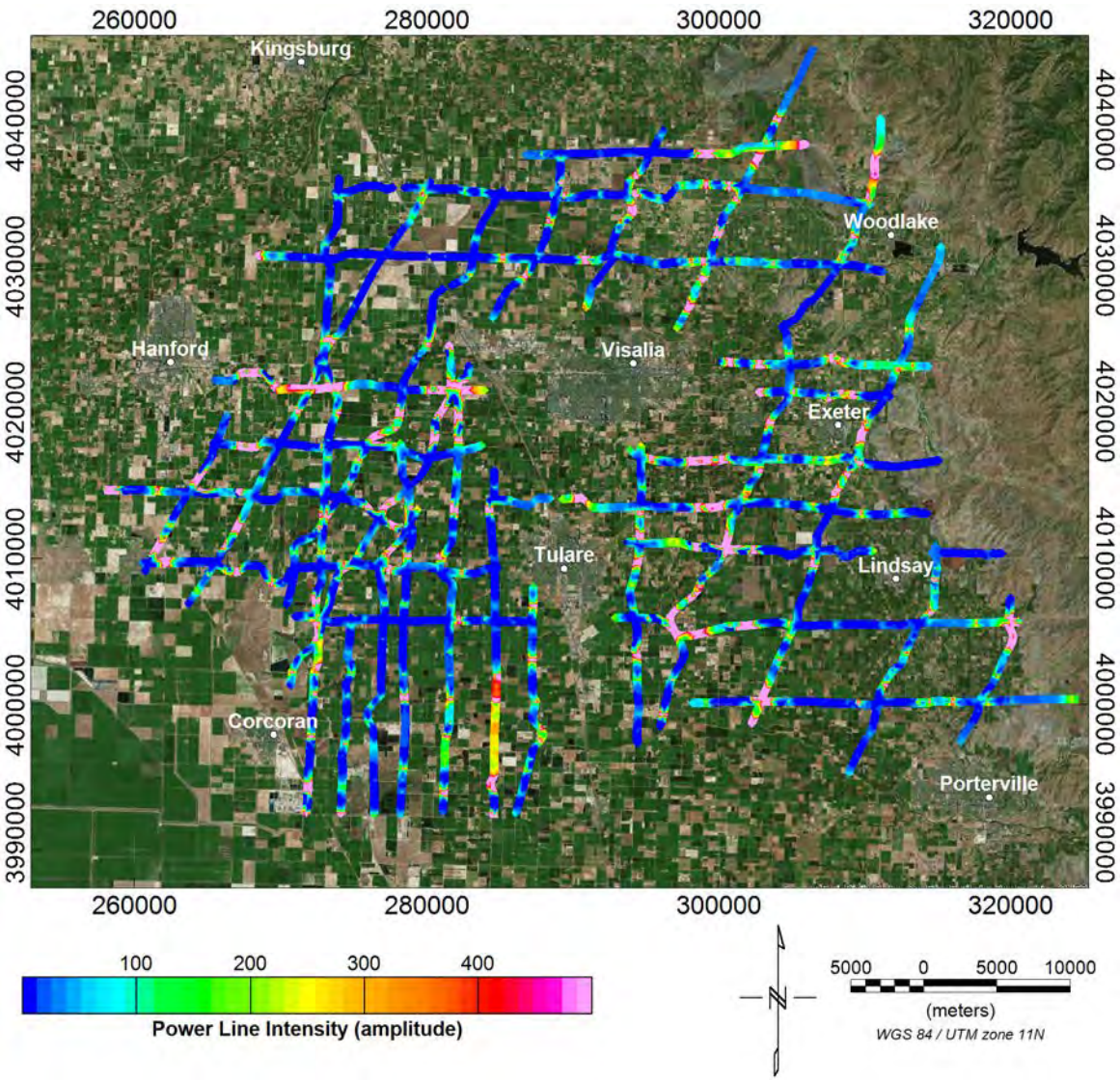

Figure 4-15. Power Line Noise Intensity (PLNI) map of the Kaweah Subbasin AEM project area.

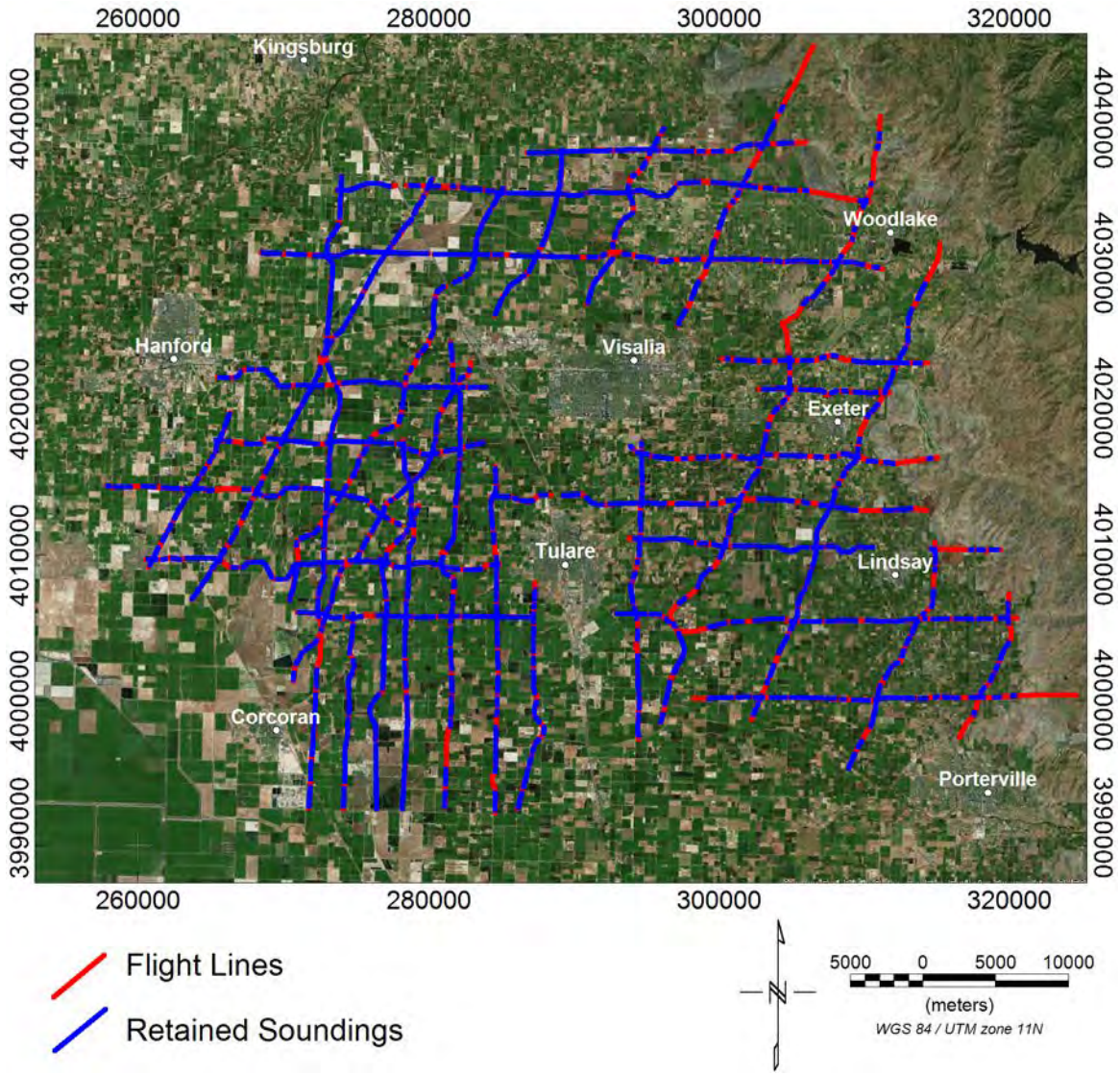

Figure 4-16. Locations of inverted data (blue lines) along the AEM flight lines (red lines) in the Kaweah Subbasin AEM survey area. Where blue lines are not present indicates decoupled (removed) data. Google Earth kmz's of the inverted data locations as well as the flight lines are included in Appendix 3\KMZ.

4.4.6 Magnetic Field Data

As discussed above, the SkyTEM 312 system includes a Total Field magnetometer whose location is listed in Table 4-1. The magnetic Total Field data can yield information about infrastructure as well as geology. Figure 4-17 shows the residual magnetic Total Field intensity data for the Kaweah Subbasin AEM survey area after correcting for diurnal drift and removing the International Geomagnetic Reference Field (IGRF). This data is also used in decoupling efforts.

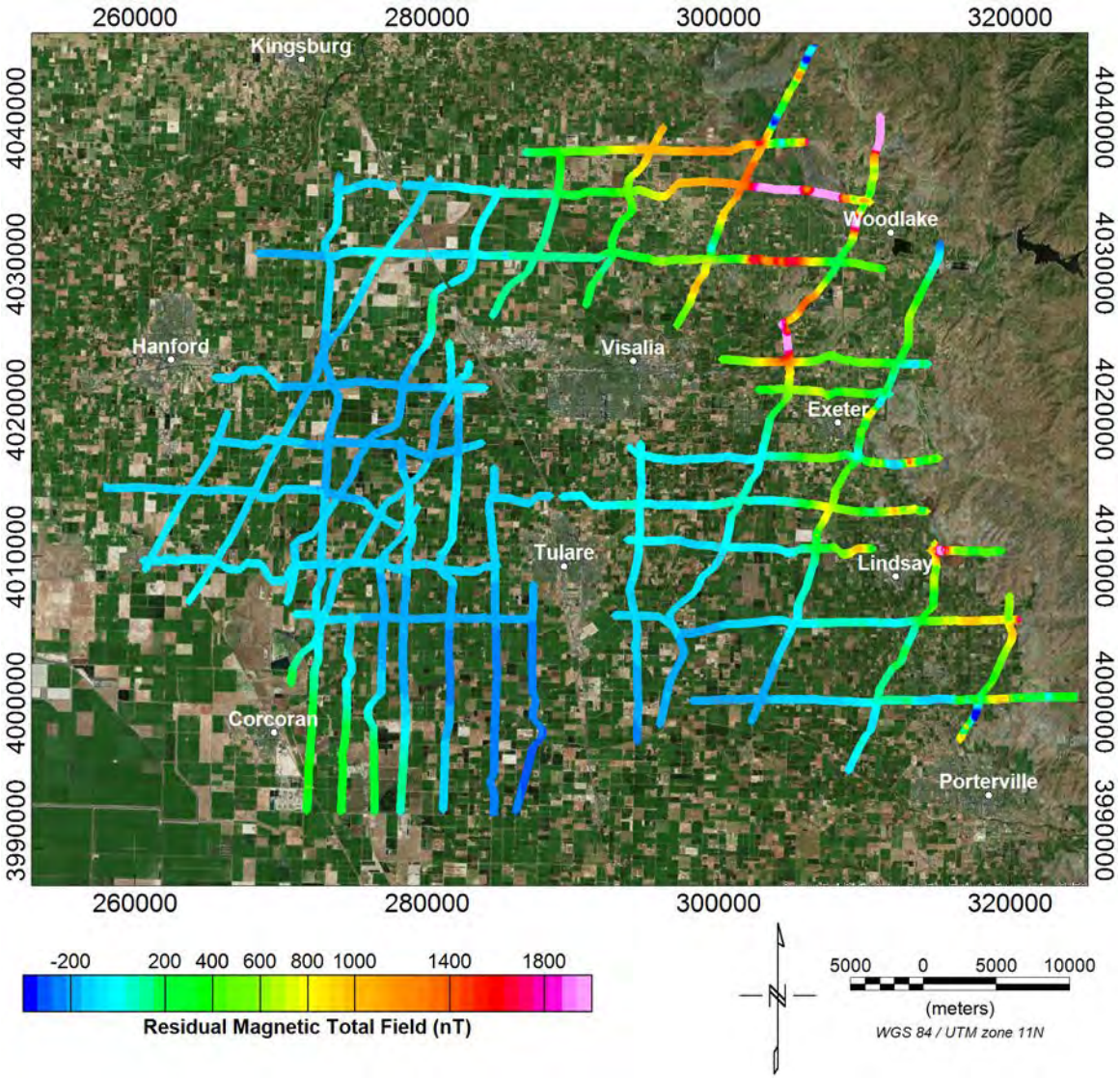

Figure 4-17. Residual magnetic Total Field intensity data for the Kaweah Subbasin AEM survey area corrected for diurnal drift, with the International Geomagnetic Reference Field (IGRF) removed.

4.5 Spatially-Constrained Inversion

Following the initial decoupling and LCI analysis, Spatially-Constrained Inversions (SCI) were performed. SCI's use EM data along, and across, flight lines within a user-specified distance criteria (Viezzoli et al., 2008).

The Kaweah Subbasin AEM data were inverted using SCI smooth models with 40 layers, each with a starting resistivity of 50 Ohm-m (equivalent to a 50 ohm-m halfspace). The thicknesses of the layers increase with depth as the resolution of the technique decreases (an example of a 30-layer model is presented in Figure 4-18). The thicknesses of the first layer of the 312 models (Table 4-5) were about 3 m with the thicknesses of the consecutive layers increasing by a factor of about 1.07. The depths to the bottoms of the 39th layers for the 312 were set to 549.9 m, with maximum thicknesses up to about 38.5 m. The spatial reference distance, ***s***, for the constraints were set to 100 m with a power law fall-off of 0.75. The vertical and lateral constraints, ***ResVerSTD*** and ***ResLatStD***, were set to 2.3 and 1.3, respectively, for all layers.

In addition to the recovered resistivity models, the SCI's also produce data-model residual error values (single sounding error residuals) and Depth of Investigation (DOI) estimates. The data residuals compare the measured data with the response of the individual inverted models (Christensen et al., 2009; SkyTEM Airborne Surveys Worldwide, 2012). The DOI provides a general estimate of the depth to which the AEM data are sensitive to changes in the resistivity distribution at depth (Christiansen and Auken, 2012). Two DOI's are calculated: an "Upper" DOI at a cumulative sensitivity of 1.2 and a "Lower" DOI set at a cumulative sensitivity of 0.6. Examination of the SCI results indicated that a much lower cumulative sensitivity, maybe 0.1 to 0.2, would still be sufficient to delineate the Kaweah Subbasin AEM DOI. A more detailed discussion on the DOI can be found in Asch et al. (2015).

Table 4-5: Thickness and depth to bottom for each layer (in meters and feet) in the Spatially Constrained Inversion (SCI) AEM earth models for the SkyTEM312. The thickness of the model layers increase with depth as the resolution of the AEM technique decreases.

Layer	Depth to Bottom (m)	Thickness (m)	Depth to Bottom (ft)	Thickness (ft)	Layer	Depth to Bottom (m)	Thickness (m)	Depth to Bottom (ft)	Thickness (ft)
1	3.0	3.0	9.8	9.8	21	133.9	11.5	439.2	37.7
2	6.2	3.2	20.3	10.5	22	146.1	12.3	479.5	40.3
3	9.6	3.4	31.4	11.2	23	159.3	13.2	522.8	43.3
4	13.3	3.7	43.6	12.1	24	173.4	14.1	569	46.2
5	17.2	3.9	56.4	12.8	25	188.4	15.0	618.2	49.2
6	21.4	4.2	70.2	13.8	26	204.5	16.1	671	52.8
7	25.9	4.5	84.9	14.8	27	221.7	17.2	727.5	56.4
8	30.7	4.8	100.7	15.7	28	240.1	18.4	787.8	60.4
9	35.8	5.1	117.4	16.7	29	259.8	19.7	852.4	64.6
10	41.3	5.5	135.4	18	30	280.9	21.1	921.6	69.2
11	47.2	5.9	154.8	19.4	31	303.4	22.5	995.4	73.8
12	53.5	6.3	175.4	20.7	32	327.5	24.1	1074.5	79
13	60.2	6.7	197.4	22	33	353.3	25.8	1159.1	84.6
14	67.4	7.2	221	23.6	34	380.8	27.5	1249.3	90.2
15	75.1	7.7	246.3	25.3	35	410.3	29.5	1346.1	96.8
16	83.3	8.2	273.2	26.9	36	441.8	31.5	1449.4	103.3
17	92.0	8.8	302	28.9	37	475.4	33.7	1559.9	110.5
18	101.5	9.4	332.9	30.8	38	511.4	36.0	1678	118.1
19	111.6	10.1	366	33.1	39	549.9	38.5	1804.3	126.3
20	122.3	10.8	401.4	35.4					

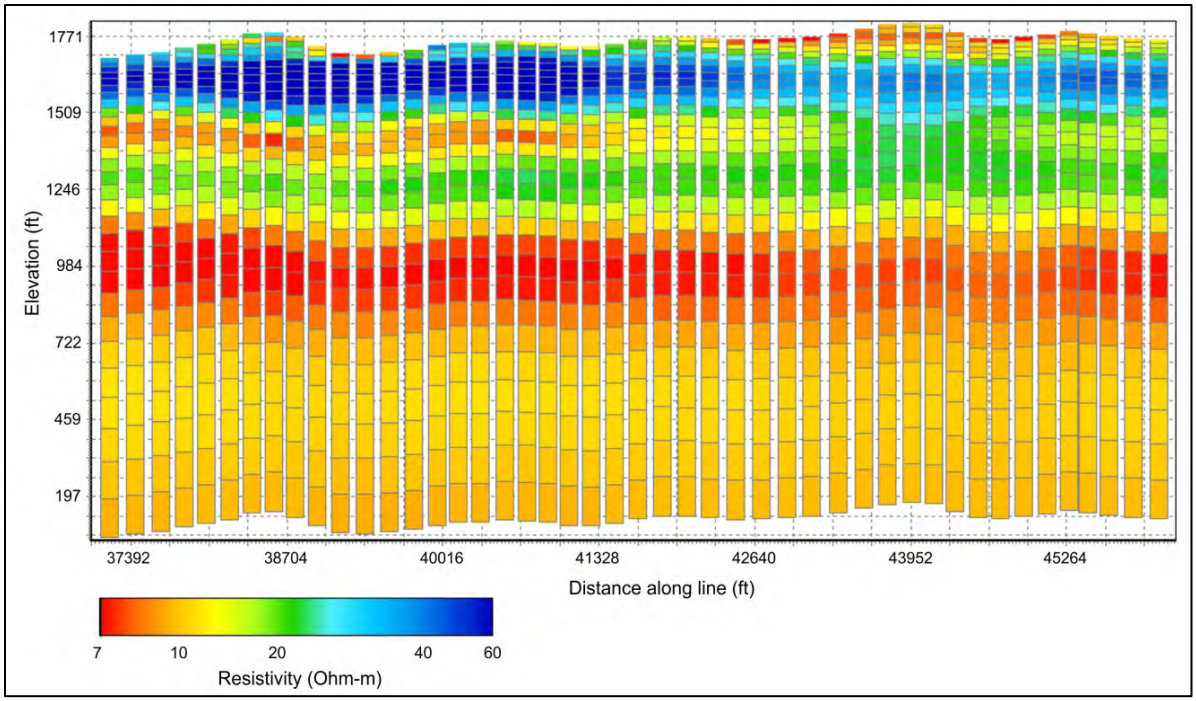

Figure 4-18. An example of an AEM profile illustrating increasing model layer thicknesses with depth. This is a 30-layer model.

Figure 4-19 presents a histogram of the Kaweah Subbasin SkyTEM 312 SCI inversion data/model residuals. A map of data residuals for the Kaweah Subbasin AEM study area is presented for the SkyTEM 312 inversion results in Figure 4-20.

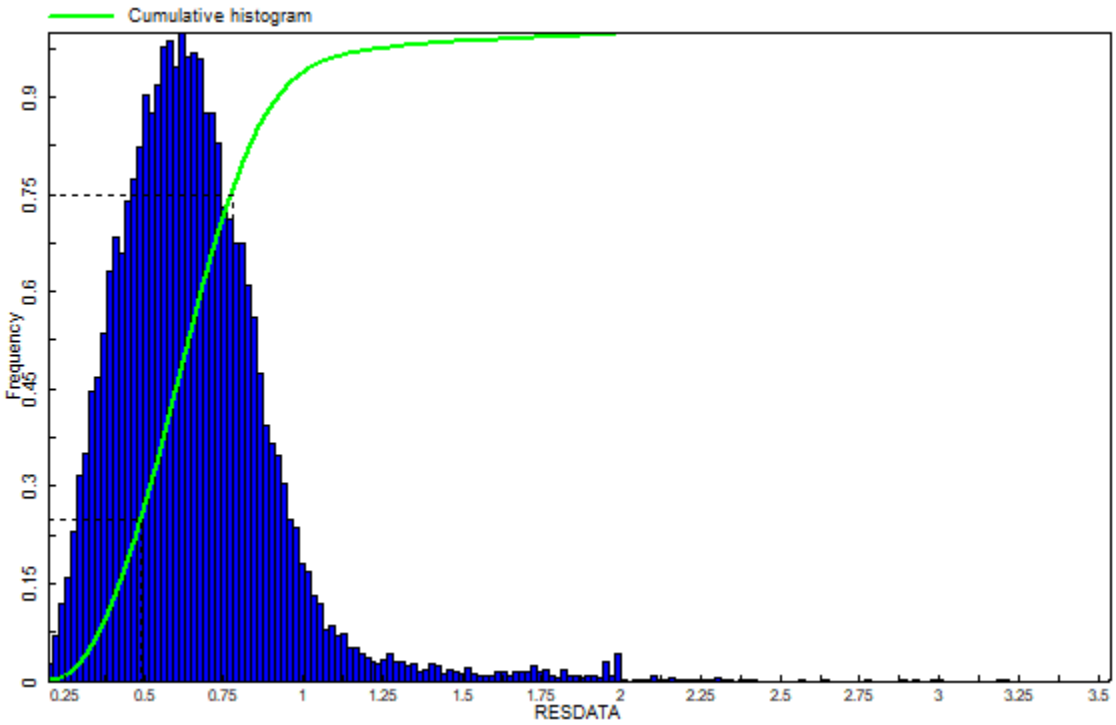

Figure 4-19. Data/model residual histogram for the Kaweah Subbasin SCI inversion results.

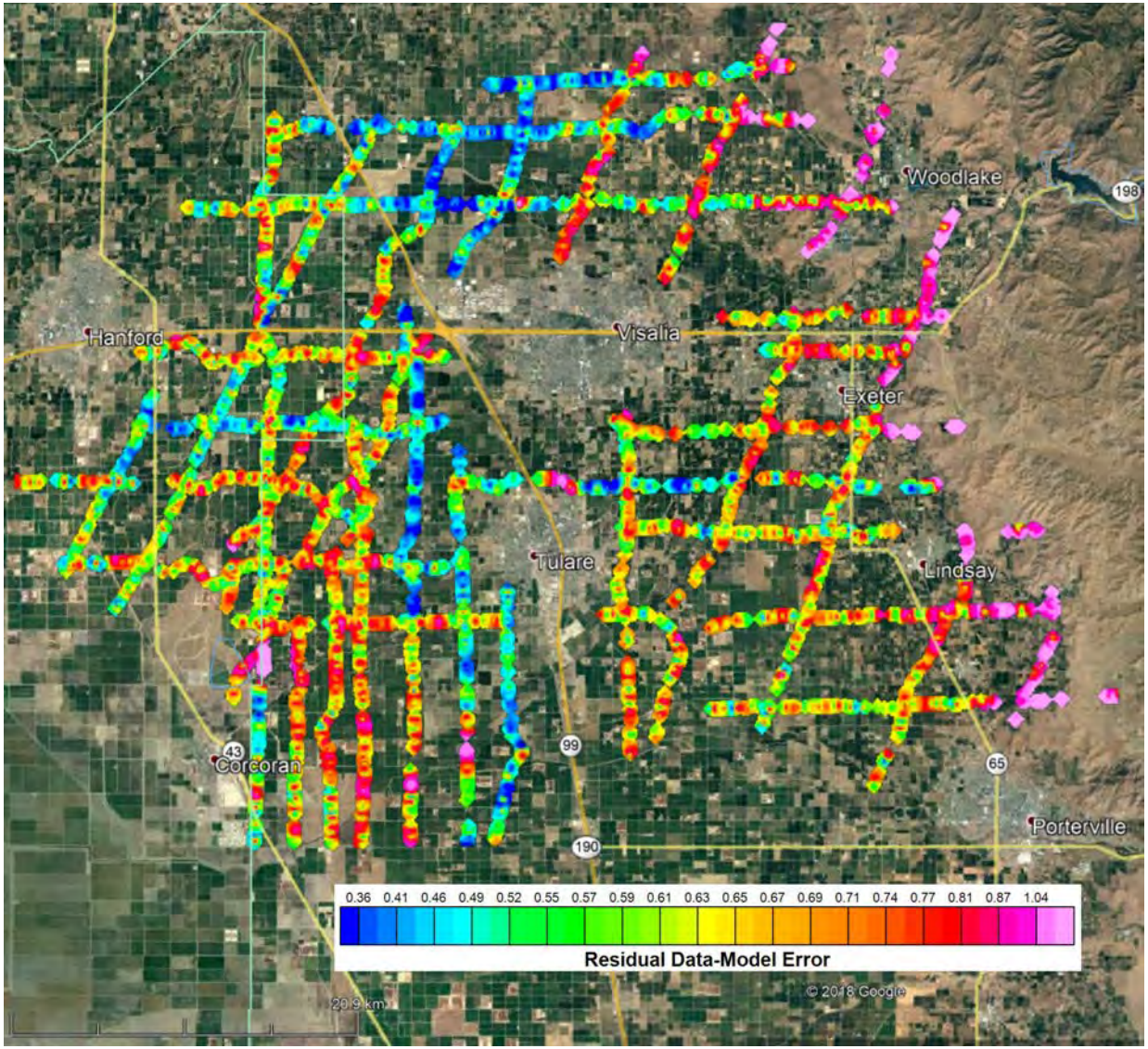

Figure 4-20. Map of data residuals for the Kaweah Subbasin SCI inversion results.

5 AEM Results and Interpretation

This section provides the details on the process involved in the interpretation of the Kaweah Subbasin AEM data and inversion results.

5.1 Interpretive Process – Merge AEM Flight Lines, Construct DEM

5.1.1 Merge AEM Flight Lines and Databases from Different Flights

After the inversion process several short lines were combined to form continuous lines within the survey area. These continuous lines allow for improved viewing and interpretation of the AEM inversions results. Table 5-1 lists the original flown lines and the new combined lines for the SkyTEM 312.

Table 5-1. Combination of SkyTEM 312 flight lines within the Kaweah Subbasin AEM survey area.

Original Line	Original Line	Merged Line
L100201	L100203	L100200
L100301	L100302	L100300
L100602	L101601	L100600
L200201	L200203	L200200
L200301	L200303	L200300
L201101	L201103	L201100
L201201	L201202	L201200
L201301	L201401	L201300

5.1.2 Construct the Project Digital Elevation Model

To ensure that the elevation used in the project is constant for all the data sources (i.e. AEM and boreholes) a Digital Elevation Model (DEM) was constructed for the Kaweah Subbasin AEM survey area. The data was downloaded from the U.S. Geological Survey National Elevation Dataset (NED) located on the National Map Website (USGS, 2019) at a spatial resolution of 1/3 arc-second or approximately 10 meters. The geographic coordinates are North American Datum of 1983 (NAD 83) and the elevation values are referenced to the North American Vertical Datum of 1988 (NAVD 88) meters. Figure 5-1 is a map of the DEM for the Kaweah Subbasin AEM survey area having a vertical relief within the flight line coverage of 427 m with a minimum elevation of 63 m and a maximum elevation of 490 m. This DEM was used to reference all elevations within the AEM and borehole datasets.

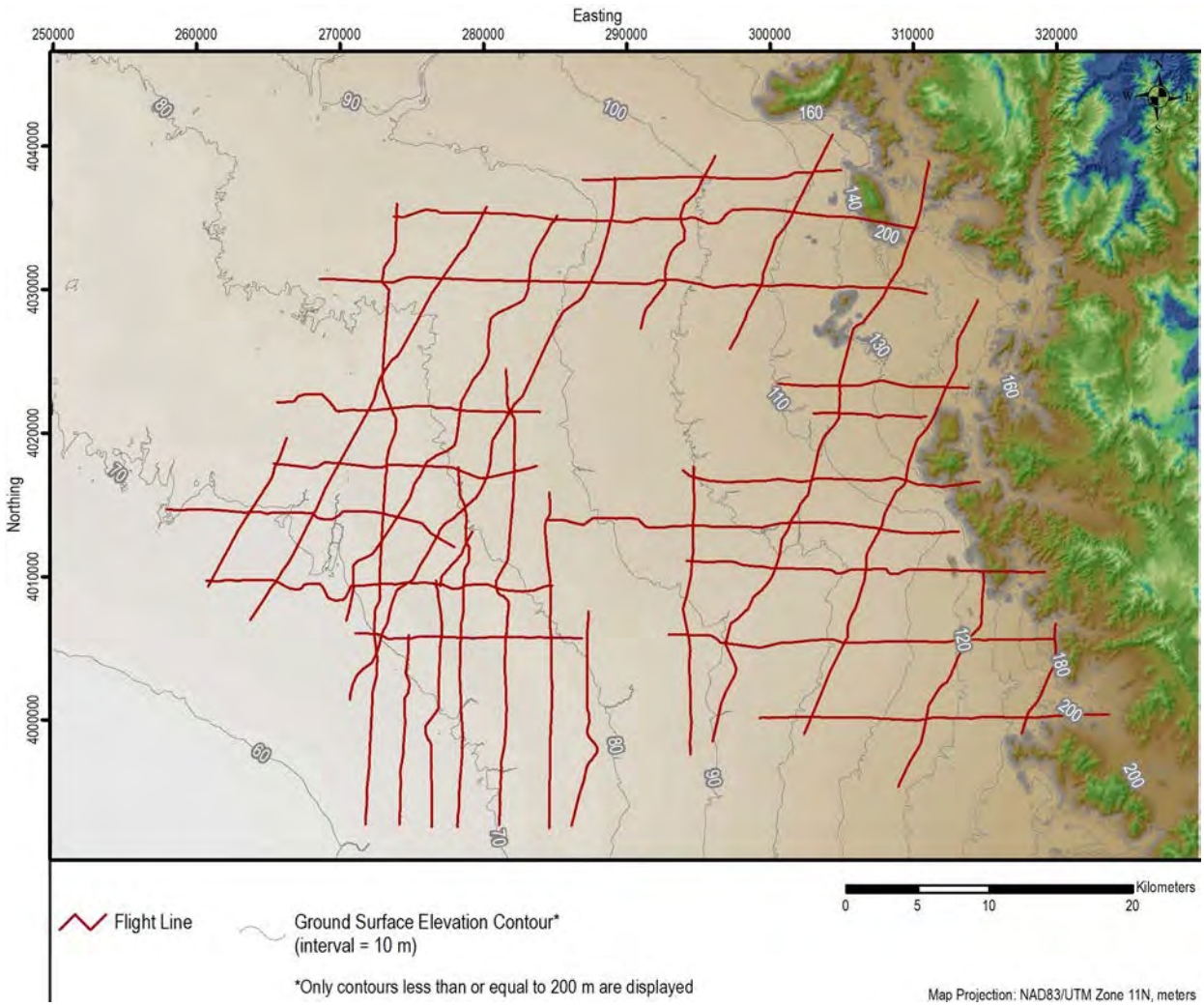

Figure 5-1. Map of the Digital Elevation Model for the Kaweah Subbasin AEM survey area. Data source is the one (1) arc-second National Elevation Dataset (USGS, 2019). North American Datum of 1983 (NAD 83) meters and the elevation values are referenced to the North American Vertical Datum of 1988 (NAVD 88) meters.

5.2 Create Interpretative 2D Profiles

After final combination of the AEM data, characterization of the subsurface was performed in cross-section format using Datamine Discover Profile Analyst (DatamineDiscover, 2018). During interpretation, the horizontal and vertical scale of the profiles were adjusted to facilitate viewing. The color scale of the resistivity data was also adjusted to illuminate subtle differences in the resistivity structure within the inverted AEM resistivity model related to the area being interpreted. The first step in the interpretation process was reviewing the previous work that was completed in the area as referenced in Section 2.0. This included the reports Groundwater Availability of the Central Valley Aquifer, California (Faunt, 2009), and Water Resources Investigation of the Kaweah Delta Water Conservation District 2003, Revised 2007 (Fugro West, 2007), and research journal articles including Mapping aquifer systems with airborne electromagnetics in the Central Valley of California (Knight et al., 2018) and Glacially driven cycles in accumulation space and sequence stratigraphy of a stream-dominated alluvial fan, San Joaquin Valley, California, U.S.A (Weissmann et al., 2002, 2004). Each of these reports and research articles helped to provide insight into understanding what was imaged by the Kaweah Subbasin AEM reconnaissance survey.

In the Fugro West (2007) report there are six cross-sections (plates 14-19) that span the Kaweah Subbasin AEM survey area. Figure 5-2 presents a Google Earth image that presents the spatial relation between the Fugro cross-sections and the AEM Reconnaissance flight lines. As an example, Fugro West cross-section A-A', plate 14 in Fugro West (2007), is presented in Figure 5-3. Cross-section A-A', running east-west, crosses the whole of the Kaweah Subbasin AEM survey area. There are two stratigraphic units of note on cross-section A-A'. The first is the pre-Tertiary basement material on the east side of the flight line (the pinkish-colored area) which is indicated to be on the up-side of the normal Rocky Hill Fault. The second stratigraphic unit of note is the thin zone identified as the "E-Clay" that is thicker on the west side of the line and thins out to the east, about half-way across A-A'. All six cross-sections in the Fugro West (2007) report are presented as a 3D fence diagram in Figure 5-4. Comparisons between the Fugro West (2007) cross-sections and the Kaweah Subbasin AEM inversion results are discussed below in Section 5.6.

An example of the AEM resistivity inversion results for the Kaweah Subbasin Reconnaissance AEM survey is presented in Figure 5-5. This is AEM flight line L200300. The dotted blue line is the Fall 2017 water table elevation data acquired at the CA-DWR website (CA-DWR, 2018a) and the grey dashed line is the "standard", deeper, depth of investigation (DOI). After examination of the Fugro West (2007) cross-sections, the high resistivity material on the east side of L200300 is interpreted to be representative of the pre-Tertiary basement material indicated on Fugro cross-section A-A' (Figure 5-3) and the solid black line is the approximate upper contact of the granitic material. Although Fugro cross-section A-A' indicates that the sub-vertical contact on western side of the granitic material is the location of the Rocky Hill Fault, no displacement can be identified in the resistivity inversion results in Figure 5-5. Thus, it has not been interpreted as a fault contact, but rather a depositional contact of the Quaternary and Tertiary sedimentary material against the pre-Tertiary intrusive granitic material. This is

not to say that the contact is not a fault contact, but rather there is no visual evidence in the AEM inversion results to definitely say that the interface is a fault contact.

There are several other observations to note on AEM flight line L200300 (Figure 5-5) including that there is no indication of the presence of the E-Clay on the western end of the flight line. Another is the slightly more resistive zone, whose boundary is marked in a red dashed line in Figure 5-5, sitting between two electrically more conductive zones. Backing up a bit and taking a more general view, it can be observed that there is a thin blue conductive zone, about 40 m thick, sitting on the granite on the eastern end of L200300 that continues west off the edge of the granite across the length of the flight line where it has thickened, up to about 100 m. Closer to the granite, beneath the 40 m conductive zone, is the slightly more resistive zone whose bounds are marked with the dashed red line in Figure 5-5. Then beneath this slightly more resistive zone is another conductive zone, also about 80 m – 100 m thick. While the conductivity indicates that all three of these units have a high clay content, the slightly increased resistivity of the zone marked with the red dashed line indicates that this zone might be more silty clay or possibly even sandy clay. So, what is the significance of marking out these three zones?

Figure 5-6 presents, from Weissmann et al. (2002), a stratigraphic sequence for the development of an alluvial fan coming out of Kings River canyon, the next valley north about 24 km (15 miles) from Kaweah River canyon. Weissmann et al. (2002) in Figure 5-6 show the prograding development of an alluvial fan with intermittent periods of deposition of sedimentary materials with, possibly, different lithological composition. Different lithological composition could translate to materials having varying electrical resistivities. Thus, it is interpreted here that the three zones of varying resistivity in Figure 5-5 *possibly* represent the prograde development of an alluvial fan coming out of the Kaweah River canyon/valley. However, as indicated in Figure 5-6 by the example of a thick black line with the red arrow pointing at it, the development of an alluvial fan involves some degree of valley incision. This is further discussed in Weissmann et al. (2004) which models the development of the incised valley fill.

What is important about identifying the alluvial fan coming out of Kaweah River canyon is that in the Kaweah Subbasin AEM survey, the indication of an alluvial fan is only clearly observed on one flight line, L200300, because this AEM survey was designed as a reconnaissance survey with a flight line separation of 5 km. The flight lines to the north (L200401, Figure 5-7) and to the south (L200200, Figure 5-8) do show the thin conductor overlying the granitic basement material, but it is not very clear if there is interbedded coarse material underlying the thin conductor along these two lines. There is some indication along L200401 (Figure 5-7), but it is not extensive or well defined. This illustrates that if conclusive characterization of such a feature, or other geologic features, is desired, then a “block” AEM flight plan of tightly-spaced flight lines would be necessary.

Also note in Figure 5-7 is a black arrow indicating an area where the data was cut due to EM coupling from infrastructure. Note the high topographic peak of the basement stratigraphic contact at this location. This does not seem normal for granitic intrusives. The circled areas of the geologic map in Figure 2-1 indicate locations where the flight lines cross pre-Tertiary metavolcanic geologic material (including ophiolites). This is the material in the peak in Figure 5-8 which creates topography in the basement. Figure 5-9 presents another AEM flight line, L100901, which also crosses over some of the

pre-Tertiary metavolcanics. It is observed that the electrical resistivities of the metavolcanics and the granitic material are both high and the units cannot be distinguished from one another based on electrical resistivity. Thus, in this report, the pre-Tertiary metavolcanics and granitic basement material are grouped together for interpretation purposes.

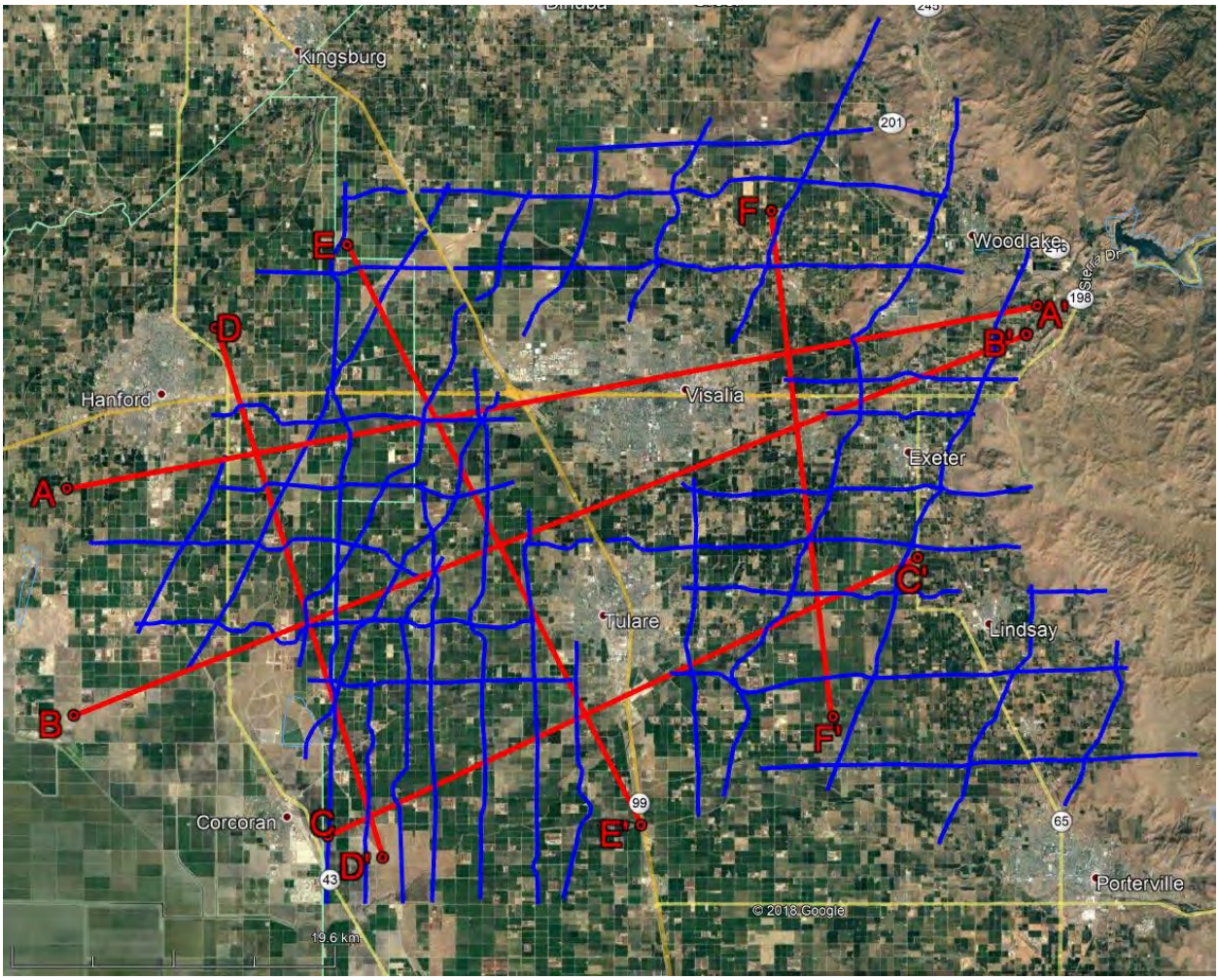

Figure 5-2. Google Earth image of Kaweah Subbasin AEM flight lines (blue lines) and the six Fugro West (2007) cross-sections.

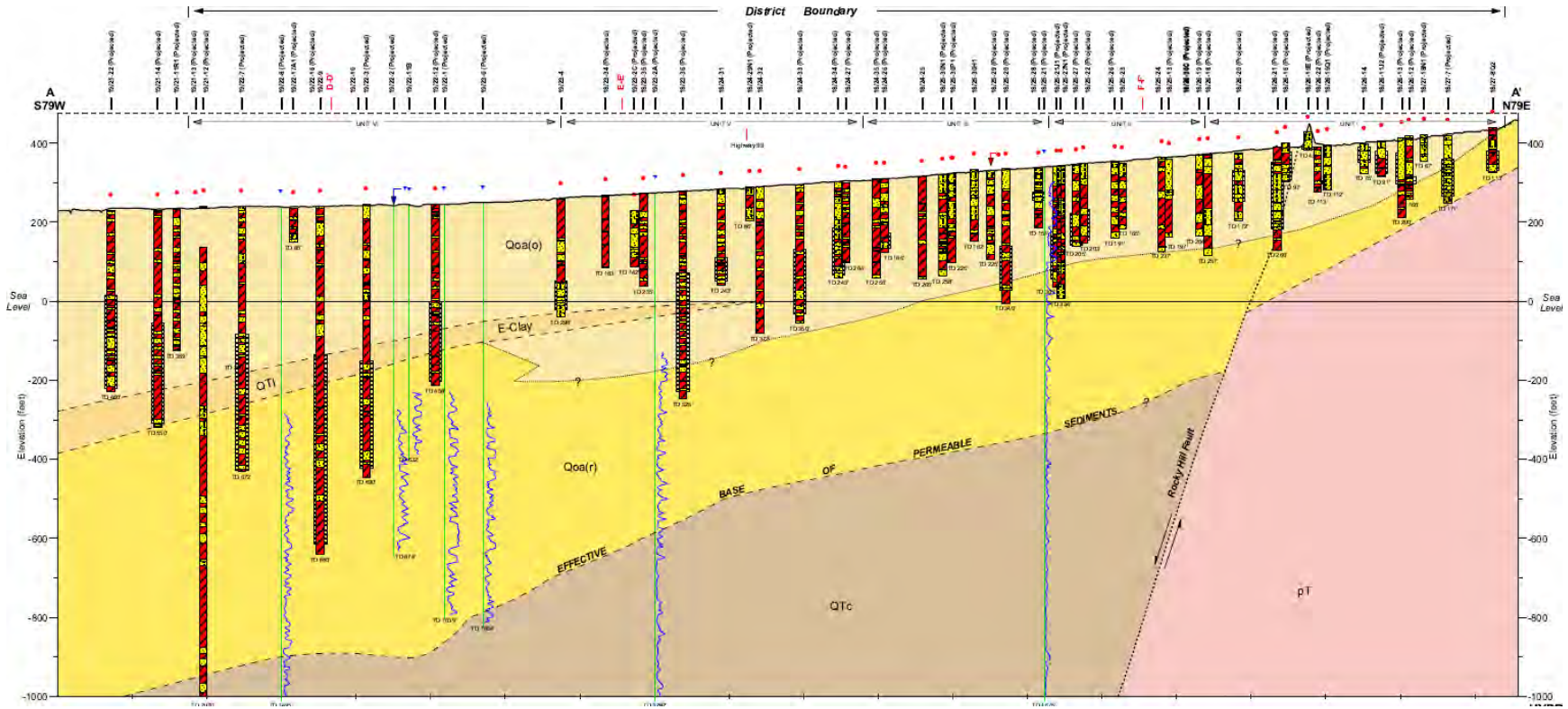

Figure 5-3. Cross-section A-A' from Plate 14 of Fugro West (2007).

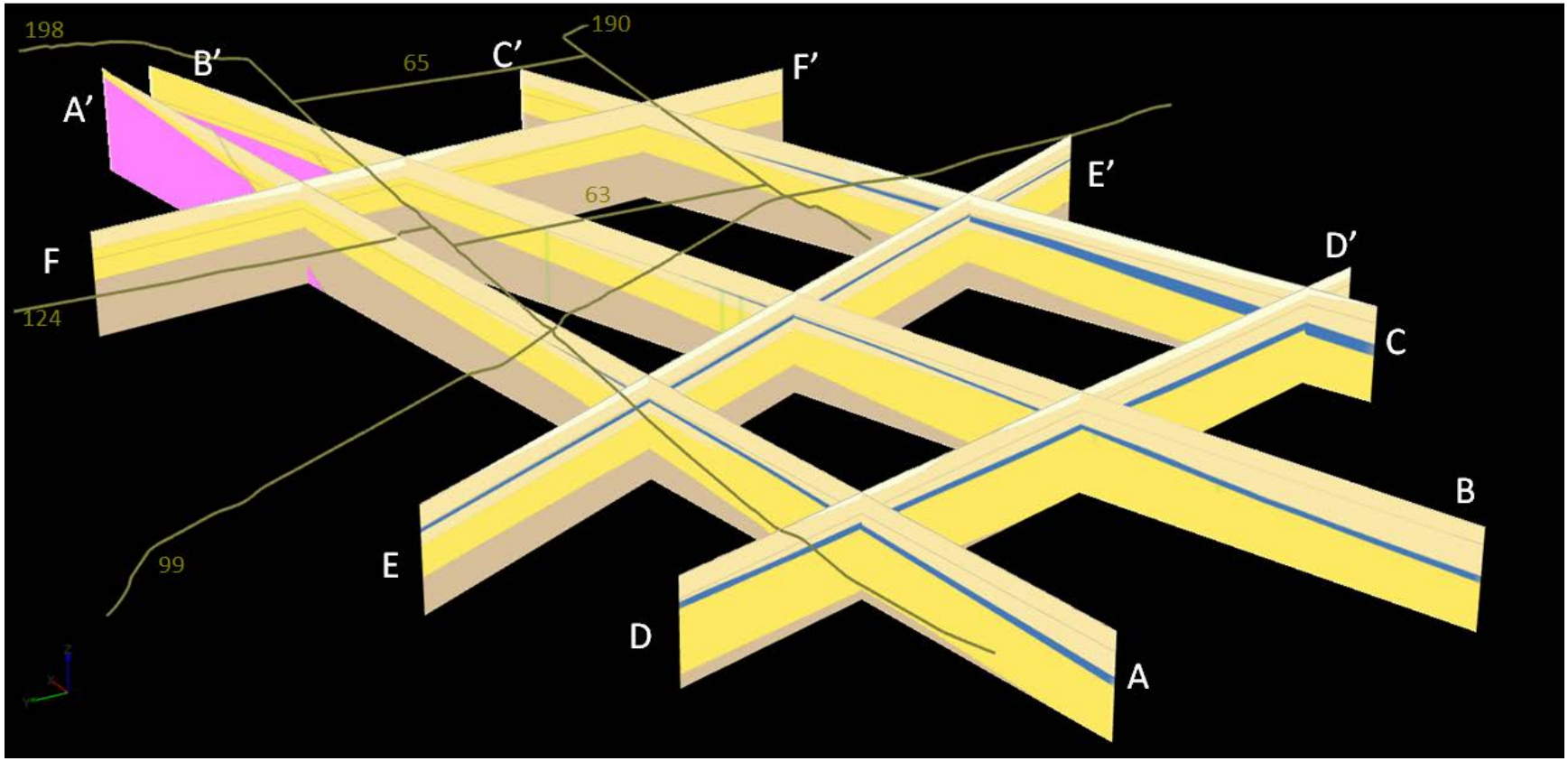

Figure 5-4. 3D fence diagram of the six cross-sections A-F from Fugro West (2007), modified with the boreholes and resistivity logs removed and different coloring applied to the E-Clay and the basement material. The brown lines are local highways (99, 163, etc.) to help the user locate themselves in the 3D space.

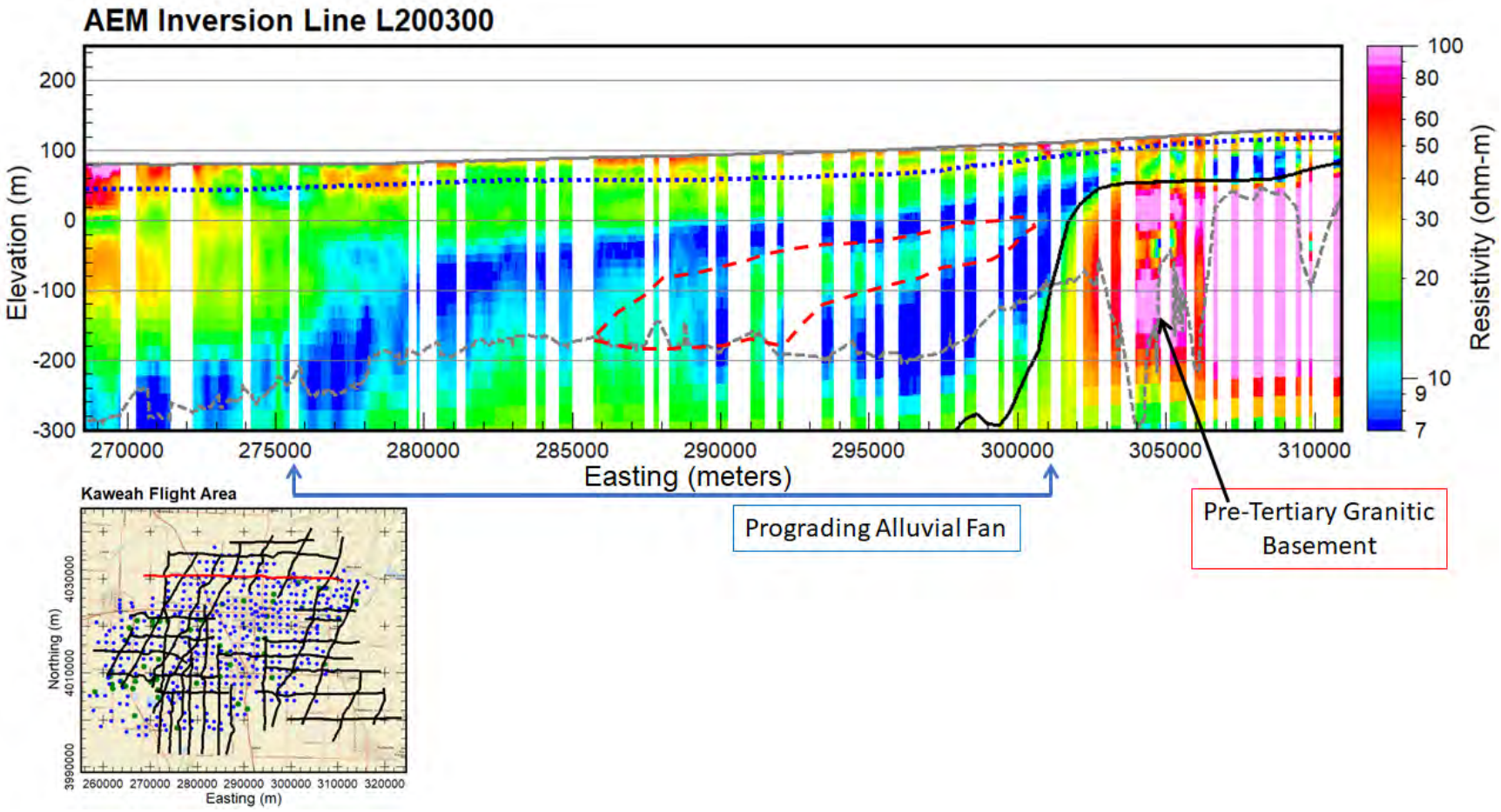

Figure 5-5. 2D profile of inverted resistivity data from Kaweah Subbasin AEM flight line L200300, located across the northern extent of the AEM survey area. The dotted blue line is the CA-DWR Fall 2017 water table (CA-DWR, 2018a). The dashed grey line is the "standard" depth of investigation (DOI). The solid black line is a stratigraphic contact, in this case the top contact of the basement material on the east side of the flight line. The red dashed line separates zones of more conductive sediments with a zone of more resistive material. The projection is NAD83, UTM 11N, meters, NAVD88 meters.

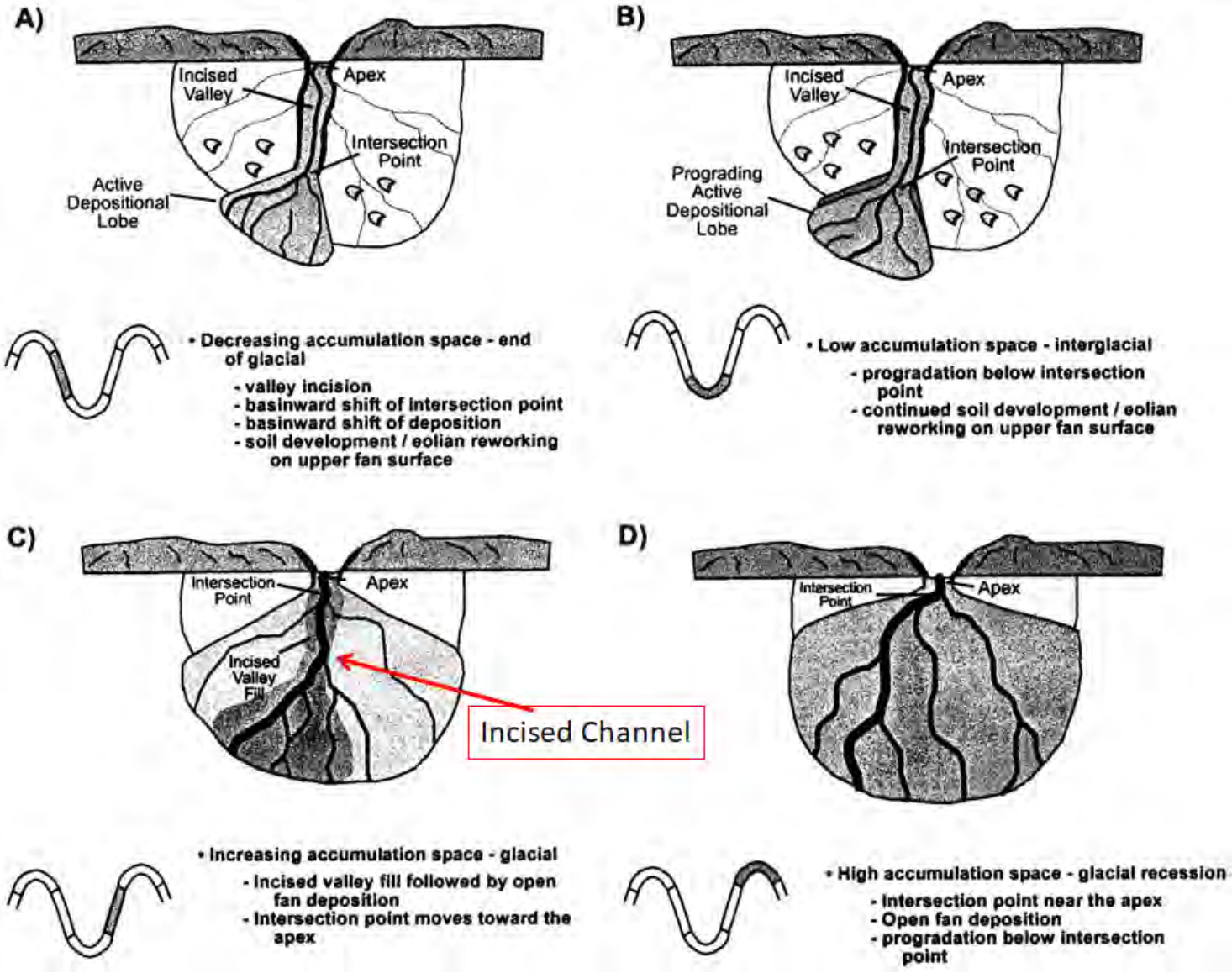

Figure 5-6. Illustration of the development sequence of stratigraphic cycles on an alluvial fan (Figure 8 modified from Weissmann et al., 2002). Darker shading indicates active areas of the alluvial fan. The red arrow indicates the incised channel discussed in the text.

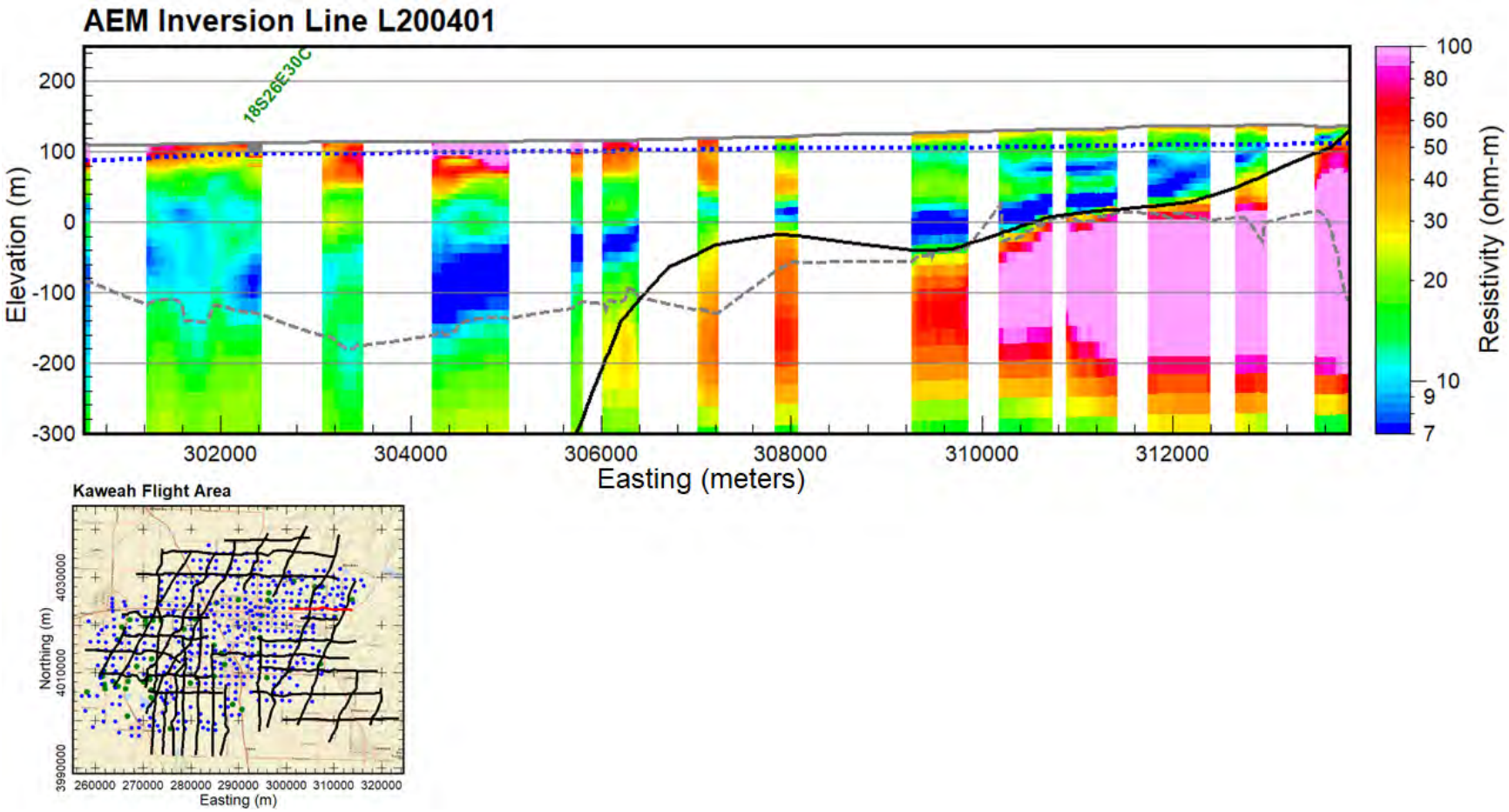

Figure 5-7. 2D profile of inverted resistivity data from Kaweah Subbasin AEM flight line L200401, located southeast of L200300. The dotted blue line is the CA-DWR Fall 2017 water table (CA-DWR, 2018a). The dashed grey line is the "standard" depth of investigation (DOI). The solid black line is a stratigraphic contact, in this case the top contact of the basement material on the east side of the flight line. There is a slight indication of a distinct prograding alluvial fan just west of the granitic body with a conductive body overlying a slightly more resistive zone. The projection is NAD83, UTM 11N, meters, NAVD88 meters.

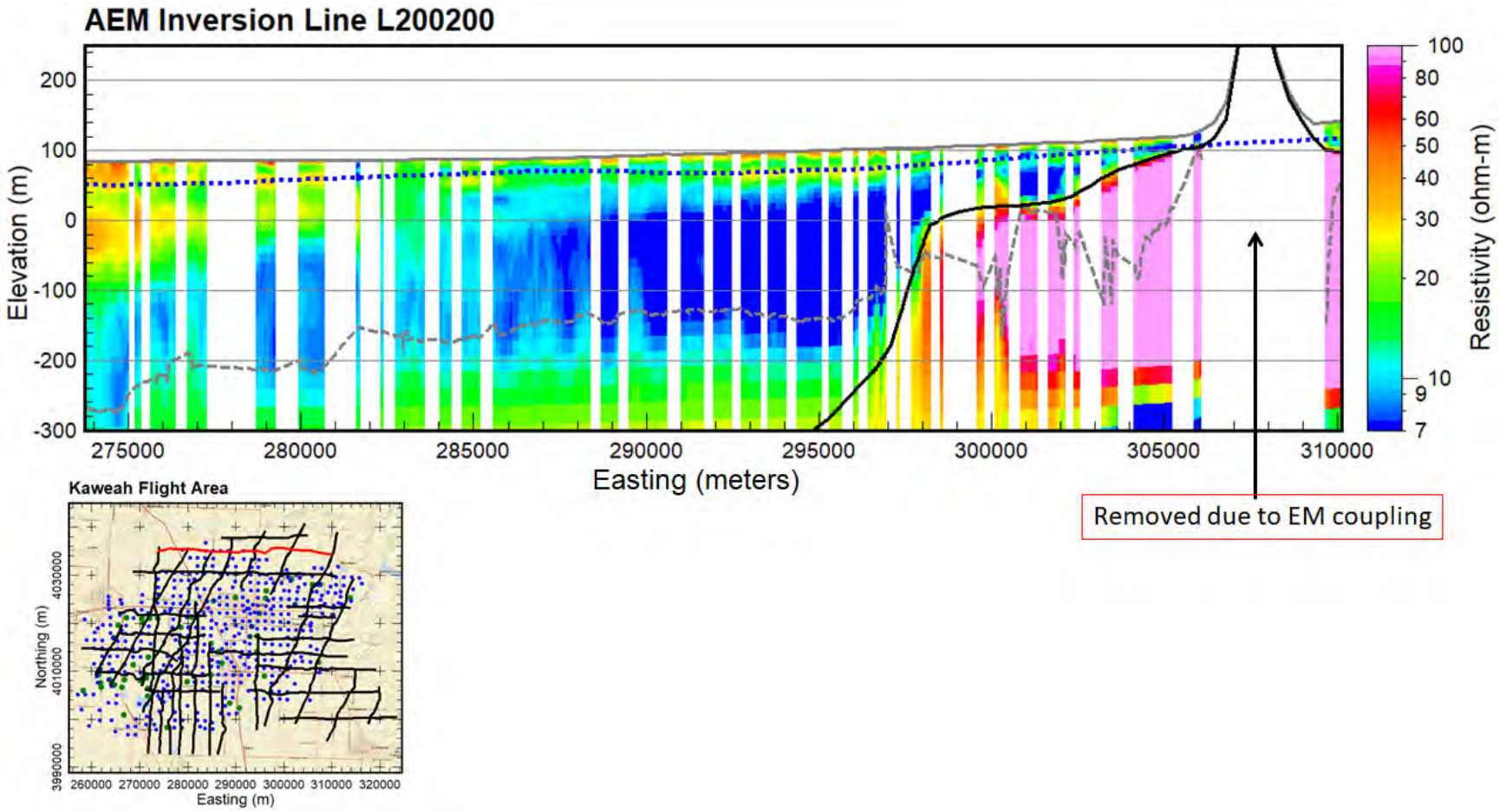

Figure 5-8. 2D profile of inverted resistivity data from Kaweah Subbasin AEM flight line L200200, located north of L200300. The dotted blue line is the CA-DWR Fall 2017 water table (CA-DWR, 2018a). The dashed grey line is the "standard" depth of investigation (DOI). The solid black line is a stratigraphic contact, in this case the top contact of the basement material on the east side of the flight line. There is no indication of a distinct *interbedded* prograding alluvial fan as there is on AEM flight line L200300 (Figure 5-5). The projection is NAD83, UTM 11N, meters, NAVD88 meters.

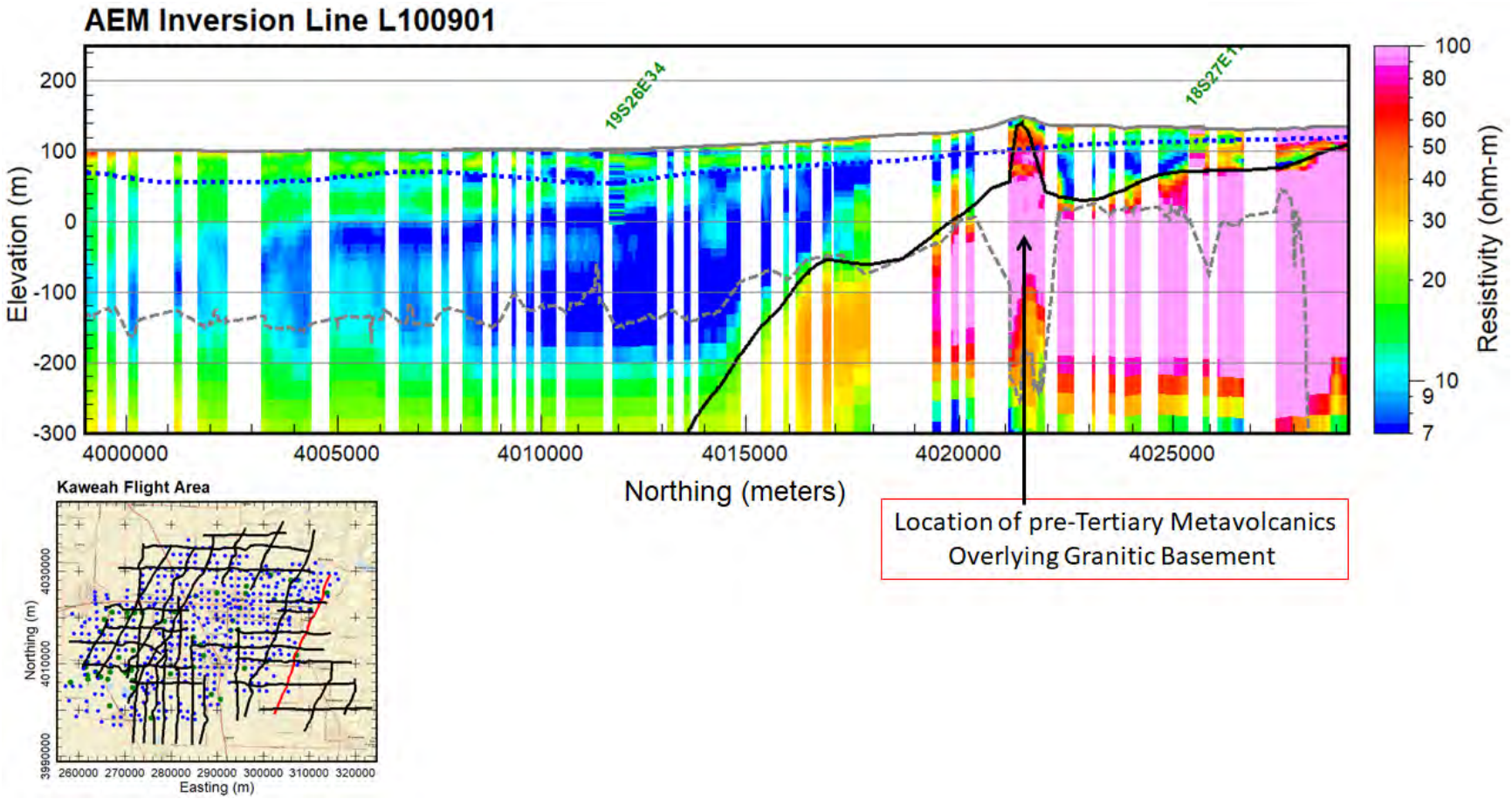

Figure 5-9. Inversion results for Kaweah Subbasin AEM flight line L100901. The dotted blue line is the CA-DWR Fall 2017 water table (CA-DWR, 2018a). The dashed grey line is the "standard" depth of investigation (DOI). The solid black line is a stratigraphic contact, in this case the top contact of the basement material on the east side of the flight line. The arrow is pointing at the location where pre-Tertiary metavolcanics are overlying granitic material. The electrical resistivities of the metavolcanics and granitic material are similar, which is high, and so cannot be distinguished from one another by resistivity alone. The projection is NAD83, UTM 11N, meters, NAVD88 meters.

As noted above, E-Clay is identified on the western end of Fugro West cross-section A-A' in Figure 5-3. As discussed in Section 2.1, the E-Clay includes the Corcoran Clay which is known to extend further to the west and southwest. One of the goals of this AEM investigation was to map the extent and thickness of the Corcoran Clay. To this end, examination of the Kaweah Subbasin AEM resistivity inversion results on the western side of the survey area show that the AEM is able to map the location and extent of the Corcoran Clay. East-west AEM flight line L20001001 in Figure 5-10 indicates that a westward-dipping conductive zone is present at about the same elevation and about the same thickness as in Fugro West cross-section A-A'. That conductive zone is interpreted to be the Corcoran Clay. North-south AEM flight line L100600 (Figure 5-11) not only shows the Corcoran Clay but also indicates that it is thins out to the north.

Also note along AEM flight line L100600 (Figure 5-11) the high resistivities of the unsaturated material above the water table (dotted blue line).

The next step was to study the available geophysical and lithological logs provided by GEI Consultants (Section 3) and then overlay them on the profiles if they are within 1,000 m (3,281 ft) of a flight line. On the profiles geophysical electrical resistivity logs are labeled in green and lithological logs are labeled in blue. The lithology color legend is in the upper right corner of the image. On the geophysical logs of interest were locations and depths of resistive and conductive zones. Then lithology logs were studied to correlate borehole lithologies with the observed resistivities.

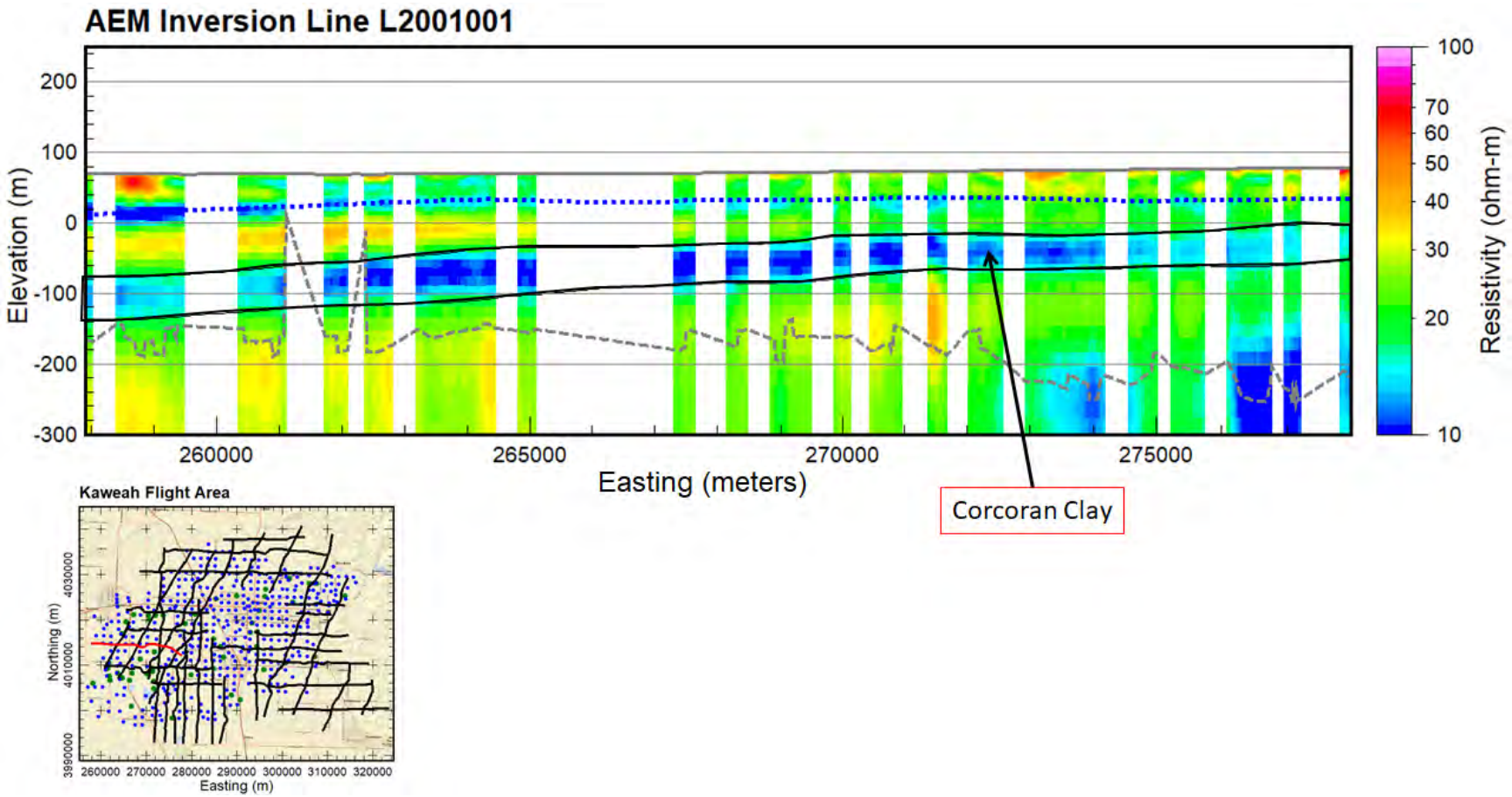

Figure 5-10. 2D profile of inverted resistivity data from Kaweah Subbasin east-west AEM flight line L2001001, located on the western side of the AEM survey area. The dotted blue line is the CA-DWR Fall 2017 water table (CA-DWR, 2018a). The dashed grey line is the "standard" depth of investigation (DOI). The solid black lines are stratigraphic contacts, in this case the top and bottom contacts of the Corcoran Clay which is dipping to the west. The projection is NAD83, UTM 11N, meters, NAVD88 meters.

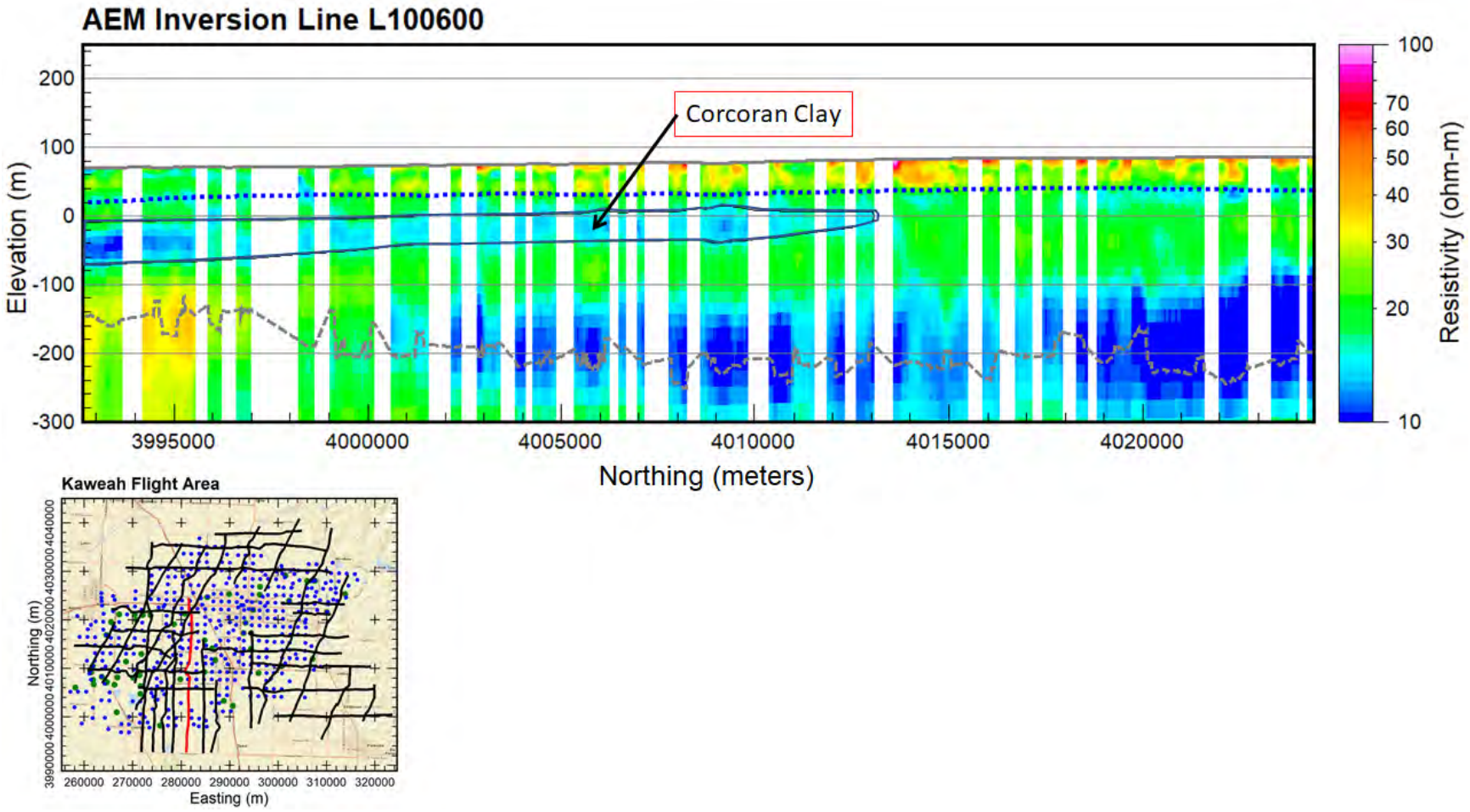

Figure 5-11. 2D profile of inverted resistivity data from Kaweah Subbasin AEM north-south flight line L100600, located on the western side of the AEM survey area. The dotted blue line is the CA-DWR Fall 2017 water table (CA-DWR, 2018a). The dashed grey line is the "standard" depth of investigation (DOI). The solid black line is the stratigraphic contacts, in this case the top and bottom contacts of the Corcoran Clay which dips slightly to the south and thins out to the north. The projection is NAD83, UTM 11N, meters, NAVD88 meters.

5.3 Comparison of Borehole Logs and the AEM Inversion Results

It is important to compare the AEM earth-model inversion results to the available borehole information. You want to look how the patterns of inverted AEM resistivities match up with the majority of geophysical borehole logs. It is quite often the case that borehole logs are not well calibrated or not operated correctly. This is not to say that when the borehole data was acquired that the tool was perfectly suitable for what was expected from the logging results. What follows in this section are samples from across the investigation area of a comparison of the inverted AEM earth model resistivities with the borehole electrical resistivity and lithology logs. Note that from the map of geophysical and lithological borehole locations (Figure 3-1), it is clear that there are many more lithology logs in the Kaweah Subbasin AEM survey area than geophysical logs.

A comparison of borehole resistivity and lithology logs and AEM flight line L100200 is presented in Figure 5-12. The geophysical logs have green labels and the lithology logs have blue labels. The resistive zones on the geophysical logs *20S22E20D2*, *19S22E11B*, and *19S22E1* line up nicely with the resistive AEM inversion results. There is also a good lithology match of the logs that pass through the Corcoran Clay such as *19S22E28* and *19S22E27*. Lithology log *18S22E36P* indicates more of an interbedded nature in the area where the Corcoran thins out and terminates about half way along the flight line.

Figure 5-13 presents a comparison of borehole resistivity and lithology logs with AEM flight line L101202. Again, the resistive zones on the geophysical logs *20S22E24*, *19S22E36*, and *19S23E6* line up nicely with the resistive (and conductive zones) in the AEM inversion results. Note that geophysical log *20S22E25* does not match the AEM inversion results at all, or even with log *20S22E24* which is right next to it, which means that *20S22E25* is either not calibrated correctly or was not set correctly prior to commencing the resistivity logging. There is a good match of most of the lithology logs that pass through the Corcoran Clay including *21S23E7*, *21S22E12A*, *20S22E36*, and *19S22E24J*.

A comparison of borehole resistivity and lithology logs with AEM flight line L101702 is presented in Figure 5-14. The interbedded nature of the resistive and conductive zones on geophysical log *20S24E8* line up nicely with the AEM inversion results. There is a good match of most of the lithology logs that pass through the Corcoran Clay, or just beyond it, including *21S24E16*, *21S24E9L1*, *20S24E8*, and *19S24E32K1*.

A final example of a comparison of borehole lithology logs with the AEM inversion results is presented in Figure 5-15 for flight line L200300. There are no geophysical logs on this section. Note the pattern of the bottoms of the logs – most logs stop in the more resistive zone (coarser material) sitting above the conductive zone (very likely clay). Note that a couple of the boreholes (*18S23E5* and *18S24E6*) were drilled through the clay and into the next coarser material zone.

These profiles presented show a good match but also are excellent examples that show how new, more continuous, information adds higher definition to the results when compared to boreholes alone.

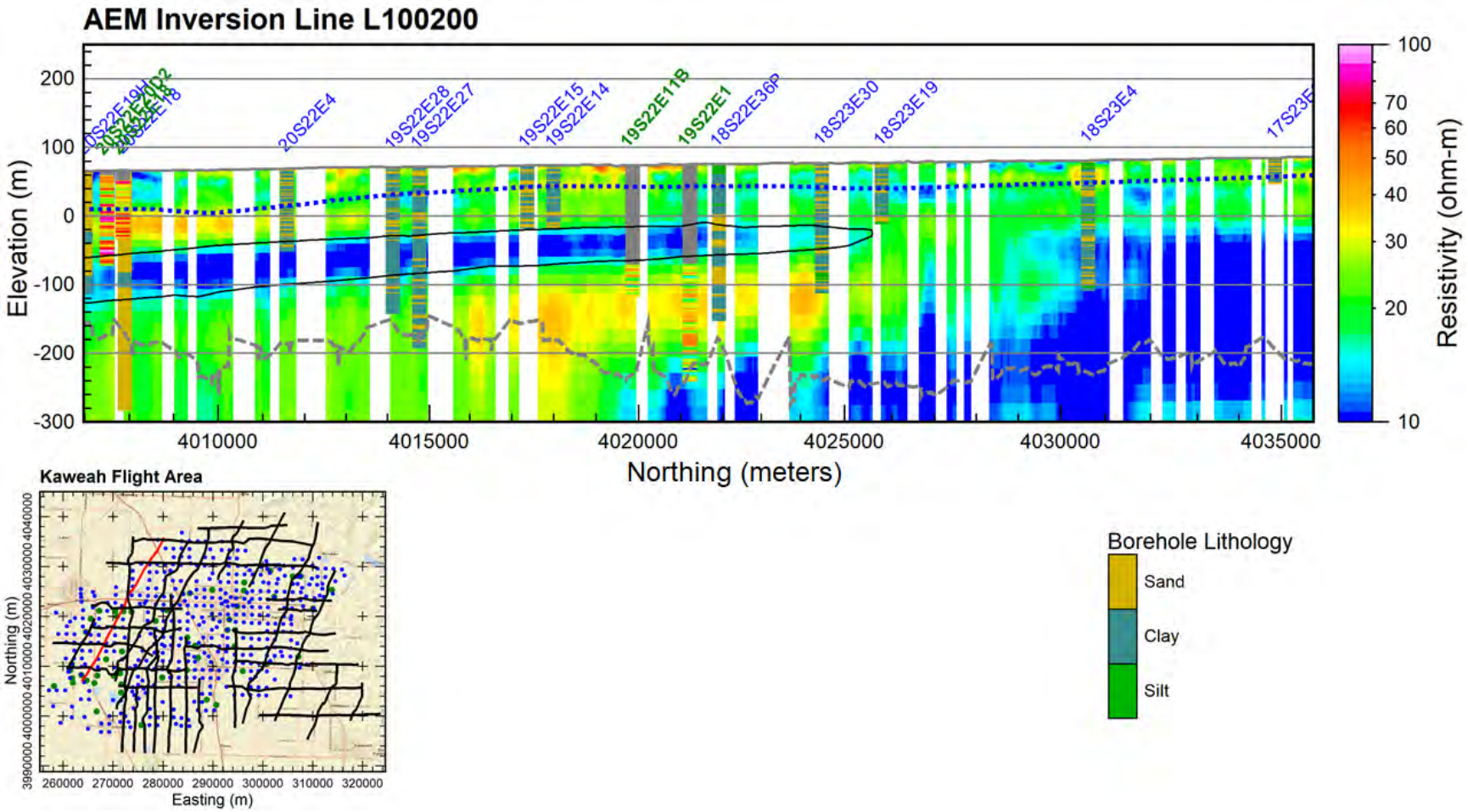

Figure 5-12. Comparison of borehole resistivity and lithology logs and AEM flight line L100200. The geophysical logs have green labels and the lithology logs have blue labels. The resistive zones on the geophysical logs *20S22E20D2*, *19S22E11B*, and *19S22E1* line up nicely with the resistive AEM inversion results. Also note the good lithology match of the logs that pass through the Corcoran Clay such as *19S22E28*, *19S22E27*, and even *18S22E36P* which is showing more of an interbedded nature in the area where the Corcoran thins out and terminates. Projection is NAD83, UTM 11N, meters, NAVD88 meters.

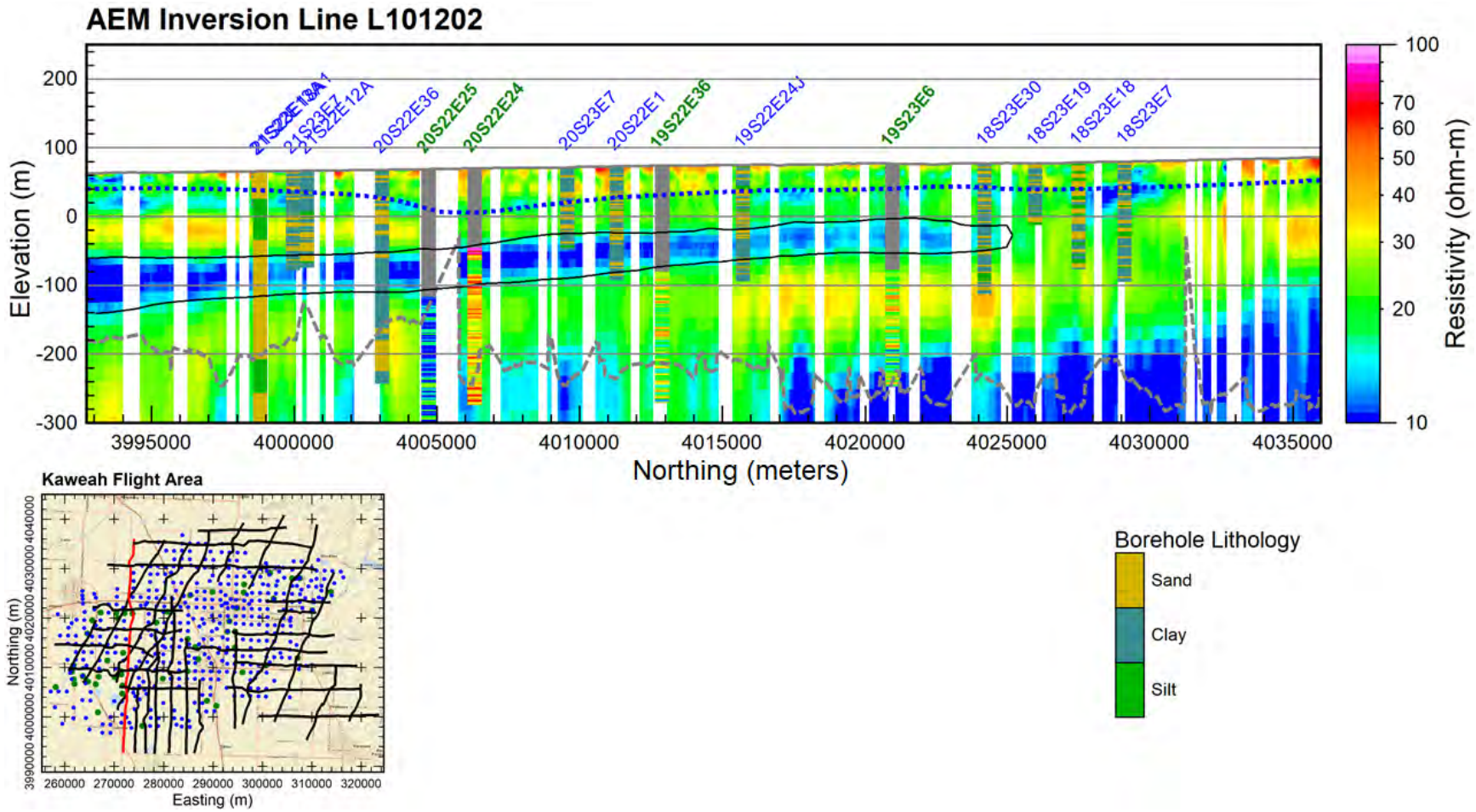

Figure 5-13. Comparison of borehole resistivity and lithology logs and AEM flight line L101202. The geophysical logs have green labels and the lithology logs have blue labels. The resistive zones on the geophysical logs *20S22E24*, *19S22E36*, and *19S23E6* line up nicely with the resistive (and conductive zones) in the AEM inversion results. Note also that geophysical log *20S22E25* does not match the inversion results at all, even to log *20S22E24* which is right next to it, which means that *20S22E25* is either not calibrated correctly or was not set up correctly prior to commencing the resistivity logging. There is a good match of most of the lithology logs that pass through the Corcoran Clay including *21S23E7*, *21S22E12A*, *20S22E36*, and *19S22E24J*. Projection is NAD83, UTM 11N, meters, NAVD88 meters.

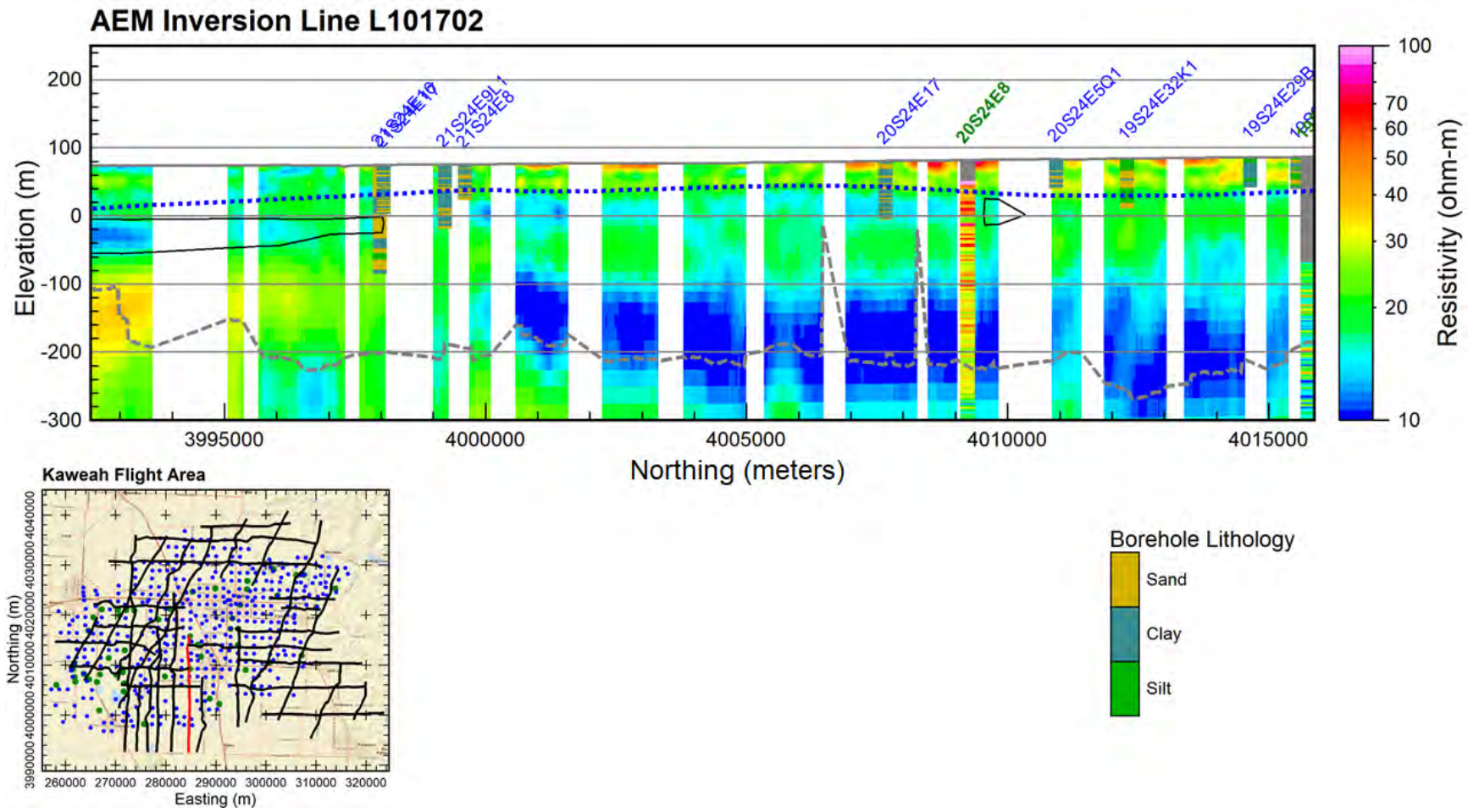

Figure 5-14. Comparison of borehole resistivity and lithology logs and AEM flight line L101702. The geophysical logs have green labels and the lithology logs have blue labels. The interbedded nature of the resistive and conductive zones on geophysical log *20S24E8* line up nicely with the AEM inversion results. There is a good match of most of the lithology logs that pass through the Corcoran Clay, or just beyond it, including *21S24E16*, *21S24E9L1*, *20S24E8*, and *19S24E32K1*. Projection is NAD83, UTM 11N, meters, NAVD88 meters.

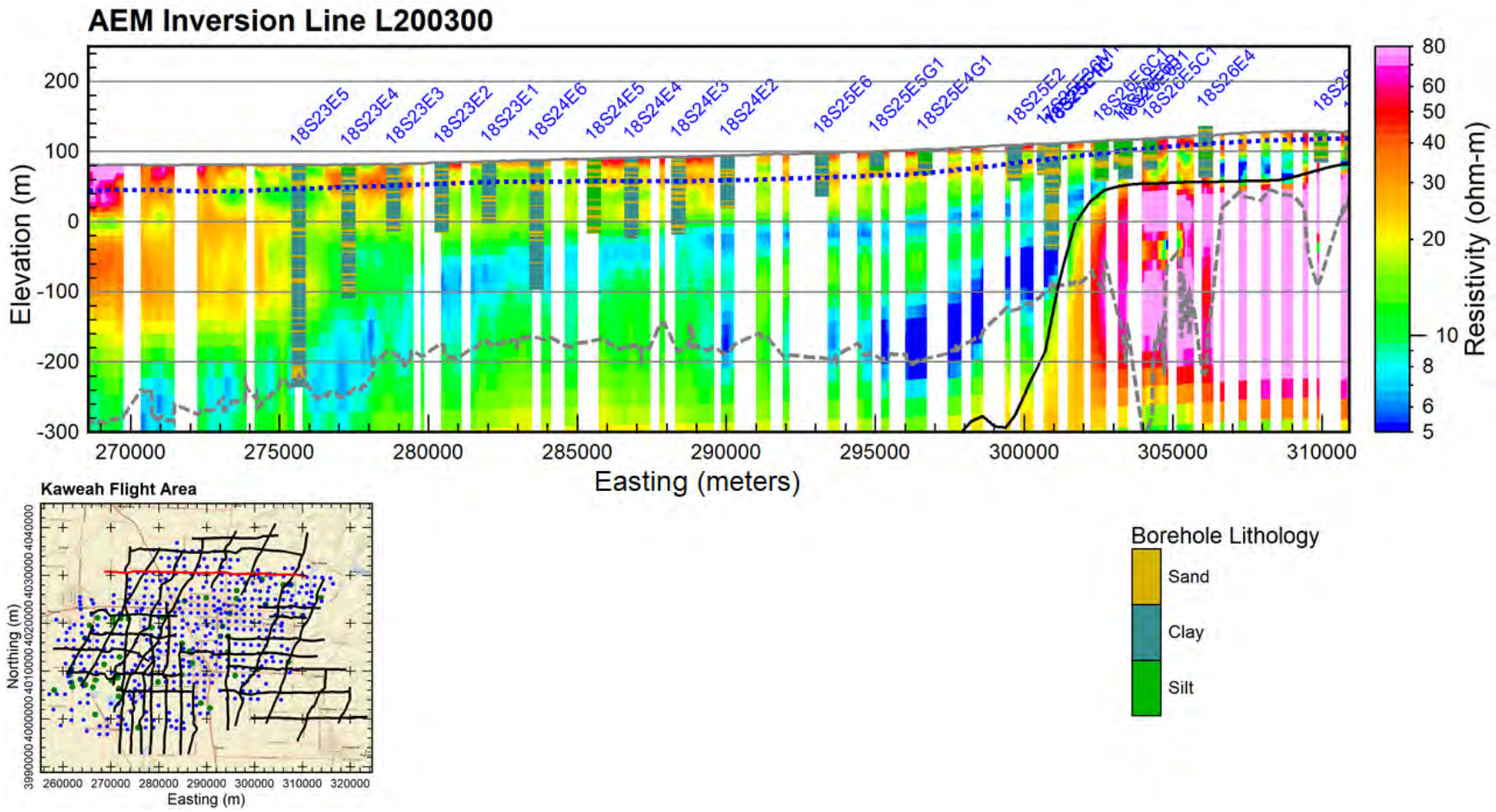

Figure 5-15. Comparison of borehole resistivity and lithology logs and AEM flight line L200300. The lithology logs have blue labels; there are no geophysical logs on this section. Note the pattern of the bottoms of the logs – most logs stop in the more resistive zone (coarser material) sitting above the conductive zone (very likely clay). A couple of the boreholes (*18S23E5* and *18S24E6*) were drilled through the clay and into the next coarse zone. Projection is NAD83, UTM 11N, meters, NAVD88 meters.

5.4 Create Interpretative Surface Grids

The Kaweah Subbasin AEM survey area surface elevation and thickness grids were produced by importing data such as a ground surface digital elevation model (DEM) and AEM interpreted point data of the AEM survey area and into ESRI's ArcMap where they were processed using the Spatial and Geostatistical Analyst extensions.

An elevation grid of the Kaweah Subbasin AEM survey area water table was produced in ArcMap using the Spatial Analyst extension. To create the grid, elevation contours representing the water table elevation during the fall of 2017 were downloaded from the California Department of Water Resources Groundwater Information Center Interactive Map Application (CA-DWR, 2018a). The contours were converted to a 30 m resolution (cell size) raster dataset with the 'Topo to Raster' tool available in ArcMap's Spatial Analyst extension and then converted to meters above sea level with ArcMap's raster calculator. Figure 5-16 is a map of the water table elevation within and surrounding the Kaweah Subbasin AEM survey area.

The top elevation, bottom elevation, thickness of, and depth to the Corcoran Clay raster grids were produced in ArcMap using the Geostatistical and Spatial Analyst extensions. To create the grids, over 600 data points with top and bottom elevation values were extracted from the AEM interpretation and input into ArcMap. The points were interpolated into a continuous surface using a kriging geostatistical model and exported to a 500 m cell size grid. The cell size is based on the approximate 5 km line spacing and 25 m down line spatial distribution of the point data. The resultant bottom elevation grid was subtracted from the top elevation grid to calculate the thickness of the Corcoran Clay. To calculate the depth to the Corcoran Clay, the 10 m resolution DEM was first masked with the top elevation grid so that the extent and cell size of the DEM were equal to the interpolated elevation grids. Then, the top elevation grid was subtracted from the masked, 500 m resolution DEM to produce a grid representing the depth to the Corcoran Clay. Figure 5-17, Figure 5-18, and Figure 5-19 are maps of the top elevation, depth to, and thickness of the Corcoran Clay within the Kaweah Subbasin AEM survey area.

The top elevation and depth to basement rock raster grids were also produced in ArcMap using both the Geostatistical and Spatial Analyst extensions. To the create the grids, over 550 data points with top elevation values of the basement rock were extracted from the AEM interpretation and input into ArcMap. The points were interpolated into a continuous surface using the kriging geostatistical model and exported to a 500 m cell size grid. The cell size is based on the approximate 5,000 m spacing across line and approximate 25 m down line spatial distribution of the point data. To calculate the depth to basement rock the 10 m resolution DEM was first masked with the basement top elevation grid so that the extent and cell size of the DEM equaled the interpolated top elevation grid. Then, the top elevation grid was subtracted from the masked, 500 m resolution, DEM resulting in a grid that represents the depth to basement rock. It is important to note that the top elevation of the basement rock was only calculated down to approximately -380 m and the depth to approximately 500 m due to the DOI of the AEM data collected; the basement rock extends further west than what the figures display. Figure 5-20 and Figure 5-21 are maps of the top elevation and depth to the basement rock within the Kaweah Subbasin AEM survey area, respectively.

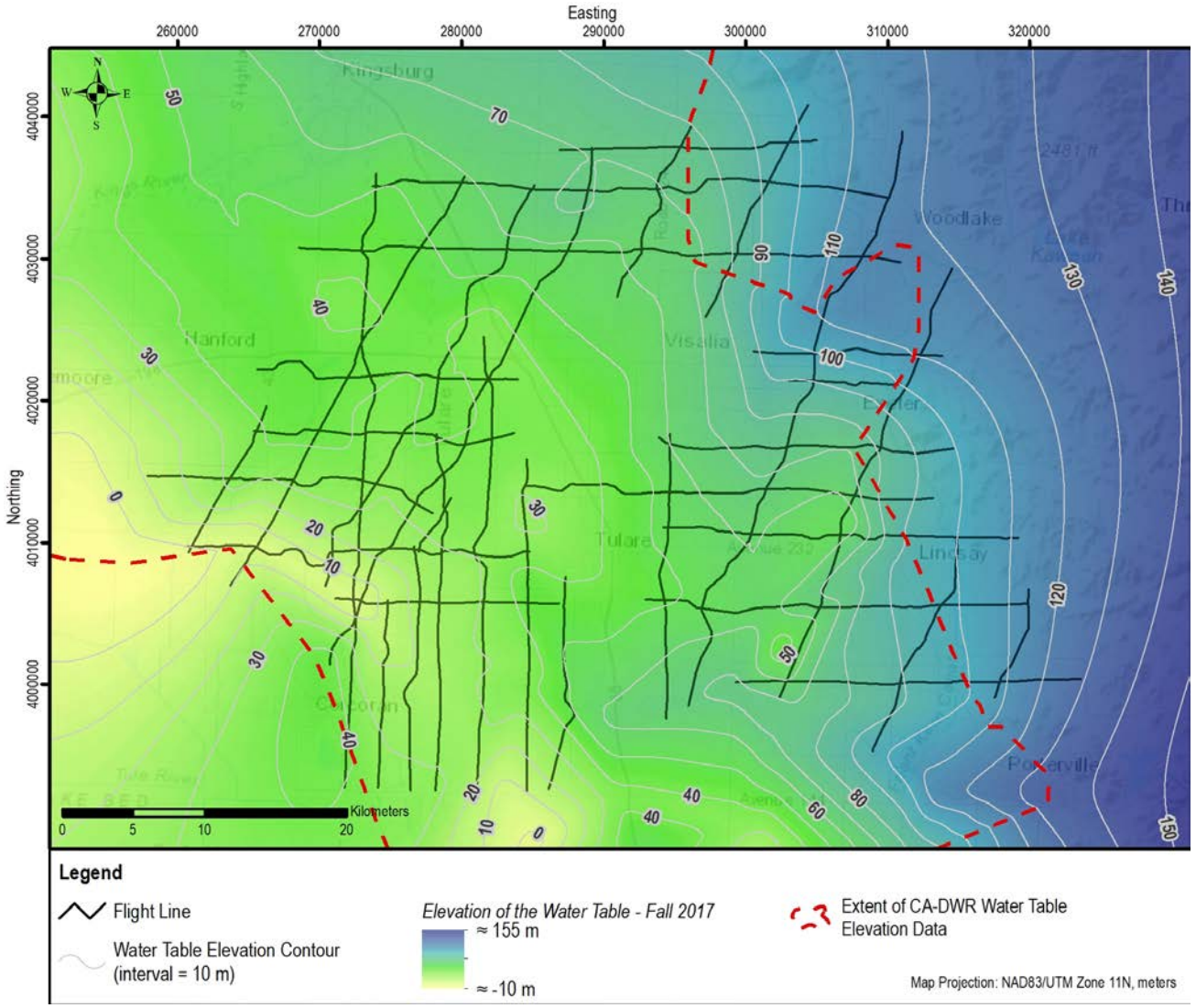

Figure 5-16. Map of the water table elevation during the fall of 2017 (CA-DWR, 2018a) within and surrounding the Kaweah Subbasin AEM survey area. The projection is NAD83 UTM Zone 11N (meters) and the elevation values are referenced to NAVD 88 (meters).

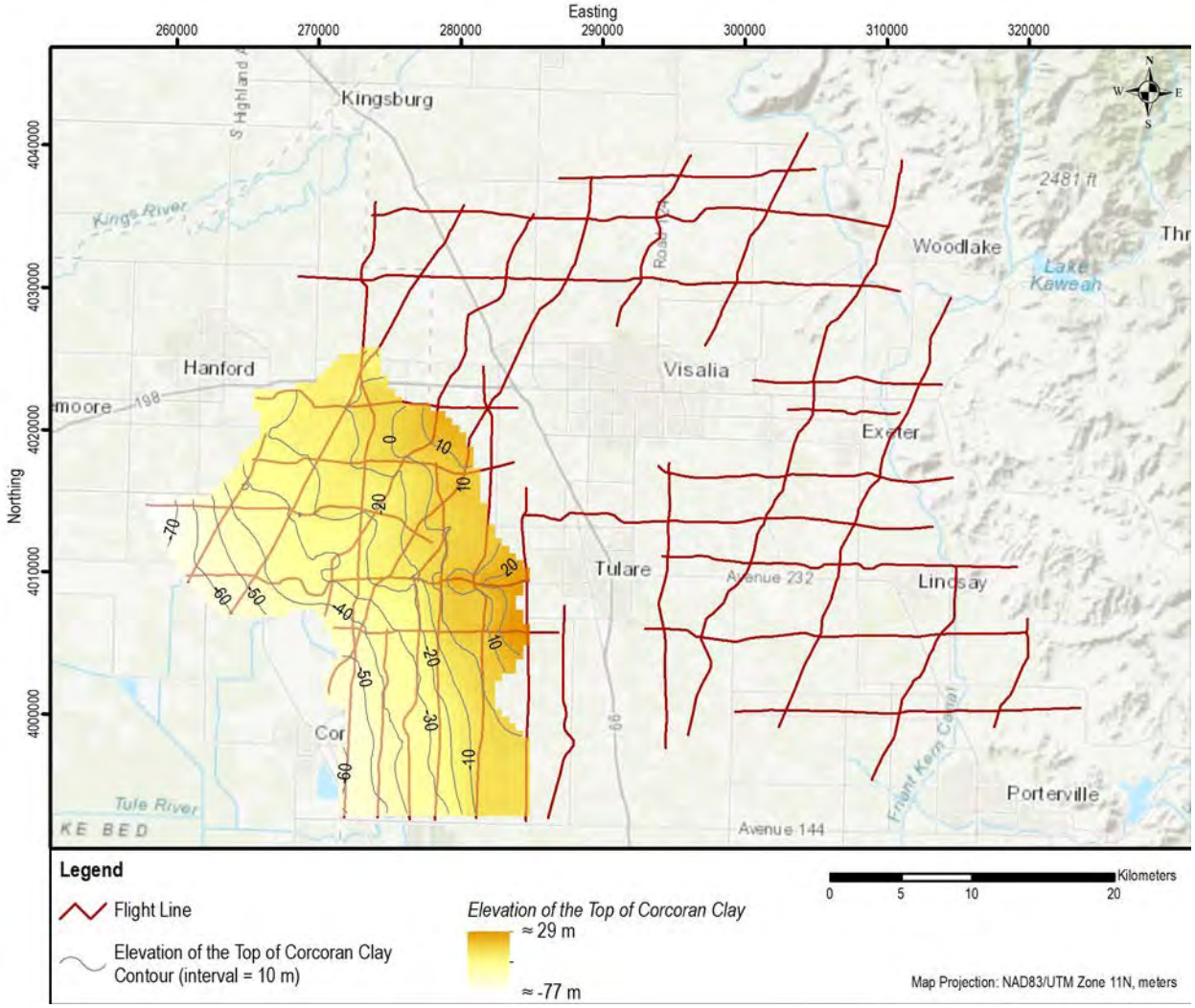

Figure 5-17. Map of the top elevation of the Corcoran Clay within the 2018 Kaweah Subbasin AEM survey area. The projection is NAD83 UTM Zone 11N (meters) and the elevation values are referenced to NAVD 88 (meters).

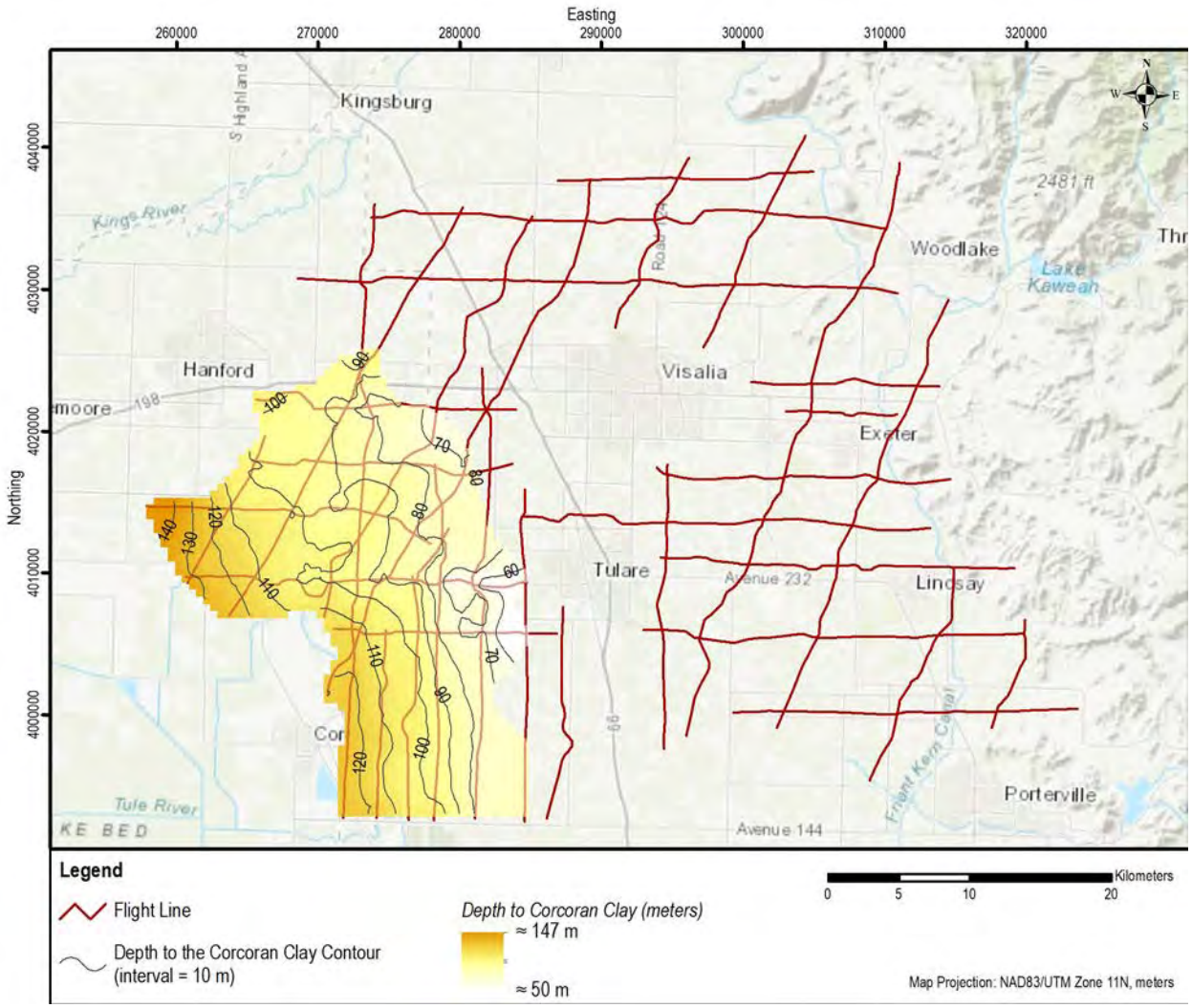

Figure 5-18. Map of the depth to the top of the Corcoran Clay within the 2018 Kaweah Subbasin AEM survey area. The projection is NAD83 UTM Zone 11N (meters) and the elevation values are referenced to NAVD 88 (meters).

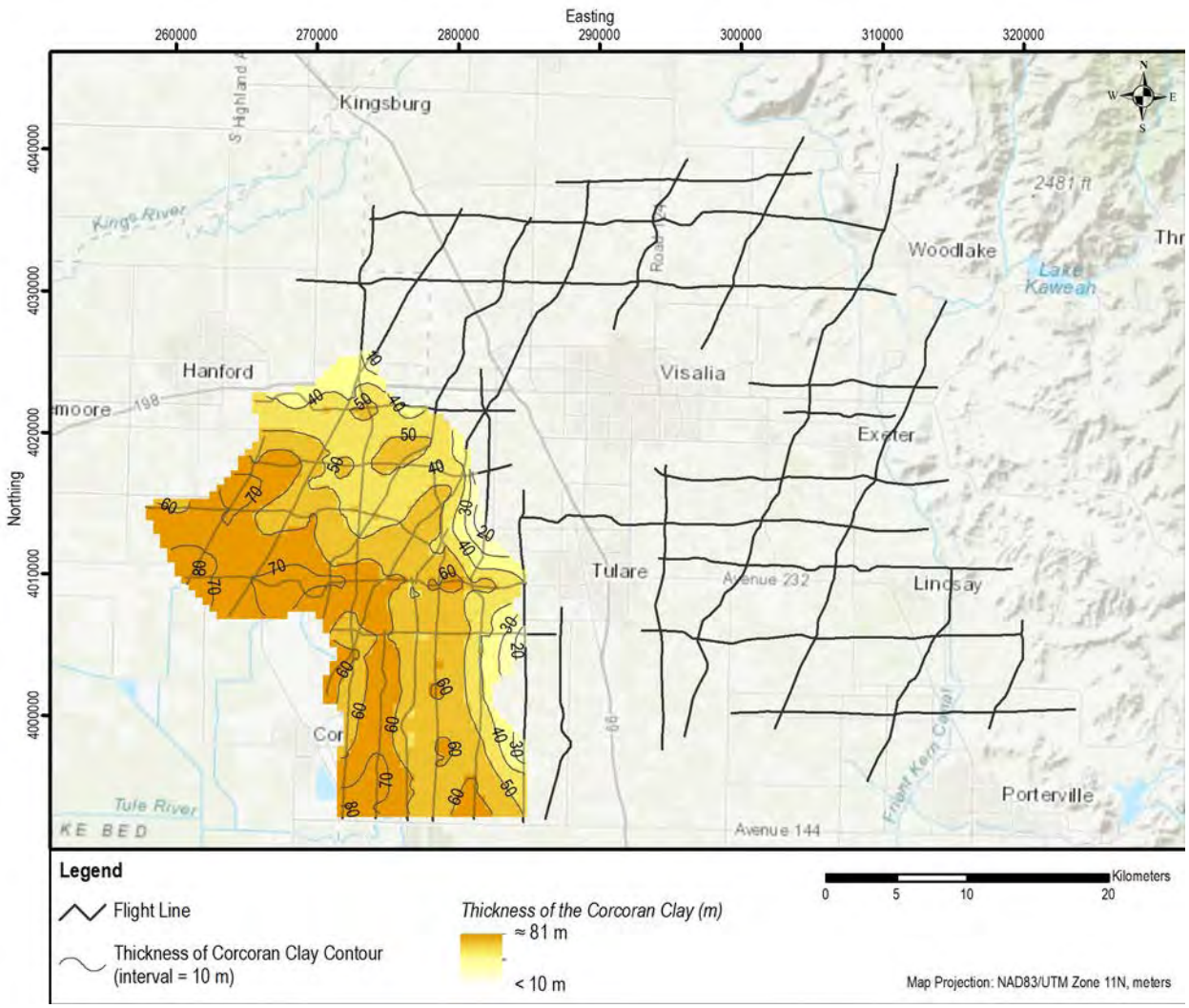

Figure 5-19. Map of the thickness of the Corcoran Clay within the 2018 Kaweah Subbasin AEM survey area. The projection is NAD83 UTM Zone 11N (meters) and the elevation values are referenced to NAVD 88 (meters).

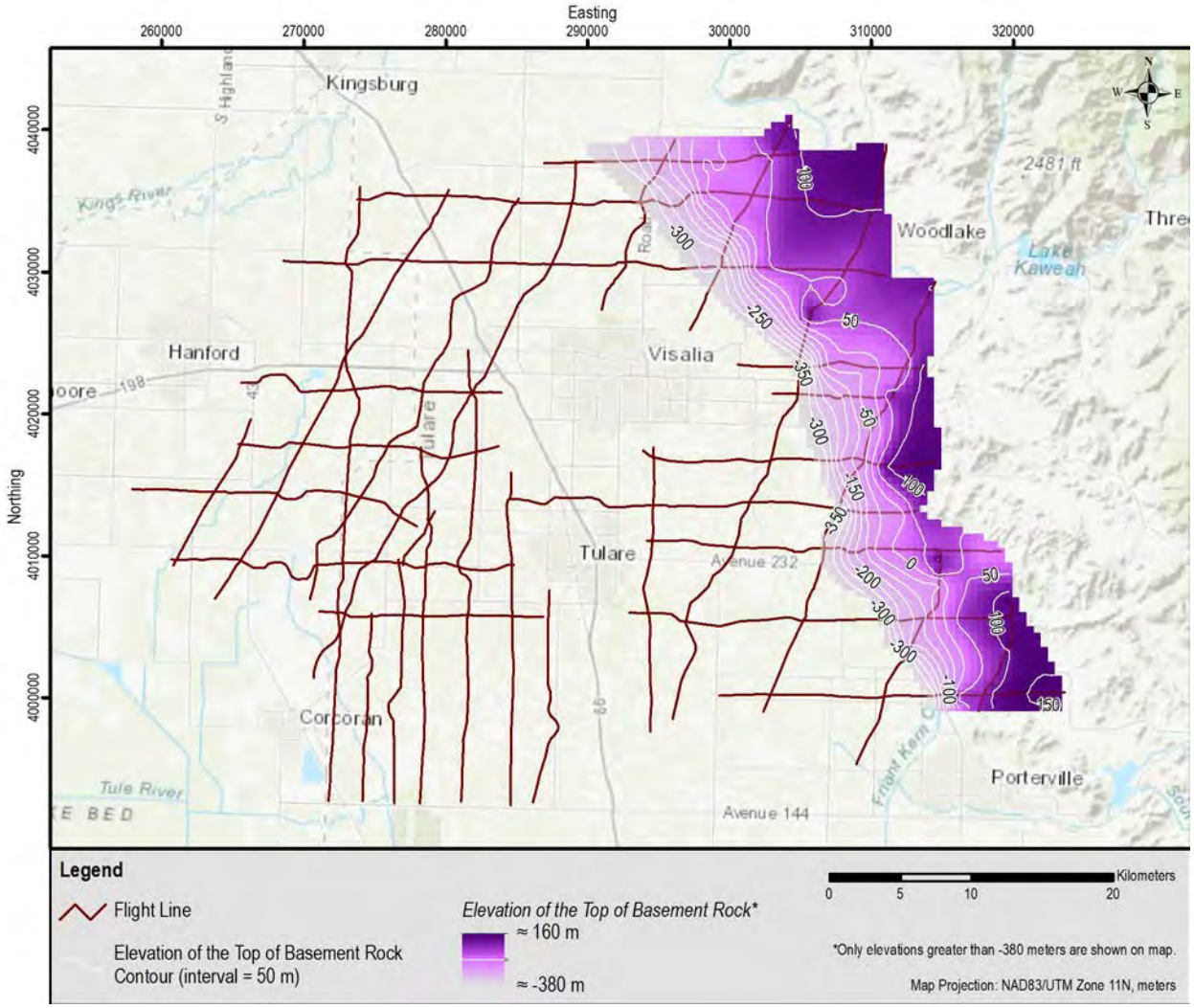

Figure 5-20. Map of the top elevation of the basement rock within the 2018 Kaweah Subbasin AEM survey area. The projection is NAD83 UTM Zone 11N (meters) and the elevation values are referenced to NAVD 88 (meters).

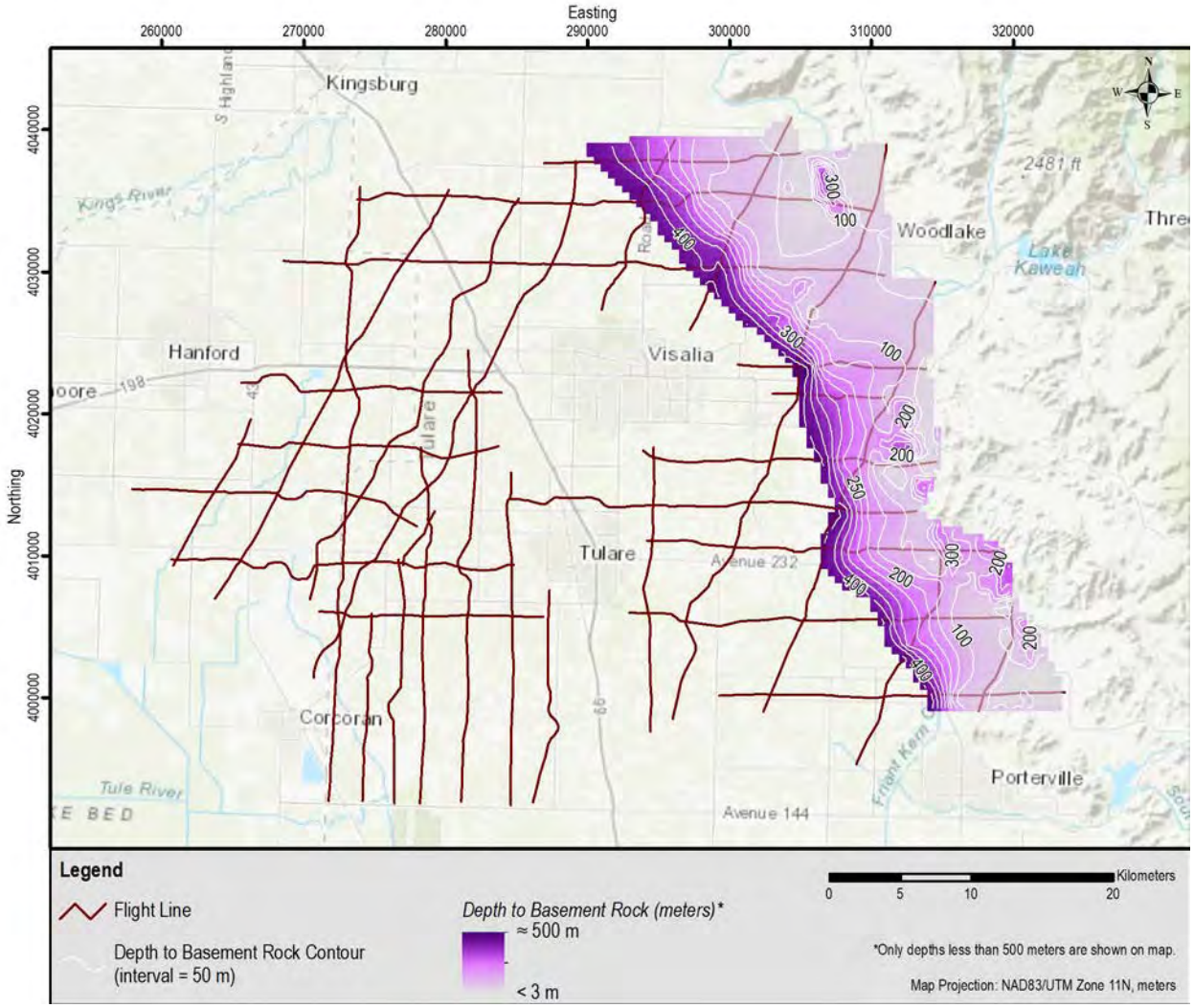

Figure 5-21. Map of the depth to the top of the basement rock within the 2018 Kaweah Subbasin AEM survey area. The projection is NAD83 UTM Zone 11N (meters) and the elevation values are referenced to NAVD 88 (meters).

5.5 Comparison of 2018 SkyTEM 312 with 2015 SkyTEM 508 AEM Inversion Results

Part of the analysis of the Kaweah Subbasin AEM investigation was a comparison between the AEM earth-model inversion results for the 2018 survey with the SkyTEM 312 and the 2015 survey that acquired data with the SkyTEM 508 just west and north of Tulare, California (Knight et al., 2018), the deeper imaging system available at the time (and which is no longer available from SkyTEM).

Figure 5-22 presents the AEM inversion results for 2018 AEM flight line L100400 and 2015 flight line L100401. There is a little finer detail in the near-surface layers for the 2018 312 inversion results than for the 2015 508 inversion results, but otherwise, they match up very well. The Corcoran Clay is easily identified on both profiles. However, the 2015 508 system is able to image deeper – the 2015 508 profile vertical axis has been set to start at -450 m versus -350 m for the 2018 SkyTEM 312 system. Note the resistive zones at an elevation of about -300 m in both the 312 and 508 profiles representing coarser sedimentary material at a northing of about 4005000.

A comparison of 2018 AEM flight line L100600 and 2015 flight line L100601 is presented in Figure 5-23. Again, there is a little more detail in the near-surface for the 2018 SkyTEM 312 inversion results than for the 2015 SkyTEM 508 inversion results. Otherwise, they match up very well. The Corcoran Clay is easily identified on both profiles. The 2015 508 system is able to image deeper – the 2015 508 profile vertical axis starts at -450 m versus -350 m for the 2018 312 system. Also, again note the resistive zones at an elevation of about -250 m in both profiles presenting the 312 and 508 results which represent coarser sedimentary material at northings of about 4000000-4005000.

Figure 5-24 presents a comparison of AEM inversion results for 2018 AEM flight line L101501 and 2015 flight line L100501. As note before, there is a more detail in the near-surface for the 2018 312 than for the 2015 508 inversion results, but otherwise, they match up very well. The Corcoran Clay is easily identified on both profiles, but is observed to terminate at the north end of 2015 L100501. The slight difference in location of the northern ends of the lines relative to the spatial extent of the Corcoran Clay is the reason for this difference in the observed Corcoran Clay extent. The 2015 508 system is able to image deeper – the 2015 508 profile vertical axis starts at -450 m versus -350 m for the 2018 312 system. Again, note the presence of the resistive zones at depth indicated by both systems representing coarser sedimentary material at northings of about 4000000-4006000.

Finally, Figure 5-25 presents a comparison of AEM inversion results for 2018 AEM flight line L200701 and 2015 flight line L100401. Note that 2018 L200701 is the approximately 5 km repeat line located directly on a 2015 AEM flight line, L100401, along which an electrical resistivity profile may have been acquired. The sections match up very well. The Corcoran Clay is easily identified on both profiles.

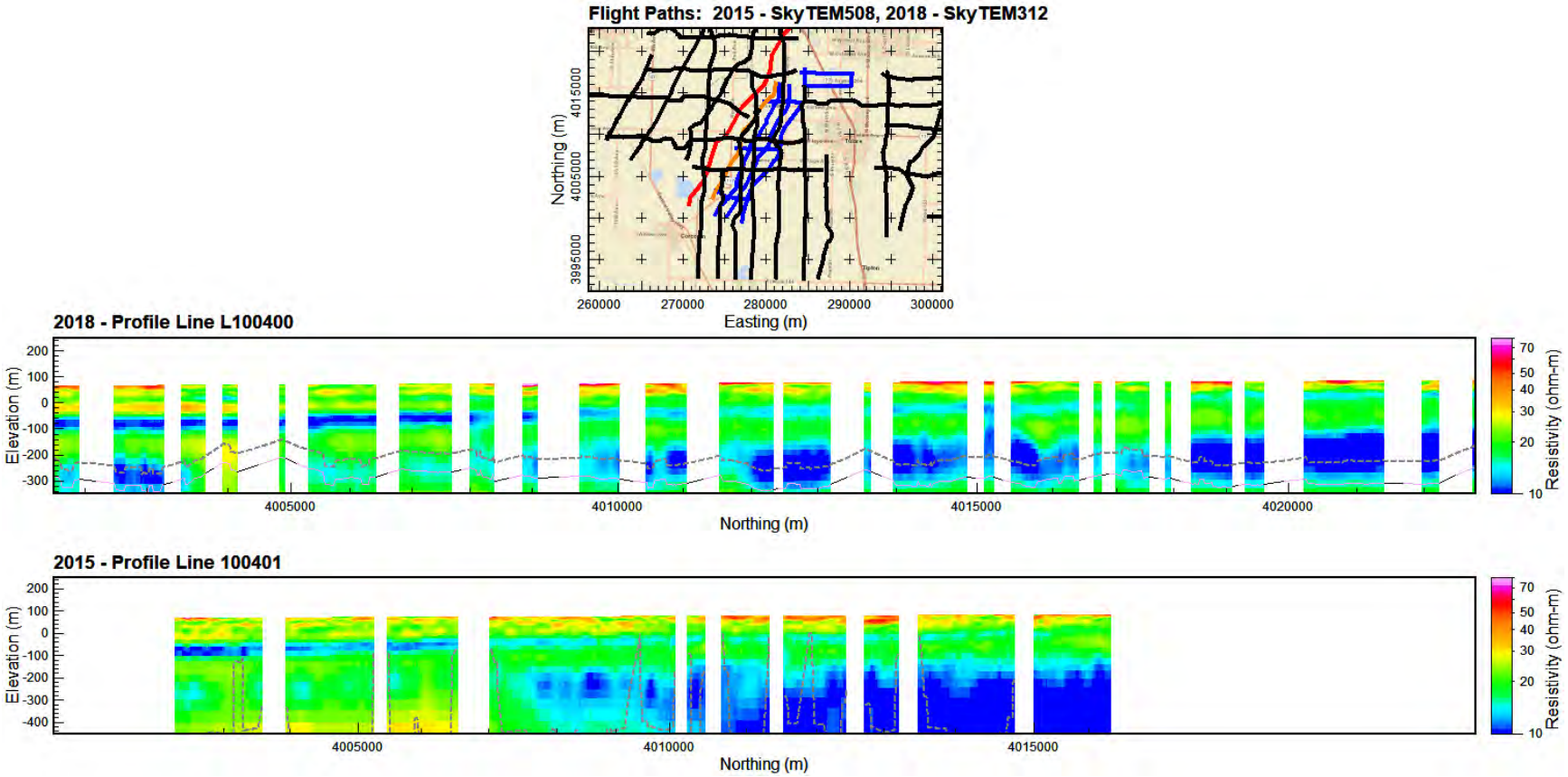

Figure 5-22. Comparison of 2018 SkyTEM 312 (black lines) and the 2015 SkyTEM 508 (blue lines) AEM inversion results for 2018 AEM flight line L100400 (top profile, red line in location map) and 2015 flight line 100401 (bottom profile, orange line in location map). There is a little more detail in the near-surface for the 2018 312 inversion results than for the 2015 508 inversion results, but otherwise, they match up very well. The Corcoran Clay is easily identified on both profiles. However, the 2015 508 system is able to image deeper – the 2015 508 profile vertical axis starts at -450 m versus -350 m for the 2018 312 system. Note the resistive zones at depth in both the 312 and 508 systems representing coarser sedimentary material at a northing of about 4005000. The projection is NAD83, UTM 11N, meters, NAVD88 meters.

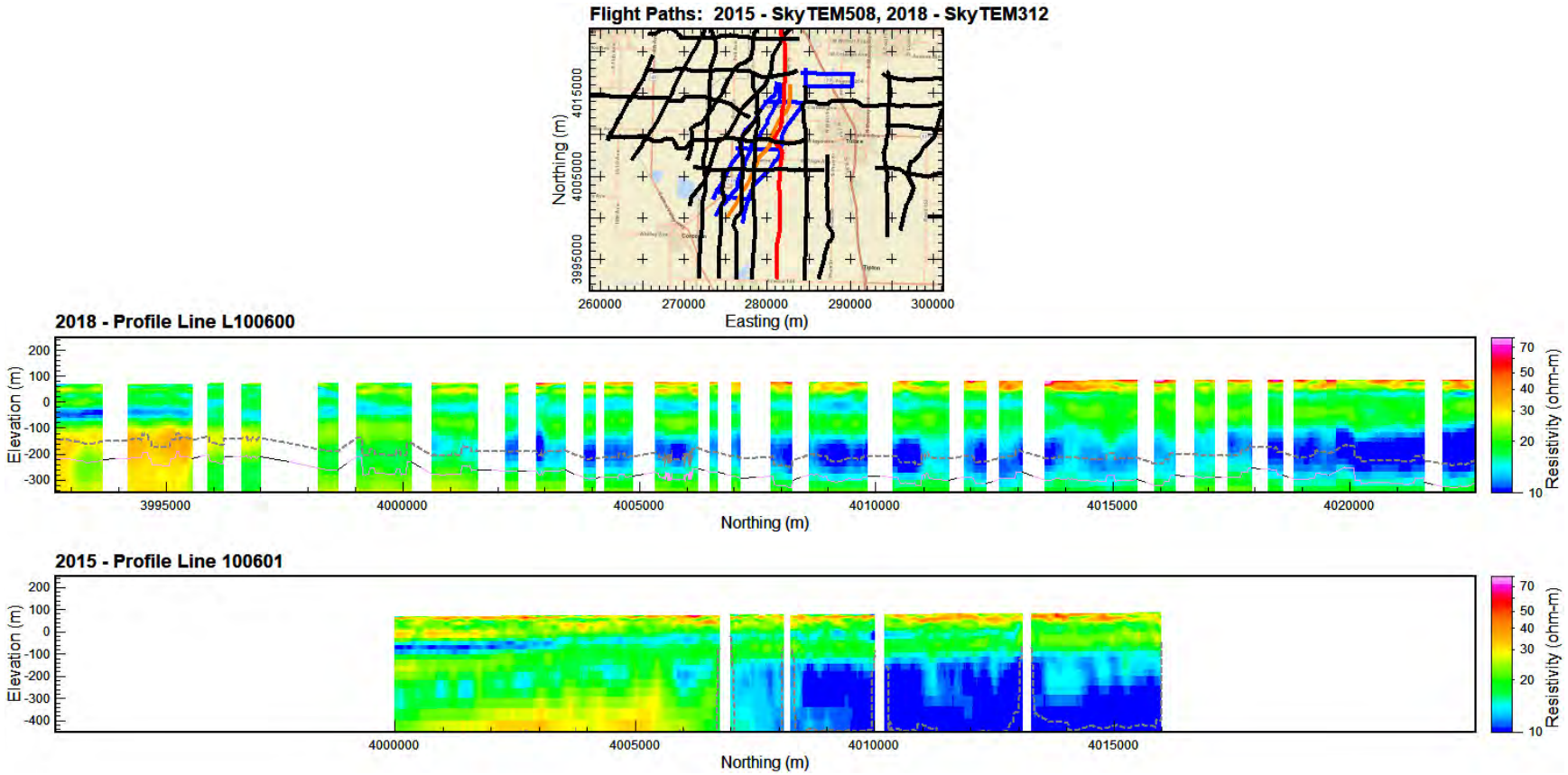

Figure 5-23. Comparison of 2018 SkyTEM 312 (black lines) and the 2015 SkyTEM 508 (blue lines) AEM inversion results for 2018 AEM flight line L100600 (top profile, vertical red line in location map) and 2015 flight line 100601 (bottom profile, southwest-northeast orange line in location map). There is a little more detail in the near-surface for the 2018 312 inversion results than for the 2015 508 inversion results, but otherwise, they match up very well. The Corcoran Clay is easily identified on both profiles. The 2015 508 system is able to image deeper – the 2015 508 profile vertical axis starts at -450 m versus -350 m for the 2018 312 system. Note the resistive zones at depth in both the 312 and 508 systems representing coarser sedimentary material at northings of about 4000000-4005000. The projection is NAD83, UTM 11N, meters, NAVD88 meters.

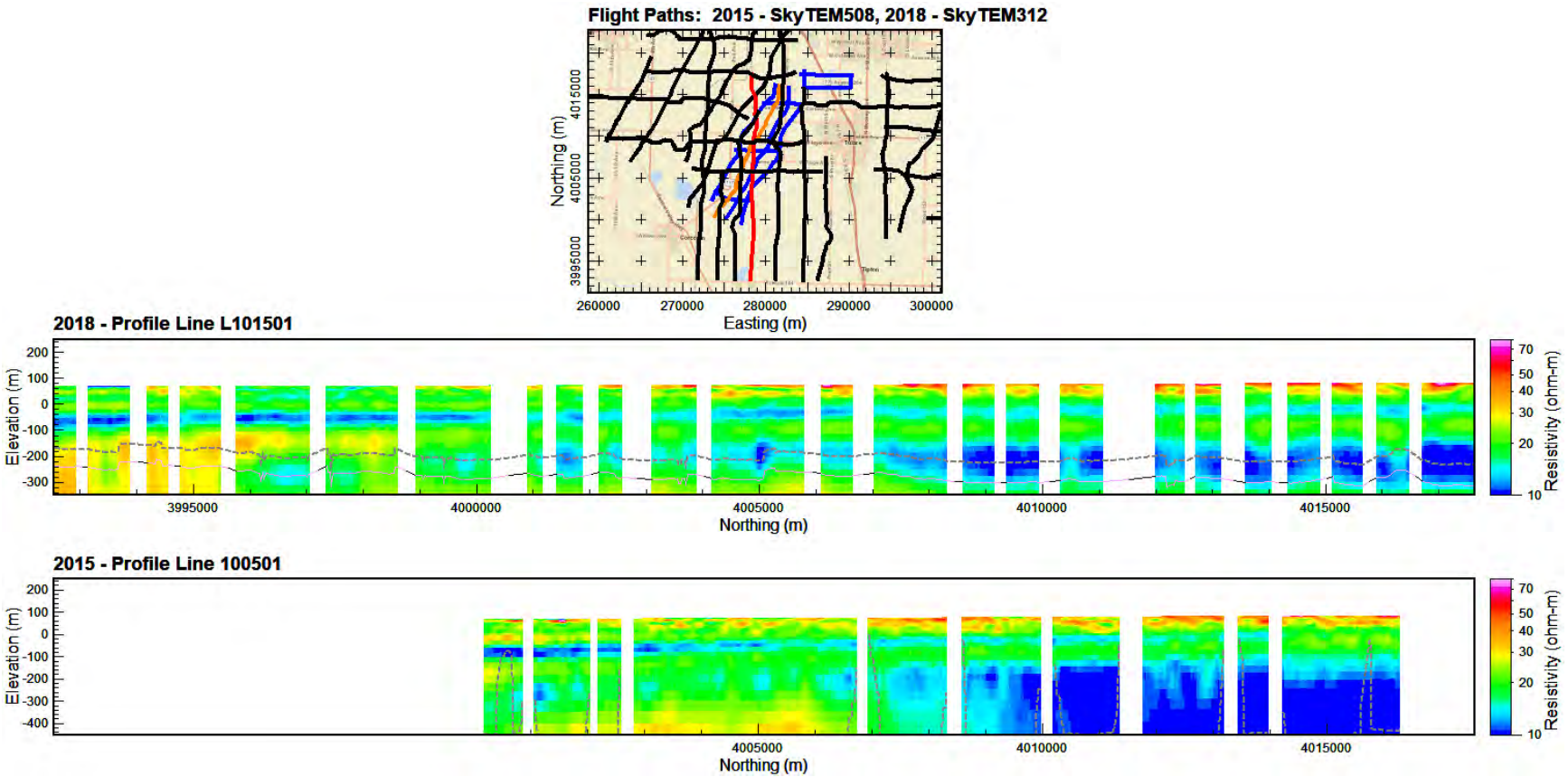

Figure 5-24. Comparison of 2018 SkyTEM 312 (black lines) and the 2015 SkyTEM 508 (blue lines) AEM inversion results for 2018 AEM flight line L101501 (top profile, vertical red line in location map) and 2015 flight line 100501 (bottom profile, southwest-northeast orange line in location map). There is a little more detail in the near-surface for the 2018 312 inversion results than for the 2015 508 inversion results, but otherwise, they match up very well. The Corcoran Clay is easily identified on both profiles, but is observed to terminate at the north end of 2015 L100501. The slight difference in location of the northern ends of the lines relative to the spatial extent of the Corcoran Clay is the reason for this difference in the Corcoran Clay extent. The 2015 508 system is able to image deeper – the 2015 508 profile vertical axis starts at -450 m versus -350 m for the 2018 312 system. Note the resistive zones at depth in both the 312 and 508 systems representing coarser sedimentary material at northings of about 4000000-4006000. The projection is NAD83, UTM 11N, meters, NAVD88 meters.

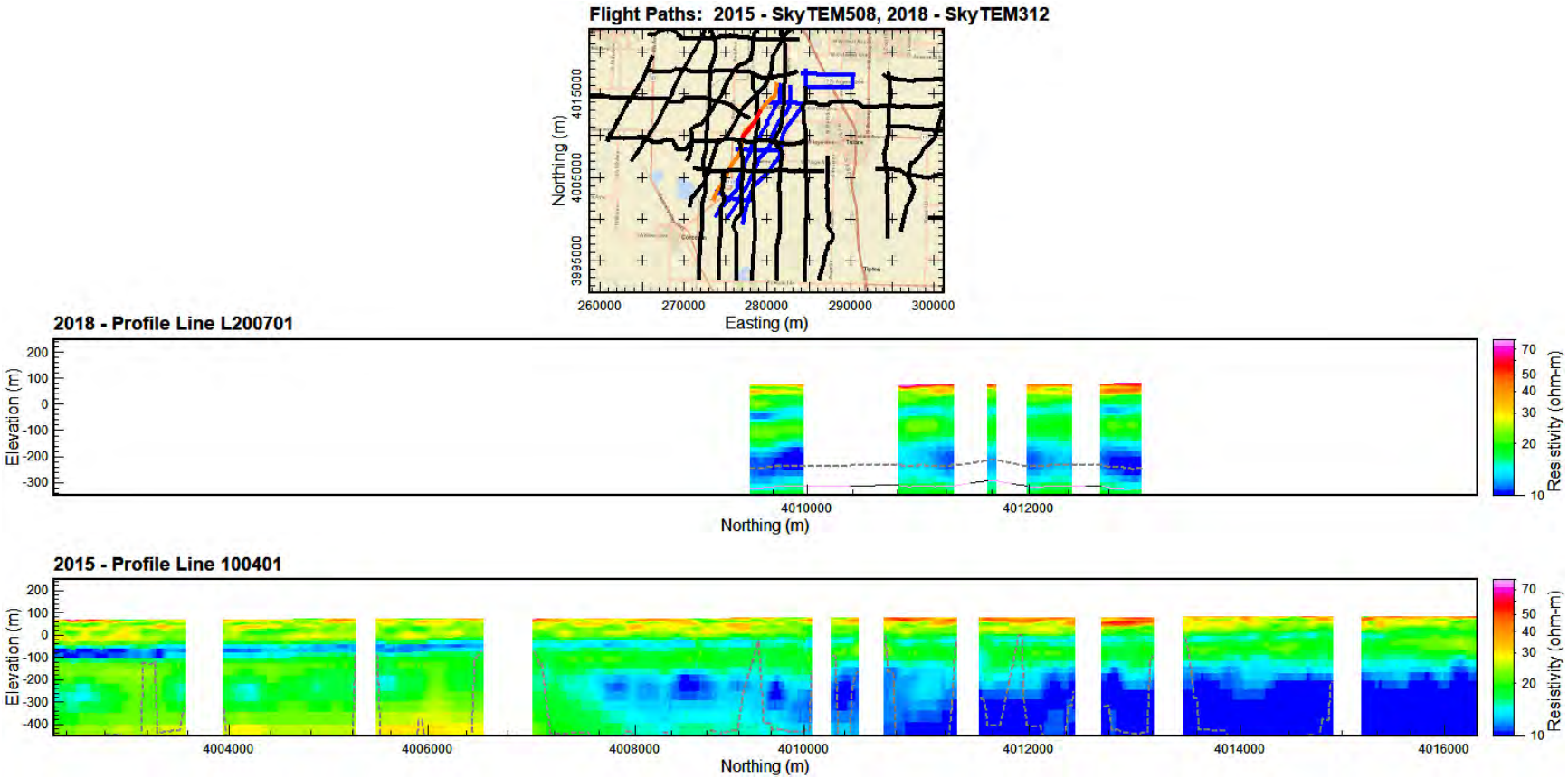

Figure 5-25. Comparison of 2018 SkyTEM 312 (black lines) and the 2015 SkyTEM 508 (blue lines) AEM inversion results for 2018 AEM flight line L200701 (top profile, short red line in location map overlying the orange line) and 2015 flight line 100401 (bottom profile, southwest-northeast orange line in location map). 2018 L200701 is the approximately 5 km repeat line located directly on a 2015 AEM flight line L100401. The sections match up very well. The Corcoran Clay is easily identified on both profiles. The projection is NAD83, UTM 11N, meters, NAVD88 meters.

5.6 Resistivity-Lithology Relationship

A critical aspect of a geophysical survey, for whatever purpose, is assessing the nature of the material detected by the geophysical method applied in the investigation. In regard to the Kaweah Subbasin AEM survey, an assessment of the lithologic character of the sediments above and below the water table was conducted by Knight et al. (2018) for the Tulare 2015 SkyTEM 508 survey (Figure 5-26). Note that the resistivity ranges listed in Figure 5-26 for the different lithologies overlap (e.g. Clay 8-31 ohm-m, Sand and Gravel 25-150 ohm-m). Thus, in application of these resistivity ranges for the lithologies listed to the Kaweah Subbasin AEM survey inversion results, the midpoint between range overlaps were used as the range bounds. That is, if the ranges above the water table overlap between 25-31 ohm-m, then the midpoint would be 28 ohm-m. Similarly, for the ranges below the water table in Figure 5-26: (6-18, 12-22) become (6-15,15-22) and (12-22,17-43) become (15-19, 19-43). For the full Kaweah Subbasin AEM survey, using the ranges from the Tulare Study (Knight et al., 2018) and extending the upper and lower range limits to the full range of inverted resistivities, the resulting ranges and color scheme for the Kaweah Subbasin AEM survey are presented in Figure 5-27. This color scale was been applied to the AEM inversion results and an AEM lithological interpretation was developed. Several examples are presented below. The rest of the flight line profiles are located in Appendix 1 – 2D Profiles.

Range of Resistivity Values Determined for the Lithologic Units Using Method 2 and from the Histogram of All Resistivity Values in the Resistivity Model

Resistivity Range (Ω m)		Interpreted Lithology
Above the water table		
8	31	Clay
25	150	Sand and gravel
Below the water table		
6	18	Clay
12	22	Mixed fine and coarse
17	43	Sand and gravel

Figure 5-26. Table 2 from Knight et al. (2018) delineating a resistivity to lithology relationship for unsaturated and saturated sediments above and below the water table in the Tulare, CA area.

	Clay	Mixed Fine & Coarse	Sand and Gravel
Unsaturated	(0.1 - 28 ohm-m)		(28 - 500 ohm-m)
Saturated	(0.1 - 15 ohm-m)	(15 - 19 ohm-m)	(19 - 500 ohm-m)

Figure 5-27. Plot displaying the resistivities by major lithological material color categories (green – clay, yellowish green – mixed fine and coarse, orange – sand and gravel).

Examples of lithological interpretations of the Kaweah Subbasin AEM inversion results are presented for AEM flight lines L200300 (Figure 5-28), L200401 (Figure 5-29), L200200 (Figure 5-30), L2001001 (Figure 5-31), and L100600 (Figure 5-32). The interpreted lithologies for different materials including Corcoran Clay, undifferentiated Clay material, Sand and Gravel, and Basement materials are indicated on the sections. On L200300 (Figure 5-28), while the Sand and Gravel deposit on the western end of the line has the appearance of an erosional channel feature, this can't be confirmed with the current set of data because of the reconnaissance nature of the flight lines. The lithological interpretation along AEM flight line L2001001 (Figure 5-31) shows the Corcoran Clay occurs across the length of the line while that for flight line L100600 (Figure 5-32) shows that the Corcoran Clay terminates towards the northern end of the line.

The next set of examples of the lithological interpretation of the Kaweah Subbasin AEM inverted earth models are presented as 3D fence diagrams, with views from different directions (the view in Figure 5-33 looks north, Figure 5-34 looks south, and in Figure 5-35 the view is to the east). Again, examples of the different lithologies are marked in places including the Corcoran Clay, undifferentiated Clay material, Sand and Gravel, and Basement materials. The Sand and Gravel zone on the western side of the survey area (right side in Figure 5-34) may represent the edge of a large paleochannel or, at the least, a coarse zone moving into the San Joaquin Valley.

The extent of the Corcoran Clay is exhibited in Figure 5-36 using the same color scheme as is used for Clay in the rest of the interpretation. A more greying color is applied to the same Corcoran Clay extent in Figure 5-37 in order to better view the bounds of the unit.

The Fugro West (2007) cross-sections A-F are next added to the 3D fence diagram view. Figure 5-38, with a view looking towards the north, allows for comparison of the nature of the Corcoran Clay on the west side of the survey area and the Basement materials on the east side. They compare very well. The view in Figure 5-39 is a magnification of the west end of the C-C' cross-section in order to compare the Corcoran Clay on the C-section and the 2018 Kaweah Subbasin AEM interpreted lithology results. Likewise, Figure 5-40 presents a view of the combined 3D fence diagram looking to the southwest. With this view it is clear that the outline of the basement on A-A' matches that of the AEM basement lithology interpretation. What is also clear is the Fugro West (2007) cross-section F-F' is not congruent with either cross-section A-A' or the AEM interpreted results. Finally, Figure 5-41 is a view of the combined 3D fence diagram looking towards the southeast. Again, it is easy to note the good agreement between the Fugro West (2007) interpretations on cross-sections and the 2018 Kaweah Subbasin AEM interpreted lithologies, for example the depth, thickness, westerly dip, and character of the Corcoran Clay.

As mentioned above, the rest of the lithological interpretations of the AEM inversion results are located in Appendix 1/2D Profiles.

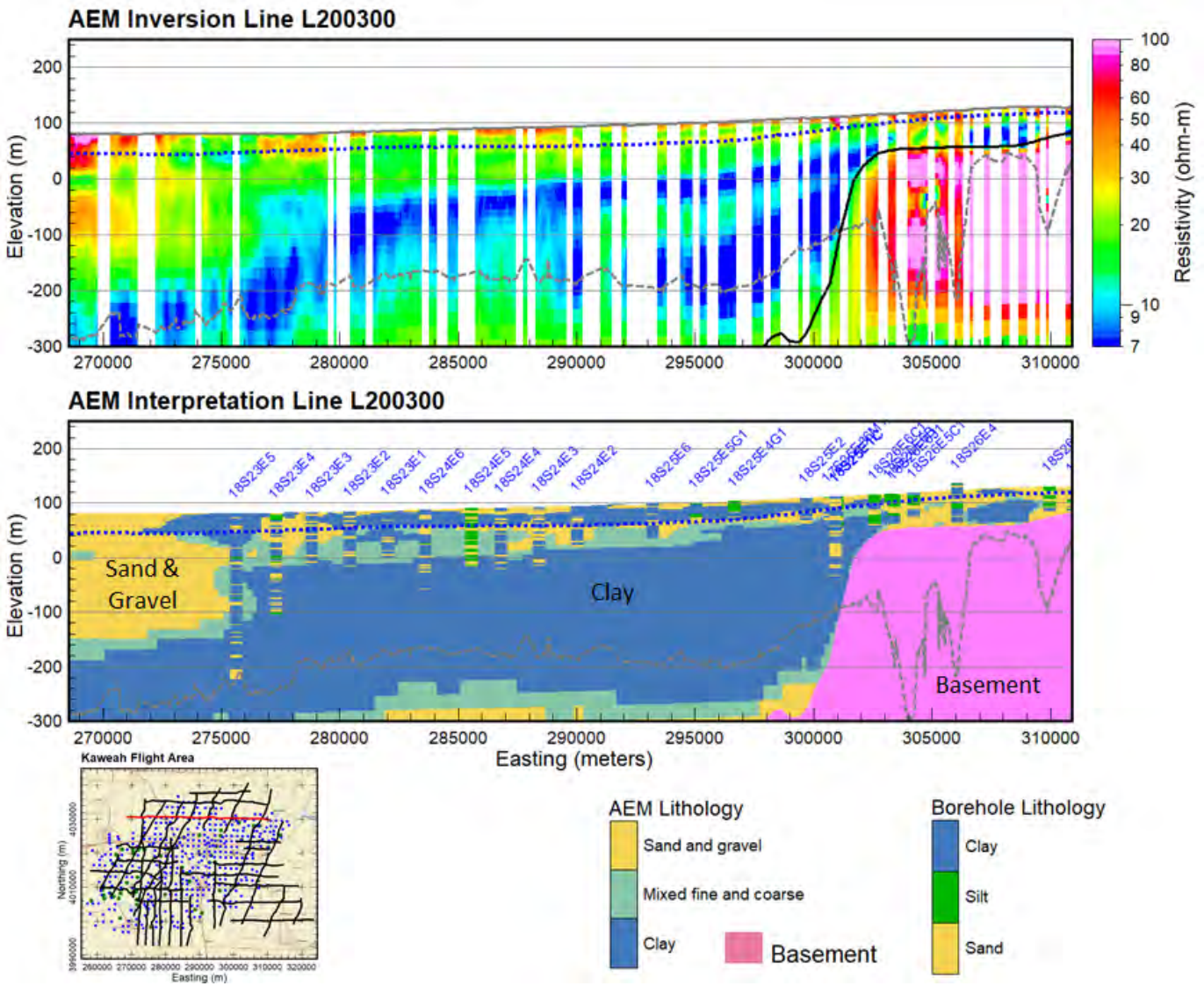

Figure 5-28. Lithological interpretation of Kaweah Subbasin AEM flight line L200300 in the bottom profile. The dotted blue line is the Fall 2017 water table (CA-DWR, 2018a). The interpreted lithologies for different materials are indicated. Projection is NAD83, UTM 11N, meters, NAVD88 meters.

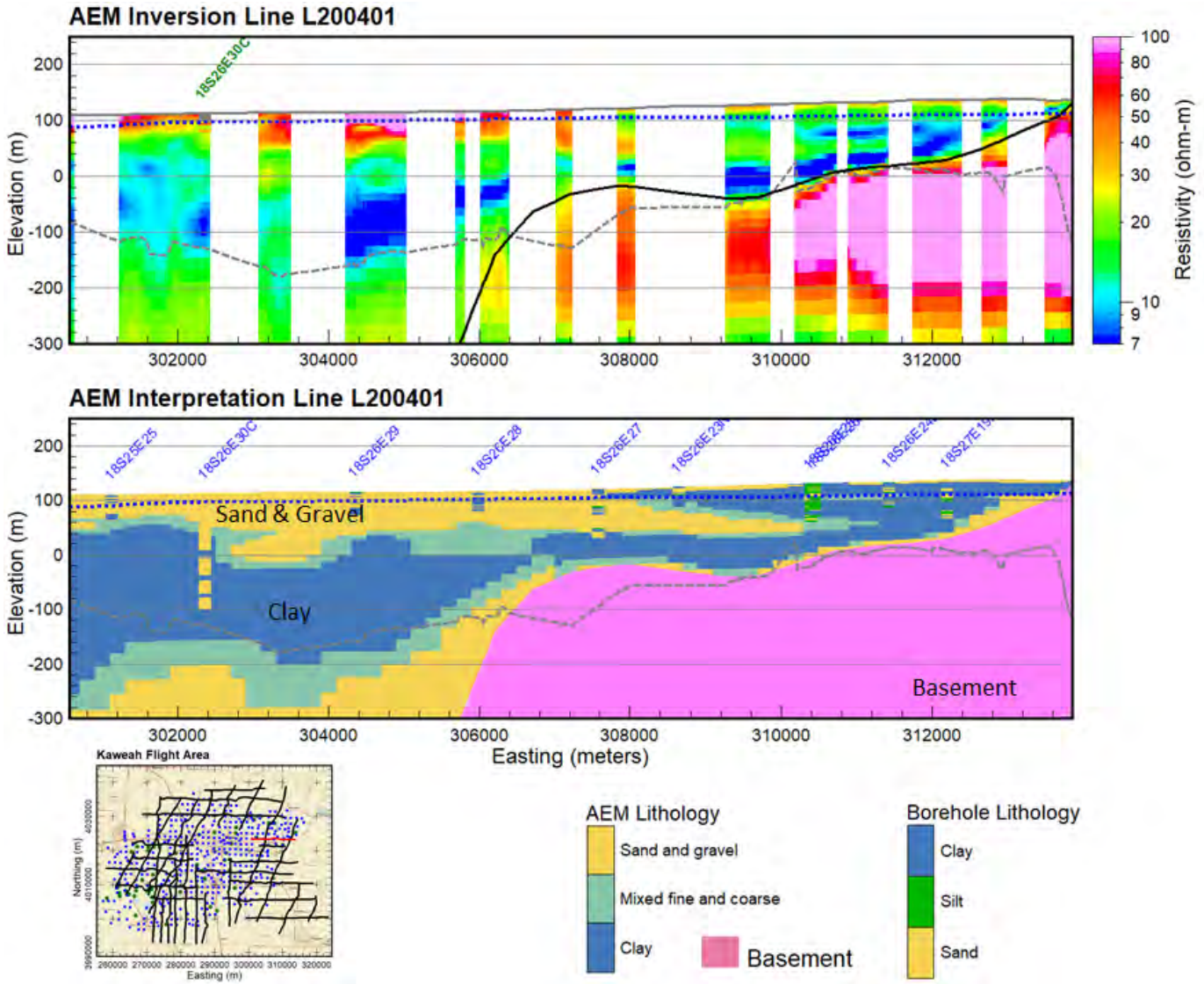

Figure 5-29. Lithological interpretation of Kaweah Subbasin AEM flight line L200401 in the bottom profile. The dotted blue line is the Fall 2017 water table (CA-DWR, 2018a). The interpreted lithologies for different materials are indicated. Projection is NAD83, UTM 11N, meters, NAVD88 meters.

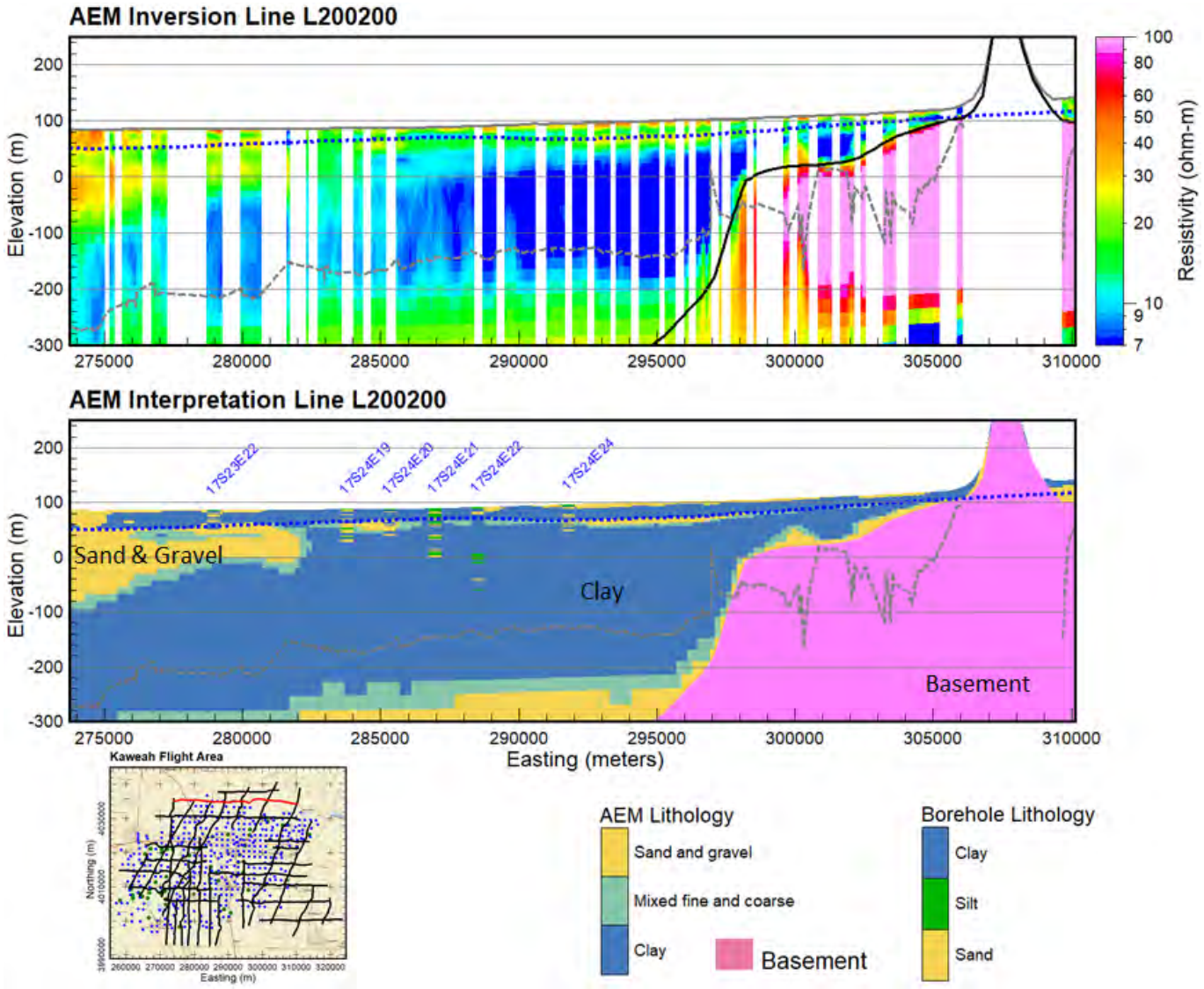

Figure 5-30. Lithological interpretation of Kaweah Subbasin AEM flight line L200200 in the bottom profile. The dotted blue line is the Fall 2017 water table (CA-DWR, 2018a). The interpreted lithologies for different materials are indicated. Projection is NAD83, UTM 11N, meters, NAVD88 meters.

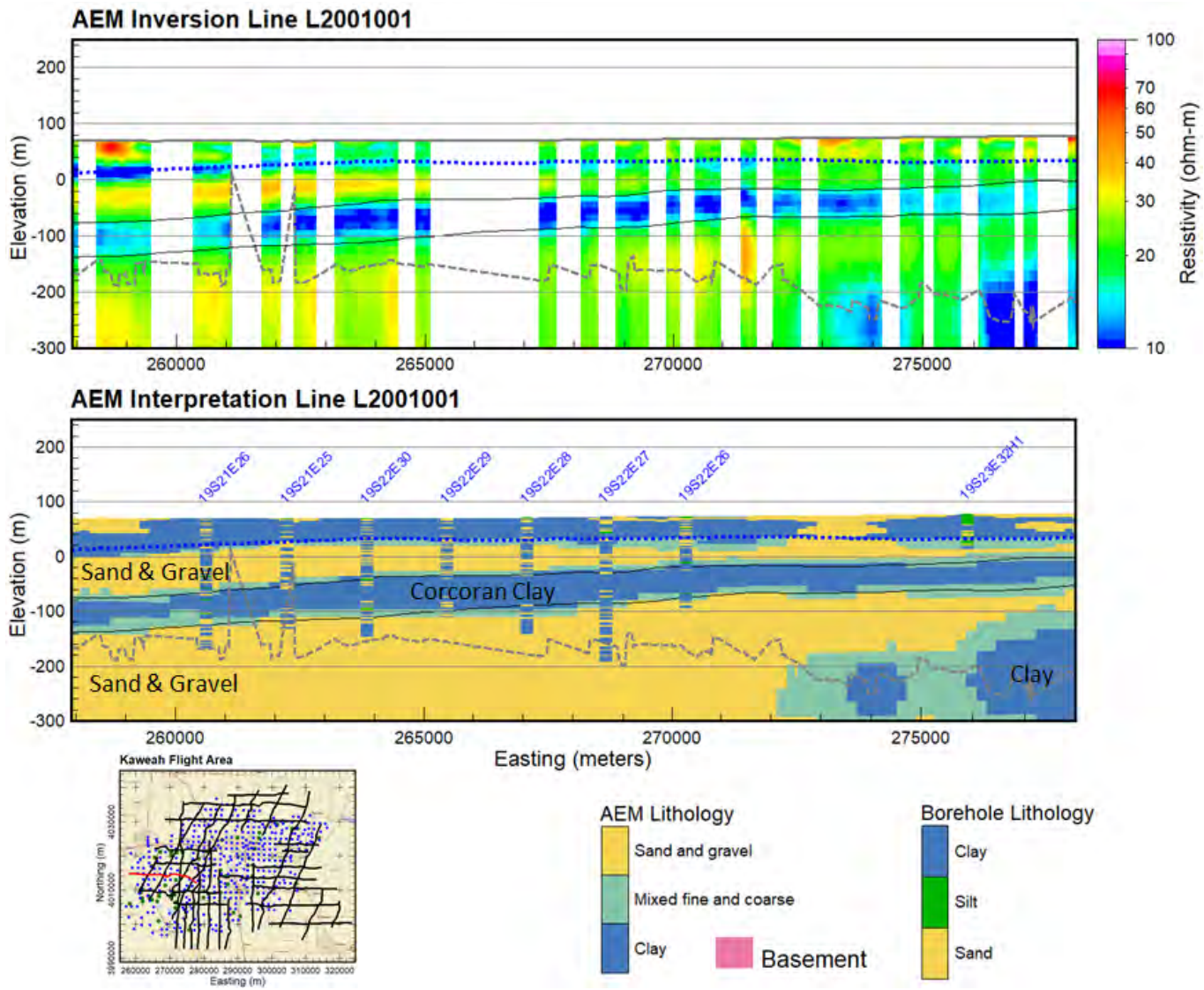

Figure 5-31. Lithological interpretation of Kaweah Subbasin AEM flight line L2001001 in the bottom profile. The dotted blue line is the Fall 2017 water table (CA-DWR, 2018a). The interpreted lithologies for different materials are indicated. Projection is NAD83, UTM 11N, meters, NAVD88 meters.

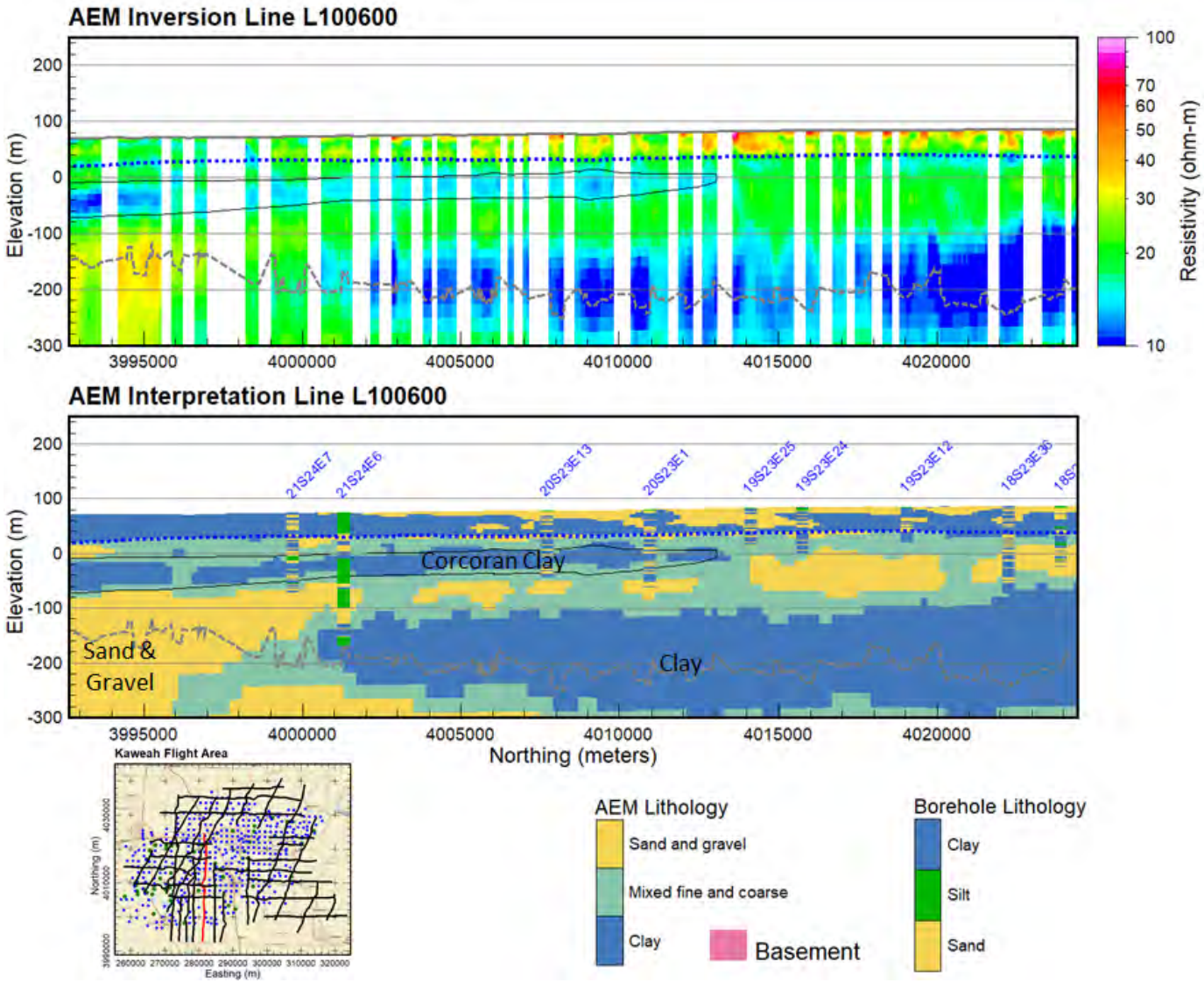

Figure 5-32. Lithological interpretation of Kaweah Subbasin AEM flight line L100600 in the bottom profile. The dotted blue line is the Fall 2017 water table (CA-DWR, 2018a). The interpreted lithologies for different materials are indicated. Projection is NAD83, UTM 11N, meters, NAVD88 meters.

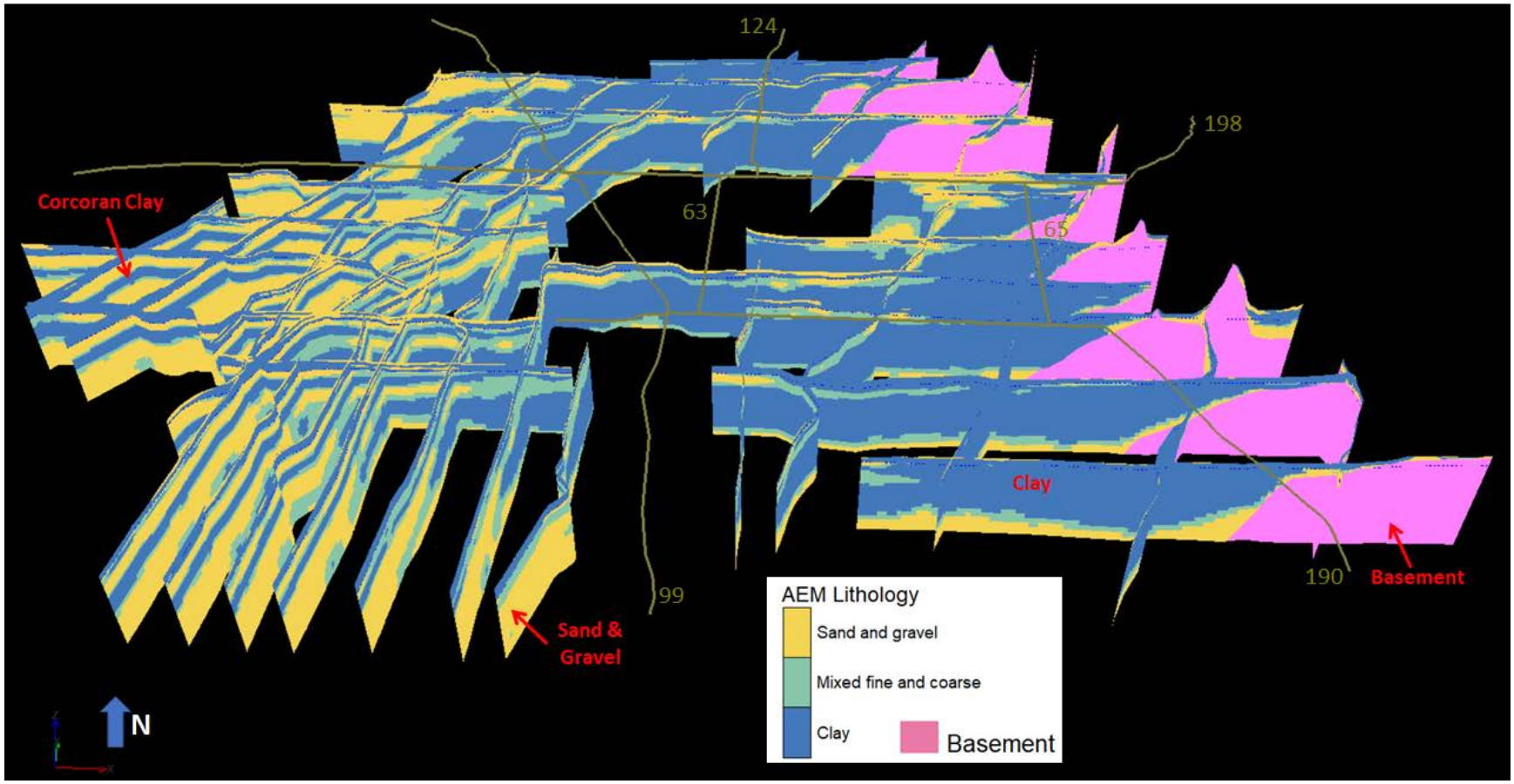

Figure 5-33. 3D lithologic interpretative fence diagram of the Kaweah Subbasin AEM inverted earth models, looking north. Greenish lines are local highways. Examples of the different lithologies are marked including the Corcoran Clay, undifferentiated Clay material, Sand and Gravel, and Basement materials.

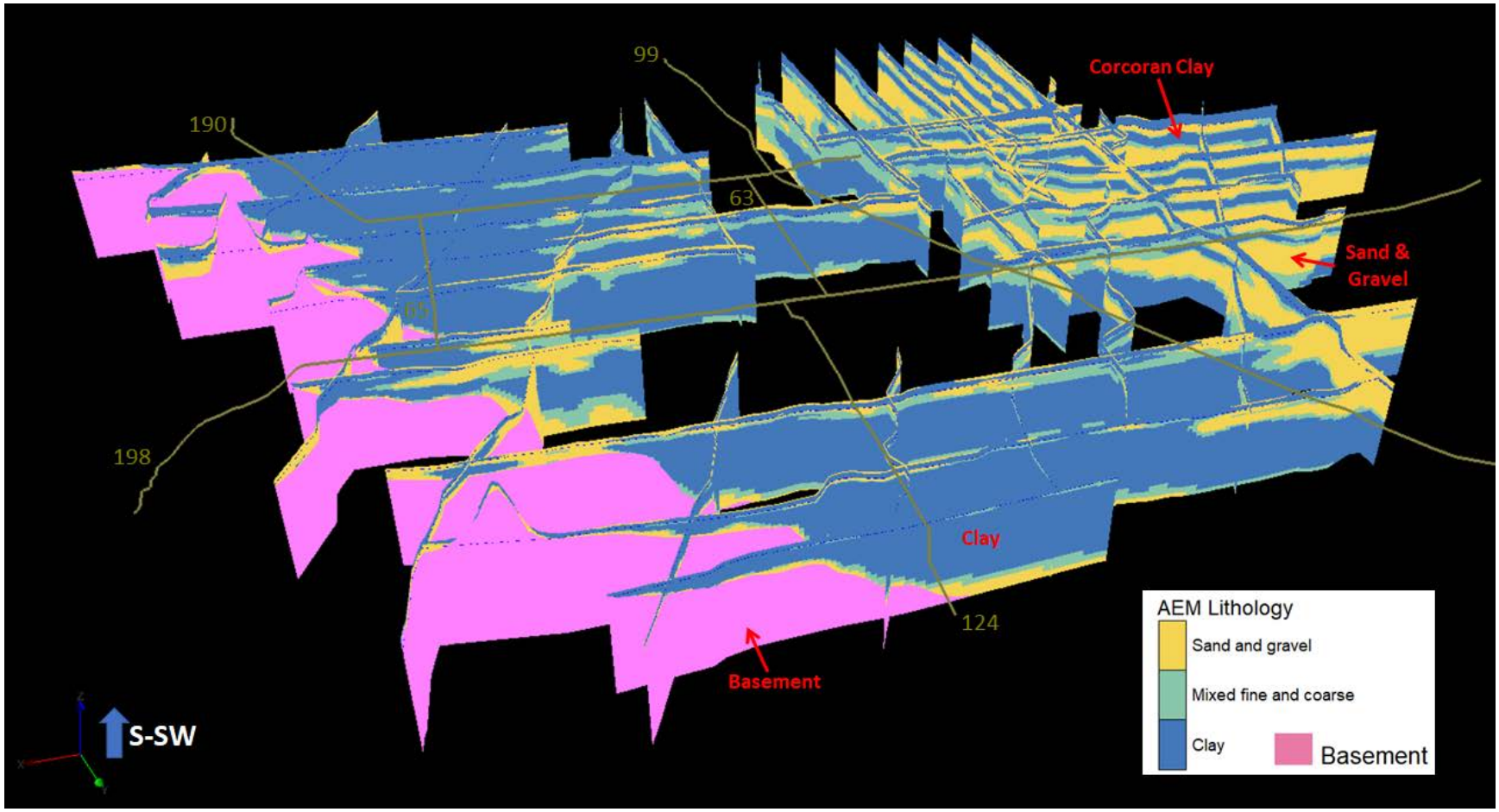

Figure 5-34. 3D lithologic interpretative fence diagram of the Kaweah Subbasin AEM inverted earth models, looking south. Greenish lines are local highways. Examples of the different lithologies are marked including the Corcoran Clay, undifferentiated Clay material, Sand and Gravel, and Basement materials. The Sand and Gravel zone on the western side of the survey area (right side here) may represent the edge of a large paleochannel or, at the least, a very coarse zone moving into the San Joaquin Valley.

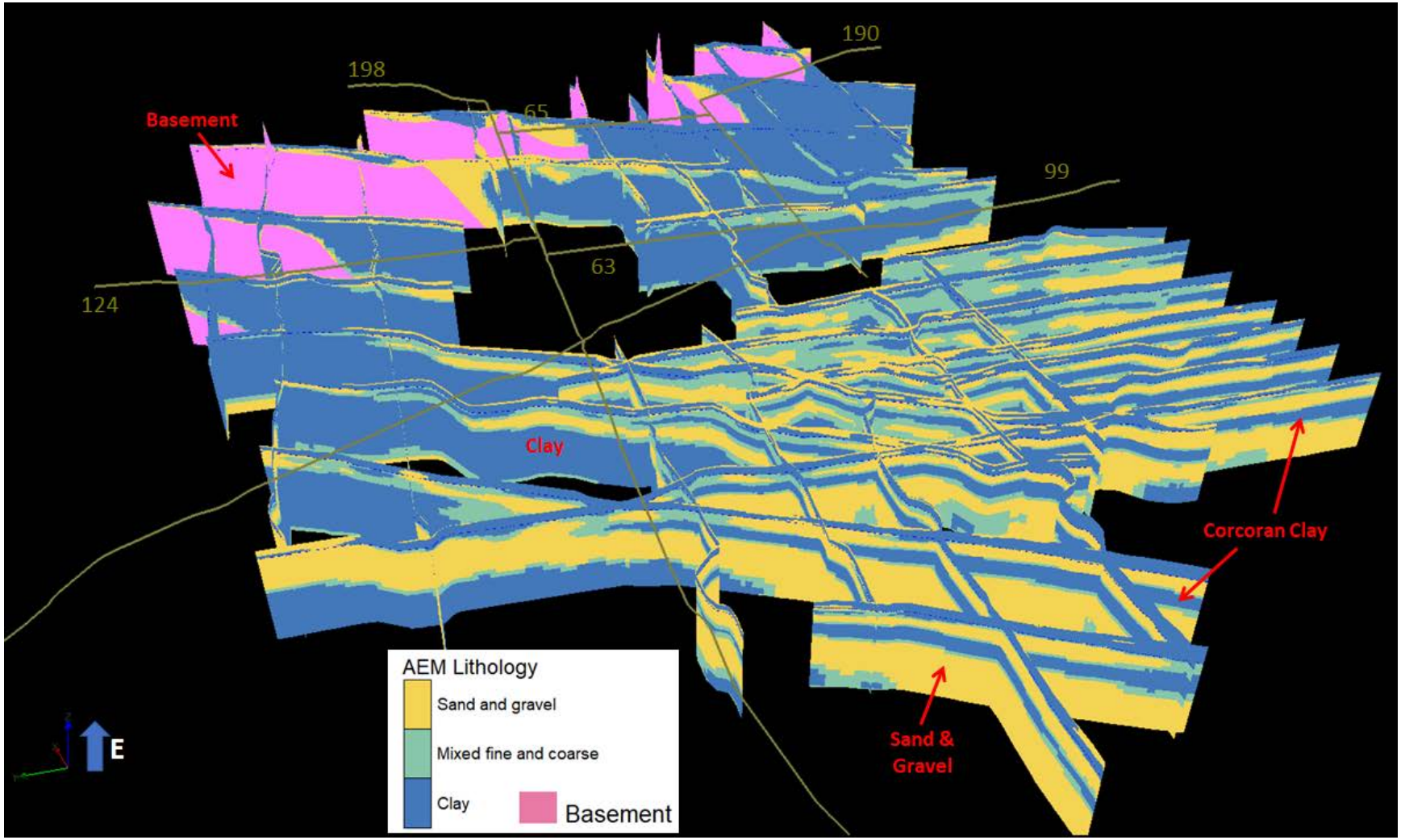

Figure 5-35. 3D lithologic interpretative fence diagram of the Kaweah Subbasin AEM inverted earth models, looking east. Greenish lines are local highways. Examples of the different lithologies are marked including the Corcoran Clay, undifferentiated Clay material, Sand and Gravel, and Basement materials.

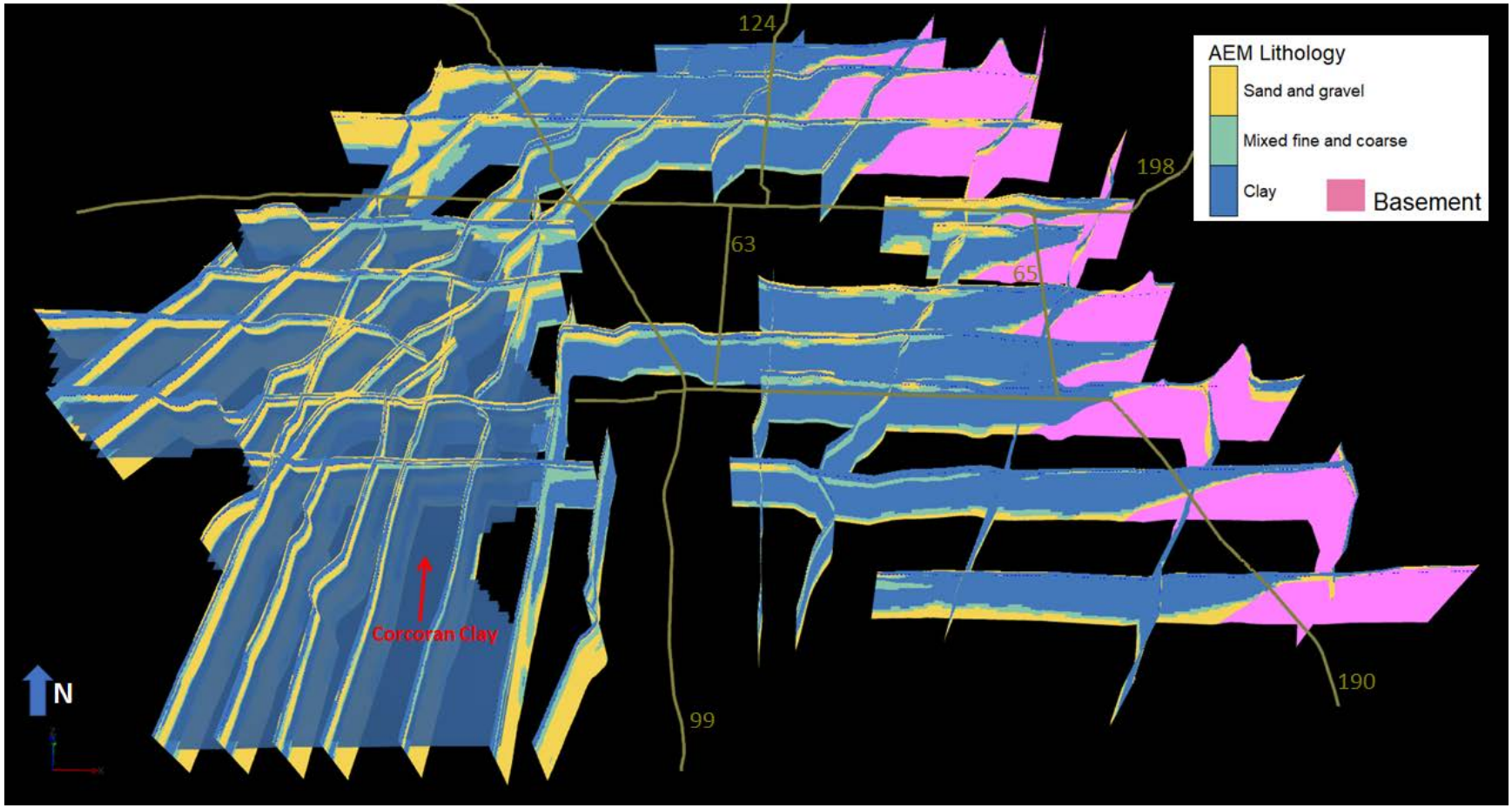

Figure 5-36. 3D lithologic interpretative fence diagram of the Kaweah Subbasin AEM inverted earth models, looking north. Greenish lines are local highways. The top and bottom extents of the Corcoran Clay are indicated on the western side (the left side in the image) using the same color scheme for Clay as for the rest of the data, except slightly more transparent. A slightly different color scheme outlining the extents of the Corcoran Clay in the survey area is presented in Figure 5-37.

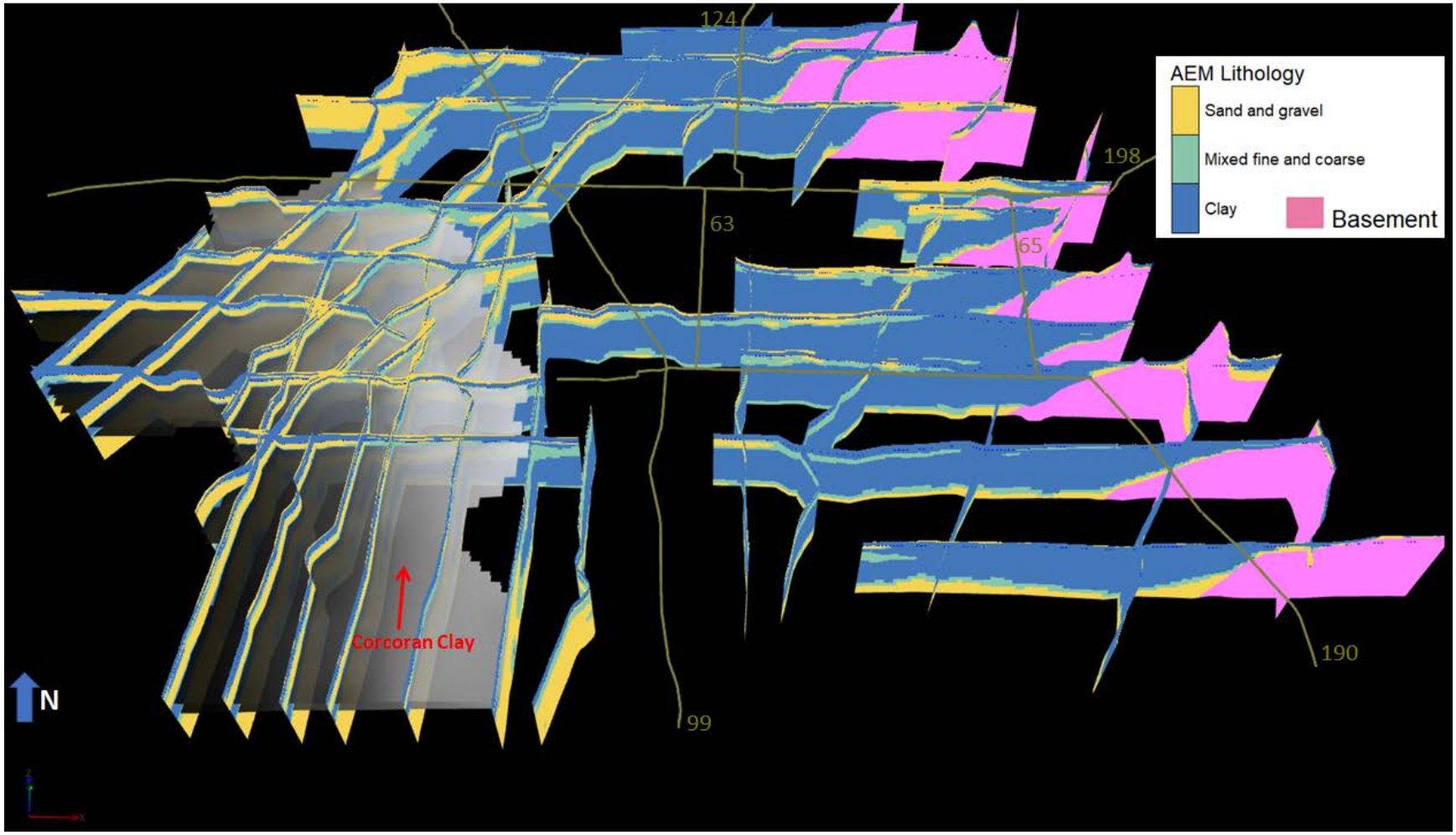

Figure 5-37. This is the same 3D fence diagram view as in Figure 5-36 except the top and bottom extents of the Corcoran Clay are highlighted with a transparent grey color instead of blue.

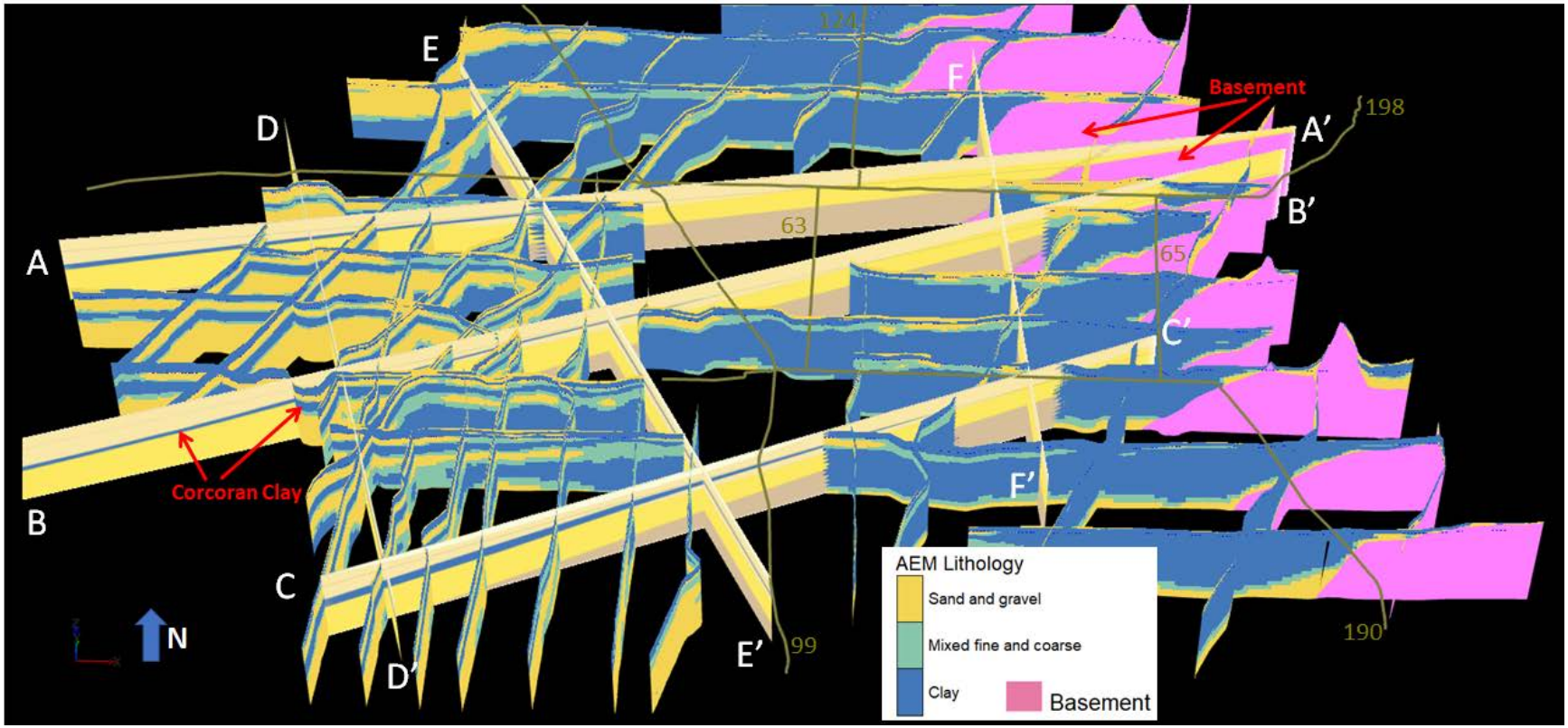

Figure 5-38. 3D lithologic interpretative fence diagram of the Kaweah Subbasin AEM inverted earth models, looking north, along with the Fugro West (2007) cross-sections, A-F. Greenish lines are local highways. The beginning and end of each Fugro West (2007) cross-section is labeled. Note the similar expressions and locations of the Corcoran Clay on the west (left side) and the Basement material on the east (right side) between the 2018 Kaweah Subbasin AEM investigation and the Fugro West (2007) cross-sections.

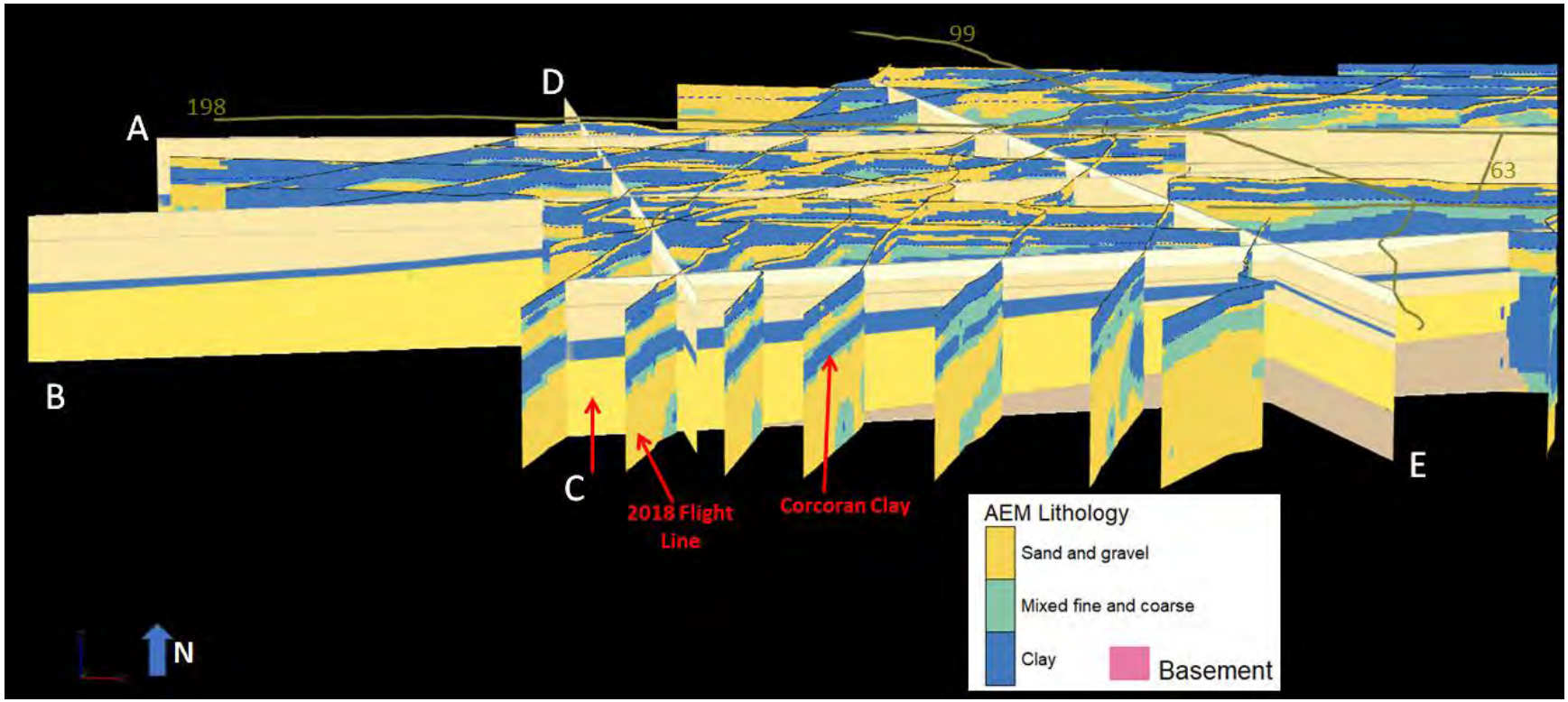

Figure 5-39. 3D lithologic interpretative fence diagram of the Kaweah Subbasin AEM inverted earth models, looking north, along with the Fugro West (2007) cross-sections, A-F. Greenish lines are local highways. The western ends of the Fugro West (2007) A, B, and C cross-sections are labeled. Note the similar expressions and locations of the Corcoran Clay on both the C-C' Fugro West (2007) cross-section and the 2018 Kaweah Subbasin AEM interpreted inversion results.

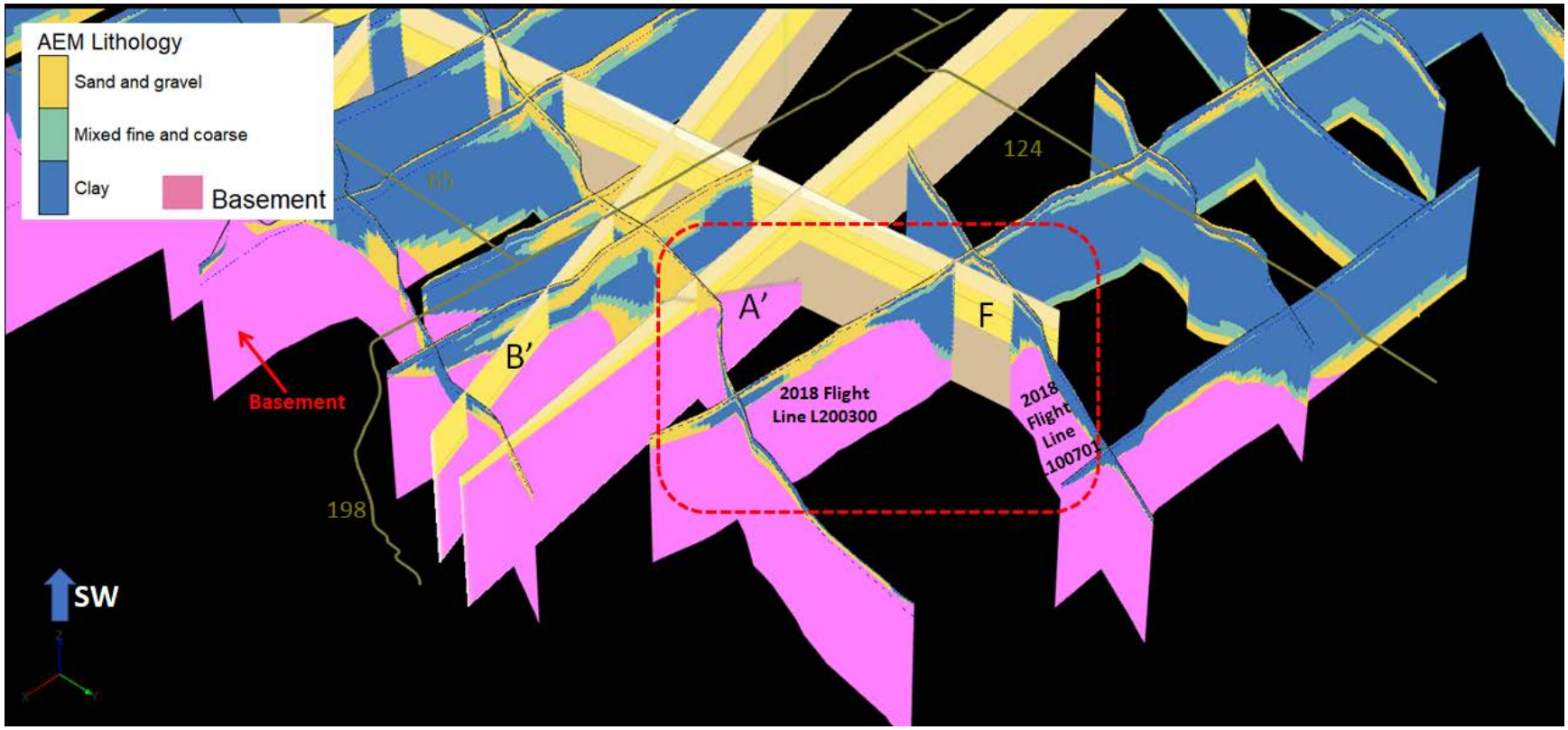

Figure 5-40. 3D lithologic interpretative fence diagram of the Kaweah Subbasin AEM inverted earth models, looking southwest, along with the eastern/northern ends of the Fugro West (2007) A, B, and F cross-sections. Greenish lines are local highways. The eastern ends of the Fugro West (2007) A, B, and F cross-sections are labeled. Of interest here is the similar nature of the basement expression on the A-A' cross-section and the 2018 AEM interpreted results on lines L200300 and L100701circled by the red dash box. Also of interest is how Fugro West (2007) cross-section F-F' does not match either the A-A' cross-section or the 2018 AEM interpreted lithology results at depth.

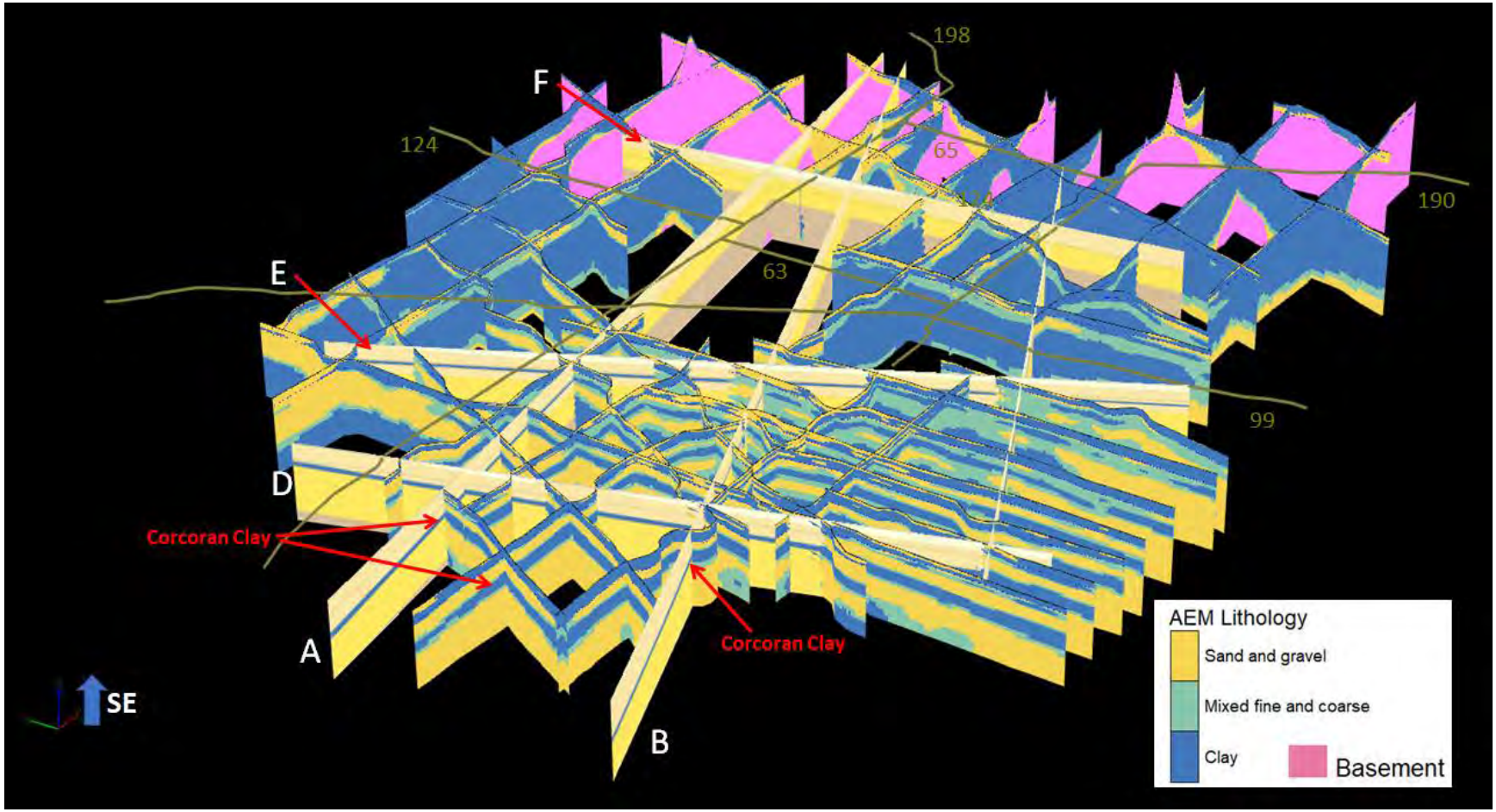

Figure 5-41. 3D lithologic interpretative fence diagram of the Kaweah Subbasin AEM inverted earth models, looking southeast, along with the Fugro West (2007) cross-sections. Greenish lines are local highways. Note the good agreement between all the Fugro West (2007) cross-sections and the 2018 Kaweah Subbasin AEM interpreted lithologies including the very good match of the Corcoran Clay exhibited by both sets of data.

5.7 Hydrogeological Framework of the Kaweah Subbasin AEM Survey Area

The 2018 Kaweah Subbasin AEM project area provides high resolution data of the subsurface along the reconnaissance flight paths within the survey area. These AEM-derived results provide new and updated information on the geology and hydrogeology in areas that were previously unknown or were only known to a limited extent from just the borehole information. The AEM profiles provide for greater understanding of the heterogeneity within and between all geologic formations in the survey area. This heterogeneity will be shown to be an important control to groundwater flow, storage, and quality. This survey completed in 2018 by AGF provides the basis for this hydrogeologic discussion.

The 2018 Kaweah Subbasin AEM survey reveals limited variability in the thick Quaternary and Tertiary deposits across the project area (Figure 5-33). While the stratigraphy between these units have not been delineated, these units have been subdivided, as discussed above in Section 5.6, into geologic materials including Sand and Gravel, Mixed Fine and Coarse materials, and Clay which make up the aquifer (and non-aquifer) materials overlying the basement units. The thick deposits of sand and gravel in the western part of the survey area are one of the dominant hydrogeologic features in the Kaweah Subbasin AEM project area and are important aquifers. These deposits have been identified in previous studies, for example Page (1986). The undifferentiated Quaternary and Tertiary units are considered aquifers where the lithology is made up of Sand and Gravel or Mixed Fine and Coarse. As discussed above in Section 5.2, the general source of material and the pattern of deposition of the Quaternary deposits originates from the Sierra Nevada Mountains to the east.

A strong presence of clay-bearing materials (blue) near the foothills of the Sierra Nevada and for some distance out into the Valley until the coarser Sand and Gravel (yellow) material is indicated in Figure 5-34. The extent of the Corcoran Clay (Figure 5-37), which was mapped in the southwest corner of the survey area by AEM, overlies the coarser, underlying Sand and Gravel. Corcoran Clay is not aquifer material and where present acts as a barrier to groundwater flow.

In some areas of the survey there are profiles that show many of the objectives of this project. Interpreted Profile L201100, presented in Figure 5-42, is in the center-east of the Kaweah Subbasin AEM project area and is approximately perpendicular to the dip of the Quaternary and Tertiary deposits which are coming/have come west off the slope of the Sierra Nevada to the east. This profile shows the relationship to the borehole resistivity information in the upper profile which allows for an understanding of how the lithology was determined. The two electric logs in the upper resistivity profile match the AEM inversion results quite well. In the interpretation profile, areas of unconfined and semi-confined to confined areas are indicated by the location and nature of the bounds on the saturated Sand and Gravel zone located just below the water table (dotted blue line). Also, note the sharp contact on the east side between the basement and the thick clay of the sediments to the west. These thick clays near the basement contact and which extend west are a common feature along the foothills of the Sierra Nevada. The details provided by the AEM allows for high definition of where these sharp flow boundaries are within the aquifer systems.

Zones along Profile L101202, presented in Figure 5-43, are aquifers where there are coarse grained materials like Sand and Gravel in its makeup. The Corcoran Clay can be seen in the profile from the southern end to about northing 4025000. This area is one of the important parts of the hydrogeologic framework of the survey area as the Corcoran Clay, as already noted, acts as a confining to a semi-confining unit. Recharge can come from the northern end of the line where there are permeable sediments that can accept recharge at the surface and transmit the water to the aquifers downgradient. Note that this profile was discussed in Section 5.3 which discussed the quality of (or not) of some of the borehole geophysical logs.

Using the interpretive surfaces and grids that were produced as described above in Section 5.4, an enhanced understanding of the hydrogeological framework of the Kaweah Subbasin AEM project area survey area can be developed. Figure 5-20 is the map of the elevation of the top of the basement upon which water can flow downhill into the project area. Note that since only the basement that could be imaged by the AEM is shown, it is only on the east side of the project area and is a steep feature across Rocky Hill Fault. The elevation relief is about 540 m in the AEM survey area. Figure 5-21 shows the depth to the top of the basement from the land surface, indicating a relief of about 500m and also a thickening of the Quaternary and Tertiary sediments from east to west.

As noted above in Section 2.2.3 – *Connectivity to Surface Water and to Other Aquifers*, groundwater connectivity to surface-water systems in the project area is complex due to the numerous surface-water features that recharge the groundwater system. Thus, it helps to have the extent of (Figure 5-37), depth to (Figure 5-18), elevation of the top (Figure 5-17), and thickness (Figure 5-19) of the Corcoran Clay which can act as a strong barrier to groundwater-surface water connectivity.

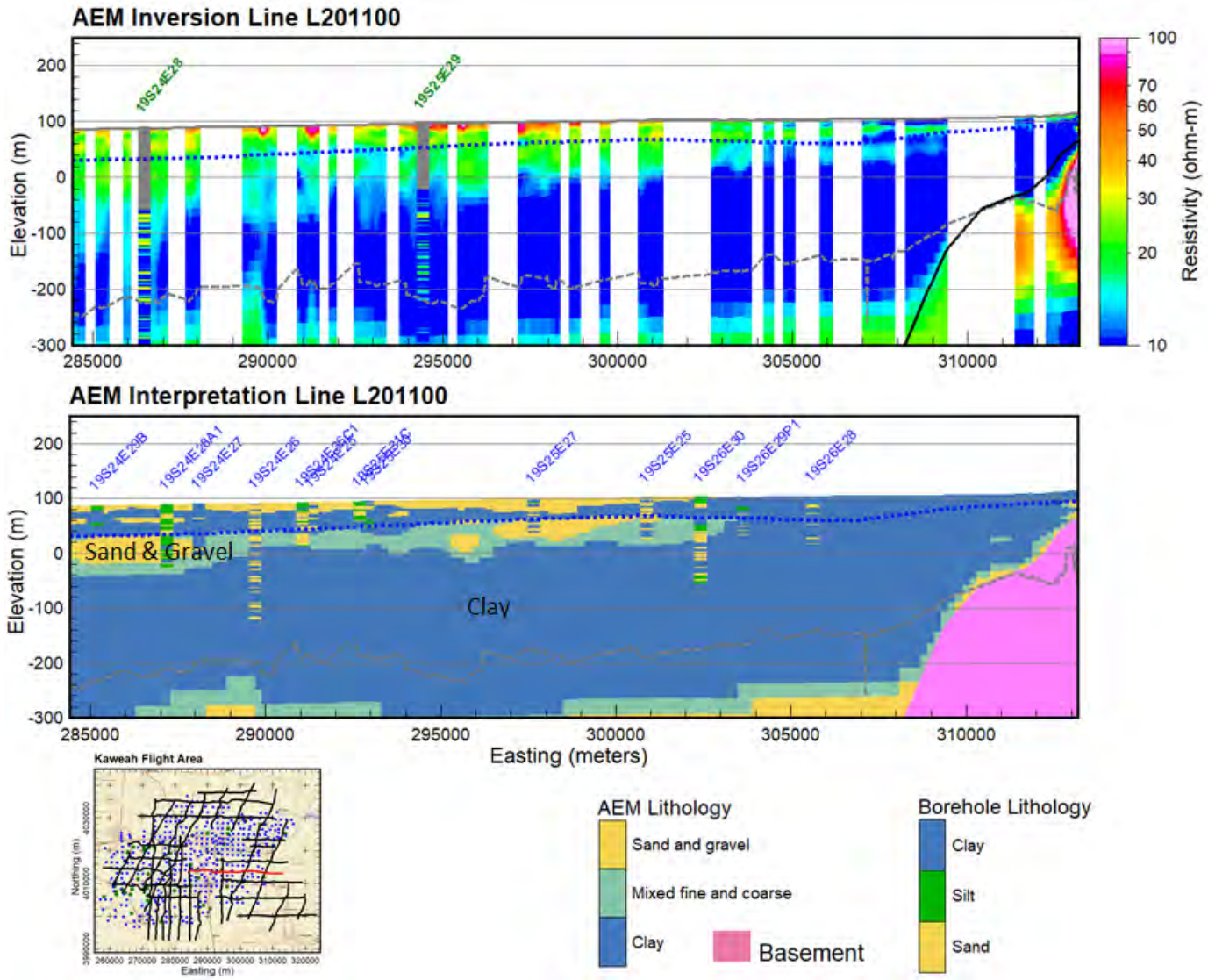

Figure 5-42. Lithological interpretation of Kaweah Subbasin AEM flight line L201100 in the bottom profile. The dotted blue line is the Fall 2017 water table (CA-DWR, 2018a). The interpreted lithologies for different materials are indicated. Projection is NAD83, UTM 11N, meters, NAVD88 meters.

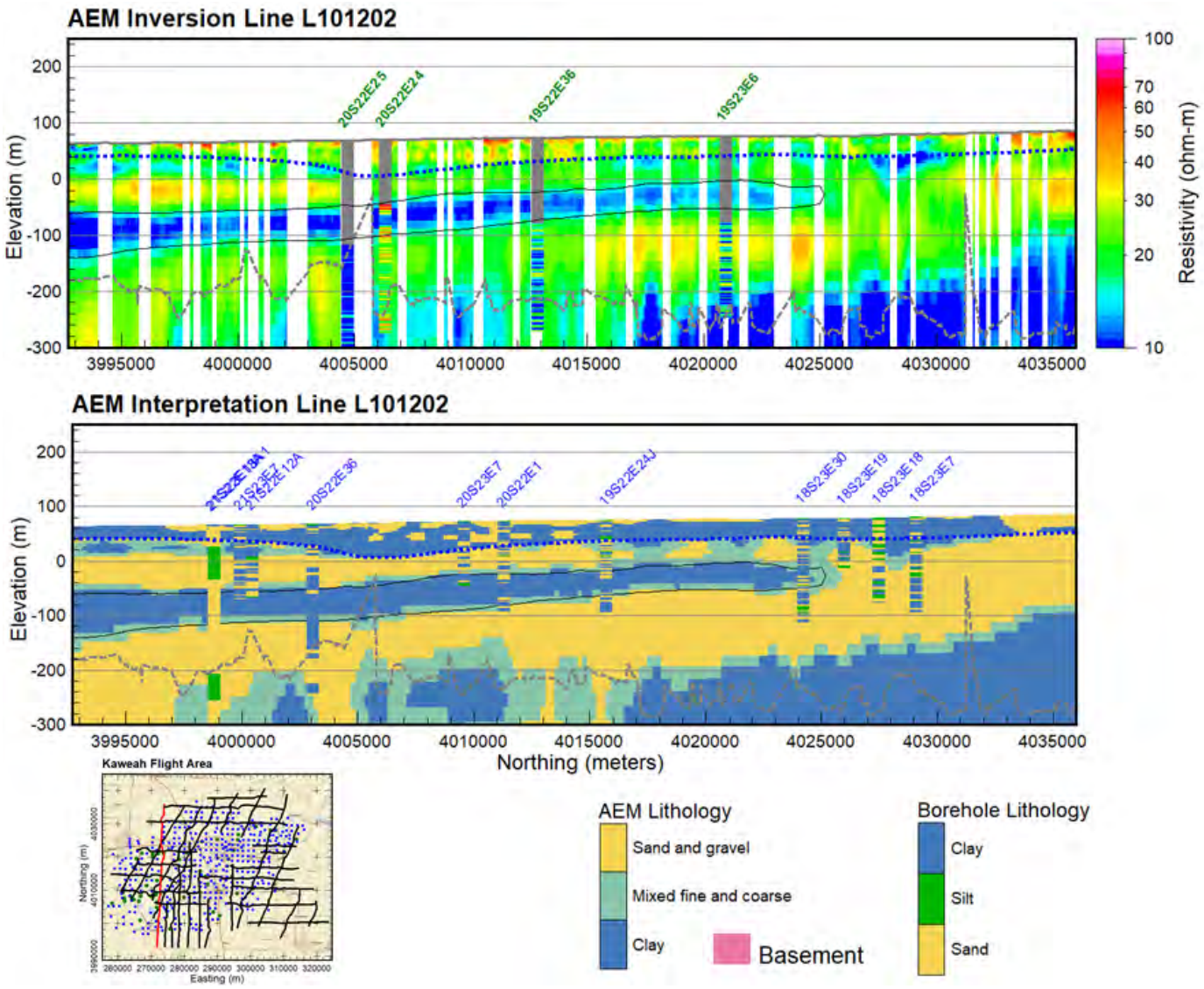

Figure 5-43. Lithological interpretation of Kaweah Subbasin AEM flight line L101202 in the bottom profile. The dotted blue line is the Fall 2017 water table (CA-DWR, 2018a). The interpreted lithologies for different materials are indicated. Projection is NAD83, UTM 11N, meters, NAVD88 meters.

5.8 Recharge Areas within the Kaweah Subbasin AEM Survey Area

This discussion on areas of potential recharge in the Kaweah Subbasin AEM survey area begins with two maps, one from the USGS, "*Groundwater Availability of the Central Valley Aquifer, California*" (Faunt et al., 2009) and the Fugro West (2007) report "*Water Resources Investigation of the Kaweah Delta Water Conservation District 2003, Revised 2007*". The USGS map, presented in Figure 5-44, is a modification of Figure A14 from Faunt et al. (2009) and presents the percent of coarse material in the first 50 ft in the southern San Joaquin Valley. A red box has been drawn around the general Kaweah Subbasin AEM survey area. The second map, presented in Figure 5-45, is a modification of Plate 10 from Fugro West (2007) and presents a map of "current and proposed" (as of 2007) locations of recharge basins in the Kaweah Delta Water Conservation District. The USGS map (Figure 5-44) indicates a mixture of coarse and fine-grained material in the near-surface of the field area, with more fine-grained material present than coarse grained. The Fugro West (2007) map (Figure 5-45) indicates areas that have been determined to be good locations for recharge into the subsurface. Note that these recharge basins are spread across the KDWCD. The near-surface recharge potential as indicated by the Kaweah Subbasin AEM interpreted lithology will be compared to the locations indicated in Figure 5-45.

A Google Earth kmz has been created that presents resistivities greater than 25 ohm-m for the first eight (8) layers of the Kaweah Subbasin AEM inversion results. Google Earth images of layers 1 (0 m - 3 m or 0 ft – 10 ft), 3 (6 m – 10 m or20 ft – 31 ft), 5 (13 m – 17 m or 43 ft – 56 ft), and 8 (26 m – 31 m or 85 ft to 100 ft) are presented in Figure 5-46, Figure 5-47, Figure 5-48, and Figure 5-49, respectively. The full Kaweah Subbasin AEM Recharge kmz is included in Appendix 3-Deliverables\KMZ\Recharge. Materials in blue are more coarse than brown materials.

While it is clear that there are subtle changes between the different layers, it is also clear that the areas with potentially good recharge are spatially distributed across the area, in a fashion similar to that indicated in the Fugro West (2007) report. A comparison of the Fugro West (2007) recharge basin map and layer 1 (0 ft – 10 ft, 0 m-3 m) of the Kaweah Subbasin AEM interpreted lithologies is presented in Figure 5-50.

Many of the locations of the 2007 current and proposed recharge basins are overlain with AEM-interpreted coarse to very coarse materials and there are many more locations indicated by the AEM that could still be developed for recharge. Using the maps and cross-sections from this report will allow for a greater understanding of the pathways the recharge takes for management purposes. Water quality management can be improved by tailoring the management practices for the recharge in an area. An example is that you would want to limit fertilizer application over areas of good recharge versus areas of low recharge. For water quantity management an example is to site managed aquifer recharge areas to locations that have the greatest recharge potential, greatest unsaturated thickness, and the ability to move water to the site. The use of AEM data along with other sources of information like soils maps will be beneficial for many hydrogeologic decisions in the survey area.

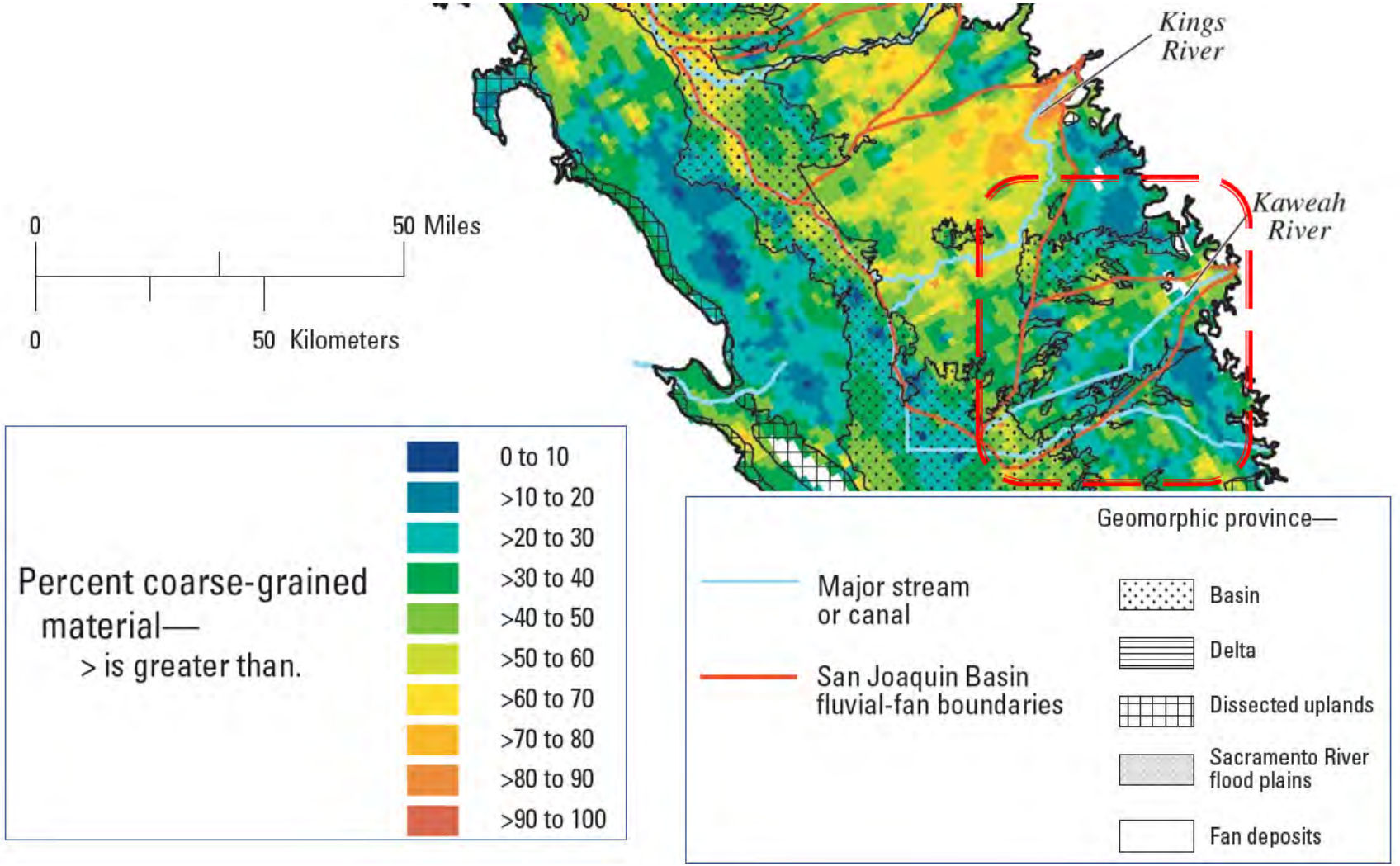

Figure 5-44. ***"Map of distribution of coarse-grained deposits for the upper 50 ft for part of the Central Valley. Map is overlain with major geomorphic provinces of the Central Valley and the fluvial fans of the San Joaquin Basin"*** **(modified from Figure A14 in Faunt et al., 2009). The dashed red box surrounds the Kaweah River discharge area.**

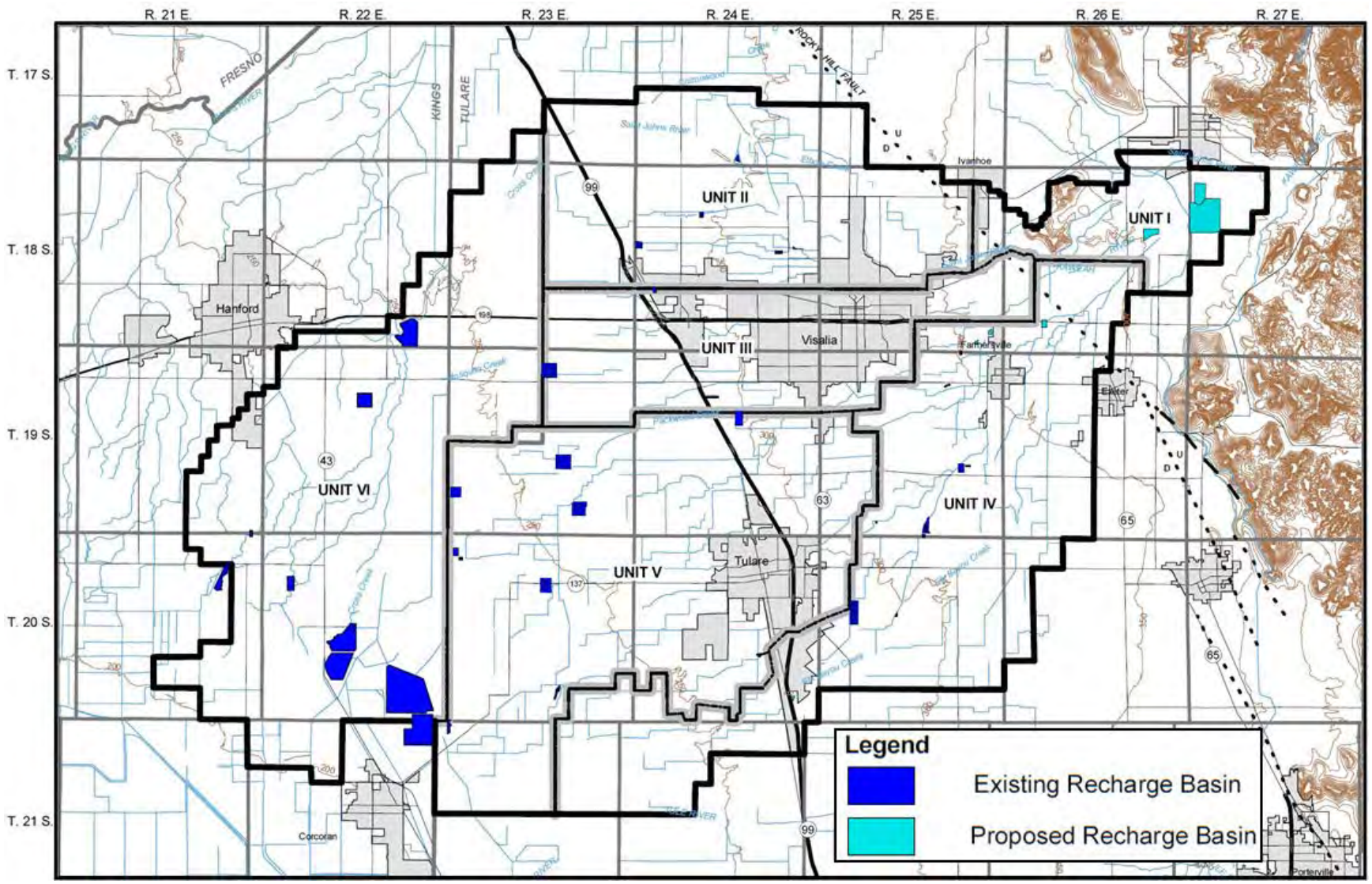

Figure 5-45. Map of "current and proposed" (as of 2007) Recharge Basins in the Kaweah Delta Water Conservation District (modified from Plate 10 in Fugro West, 2007).

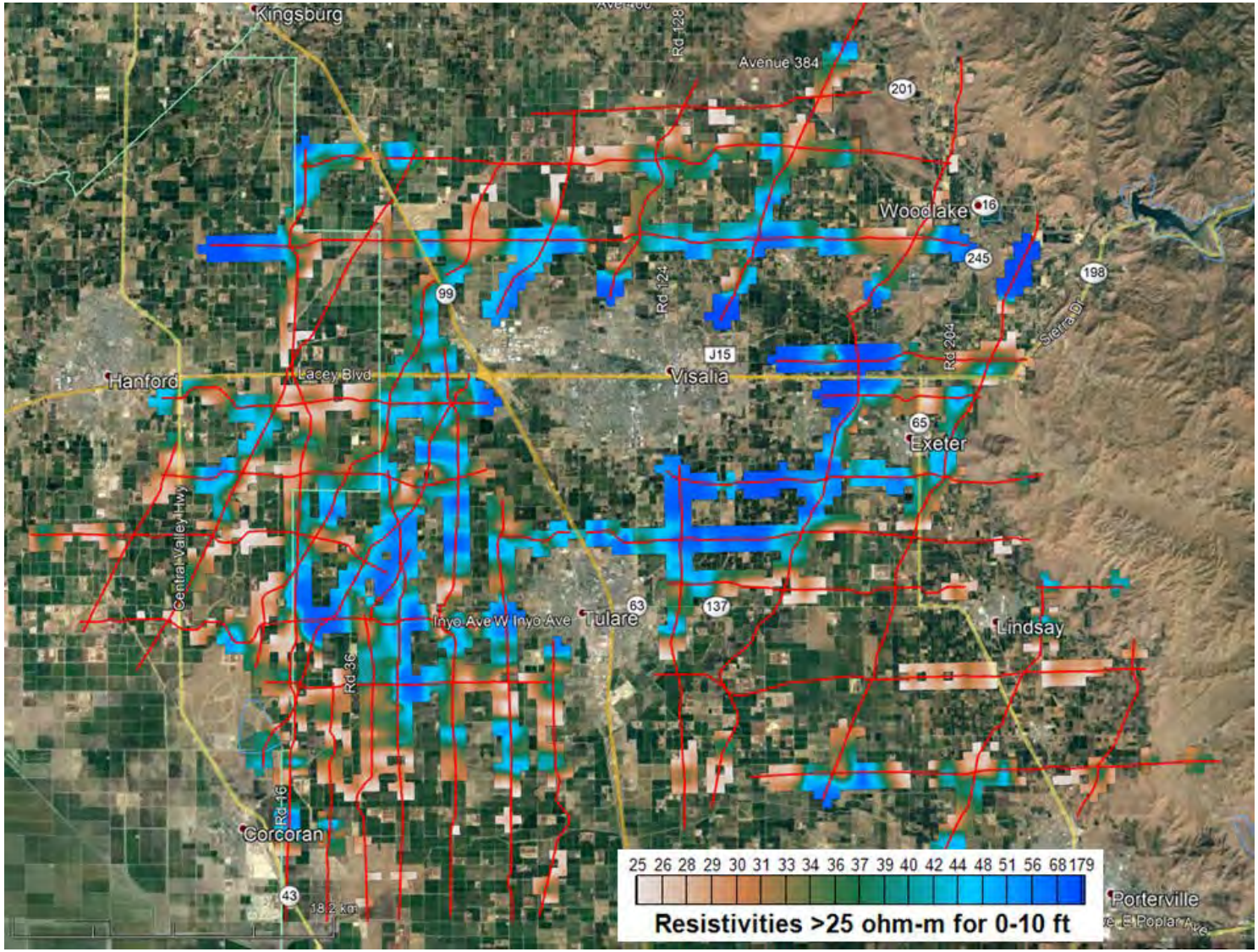

Figure 5-46. Google Earth image of areas of potential recharge showing coarse-grained material with resistivities >25 ohm-m for the depth range 0 m – 3 m or 0 ft – 10 ft. This is layer 1 of the Recharge kmz in Appendix 3\KMZ\Recharge. Materials in blue are more coarse than brown materials.

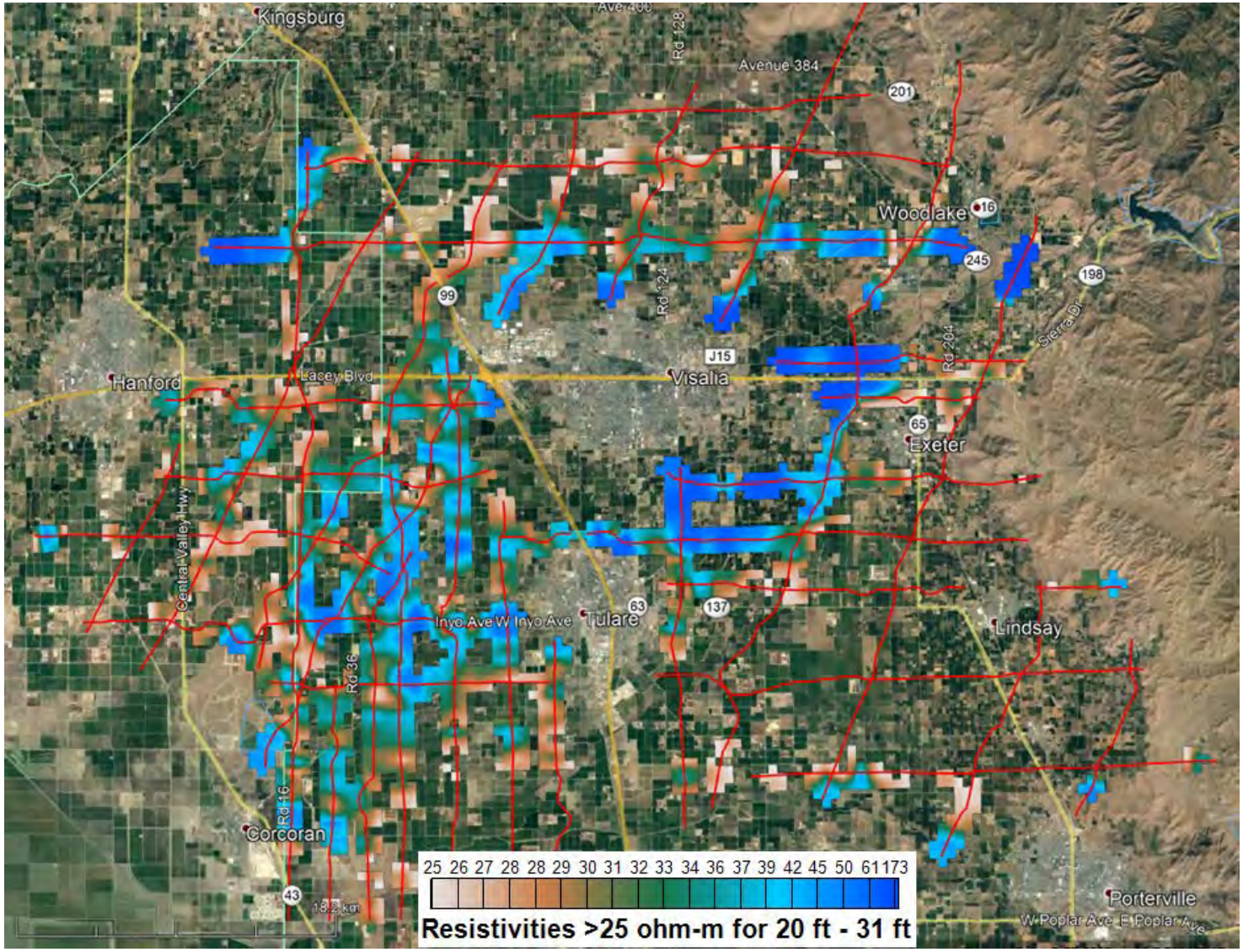

Figure 5-47. Google Earth image of areas of potential recharge showing coarse-grained material with resistivities >25 ohm-m for the depth range 6 m – 10 m or 20 ft – 31 ft. This is layer 3 of the Recharge kmz in Appendix 3\KMZ\Recharge. Materials in blue are more coarse than brown materials.

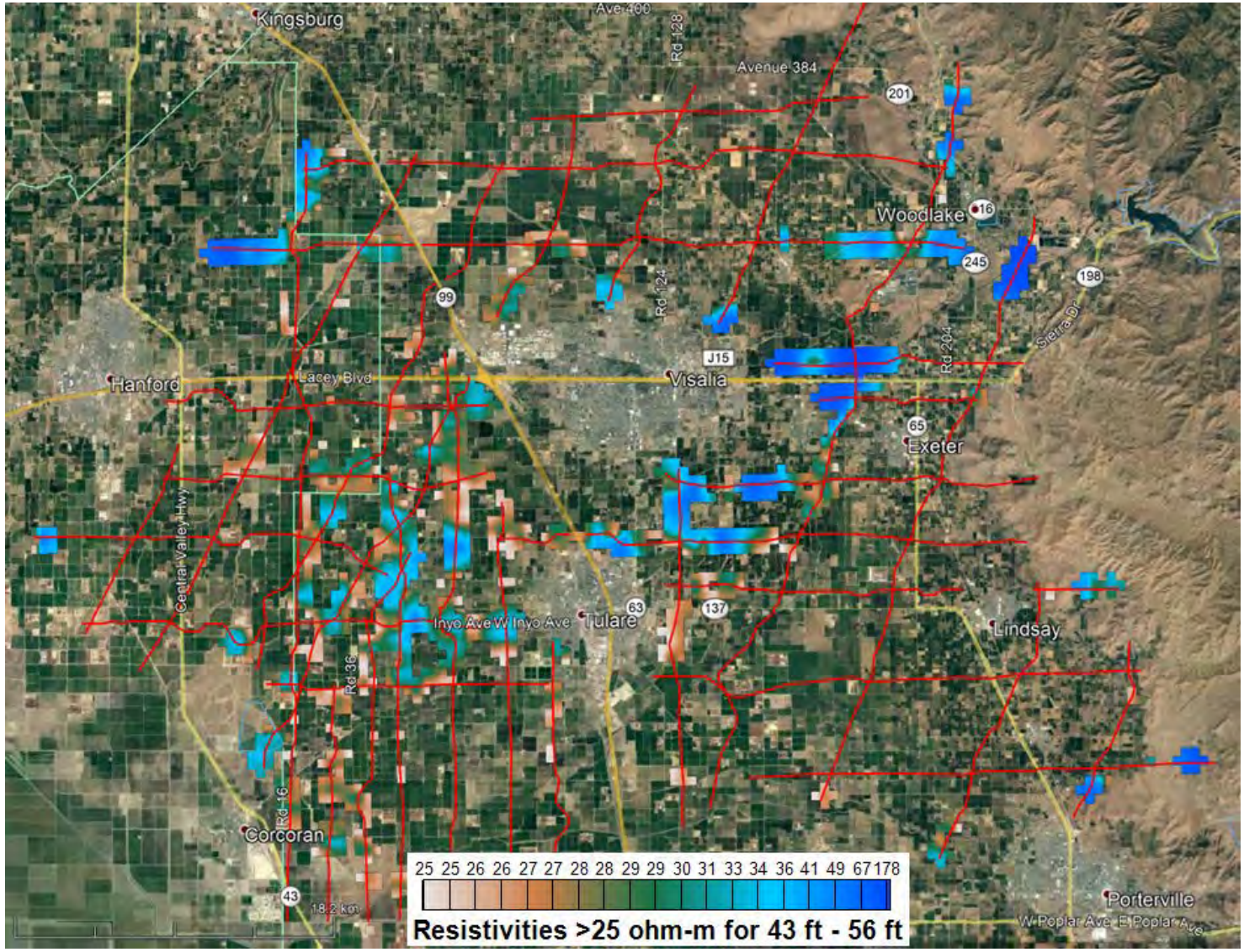

Figure 5-48. Google Earth image of areas of potential recharge showing coarse-grained material with resistivities >25 ohm-m for the depth range 13 m – 17 m or 43 ft – 56 ft. This is layer 5 of the Recharge kmz in Appendix 3\KMZ\Recharge. Materials in blue are more coarse than brown materials.

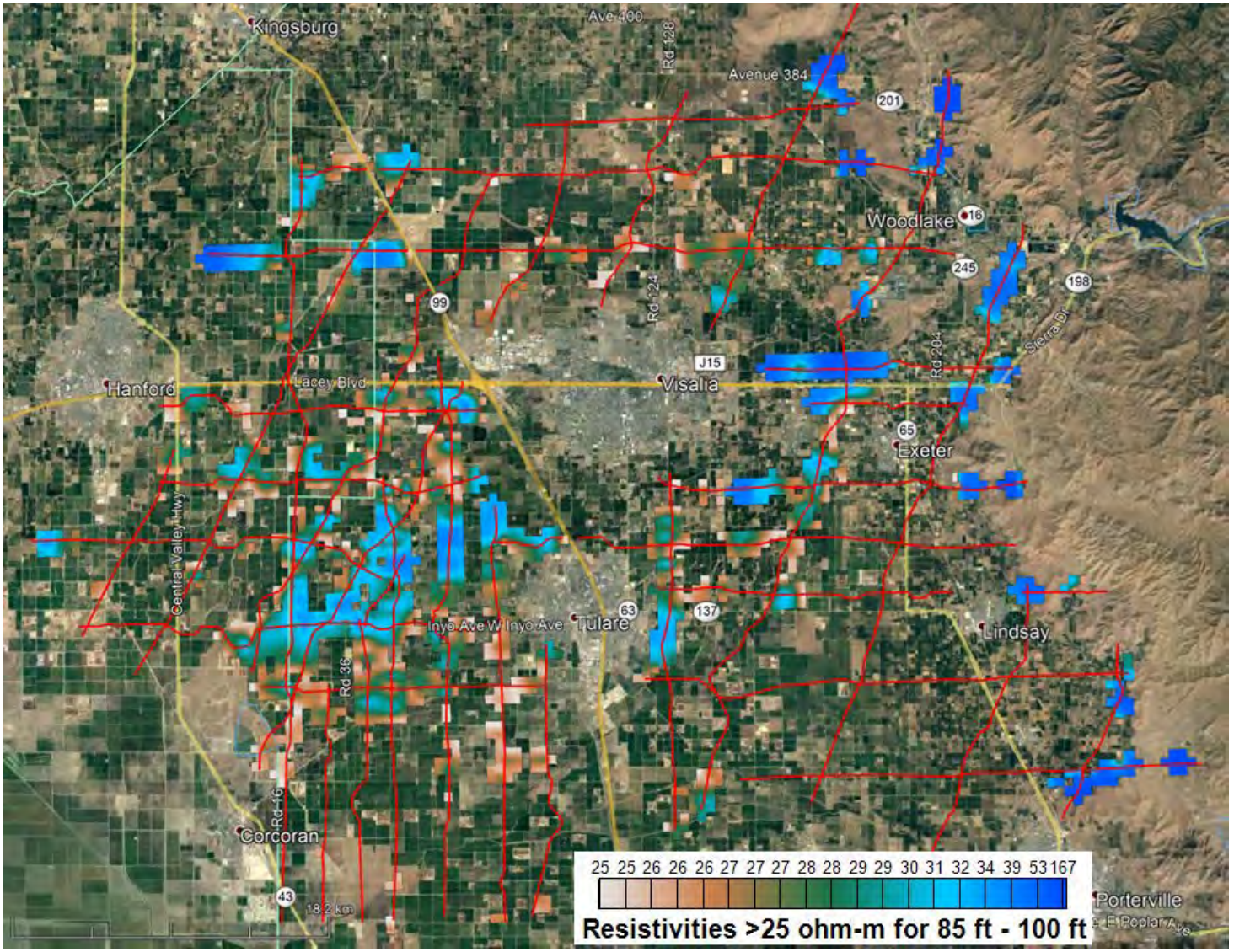

Figure 5-49. Google Earth image of areas of potential recharge showing coarse-grained material with resistivities >25 ohm-m for the depth range 26 m – 31 m or 85 ft to 100 ft. This is layer 8 of the Recharge kmz in Appendix 3\KMZ\Recharge. Materials in blue are more coarse than brown materials.

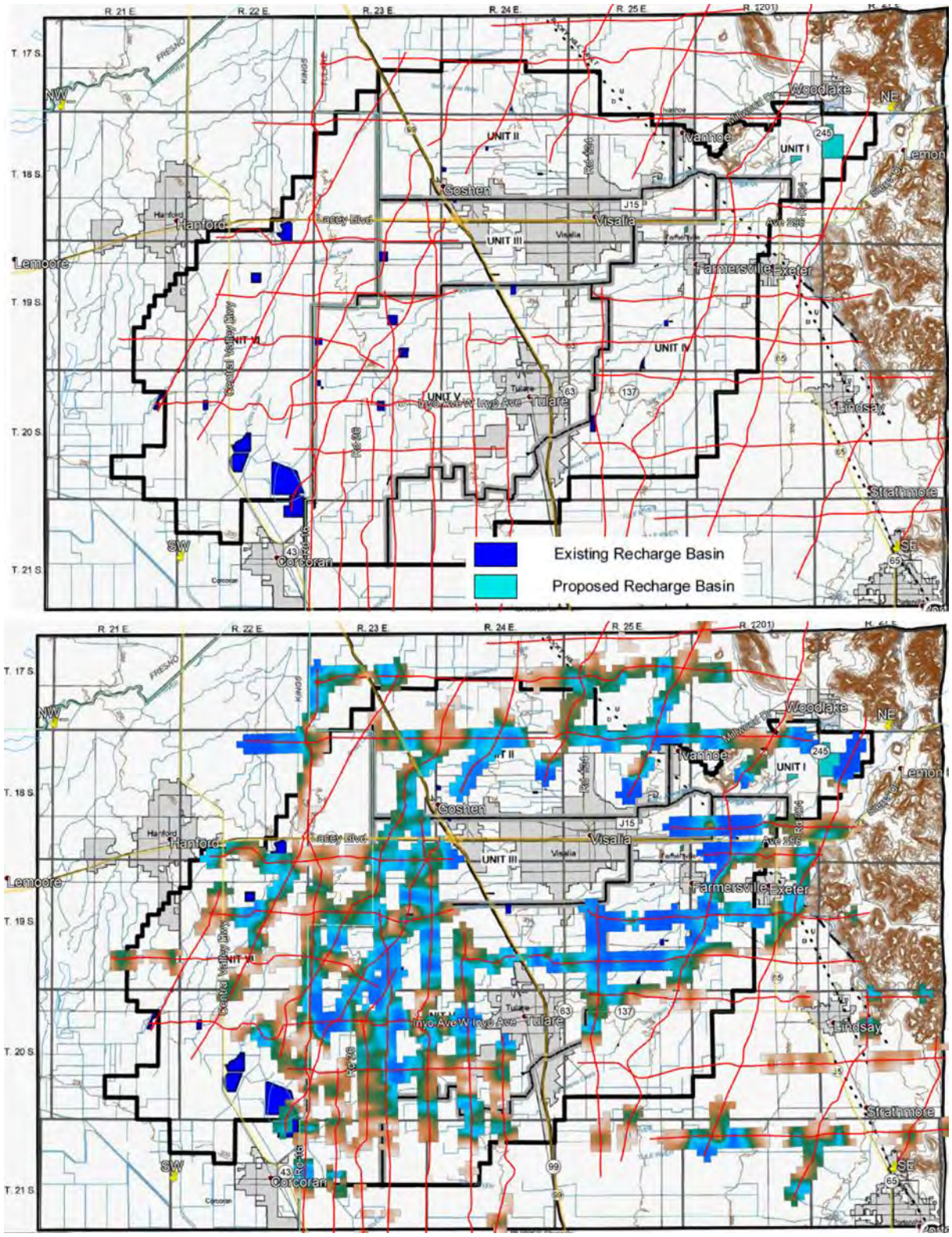

Figure 5-50. Top: Google Earth image of "current and proposed" (as of 2007) Recharge Basins in the Kaweah Delta Water Conservation District (modified from Plate 10 in Fugro West, 2007); Bottom: Same as top image plus first layer (0-10 ft) of AEM earth model for resistivities >25 ohm-m. With 2018 AEM flight lines.

5.9 Key AEM Findings

5.9.1 Boreholes

Information from boreholes was used to analyze the Kaweah Subbasin AEM inversion results. A total of 440 holes contained lithology information and 52 holes contained geophysical information within the Kaweah Subbasin AEM survey area. These boreholes were provided by GEI Consultants under separate contract to Stanford University. The AEM inversion results matched up well with most of the both the geophysical logs and also the lithological logs.

5.9.2 Digitizing Interpreted Geological Contacts

Characterization and interpretation of the subsurface was performed in cross-section and derived surface grid formats. The interpretive process greatly benefited from the use of the borehole logs. The upper and lower Corcoran Clay contacts as well as extent and the top of the pre-Tertiary granitic and metavolcanic materials have been mapped. Surface grids of the interpreted geologic formations were produced as well as interpretative profiles. Each flight line profile with interpretation is included in the appendices as well as the interpretative surface grids.

5.9.3 Comparing the 2018 Kaweah 312 AEM Results with the 2015 Tulare 508 AEM Results

A comparison was performed between the 2018 SkyTEM312 Kaweah inversion results and the 2015 SkyTEM508 inversion results via profile comparisons along multiple flight lines. The results compare very well down to about -350 m (-1,150 ft) depth. The greater depth of investigation of the 508 stands out as the primary difference between the two systems. While the SkyTEM 312 system was able to image the top of the resistive zone that was identified at the southwestern end of the Tulare AEM flight lines, the SkyTEM 312 did not do as good a job characterizing the extent of that resistive, coarse-grained zone.

5.9.4 Resistivity/Lithology Relationship

An assessment of the lithologic character of the sediments in the Kaweah Subbasin AEM survey area was conducted to determine the overall composition of the major categories used to define aquifer and aquitard material. The resistivity-lithological relation described in Table 2 of Knight et al. (2018), *Mapping aquifer systems with airborne electromagnetics in the Central Valley of California*, for materials above and below the water table was applied to the Kaweah Subbasin AEM inversion results, with a slight modification due to overlapping ranges. The ranges are defined as: Unsaturated - Clay (<28 ohm-m) and Sand and Gravel (28-500); Saturated – Clay (<15 ohm-m), Mixed Fine and Coarse (15-19 ohm-m), and Sand and Gravel (19-500 ohm-m). This allowed for the characterization of the ranges of resistivities present in the major geologic units described in this report which were then used in understanding the hydrogeological framework.

5.9.5 Hydrogeological Framework of the Kaweah Subbasin AEM Survey Area

The 2018 Kaweah Subbasin AEM project area provides high resolution data of the subsurface along the reconnaissance flight paths within the survey area. These AEM-derived results provide new and updated information on the geology and hydrogeology in areas that were previously unknown or were only known to a limited extent from just the borehole information. The AEM

profiles provide for greater understanding of the heterogeneity within and between all geologic formations in the survey area. The result of that heterogeneity is that there is limited variability in the thick Quaternary and Tertiary deposits across the project area. While the stratigraphy between these units have not been delineated, these units have been subdivided as just discussed into geologic materials which make up the aquifer (and non-aquifer) materials overlying the basement units. The thick deposits of sand and gravel in the western part of the survey area are one of the dominant hydrogeologic features in the Kaweah Subbasin AEM project area and are important aquifers. The extent of the Corcoran Clay, which was delineated in the southwest corner of the survey area by AEM, overlies coarser Sand and Gravel deposits. Corcoran Clay is not aquifer material and, where present, acts as a barrier to groundwater flow and is also a large contributor to the subsidence in the area due to dewatering.

5.9.6 Estimation of Aquifer Volume and Water in Storage in the Kaweah Subbasin AEM Survey Area

Estimation of aquifer volume and yield were not calculated for the Kaweah Subbasin AEM survey area because of the nature of a reconnaissance flight line plan in which the AEM line spacings are approximately 5 km. AEM flight plan designs with blocks of closely spaced (250 m to 400 m) survey lines would allow for development of estimates of aquifer and water in storage, if at the same time good aquifer production information such as porosity and specific yield were available in order to quantify water availability in the different lithologies.

5.9.7 Potential Recharge Zones within the Kaweah Subbasin AEM Survey Area

Previous studies of the groundwater recharge potential in the Kaweah Subbasin AEM survey area, including the USGS which characterized the region as a diverse mix of coarse and fine materials, identified locations of recharge basins for the local water district. An overlay of the lithological interpretation of the first layer of the Kaweah Subbasin AEM inversion results (covering depths from the surface to 3 m or 10 ft) on a map developed by Fugro West from 2007 for the Kaweah Delta Water Conservation District, which shows the locations of current and proposed recharge basins (as of 2007), indicates that even given the reconnaissance nature of the Kaweah AEM investigation, the recharge areas indicated by the AEM match up well with the locations of existing and proposed recharge basin locations and also indicate additional areas where recharge to groundwater aquifers could be developed.

5.10 Recommendations

Recommendations provided to the Greater Kaweah, East Kaweah, and Mid-Kaweah Groundwater Sustainability Agencies in this section are based on the interpretation and understanding gained from the addition of the AEM data to existing information and from discussions with the representatives of the GSA's and water districts about their management challenges.

5.10.1 Additional AEM Mapping

If it is determined that greater fidelity is necessary in terms of groundwater flow, aquifer sustainability, volumes, and water in storage estimates, depletion to streams, well interference, groundwater withdrawal, and other management considerations, it is recommended that areas of closely spaced lines or "block-flights" be collected to develop more-detailed frameworks. The current 5 km line spacing between flight lines could be reduced to a 250 m to 400 m flight line spacing for greater detail on the natural system. Block flights, by providing AEM data, will also assist other studies in the San Joaquin Valley such as that by Smith and Knight (2019) which combines AEM and INSAR to study and model the mechanics of subsidence in the CV.

5.10.2 Update the Water Table map

The groundwater data used the CA-DWR Fall 2017 (CA-DWR, 2018a) water table map. Additional water level measurement locations would improve the water table map. This may be available after the delivery of this report.

5.10.3 Siting new test holes and production wells

The AEM framework maps and profiles provided in this report provide insight on the relationship between current test holes and production groundwater wells. At the time of this report, the currently available lithology and geophysical log data for the Kaweah Subbasin area were used in building the framework maps and profiles. It is recommended that the results from this report be used to site new test holes and monitoring wells. Often test holes are sited based on previous work that is regional in nature or for local projects of small size. By utilizing the maps in this report new drilling locations can be sited in optimal locations. Consideration for the areas that have been identified as confined to semi-confined aquifers is a good place to start doing this work. These wells need to be screened in discreet zones in order to understand the potentiometric surfaces from each zone. These wells should also be spaced geographically for water level/potentiometric head measurements as well as water quality sampling. Small screened intervals would allow for age dating the water for improved understanding of recharge, time of travel along flow paths and groundwater-surface water interaction.

The location of new water supply wells for communities can also use the AEM results in this report to guide development of new water supply wells. Planners should locate wells in areas of greatest saturated thickness with the least potential for non-point source pollution.

5.10.4 Aquifer testing and borehole logging

Aquifer tests are recommended to improve estimates of aquifer characteristics. A robust aquifer characterization program is highly recommended at the state, county, and smaller municipal levels. Aquifer tests can be designed based on the results of AEM surveys and existing production wells could be used in conjunction with three or more installed water level observation wells (which can be used as monitoring wells for levels and water quality sampling after the test).

Additional test holes with detailed, functional, and well calibrated geophysical logging for aquifer characteristics are highly recommended. Most of the borehole geophysical logs provided for this investigation were well calibrated. However, there were also quite a few that demonstrate that additional calibrated and verified geophysical logs would be useful in the Kaweah Subbasin.

Examples of additional logging would be flow meter logs and geophysical logs including gamma, neutron, electrical, and induction logs. Detailed aquifer characteristics can be accomplished with nuclear magnetic resonance logging (NMR). This is a quick and effective way to characterize porosity and water content, estimates of permeability, mobile/bound water fraction, and pore-size distributions with depth. NMR logs compare well with the aquifer tests in our experience (Knight et al., 2012) and are very cost effective when compared to traditional aquifer tests.

5.10.5 Recharge Zones

The Kaweah Subbasin hydrogeologic framework in this report provides areas of recharge, that are widely spatially distributed, from the ground surface to the groundwater aquifers. Block flights of AEM data acquisition can provide the most detailed information for understanding recharge throughout the block flight areas. It is, again, recommended that additional AEM data be collected and interpreted utilizing closely-spaced flight lines using an AEM system that has near-surface resolution in the reconnaissance line flight areas. It is further recommended that future work integrate new soils maps with the results of this study to provide details on soil permeability, slope, and water retention to provide a more complete understanding of the transport of water from the land surface to the groundwater aquifers.

6 Description of Data Delivered

6.1 Tables Describing Included Data Files

Table 6-1 describes the raw data files included in Appendix 3_Deliverables \Raw_Data. As discussed above, six (6) 312 flights were required to acquire the Kaweah Subbasin AEM data (Figure 4-5). Grouped by flight date, there are four (4) data flies included in Appendix 3\Raw_Data for each flight. These files have extensions of "*.sps" and "*.skb". The "*.sps" files include navigation and DGPS location data and the "*.skb" files include the raw AEM data that have been PFC-corrections (discussed in Section 4.4.2). Two additional sets of files are used for all the flights. These are the system description and specifications file (with the extension "*.gex") in the GEO subdirectory and the 'mask' file (with the extension "*.lin"), in the MASK subdirectory, which correlates the flight dates, flight numbers, and assigned line numbers.

Table 6-2 describes the data columns in the ASCII *.xyz file Kaweah_EM312_MAG.xyz. This file contains the electromagnetic data, plus the magnetic and navigational data, as supplied directly from SkyTEM.

The result of the SCI is included in Kaweah_AEM_SCI_Inv_v1.xyz and the data columns of these databases are described in Table 6-3.

The borehole data used to assist in the interpretation of the SCI inversion results are included in the files listed in Table 6-4. Each type of borehole information has both a collar file containing the location of each of the wells, and a second file containing the borehole data for the individual wells. The data column descriptions for the collar files are listed in Table 6-5. Table 6-6 describes the channels in the lithology borehole data files and Table 6-7 describes the channels in the geophysical borehole data files.

The various interpretation results are included in the data file Kaweah_InterpSurfaces_v1.xyz in ASCII format. Table 6-8 describes the data columns of those files.

ESRI Arc View Binary Grids of the surfaces that were used in the interpretation (DEM, water table) and derived from the interpretation (top of geological units) of the AEM and borehole are listed in Table 6-9 and stored in Appendix 3_Deliverables\Grids.

In summary, the following are included as deliverables:

- Raw EM Mag data as ASCII *.xyz
- SCI inversion as ASCII *.xyz
- Borehole databases as ASCII *.xyz
- Interpretations as ASCII *.xyz
- Raw Data Files - SkyTEM files *.geo, *skb, *.lin
- ESRI ArcView grid files – surface, topo, etc.
- 3D fence diagrams of the lithologic interpretation

KMZs for AsFlown, Retained, Recharge, and Interpretation results (Discussed in Section 6.2)

Table 6-1. Raw SkyTEM data files

Folder	File Name	Description
Data	..NavSys.sps, …PaPc.sps, ...RawData_PFC.skb, …DPGS.sps	Raw data files included for each flight used in importing to Aarhus Workbench
Geo	20181205_456_Kaweah_312_DualWaveform_60Hz_SR2.gex 20181205_456_Kaweah_312_DualWaveform_60Hz_SR2.sr2	312 System Description
Mask	20181109_456_Kaweah_USA_Prod.lin	Production file listing dates, flights, and assigned line numbers

Table 6-2. Channel name, description, and units for Kaweah_EM312_MAG.xyz with EM, magnetic, DGPS, Inclinometer, altitude, and associated data.

Parameter	Description	Unit
Fid	Unique Fiducial Number	
Line	Line Number	
Flight	Name of Flight	yyyymmdd.ff
DateTime	DateTime Format	Decimal days
Date	DateTime Format	yyyymmdd
Time	Time UTC	hhmmss.sss
AngleX	Angle (in flight direction)	Degrees
AngleY	Angle (perpendicular to flight direction)	Degrees
Height	Filtered Height Measurement	Meters [m]
Lon	Longitude, WGS84	Decimal Degrees
Lat	Latitude, WGS84	Decimal Degrees
E_UTM11N_m	Easting, NAD83 UTM Zone 11N	Meters [m]
N_UTM11N m	Northing, NAD83 UTM Zone 11N	Meters [m]
DEM_m	Digital Elevation	Meters [m]
Alt	DGPS Altitude above sea level	Meters [m]
GDSpeedL	Ground Speed	Kilometers/hour [km/h]
Curr_LM	Current, Low Moment	Amps [A]
Curr_HM	Current, High Moment	Amps [A]
LMZ_G01	Normalized (PFC-Corrected) Low Moment Z-RxCoil values array	$pV/(m^4*A)$
HMZ_G01	Normalized (PFC-Corrected) High Moment Z-RxCoil values array	$pV/(m^4*A)$
HMX_G01	Normalized (PFC-Corrected) High Moment X-RxCoil values array	$pV/(m^4*A)$
PLNI	Power Line Noise Intensity monitor	V/m^2
Bmag	Raw Base Station Mag Data filtered	nanoTesla [nT]
MAG_Raw	Raw Mag Data	nanoTesla [nT]
Mag_ED	Mag filtered	nanoTesla [nT]
Diurnal	Diurnal Mag Data	nanoTesla [nT]
Mag_Cor	Mag Data Corrected for Diurnal Drift	nanoTesla [nT]
RMF	Residual Magnetic Field	nanoTesla [nT]
TMI	Total Magnetic Intensity	nanoTesla [nT]

Table 6-3. Channel name, description, and units for Kaweah_AEM_SCI_Inv_v1.xyz with EM inversion results.

Parameter	Description	Unit
LINE	Line Number	
East	Easting NAD83, UTM Zone 11	Meters [m]
North	Northing NAD83, UTM Zone 11	Meters [m]
DEM	DEM from 30 m grid NED NAVD88	Meters [m]
FID	Unique Fiducial Number	
TIME	Date Time Format	Decimal days
ALT_M	Altitude of system above ground	Meters [m]
INVALT	Inverted Altitude of system above ground	Meters [m]
INVALTSTD	Inverted Altitude Standard Deviation of system above ground	Meters [m]
DELTAALT	Change in Altitude of system above ground	Meters [m]
RESDATA	Residual of individual sounding	
RESTOTAL	Total residual for inverted section	
DOI_CONSERVATIVE	More conservative estimate of DOI, bgs	Meters [m]
DOI_STANDARD	Less conservative estimate of DOI, bgs	Meters [m]
RHO_0 THROUGH RHO_38	Inverted resistivity of each later	Ohm-m
RHO_STD	Inverted resistivity error per layer	
SIGMA_I_0 THROUGH SIGMA_I_39	Conductivity	S/m
DEP_TOP_0 THRU DEP_TOP_38	Depth to the top of individual layers	Meters [m]
DEP_BOT_0 THRU DEP_BOT_38	Depth to the bottom of individual layers	Meters [m]
THK_0 THROUGH THK_38	Thickness of individual layers	Meters [m]

Table 6-4. Files containing borehole information.

Database (*.xyz)	Description
Kaweah_ELogs_Collar.xyz	Geophysical Short Normal Resistivity Elogs
Kaweah_ELogs_Data.xyz	
Kaweah_Lith_Collar.xyz	Lithology logs
Kaweah_Lith_Data.xyz	

Table 6-5: Channel name, description, and units for collar files.

Parameter	Description	Unit
DH_Hole	Name of individual boreholes	
DH_East	Easting of boreholes, NAD83, UTM Zone 11	Meters (m)
DH_North	Northing of boreholes, NAD83, UTM Zone 11	Meters (m)
DH_RL	Elevation of top of borehole	Meters (m)
DH_Dip	Dip of borehole	Degrees
DH_Azimuth	Azimuth of borehole	Degrees
DH_Top	Depth to top of borehole	Meters (m)
DH_Bottom	Depth to bottom of borehole	Meters (m)

Table 6-6. Channel name description and units for Lithology borehole data.

Parameter	Description	Unit
DH_Hole	Name of Borehole	
DH_East	Easting of boreholes, NAD83, UTM Zone 11	Meters (m)
DH_North	Northing of boreholes, NAD83, UTM Zone 11	Meters (m)
DH_RL	Elevation of top of borehole	Meters (m)
DH_From	End of interval	Meters (m)
DH_To	Start of interval	Meters (m)
Lithcode	Lithology description associated with 30 categories	
DH_Description	Description of lithology material	

Table 6-7. Channel name description and units for E-Logs borehole data.

Parameter	Description	Unit	Type of Log
DH_Hole	Name of Borehole		
DH_East_SPZ4_ft	Easting of boreholes, Calif. State Plane, Zone 4	Feet (ft)	
DH_North_SPZ4_ft	Northing of boreholes, Calif. State Plane, Zone 4	Feet (ft)	
DH_RL_ft	Elevation of borehole data point	Feet (ft)	
DH_Depth_FT	Depth	Feet (ft)	
SN	Short Normal Resistivity 16in	Ohm-m	GP
DH_East_m	Easting of boreholes, WGS84, UTM Zone 11	Meters (m)	All
DH_North_m	Northing of boreholes, WGS84, UTM Zone 11	Meters (m)	All
DH_RL_m	Elevation of top of borehole	Meters (m)	All
DH_Depth_m	Depth	Meters (m)	GP

Table 6-8: Channel name, description, and units for the interpretation results file Kaweah_InterpSurfaces_v1.xyz.

Parameter	Description	Unit
LINE	Line Number	
Easting	Easting NAD83, UTM Zone 11	Meters (m)
Northing	Northing NAD83, UTM Zone 11	Meters (m)
DEM_m	Topography at 30m sampling (NAVD 1988)	Meters (m)
RHO[0] through RHO[38]	Array of Inverted model resistivities of each later	Ohm-m
RESDATA	Inversion model residuals of each individual sounding	
DEP_TOP[0] through DEP_TOP[38]	Depth to the top of individual layers	Meters (m)
DEP_BOT[0] through DEP_BOT[38]	Depth to the bottom of individual layers	Meters (m)
DOI_Conservative	More conservative estimate of DOI from Workbench	Meters (m)
DOI_Standard	Less conservative estimate of DOI from Workbench	Meters (m)
WaterTable_2017	Elevation of the top of the water table from the 2017 report.	Meters (m)
Top_Corcoran	Top of Corcoran Clay in the Kaweah AEM survey area	Meters (m)
Bot_Corcoran	Bottom of Corcoran Clay in the Kaweah AEM survey area	Meters (m)
Top_Granite	Top of Granite which only occurs on L730300	Meters (m)

Table 6-9. Files containing ESRI ArcView Binary Grids *.flt (NAD 83 UTM 11 North)

Grid File Name	Description	Grid Cell Size (meters)
Kaweah_DEM	Digital Elevation Model (ground surface elevation) (NAVD88 meters) of the 2018 Kaweah survey area, NAD83/UTM Zone 11N, meters	10
Kaweah_WT_F2017	Elevation (NAVD88 meters) of the water table (Fall 2017) for the 2018 Kaweah Survey area, NAD83/UTM Zone 11N, meters	30
Kaweah_Basement_DepthTo	Depth to Top of Basement (NAVD88 meters) for the 2018 Kaweah Survey area, NAD83/UTM Zone 11N, meters	500
Kaweah_Basement_TopEle	Elevation of the Top of Basement (NAVD88 meters) for the 2018 Kaweah Survey area, NAD83/UTM Zone 11N, meters	500
Kaweah_CorClay_TopEle	Elevation of the Top of the Corcoran Clay (NAVD88 meters) for the 2018 Kaweah Survey area, NAD83/UTM Zone 11N, meters	500
Kaweah_CorClay_BotEle	Elevation of the Bottom of the Corcoran Clay (NAVD88 meters) for the 2018 Kaweah Survey area, NAD83/UTM Zone 11N, meters	500
Kaweah_CorClay_DepthTo	Depth to the Top of the Corcoran Clay (NAVD88 meters) for the 2018 Kaweah Survey area, NAD83/UTM Zone 11N, meters	500
Kaweah_CorClay_Thickness	Thickness of the Corcoran Clay (NAVD88 meters) for the 2018 Kaweah Survey area, NAD83/UTM Zone 11N, meters	500

6.2 Description of Included Google Earth KMZ Data and Profiles

In addition to the data delivered in ".xyz" format, a Google Earth .KMZ file was generated to view the geophysical AEM flight line locations and interpreted geologic data. KMZ files for all "*As-Flown*" flight lines and data "*Retained*" for inversion after editing are included in the folder "*Appendix_3_Deliverables\KMZ\FlightLines*".

KMZ files of the potential recharge zones in the Kaweah Subbasin AEM investigation area are included in the folder "*Appendix_3_Deliverables\KMZ\Recharge*"

Unique KMZ files were created for each individual flight line. Within this specialized KMZ file, the AEM flight line is shown as well as place marks at each location where there are interpreted geologic results. The attribute data for each unique place mark contains location information plus the elevations of tops of the interpreted stratigraphy as well as the 2017 water table. This KMZ file is located within the "*Appendix_3_Deliverables\KMZ\Interpretation\Kaweah_Profiles*" folder. Also, in this folder is a "*GoogleE_Readme.pdf*" file that provides instructions in regard to the "*Settings*" changes that need to be made in Google Earth, and how to use the KMZ files in Google Earth including a legend of what attributes are displayed when an AEM sounding location is clicked. This file is repeated below as a convenience. An example of the Kaweah AEM Interpretation KMZ is presented in Figure 6-1.

6.2.1 Included README for the Kaweah Subbasin AEM Interpretation KMZ

README for:

Kaweah_AEM_Interpretation.kmz

Data Files - Please copy the folder *Kaweah_Profiles* to your C:\ drive. Do not rename any of the images within the folder.

Google Earth Instructions:

STEP 1: In Google Earth, click "*Tools*", then "*Options*".

STEP 2: In the Google Earth Options box, click the "*General*" tab.

STEP 3: Under "*Placemark balloons*", make sure the box is checked to allow access to local files (the profiles).

STEP 4: Under "*Display*", make sure the box is checked to show web results in external browser.

STEP 5: The *Kaweah_AEM_Interpretation.kmz* file within the folder named *Kaweah _Profiles* can now be opened and viewed in Google Earth.

Data:

Line – AEM line number

Easting (m) – Easting coordinate in NAD83, UTM 11N, in meters

Northing (m) – Northing coordinate in NAD83, UTM 11N, in meters

Elevation (m) – Digital Elevation Model (DEM) elevation in meters

WaterTable2017 Elev (m) – 2017 Water Table elevation, in meters (From CA-DWR)

Top of Corcoran Clay (m) – Top of Corcoran Clay, in meters

Bottom of Corcoran Clay (m) – Bottom of Corcoran Clay, in meters

Top of Basement (m) – Top of the Mesozoic Basement materials (Granite, Ophiolite), meters

Profiles – Link to AEM Interpreted Lithology profile images

Legend – Link to this write-up describing data channels listed here

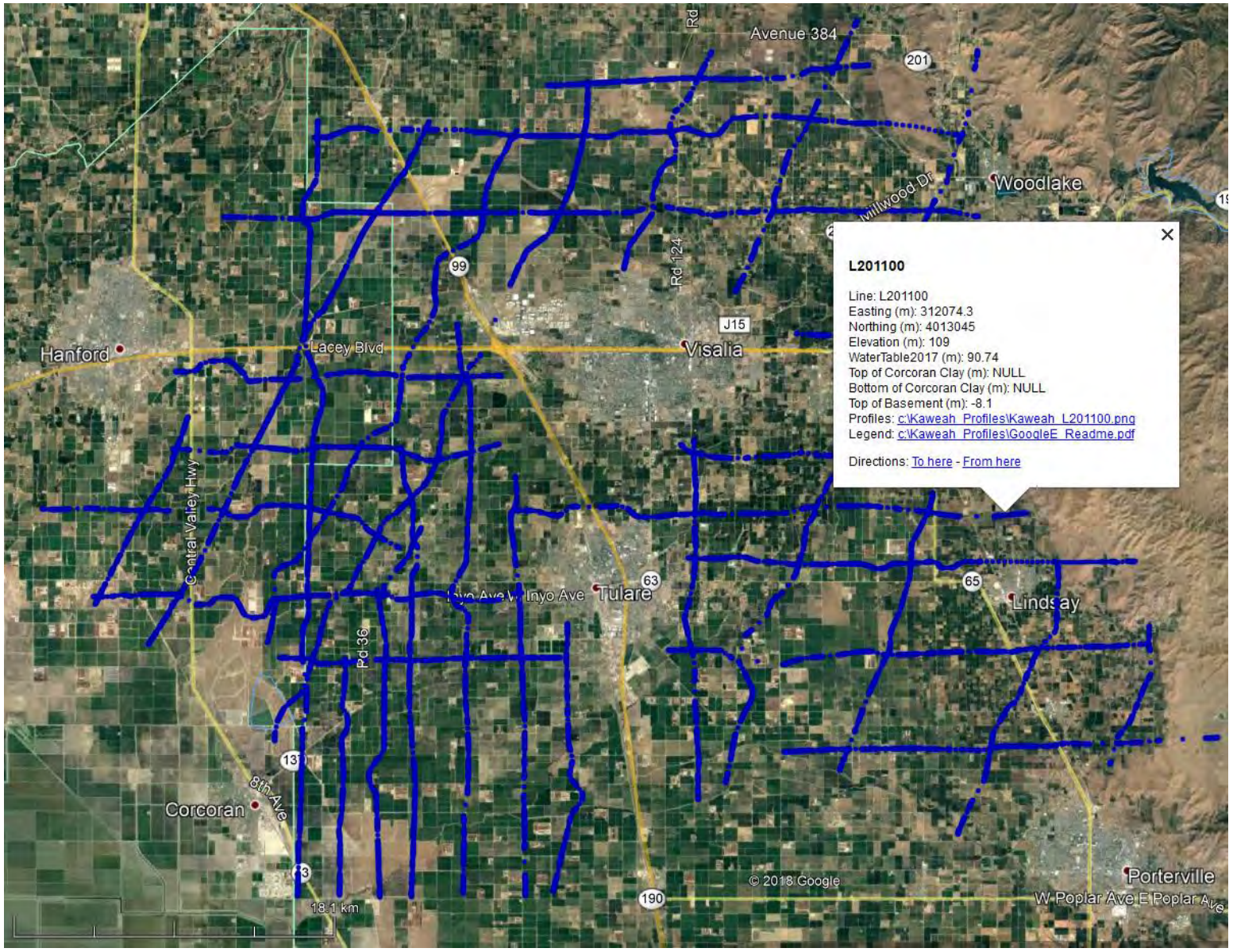

Figure 6-1. Example Google Earth image for the Kaweah AEM Interpretation kmz.

7 References

Asch, T.H., Abraham, J.D., and Irons, T., 2015, A discussion on depth of investigation in geophysics and AEM inversion results, Presented at the Society of Exploration Geophysicists Annual Meeting, New Orleans.

Asch, T.H., Abraham, J.D., Cannia, J.C., 2017, AEM-based hydrogeological frameworks in the Owens and Central valleys of California: Fast Times, v.22, no.3, p.47-57.

Asch, T.H., Gottschalk, I., Knight, R., Abraham, J.D., Cannia, J.C., Van Der Maaten, K., 2018, An airborne electromagnetic investigation of the Marina, CA hydrogeologic framework: presented at the Symposium on the Application of Geophysics to Environmental and Engineering Problems, Nashville, Tennessee, 27 March 2018.

Barow, K.R., Stork, S.V., and Dubrovsky, N.M., 1998, Nitrate and Pesticides in groundwater in the eastern San Joaquin Valley, California—Occurrence and Trends: U.S. Geological Survey Water-Resources Investigations Report 98-4040, 33 p., accessed April 19, 2019 at https://pubs.er.usgs.gov/publication/wri984040A.

Bartow, J.A., 1984, Geologic map and cross-sections of the southeastern margin of the San Joaquin Valley, California: U.S. Geological Survey, Miscellaneous Investigations Series, Map I-1496, 2pl., accessed April 19, 2019 at https://ngmdb.usgs.gov/Prodesc/proddesc_22.htm.

Bartow, J.A., 1991, The Cenozoic evolution of the San Joaquin Valley, California: U.S. Geological Survey Professional Paper 1501, 40 p., 2 pl., accessed April 19, 2019 at https://pubs.er.usgs.gov/publication/pp1501.

Bear, J., 1979, Hydraulics of groundwater: McGraw-Hill, New York, 569 p.

California Department of Water Resources, 2003, San Joaquin Valley – Kaweah: State of California Department of Water Resources, Bulletin 118 Groundwater Basin Descriptions, accessed November 30, 2018 at: https://water.ca.gov/Programs/Groundwater-Management/Bulletin-118

California Department of Water Resources, 2014, Geology, hydrology, quality of water, and water supply of the Three Rivers area, California: State of California Department of Water Resources, Division of Integrated Regional Water Management, accessed November 30, 2018 at: http://tularecounty.ca.gov/rma/index.cfm/planning-building/community-plans/updated-community-plans/three-rivers-community-plan/geology-hydrology-quality-of-water-and-water-supply-of-the-three-rivers-area-california/

California Department of Water Resources, 2018a, Groundwater Information Center Groundwater Interactive Map Application: California Department of Water Resources, accessed November 30, 2018 at: https://gis.water.ca.gov/app/gicima/#bookmark_GroundwaterElevation

California Department of Water Resources, 2018b, Success Dam (SCC): California Department of Water Resources, California Data Center accessed April 15, 2019 at: https://cdec.water.ca.gov/dynamicapp/selectQuery

California Geological Survey (CGS), 2010, Geologic Map of California, Version 2: Department of Conservation, California Geologic Data Map Series, GDM No. 2, accessed April 23, 2019 at https://data.ca.gov/dataset/geologic-map-california/resource/ffbd7759-dd0c-4be1-b99d-5a93e17ac359

Carney, C.P., Abraham, J.D., Cannia, J.C., and Steele, G.V., 2015, Airborne Electromagnetic Geophysical Surveys and Hydrogeologic Framework Development for Selected Sites in the Lower Elkhorn Natural Resources District: prepared for the Lower Elkhorn Natural Resources District by Exploration Resources International Geophysics LLC, Vicksburg, MS. .http://www.enwra.org/LENRD2014AEMDataDownload.html (accessed December 31, 2018)

Christensen, N. B., J. E. Reid, and M. Halkjaer, 2009, "Fast, laterally smooth inversion of airborne time-domain elecromagnetic data." *Near Surface Geophysics* 599-612.

Christiansen, A. V. and E. Auken, 2012, "A global measure for depth of investigation." *Geophysics,Vol. 77, No. 4* WB171-177.

DatamineDiscover, 2018, Datamine Discover Profile Analyst, available on the world-wide web at: https://www.dataminesoftware.com/discover/.(accessed December 31, 2018)

Davis, G.H., Lofgren, B.E., and Seymour, Mack, 1964, Use of ground-water reservoirs for storage of surface water in the San Joaquin Valley, California: U.S. Geological Survey Water-Supply Paper 1618, 125 p. 11 pl.

Driscoll, F.G, 1987, "Groundwater and Wells", Published by Johnson Division, St. Paul, MN.

Faunt, C.C., ed., 2009, Groundwater Availability of the Central Valley Aquifer, California: U.S. Geological Survey Professional Paper 1766, 225 p., accessed April 19, 2019 at https://pubs.usgs.gov/pp/1766/.

Foged, N., Auken, E., Christiansen, A.V., and Sorensen, K.I., 2013, Test-site calibration and validation of airborne and ground based TEM systems: Geophysics, V.78, No.2, E95-E106.

Fugro West, 2007, Water Resources Investigation of the Kaweah Delta Water Conservation District 2003, Revised 2007: Fugro West, Inc., 177 pp., 71 plates (Received from KDWCD, Larry Dotson, April 16, 2019).

Galloway, D., 1999, San Joaquin Valley, California; in Land subsidence in the United States (Galloway, D., Jones, D.R., and Ingebritsen, S.E., *ed.*), U.S. Geological Survey Circular 1182, pp 23-34, accessed April 18, 2019 at https://pubs.usgs.gov/circ/circ1182/

Heath, R.C., 1983. Basic ground-water hydrology, U.S. Geological Survey Water-Supply Paper 2220, 86p, http://pubs.er.usgs.gov/publication/wsp2220 (accessed April 18, 2017)

Hilton, G.S., Klausing, R.L., and Kunkel, F., 1963, Geology of the Terra Bella-Lost Hills Area, San Joaquin Valley, California: U.S. Geological Survey, Open-File Report 63-47, 64p., 28 pl., accessed on April 18, 2019 at https://pubs.er.usgs.gov/publication/ofr6347.

HydroGeophysics Group, Aarhus University, 2010, "Validation of the SkyTEM system at the extended TEM test site." Aarhus, Denmark.

HydroGeophysics Group, Aarhus University, 2011, "Guide for processing and inversion of SkyTEM data in Aarhus Workbench", Version 2.0."

Johnson, T.D. and Belitz, K., 2014, California Groundwater Units: U.S. Geological Survey Data Series 796, 34 p., accessed April 18, 2019 at https://pubs.usgs.gov/ds/796/.

Kaweah Delta Water Conservation District, 2015, Groundwater management plan: Kaweah Delta Water Conservation District, amended July 7, 2015, accessed on December 6, 2018 at: www.kdwcd.com/water-resources/

Kaweah Delta Water Conservation District, 2017, 2017 annual groundwater report: Kaweah Delta Water Conservation District, accessed on December 6, 2018 at: www.kdwcd.com/water-resources/

Kaweah Delta Water Conservation District, 2018, Kaweah Delta Water Conservation District: Kaweah Delta Water Conservation District, accessed on December 6, 2018 at: www.kdwcd.com

Knight, R., E. Grunewald, T. Irons, K. Dlubac, Y. Song, H. N. Bachman, B. Grau, D. Walsh, J. D. Abraham, and J. Cannia, 2012, Field experiment provides ground truth for surface nuclear magnetic resonance measurement: Geophysical Research Letters, v.39, no. 3, 7p, accessed April 27, 2019 at https://agupubs.onlinelibrary.wiley.com/doi/10.1029/2011GL050167.

Knight, R., Smith, R., Asch, T., Abraham, J., Cannia, J., Viezzoli, A., and Fogg, G., 2018, Mapping aquifer systems with airborne electromagnetics in the Central Valley of California: Groundwater, v.55, no.6, p.893-908.

Ley-Cooper, Y. and Davis, A., 2010. Can a borehole conductivity log discredit a whole AEM survey?: *in* Extended abstracts of the Australian Society of Exploration Geophysicists Annual meeting Aug 20-24, Sydney, Australia.

Matthews, R.A., and Burnett, J.L., 1965 Geologic map of California – Fresno sheet: California Division of Mines and Geology, scale 1:250,000.

McClelland, E.J., 1962, Aquifer-test compilation for the San Joaquin Valley, California: U.S. Geological Survey Open-File Data Report 62-80, 38 p, accessed April 18, 2019 at https://doi.org/10.3133/ofr6280.

Muir, K.S., 1977, Ground water in the Fresno area, California: U.S. Geological Survey Water-Resources Investigations Report 77-59, 22 p., accessed April 18, 2019 at https://pubs.usgs.gov/wri/1983/4246/report.pdf

Page, R.W., 1983, Geology of the Tulare Formation and other continental deposits, Kettleman City area, San Joaquin Valley, California, *with a section on* ground-water management considerations and use of texture maps: U.S. Geological Survey Water-Resources Investigations Report 83-4000, 28 p., 2 pl., accessed on April 18, 2019 at https://ngmdb.usgs.gov/Prodesc/proddesc_35648.htm

Page, R.W., 1986, Geology of the fresh ground-water basin of the Central Valley, California, with texture maps and sections; Regional Aquifer System Analysis: U.S. Geological Survey Professional Paper 1401-C, 54 p., 6 pl.

Page, R.W., and LeBlanc, R.A., 1969, Geology, hydrology, and water quality in the Fresno area, California: U.S. Geological Survey Open-File Report 69-328, 193 p., 29 pl., accessed on April 18, 2019 at https://pubs.er.usgs.gov/publication/ofr69328.

Planert, M. and Williams, J.S., 1995, Ground Water Atlas of the United States, Segment 1, California, Nevada: U.S. Geological Survey Hydrologic Investigations Atlas, 730-B, 28 p.

Provost & Pritchard Consulting Group, 2015, Groundwater management plan James Irrigation District and the City of Sand Joaquin (*ed* Owen Kubit); Provost & Pritchard Consulting Group, November 10, 2015, accessed December 10, 2018 at: water.ca.gov/LegacyFiles/wateruseefficiency/sb7/docs/2016/James ID 2016 AWMP.pdf

Schamper, C., Auken, E., and Sorensen, K., 2014, Coil response inversion for very early time modelling of helicopter-borne time-domain electromagnetic data and mapping of near-surface Geologic Layers. European Association of Geoscientistis & Engineers, Geophysical Prospecting.

SkyTem Airborne Surveys Worldwide, 2019, SkyTEM304M, https://skytem.com/tem-systems/ (accessed March 28, 2019)

Smith, R. and Knight, R., 2019, Modeling land subsidence using InSAR and airborne electromagnetic data: Water Resources Research, v.55, 19pp., https://doi.org/10.1029/2018WR024185

U.S. Census Bureau, 2018, Census 2010 total population: U.S. Census Bureau, accessed November 5, 2018, at: https://factfinder.census.gov/faces/nav/jsf/pages/index.xhtml#none.

U.S. Geological Survey (USGS), 2018, USGS Groundwater Data for California: U.S. Geological Survey National Water Information System, accessed November 26, 2018, at: https://waterdata.usgs.gov/ca/nwis/gw.

U.S. Geological Survey (USGS), 2019, The National Map, 2018, 3DEP products and services: The National Map, 3D Elevation Program Web page, http://nationalmap.gov/3DEP/3dep_prodserv.html (accessed April 1, 2019)

Weissmann, G.S., Mount, J.F., and Fogg, G.E., 2002, Glacially driven cycles in accumulation space and sequence stratigraphy of a stream-dominated alluvial fan, San Joaquin Valley, California, U.S.A: Journal of Sedimentary Research, v.72, no.2, pp.240-251, access April 19, 2019 at https://pubs.geoscienceworld.org/sepm/jsedres/article-pdf/72/2/240/2814711/240.pdf or https://doi.org/10.1306/062201720240

Weissmann, G.S., Zhang, Y., Fogg, G.E., and Mount, J.F., 2004, Influence of incised-valley-fill deposits on Hydrogeology of a Stream-Dominated Alluvial Fan: Book Chapter in Aquifer Characterization, Society for Sedimentary Geology, v.80, ed. Bridge, J.S. and Hyndman, D.W., https://doi.org/10.2110/pec.04.80.0015

White, D., 2016, Stratigraphy and transmissivity of the Kaweah River fan, Visalia, California: California State University, Fresno College of Science and Mathematics, Thesis, 119 p.

Woodring, W.P., Stewart, Ralph, and Richard, R.W., 1940, geology of the Kettleman Hills oil field, California: U.S. Geological Survey Professional Paper 195, 170 p., accessed on April 18, 2019 at https://doi.org/10.3133/pp195

Viezzoli, A., A. V. Christiansen, E. Auken, and K. Sorensen, 2008, "Quasi-3D modeling of airborne TEM data by spatially constrainted inversion." *Geophysics Vol. 73 No. 3* F105-F11

Appendix 7B

Integration of InSAR with Airborne Geophysical Data for the Development of Groundwater Models

Integration of InSAR with Airborne Geophysical Data for the Development of Groundwater Models

Decision-Making Activity; Description and Role or Authority of Water Resources Partner

Climate change and population growth are increasing concerns about the depletion of groundwater in the western U.S. Among all states, California uses the most groundwater, extracting on average 30 cubic kilometers per year. In 2014, the California Legislature passed the Sustainable Groundwater Management Act (SGMA). Local agencies, referred to as Groundwater Sustainability Agencies (GSAs), are responsible for achieving sustainability, with plans due in 2020 or 2022 for the original 127 medium and high priority basins. As a way of defining sustainability, SGMA lists six "undesirable effects" associated with groundwater use: chronic lowering of water levels, significant and unreasonable reduction of groundwater storage, significant and unreasonable seawater intrusion, significant and unreasonable degraded water quality, significant and unreasonable land subsidence, depletions of interconnected surface water. The management challenge, within any GSA, is to assess possible risks to the long-term sustainability of the groundwater resource, and to decide on the management actions required (e.g. the location, timing and magnitude of groundwater pumping or aquifer recharge) so as to avoid the undesirable effects.

The decision-making activity to be enhanced through this project is the development of the groundwater model. Developing the groundwater model is a key decision-making activity, as it provides the modeling tools required to predict and assess changing conditions (e.g. climate, land use) and the outcomes of possible alternate water management actions; so is thus the foundation on which to build effective groundwater management. Enhancing this decision-making activity directly supports decision-making, within the GSAs, related to sustainable groundwater management.

The groundwater model should be a 3D lithologic model capturing the spatial heterogeneity of the subsurface at the spatial resolution needed as input for flow modeling, parameterized in terms of the hydraulic properties required to model flow (e.g. hydraulic conductivity, porosity, specific yield, and specific storage under elastic and inelastic conditions), and capturing the various stores and fluxes in the represented system. There are a number of groundwater models in various stages of development in California. These models include C2VSIM developed by the California Department of Water Resources (DWR), the Central Valley Hydrologic Model (CVHM) developed by the U.S. Geological Survey (USGS) (Faunt et al., 2009), and local models developed by the GSAs and their consultants. With California's SGMA groundwater legislation, the newly established GSAs are given authority to limit groundwater use to ensure sustainability, so high-quality data at scales and depths relevant to these agencies are of great importance for inclusion in the groundwater models. However, most existing models utilize limited geologic data at depths relevant to these agencies; the prediction accuracy of all of the available models needs to be significantly improved in order to have confidence in the groundwater management plans that are developed using these models to support decision-making.

There is a critical need for more data to inform groundwater models. But the currently employed, traditional methods of acquiring data, through the drilling of wells with testing and logging, are slow, expensive and insufficient in terms of data coverage. What we propose is to improve the quality, and thus the usefulness, of groundwater models by incorporating

information derived from interferometric synthetic aperture radar (InSAR) data and airborne electromagnetic (AEM) data. We will develop a methodology that will update the CVHM, and obtain groundwater models, to a depth of ~500 m, with the required spatial resolution and hydrologic/geomechanical properties so as to provide accurate predictions of groundwater flow and pumping-induced aquifer system compaction and resulting subsidence. These accurate predictions are an essential component of the decision-making required for the development of sustainable groundwater management plans.

We are partnering in this project with GSAs and their consultants, directly engaged in SGMA implementation. The new methodology that we will develop, for the decision-making activity of generating a groundwater model, will directly serve GSAs as end-users who can adopt these models, particularly their supporting datasets, to support the decision-making required through SGMA to attain sustainable groundwater management. We will be working with the GSA of Butte County, interacting directly with Paul Gosselin (Director) and Christina Buck (Assistant Director) of the Butte County Department of Water and Resource Conservation. Our second study area is the Kaweah Basin. Here we are working with three GSAs (mid-Kaweah, greater Kaweah, and east Kaweah) and their consultants. Our interaction will be primarily through GEI Consultants who are responsible for the development of the groundwater model of the Kaweah Basin; Chris Petersen with GEI is acting as our main point of contact and co-ordinating activities and communication with the larger group. By project end, our partner GSAs will have in place improved groundwater models that can be used, in conjunction with any existing local models, to support the development and future implementation of their required sustainable groundwater management plans. In addition, we will have documented our workflow so that any GSA with access to the various forms of required input data would be able to use our methodology to develop their local groundwater model. We have supporting letters from Butte County and from the three GSAs in the Kaweah Basin.

At the state level, we are partnering with the California Department of Water Resources (DWR) and the State Water Resources Control Board (the Board), and have supporting letters from these two agencies. Under SGMA, DWR is specifically tasked with the development, implementation, and technical evaluation of the regulations to modify basin boundaries and develop groundwater sustainability plans. DWR also has financial and technical assistance obligations. The Board carries the responsibility of stepping in to manage groundwater once DWR has deemed that a groundwater sustainability plan is inadequate and not reasonably capable of reaching sustainability. The Board's role is referred to as state intervention and is intended to be a backstop to ensure the resource is protected. Partnering with these two agencies, in addition to the GSAs, will ensure that the product that we produce contributes significantly to the current challenges faced in sustainable groundwater management.

The proposed project will be conducted by working closely with GSAs in two areas in the Central Valley of California utilizing one of the available regional groundwater models; but we note that the methods that we will develop are readily transferrable to other geographic areas and other numerical models.

NASA Earth Observations, Models and Datasets

We begin our work with the CVHM. This will be the starting groundwater model for our work with Butte County; in the Kaweah Basin, we will work with the “Kaweah model”, an updated version of the CVHM. CVHM is a numerical model that accounts for integrated,

variable water supply and demand, and simulates surface-water and groundwater flow, and subsidence across the Central Valley system (Faunt, 2009) on a monthly basis. This model was developed at scales relevant to water management decisions for the entire Central Valley aquifer system so has one square mile grid cells and 10 layers that get thicker with depth and extend to a total depth of ~500 m in most parts of the Central Valley (Faunt, 2009). Recently, this model was extended through water year 2014 by including a scenario based on updated surface-water inflows and deliveries, updated land-use maps, and climate data (precipitation and reference evapotranspiration). The numerical code driving the model has been significantly enhanced to better simulate conjunctive use of surface water and groundwater for irrigated agriculture and aquifer system compaction (Boyce and others, in review). The CVHM is a valuable resource for water managers for addressing some needs at the state or county level, but has relatively coarse spatial resolution and limited geologic data in the deeper aquifer, which in recent years has been depleted at accelerated rates. Thus, while useful it does not provide the level of spatial detail required for predicting, with confidence, the outcome of various groundwater management actions affecting both the shallow and deeper zones of the groundwater system.

The two data sets that provide the foundation for our new approach to updating CVHM and the Kaweah model so as to develop improved groundwater models are InSAR data and AEM data. InSAR data, commonly acquired by satellites, provide a measure of land deformation. We will use InSAR data from the Envisat and Sentinel-1 missions, covering time periods from 2002-2010 and from 2015-present. Both satellites have full coverage of both study areas. They are operated by the European Space Agency, and produce estimates of land deformation at the resolution of ~100 m in agricultural areas, with deformation measurement error on the order of 5 mm. Envisat data nominally have a 40 day revisit cycle, although there are many gaps in the data due to measurement problems on the satellite. The Sentinel-1 mission includes two satellites-Sentinel-1a and Sentinel-1b. Each satellite has a revisit period of 12 days, so combining them could result in a 6-day revisit cycle. The data quality of Sentinel-1 is high, with few if any gaps in acquisition due to measurement problems. While the InSAR data to be utilized in this study are not acquired by NASA, the methods developed in this proposal can be implemented with data from the upcoming NISAR launch planned for 2020. These methods will leverage the ability of NISAR data to be used for groundwater modeling purposes.

The AEM data in the areas of Butte County and the Kaweah Basin will be acquired in the fall of 2018 with funding provided by Butte County ($200k) and the GSAs in the Kaweah Basin ($150k), and by grants to Knight from the Gordon and Betty Moore Foundation and the Danish Environmental Protection Agency. The AEM data, approximately 800 km in each area, will be acquired using a helicopter-deployed system. The result, after data processing and inversion, will be a set of 2D slices displaying the detailed variation in the electrical resistivity of the subsurface. Through calibration with well data and geologic interpretation, this can be transformed to map out the distribution of sediment textures (sand, silt, clay), defining the large-scale architecture of the groundwater system. The horizontal resolution is approximately 30 m along the flight lines, and equal to line spacing between the flight lines, typically 200 m to 1 km, depending on the objectives of the data acquisition. The depth to which the electrical resistivity can be determined, referred to as the depth of investigation (DOI), depends on the electrical resistivity of the subsurface, with shallower DOI in areas with lower electrical resistivity. In October 2015, Knight and co-workers acquired AEM data in the Tulare Irrigation District, within the Kaweah Basin (Knight et al., 2018). The data quality was superb, imaging to a depth of approximately 500 m, providing perfect overlap with the depth range of the CVHM. The vertical

resolution of the AEM data is on the scale of a meter near the ground surface, increasing to tens of meters at the DOI of 500 m.

There are a number of other ancillary datasets that will be used. Geologic logs (also referred to as drillers' logs) are included in the well completion reports and provide information about the lithology of the subsurface, as observed by the driller during drilling of the well. These logs, available from DWR as pdfs, are used to develop the relationship between electrical resistivity and sediment texture, allowing us to use the AEM data to map out the major lithologic units. In the Central Valley as a whole, approximately 10,000 drillers' logs have been digitized for various USGS studies. In the Kaweah Basin, we will have available to this project ~200 digitized logs, currently being assembled and digitized by a consultant (GSI) working in support of the AEM data acquisition. In Butte County, Todd Greene of Chico State is leading an effort to assemble and digitize the required geologic logs.

Geophysical resistivity logs are the 1D record of the electrical resistivity measurements made in water wells and oil and gas wells using instrumented tools, lowered into a well. These logs are used to assist with the inversion and interpretation of the AEM data. We are in the process of compiling and digitizing these in both of the study areas. Resistivity logs from water wells are available through the DWR website. From oil and gas wells they are available from an online mapping system provided by the California Division of Oil, Gas, and Geothermal Resources (DOGGR). While the oil and gas wells extend to greater depths, there is the tendency to not acquire data in the top ~200 m, an area where we require data for the development of groundwater models. In each of our study areas, we will have approximately 40 geophysical logs to assist with the interpretation of the AEM data. These logs are also being digitized and depth registered by GSI and Greene so as to be available as LAS files.

Information about the water level in an area is also helpful in interpreting the AEM data. At depths where the sediments are not saturated, the resistivity tends to be higher, which affects the measured AEM signal. Water level data are available in California, and will be accessed through the California Statewide Groundwater Elevation Monitoring Program (CASGEM) and the USGS National Water Information System (NWIS). The CASGEM data are acquired by DWR (or partner agency) primarily from irrigation wells and also from dedicated monitoring wells. This results in a measurement every few kilometers. The USGS data are from various studies throughout the state of California and are more sparse, but often have more complete well construction information.

Continuous global positioning system (CGPS) data will be used to calibrate and validate the InSAR data. In California, data from hundreds of CGPS stations are available on the UNAVCO website (unavco.org). There are 20+ CGPS stations within the InSAR footprints covering our two study areas. Where available (or transferable from nearby areas), extensometer data will be used to help validate the depth at which the compaction is occurring.

PROJECT ELEMENTS

Description of the Water Management Challenge

The general geographic area of our work is the Central Valley of California. Covering 50,000 km^2, bounded by the Sierra Nevada to the east and the Coast Ranges to the west, the valley yields a third of the produce grown in the United States valued at $17 billion dollars per year. Much of the irrigation water in the valley has historically been from the conjunctive use of

both surface water and groundwater. In times of drought, most recently in the periods 2007 to 2009 and 2012 to 2016, the only way to meet irrigation needs has been through more extensive pumping of groundwater. This has exacerbated an already serious problem in the Central Valley, where some areas have experienced declining water levels for several decades. We will focus in this project on two study areas: the Kaweah Basin and Butte County.

The Kaweah Basin is in an area where agriculture in an essential component of the local economy, and is an area that has seen significant subsidence due to extensive groundwater pumping. The GSAs in the Kaweah Basin are in the process of revising the Kaweah model (an updated CVHM) in their area, incorporating more geologic logs, but it is acknowledged that the model is in need of improvement in order to support the challenges faced in developing a plan for sustainable groundwater management. A key issue is this area is the continued subsidence, which during the time period from 2007 to 2010 reached 30 cm/yr in places. Not only has this aquifer system compaction led to a permanent loss in groundwater storage (Smith et al., 2017), we have recently shown that over-pumping has triggered the release of arsenic from clay layers, resulting in serious water quality concerns in the area (Smith et al., 2018). Having in place a groundwater model that can accurately predict the likelihood of aquifer system compaction and resulting subsidence due to proposed groundwater management actions is essential for sustainable groundwater management in this area.

Butte County has not experienced the same issues with groundwater depletion as seen in the Kaweah Basin. There is less groundwater demand due to higher precipitation in this more northern part of the Central Valley, lower summer temperatures, and greater availability of surface water. Our work in Butte County is intended to support a number of management decisions that need to be made as part of developing and implementing a sustainable groundwater management plan. These include decisions about the desirable locations (in plan view and in depth), timing and magnitude of groundwater pumping in existing wells and in permitting new wells, so as to avoid undesirable effects such as subsidence or impacts on shallow wells and surface water.

Methodology and Earth Observations to be Employed

In each of our study areas we will build a groundwater model that covers an area of ~ 100 km x 100 km and extends to a depth of ~500 m, using as our starting point the CVHM or an updated version, the Kaweah model. While other hydrologic models exist, the CVHM is the preferred model for the development of our new methodology due to its detailed geologic framework and extensive use in previous studies to accurately model subsidence, one of the SGMA undesirable effects of great concern in the Central Valley. Our novel methodology will use the MODFLOW framework implemented in CVHM, but update, with significantly improved spatial resolution, the description and parameterization of the subsurface by combining two data sets, both of which are sensitive to the lithology of the subsurface: InSAR data and AEM data. This approach is highly innovative. The integration of satellite and geophysical data, both of which contain information about the subsurface, is an obvious, but to-date unexploited, approach to improving our ability to quantify subsurface properties and model subsurface processes.

In this study we are in a unique position, having access to high quality InSAR data from 2002-2010 and from 2015-present, and having access to the geophysical AEM data sets to be acquired in fall 2018. Through this project we will have an opportunity to develop our new approach and demonstrate the viability of using the integration of these two data types as the

basis for developing high resolution groundwater models wherever InSAR data and AEM data are available. The resulting groundwater models will have the large-scale architecture seen in the AEM data (likely eight layers, 0 to 200 m in thickness); within these layers descriptions of sediment texture, also from the AEM data; and, by integrating AEM and InSAR, improved estimates within the CVHM and the Kaweah model of the following at the spatial resolution of the AEM data: vertical and horizontal hydraulic conductivity, porosity, specific yield, and specific storage under elastic and inelastic conditions. Such a model can be used to accurately predict total groundwater storage; and spatial and temporal changes in groundwater storage, head, subsidence and aquifer deformation, at the spatial resolution and depths relevant to local groundwater management decisions.

Introduction to the CVHM

The CVHM accounts for integrated, variable water supply and demand, and simulates surface-water and groundwater flow, and compaction and the resulting subsidence across the entire Central Valley system. The CVHM is comprised two major components: (1) a texture model to characterize the aquifer system and (2) an integrated hydrologic model. The detail and breadth of this hydrologic modeling tool provides a better understanding of valley wide hydrologic processes, as it was designed to create enough detail to be practical for water management decisions on a regional basis and provide datasets and boundary conditions that could be applied at more local scales.

The Central Valley is a large structural trough filled with heterogeneous sediments comprise of unconsolidated to semi-consolidated gravel, sand, silt, and clay as much as six miles deep. Most of the fresh water, however, is contained in the upper few thousand feet of the sediments. In order to better characterize the aquifer-system deposits, lithologic data from approximately 10,000 drillers' logs of boreholes were compiled and analyzed to develop a 3-D texture model. This texture model is an interpolation of the percentage of coarse-grained deposits on a 1-mile spatial grid at 50-foot depth intervals to 2,800 feet below land surface.

The hydrology of the present-day Central Valley, and the CVHM model, are driven by surface-water deliveries and associated groundwater pumpage, which in turn reflect spatial and temporal variability in climate, water availability, land use, and the water delivery system. The relatively detailed database on texture properties coupled with water-budgets and MODFLOW's unique subsidence capabilities make CVHM particularly useful for assessing subsidence and artificial recharge sites. CVHM has been updated to the most recent version of MODFLOW, MODFLOW-One Water Hydrologic Model-version 2 (MF-OWHM2). The Farm Process (FMP) for MODFLOW dynamically allocates groundwater recharge and groundwater pumping on the basis of crop water demand, surface-water deliveries, and depth to the water table. MF-OWHM2 includes numerous enhancements to FMP, the subsidence packages, model output, and the embedded-model technology of the local grid refinement (LGR). The CVHM includes 20,000 model cells of 1 mi^2 areal extent and 13 layers ranging in thickness from 10 to 750 ft, typically reaching a depth of 1,800 ft. The texture model was used to estimate hydraulic conductivity for every cell in the model. Land subsidence, an important consequence of intense groundwater pumpage in susceptible aquifer systems is specifically simulated as is intra-borehole flow, an important mechanism for vertical flow within and between hydrogeologic units in parts of the valley. The CVHM was constrained by comparing simulated and historically observed groundwater levels, stream flows, and subsidence. The CVHM simulates groundwater and

surface-water flow, irrigated agriculture, land subsidence, and other key processes in the Central Valley on a monthly basis for water years 1961 to 2013. Water-budget datasets, include climate, landuse and water deliveries. There are 21 water balance regions that are split into up to 100 accounting regions at various times, predominantly in the western San Joaquin Valley, to better define the conjunctive use of water in later years.

Introduction to the Information Content in InSAR Data

InSAR data provide a measure of land deformation, subsidence or rebound. During repeat passes of a location, a radio wave is transmitted to Earth's surface along the direction of the look angle and a measurement made of the phase and amplitude of the reflected wave. The change in phase between passes, along the direction of the look angle, measured at all pixels in the satellite's footprint, is called an interferogram. The change in phase, $\Delta\theta$, is measured in radians and 'wraps' every 2π radians as a full wave cycle is completed. The change in phase must first be unwrapped, and then can be related to deformation of the land surface, Δb. In areas with no tectonic activity or horizontal deformation, one can assume that the majority of the deformation is vertical. If there are no significant processes at the surface that could cause deformation, one can assume that the deformation is related to pressure changes below the surface.

The surface deformation caused by pumping of groundwater systems is an integrated measurement that is a function of hydrologic pressure changes (changes in head) in the subsurface, as well as the total thickness and compressibility of sediments experiencing pressure changes. The compressibility is a function of lithology; clays tend to have a much higher compressibility than sands. In groundwater studies, the specific skeletal storage, S_{sk}, is a commonly used term and is related to compressibility, α by the following equation:

$$S_{sk} = \rho_w g \alpha,$$

where ρ_w is the density of water and g is the acceleration due to gravity.

If we can assume that all deforming materials are experiencing the same change in head, the head change, Δh is related to surface deformation, Δb by the following equation:

$$\Delta b = \Delta h S_{sk} b_0,$$

where b_0 is the thickness of the deforming material. The variable S_{sk} is given as S_{ske} when the sediments are deforming elastically, and S_{skv} when the sediments are deforming inelastically. Inelastic deformation only occurs when the head drops below the lowest previously experienced level (preconsolidation head). The above equation assumes that all sediments undergo the same change in head. In reality, the subsurface units experience different changes in head that are a function of the screened interval of the wells that are being pumped, and the hydraulic conductivity of the sediments.

In order to model land deformation, we need information about the specific skeletal storage, the thickness of the subsurface unit that is deforming, and the change in head of the subsurface unit that is deforming. The change in head in fine-grained units often has a delayed response to a change in head experienced in an aquifer, due to the lower hydraulic conductivity of fine-grained sediments. This delayed reaction can be modeled with the 1D groundwater flow equation:

$$\frac{\partial}{\partial z}\left(K_v \frac{\partial h}{\partial z}\right) = S_s \left(\frac{\partial h}{\partial t}\right),$$

where z is the vertical location of the deforming material, K_v is the vertical hydraulic conductivity, h is the head, t is time and S_s is the specific storage. With an accurate groundwater model, we can estimate the change in head with respect to time and location, and use these estimates to model deformation of subsurface units. To obtain the required depth-dependent geologic data, an essential part of our methodology is the acquisition of AEM data.

Introduction to the Information Content in Airborne Electromagnetic (AEM) Data

The AEM method has been used for many years to map geology (Palacky 1991) and, in the last 10 or so years, has been widely used to map groundwater systems. While there have been AEM data sets acquired in California, there has not been widespread adoption for the mapping of groundwater systems. We suggest that this is due to the lack of familiarity with the method, as the value-added to groundwater management has been repeatedly demonstrated.

The theory behind the method is described in Ward and Hohmann (1988). In the SkyTEM system that will be used to acquire the data for this study, all of the hardware required for data acquisition is suspended beneath a helicopter. Current flowing in a transmitter loop generates a primary magnetic field. The termination of current causes a time-varying decay in the produced magnetic field which causes eddy currents to flow at various depths beneath the land surface. The less electrically resistive the region, the stronger the current and the more slowly the current decays. The eddy currents generate secondary magnetic fields which are measured at the receiver mounted on the transmitter loop. The measurement taken is the change in magnetic field with respect to time (dB/dt). Once acquired, the dB/dt data can be inverted to obtain the resistivity structure of the subsurface. This is done by modeling the predicted dB/dt response due to a given resistivity structure, comparing with the observed AEM response, then repeatedly modifying the resistivity structure until the inversion process converges at a resistivity structure that fits the observed data. The result is a 3D model of resistivity for the surveyed subsurface region.

Once the resistivity model is obtained, this model needs to be transformed to map out the hydrostratigraphic units. This transform requires establishing a relationship between resistivity and the lithologic units present in the area, e.g. sand, silt, clay. There have been a number of different approaches taken to establish the resistivity-lithology transform, all of which involve the use of geologic logs and geophysical measurements – either made in the well or taken from the actual SkyTEM data set (e.g. Christiansen et al., 2014; Barford et al.,2016; Knight et al., 2018). What is obtained as a final product is a 3D model of the subsurface mapping out lithology in terms of the texture (percent coarse-grained and fine-grained) and thickness of major (>10 m) subsurface aquifers and aquitards. It is important to note that the AEM method, due to constraints in the inversion routines and fundamental physics-controlled limitations in the resolution of the measurement, is capable of resolving packages of interlayered materials, but cannot resolve individual thin layers. There will be an averaging of resistivity values. As shown in the recent study in the Tulare Irrigation District (in the Kaweah Basin) (Knight et al., 2018) we are thus able to differentiate sections that are predominantly coarse-grained from those that are predominantly fine-grained but cannot map in detail the fine structure of lithology variation.

While the vertical resolution of AEM data can never match that of a well, even abundant well data yield little information in the horizontal direction. In addition, the many wells that have been drilled in the Central Valley tend to be shallow, so do not provide information about the deeper parts of the aquifer system. We note, however, that the presence of wells is a necessary part of the analysis and interpretation of AEM data.

Description of Workflow

Acquisition and Processing of InSAR and AEM Data

Acquiring and processing InSAR and AEM data from the Kaweah Basin and Butte County are the first steps in our methodology.

We plan to use InSAR data from the Envisat and Sentinel-1a and 1b missions, which cover the two study areas at time periods from 2002-2010 and from 2015-present. The processing of most of the Sentinel-1 dataset over our study area has been completed by our collaborator, Tom Lauknes. Interferograms were generated from the satellite acquisitions. Noisy pixels were identified using coherence, which is a measure of how similar the phase change is among neighboring pixels. Only pixels with consistently high coherence (low noise) were retained in the analysis. These pixels were unwrapped, then all interferograms were processed using a method called small baseline subset (SBAS; Berardino et al., 2002). To process the data with SBAS, a 'reference pixel' was selected that experienced very little deformation over the study period. This method produced a time series of land deformation at each pixel. The average deformation rate (cm/year) at each pixel was calculated from these time series.

Continued work, to be conducted over the first year of the project includes processing of the Envisat data and validating both the Sentinel-1 and Envisat data with GPS data. The validation with GPS data will help us to refine and improve the processing workflow, such as adjusting the criteria to select good pixels, removing scenes with potential unwrapping errors, and modifying the reference pixel used in the SBAS processing. The processed data will be a time series of land deformation at each pixel that has coherence high enough to be included in the analysis.

We have already acquired and processed AEM data over a portion of the Kaweah Basin and transformed it to a lithologic model (Knight et al., 2018). We have plans and funding to acquire AEM data over the rest of the Kaweah Basin and Butte County in October 2018. After the acquisition, the data will be processed, inverted and transformed to lithologic models by researchers in Knight's group with existing funding. The details of our approach are given in Knight et al. (2018).

Integration of InSAR and AEM Data to Develop the Groundwater Models

Our objective is to improve the accuracy of groundwater modeling by integrating AEM and InSAR data into the models. This would be the first time these datasets have been used together in a 3D groundwater model. Because of their high resolution relative to the data that are typically used to calibrate groundwater models, the integration of these datasets will significantly improve the accuracy of the groundwater model's storage, head, and subsidence and deformation predictions. To implement this approach, we need the InSAR deformation time series and information about the depth, thickness and texture of layers of subsurface sediments. AEM data can be used to produce these estimates at depths of up to 500 m, with a vertical resolution on the order of 10 m and horizontal resolution on the order of 30 m to 1 km (depending on line spacing

during AEM data acquisition). This depth and resolution make lithology estimates from AEM data suitable to be used in groundwater models.

Since the subsidence and rebound data from InSAR are related to changes in groundwater storage, they can be simulated with groundwater models, making them useful in parameterizing, or calibrating, groundwater models. The USGS has used InSAR data in combination with well data to calibrate the recent update to the CVHM (Faunt et al., 2018). However, this model is limited by the low density of geologic data at the depths at which subsidence historically occurs (>100 m). In our proposed approach, we will further update both the CVHM and Kaweah model by combining AEM, which images to greater depths, and InSAR data, solving for hydrologic and geomechanical properties. These two datasets, when used together, can provide high-resolution estimates of the hydraulic properties of the subsurface, and the depths at which deformation is likely occurring. The end result will be integrated groundwater models that can be used to accurately predict total groundwater storage, and spatial and temporal changes in groundwater storage, head, subsidence and aquifer deformation, at a spatial resolution and at depths relevant to local management districts.

Our workflow for developing a groundwater model is shown in Figure 1. The boundary fluxes and groundwater pumping required to run the groundwater model will be assigned based on output from the starting models. The groundwater model is composed of thirteen large-scale model layers which thicken with depth that represent the heterogenous aquifer system. The Corcoran Clay, the main confining unit, is explicitly represented. The thickness and sedimentary texture of these model layers, which we refer to as the 'textural model' in Figure 1, will be derived from our AEM data using the approach outlined in Knight et al. (2018). The hydrologic and geomechanical properties of the fine-grained and coarse-grained materials are also key inputs to the model. These values are unknown, and will be solved for by inversion. With estimates of the hydrologic and geomechanical properties of fine- and coarse-grained materials, and with estimates of the fraction of each model layer at each location in our study area that is fine-and coarse-grained from our AEM dataset, we can estimate the hydrologic

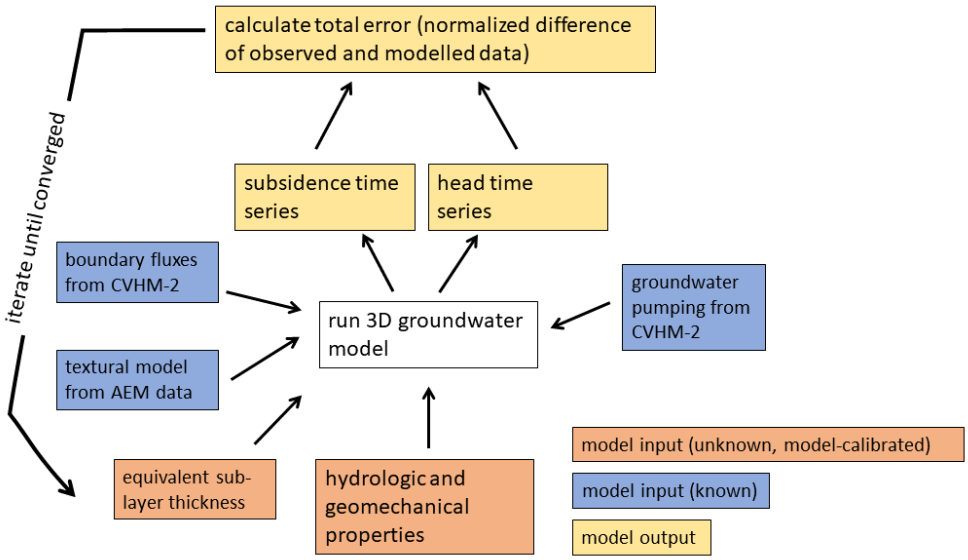

Figure 1. Workflow for developing the groundwater model.

and geomechanical properties throughout our model. This approach of using hydrologic properties of fine-grained and coarse-grained materials in combination with a textural model to solve for the properties of the subsurface follows the approach implemented in the CVHM (Faunt et al., 2009), but with a more accurate and higher-resolution textural model. Another unknown input parameter that is important for the model simulation of land deformation is the thickness of individual fine-grained sub-layers within the larger hydrostratigraphic model layers. Rather than determining the thickness of each sub-layer, we solve for an 'equivalent' thickness, that allows us to model the observed deformation, through inversion.

With the input parameters described, the groundwater model will be run, producing output time series of hydraulic head and land deformation. These outputs will be compared with head time series from wells and land deformation time series estimated with InSAR. The error will be computed based on the normalized difference between model output and observed data. To invert the data the input parameters (hydrologic and geomechanical properties and equivalent layer thickness) will be modified after each model run until the error converges at an acceptably low level. We will use the parameter estimation and uncertainty analysis (PEST) package to perform the inversion. This package has been extensively used in the hydrologic community and is well-equipped for inversions of complex 3D groundwater models (Doherty, 1994).

The inversion framework as described will be the first implementation of AEM data in a 3D groundwater model that predicts land deformation. It will provide us with estimates of vertical and horizontal hydraulic conductivity, porosity, specific yield, and specific storage under elastic and inelastic conditions. These can be used in a predictive model that allows water managers to assess the impact of changing conditions and alternate management actions on both head levels and land subsidence. Such predictive modeling is at the core of the development of sustainable groundwater management plans. Our methodology will take advantage of two data sets – InSAR and AEM – to dramatically improve the accuracy of current predictions.

Discussion of Accuracy / Uncertainty

Groundwater models have a high level of uncertainty due to the large number of parameters needed to calibrate them. One of the parameters with the highest uncertainty is sediment texture in the major subsurface layers. However, due to the complexity of estimating this, the uncertainty in this parameter is rarely quantified. We expect that introducing textural data derived from AEM will improve the accuracy of the groundwater model, and also introduce a more robust way to quantify its uncertainty. Knight et al. (2018) established a bootstrapping method to estimate the uncertainty in lithologic estimates. This approach randomly selected subsets of the AEM data to derive lithologic estimates thousands of times. The variation in these estimates was used to quantify the lithologic uncertainty. Researchers in Knight's group are continuing to develop novel methods for quantifying uncertainty in AEM-derived textural estimates, which will produce many possible realizations of the subsurface that fit the data equally well. The average of these is considered the 'most likely', and will be used for the inversion. After running the initial inversion, we will run groundwater models with the suite of possible textural realizations. The variation in model output will provide an estimate of model uncertainty related to the uncertainty of the underlying textural structure. Our inversion routine, run through PEST, will also provide uncertainty estimates of the calibrated parameters.

To test the accuracy of each developed model, we will use it to predict head and land deformation on a validation dataset that is not included in the calibration process. The closer the match between the validation data and the predicted data, the higher our confidence will

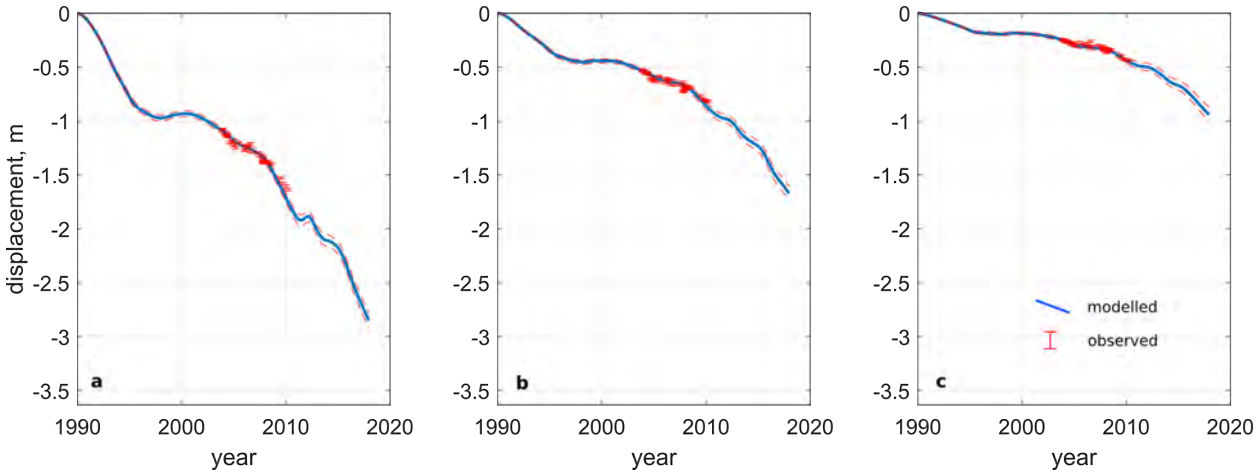

Figure 2. Modeled and observed land deformation at three locations near Tulare. Dashed red lines show the 5th and 95th percentiles in the prediction.

be in our model. To learn the relative importance of head data, the traditional groundwater model calibration dataset, and InSAR data, which are rarely used to calibrate groundwater models, we will test running the inversion holding out InSAR data and head data.

We have recently completed the development of a similar methodology in a 1D land deformation model, and tested our approach at three locations in Tulare County. In this approach, we modeled land deformation using AEM data and measured head data. In Figure 2 we show the outstanding fit of modeled to observed land deformation, revealing the our model can capture a complex pattern of land deformation. The model also fills in data gaps where no land deformation data were acquired and can be used to predict future land deformation given various scenarios. This work demonstrates that combining AEM data with head data (which in the proposed case will be computed using the groundwater model) can successfully model land deformation.

Identification and Description of the ARL of the Application

Many of the individual components of our project, such as the analysis and interpretation of the InSAR and AEM data, are at level 5 (validation in relevant environment). Claudia Faunt, with the USGS, has extensive experience developing integrated hydrologic models which simulate the components of subsidence, incorporating InSAR and numerous other forms of data (Faunt et al., 2009; Faunt et al., 2016) with over a decade of work in the Central Valley. Another of our key personnel, Tom Lauknes, senior research scientist with Norut in Norway, brings more than 10 years of experience in the processing of InSAR data (Lauknes et al., 2010a; Lauknes et al., 2010b; Eriksen et al., 2017), and has collaborated since 2007 with the Stanford researchers. Rosemary Knight's research group, including Ryan Smith now an assistant professor at Missouri University of Science and Technology, has experience applying InSAR to water resources problems (Reeves et al., 2011, 2014; Chen et al., 2015, 2016), implementing geophysics in water resource problems (Goebel et al., 2017; Knight et al., 2018), integrating satellite data into groundwater models (Smith et al. 2017), as well as established connections to local water managers in the Central Valley who will be using the products developed in this project.

While the individual components are at level 5, the integration of the combination of InSAR and AEM data into a groundwater model has not been previously explored. We therefore estimate our Start-of-Project ARL to be level 2 (application concept – invention). By working

closely with our partners in local GSAs, we plan to move to ARL 7 for End-of-Project ARL (application prototype in partner's decision-making – functionality demonstrated).

Transition Plan and Evidence of Partner Commitment

In the Kaweah Basin, we have been working closely, over the past three years, with Aaron Fukuda, General Manager of the Tulare Irrigation District and Paul Hendrix, Manager of the Mid-Kaweah GSA, demonstrating both the use of InSAR for monitoring subsidence and the use of AEM data for mapping out sediment texture. We are now working with their consultants at GEI in continued acquisition of AEM data to cover a larger area. The local agencies are providing $150k for the acquisition of AEM data, showing their commitment to the approach being taken in Knight's research. In our work in the Kaweah Basin we will start with their updated version of the CVHM, the Kaweah model, and interact with consultants and representatives from the GSAs throughout the three years to ensure our product will meet their needs. In the last six months of the project, we will work with them to allow adoption of the updated Kaweah model. Our project is completely in line with their needs related to SGMA – a reliable groundwater model that can provide accurate predictions of the outcomes of various management actions. There is a commitment to providing the staff time needed throughout this project in order to achieve the successful adoption of the improved groundwater model.

In Butte County, we have been collaborating over the past two years with Paul Gosselin, Director, and Christina Buck, Assistant Director, of Butte County Water and Resource Conservation District. We are currently in the process of planning the acquisition of AEM data to provide input for improving their groundwater model to support SGMA implementation. The methods that we will apply through the proposed research will contribute directly to their ongoing modeling efforts. They plan to compare our model with their existing model to aid in decision making, to better quantify the uncertainty of both models, and could implement our approach in their modeling code. Butte County has committed $200k to the acquisition of the AEM data, an indication of their commitment to incorporating AEM data into their work. There is a commitment to providing the staff time needed throughout this project in order to achieve the successful adoption of the improved groundwater model.

The workflow that we are developing will be applicable throughout the Central Valley, addressing a recognized need for additional data sources to improve the resolution of groundwater models. We are thus confident that the methods that we develop will be adopted by the local agencies. In addition, the methods that we will develop will be transferable to other parts of the world, where the integration of InSAR and AEM data could be used as the basis for developing groundwater models.

Our project will provide a methodology for the development of groundwater models by integrating InSAR and AEM data, using the CVHM and the Kaweah model as the starting models. The USGS is committed to providing ongoing support of CVHM. We presume that InSAR data will be available from NASA or other agencies going forward. The other critical data set is the AEM data. There is the commercially-available equipment and the expertise in the private sector to acquire AEM data. DWR, as stated in their letter of support, "is currently utilizing and providing NASA JPL InSAR data to aid local agencies in identification of subsidence conditions; and are potentially expanding collection of state-wide AEM data over the next several years. " They are therefore very supportive of this research that utilizes these two data sets to develop improved groundwater models.

Challenges and Risks Affecting Project

As described above in our discussion of the ARL, many of the individual components in this project have been validated. The primary challenge that we face in the integrated approach that we are taking to the development of a groundwater model, is acquiring the high quality data needed as input (e.g. irrigation data, groundwater pumping data). Many data are not consistently reported and of variable quality. Our approach is to work with our local partners who have local knowledge and experience with the development of groundwater models in their area. A technical challenge that we face is the complexity of system we are modeling, which includes both elastic and inelastic deformation. We are addressing this by implementing a groundwater flow model that has been developed to account for both of these. There are technical challenges in implementing the joint inversion in a way that is computationally efficient. We plan to address this by limiting the number of forward runs in a way that will reduce the range of all possible outputs while not significantly impacting our ability to quantify uncertainty.

Issues Affecting the Adoption, Transition, and Sustainable Use

We will be working closely with water managers and consultants involved with the development of groundwater management plans, so do not anticipate any issues to negatively affect the adoption, transition and sustainable use of the groundwater models, and the methodology to be developed in this project.

Anticipated Results

The successful implementation of this research project will result in 1) the development of improved groundwater models, and more importantly their supporting data sets, in our two study areas, and 2) the development of a methodology that could be adopted for implementation throughout the Central Valley and potentially the entire state, starting with CVHM (or local updates such as the Kaweah model) and incorporating InSAR and AEM data to refine the local groundwater models. The development of improved groundwater models and datasets directly supports the sustainable management of groundwater in the Central Valley, crucial for safeguarding groundwater resources, which provide drinking water for 3 million people in the valley, as well as supporting the $17 billion/yr agricultural industry. It is important to note that groundwater depletion does not just affect the quantity of groundwater available. USGS water-quality data indicate that in many areas water quality decreases with depth and various constituents may be more concentrated by groundwater usage. Recent research by the Stanford group has shown that over-pumping results in arsenic contamination, rendering the water undrinkable (Smith et al., 2018). In addition to these critical issues, over-pumping has resulted in land subsidence of greater than 20 cm/year in some parts of the Central Valley, damaging infrastructure, including canals, which are used for delivering surface water, and permanently removing groundwater storage from the system (Faunt and others, 2016). Furthermore, in some areas, though localized in the Central Valley, surface water resources have been impacted by groundwater level changes and subsidence. Sustainable groundwater management is intended to prevent these negative consequences of undesirable effects from occurring, and ideally mitigate, to the extent possible, existing problems.

Our total groundwater storage estimates, as well as the lithologic model, will be made publicly available on an online repository such as Google Earth Engine, and/or through the databases maintained by the USGS. These data could then be used by local water managers to

make decisions regarding sustainable use of groundwater resources. This dataset is one of the main deliverables of this proposed study.

Project Management

Rosemary Knight is responsible for the overall management of the project. Working with Knight at Stanford will be a post-doctoral fellow, supported by funding from this project. The post-doctoral fellow will be the primary researcher involved with the joint inversion (starting with processed and interpreted AEM and InSAR data) and development of the groundwater models. In addition, two graduate students, with funding from other sources, will be involved with the interpretation of the AEM data and the processing of the InSAR data. Smith will co-supervise the post-doctoral fellow in the development of the joint inversion. Faunt is the researcher with the in-depth understanding of CVHM so she and her team at the USGS will work closely with the post-doctoral fellow in working to develop the groundwater model.

Knight's management approach to such projects is a weekly one-hour meeting with each student or post-doctoral fellow, and a weekly one-hour meeting with the full project team, including Smith and Faunt through video-conferencing. A once-a-month meeting will involve all project partners. Twice a year Knight, students and post-doctoral fellow and Faunt will meet with the GSAs, and with representatives from DWR and SWRCB. Throughout the year, ongoing communication with the project partners will ensure that the project benefits from the local knowledge, from the perspectives of the state agencies, and remains on track to developing a valuable product that will be adopted for groundwater management.

Schedule and Milestones

January 2019: Begin project.
January to June 2019: Processing and initial interpretation of AEM data in both study areas. Data will be acquired in fall 2018 with funding from other sources. Gather more detailed surface-water delivery and diversion information needed for more localized CVHM conditions. Begin development of joint inversion code.
July to December 2019: Compilation and analysis of well data in the two study areas, with comparison with data in CVHM and the Kaweah model; finalize interpretation of AEM data. Continue work on joint inversion code. Import AEM data into joint inversion.
MILESTONE Dec 2019: Interpretation of AEM data completed.
January to June 2020: Gather and process InSAR data. Import InSAR data into joint inversion.
MILESTONE June 2020: Processing of InSAR data completed.
July 2020 to December 2020: Extract boundary conditions from CVHM and the Kaweah model to impose on a finer, localized grid where AEM data are available; import remote sensing datasets into groundwater model. Calibrate groundwater model in each area; this involves a joint inversion to solve for the rock physics transform to convert AEM data to geologic data, as well as the hydraulic properties.
MILESTONE Dec 2020: Calibration of groundwater models completed.
January to June 2021: Evaluate the groundwater models and the groundwater storage estimations against validation datasets. Testing runs with partners. Finalize models for distribution.
MILESTONE June 2021: Groundwater models distributed to partners.
July to December 2021: Prepare groundwater storage and storage change products for distribution among groundwater managers. Provide training on the use of new models, making modifications as needed.
MILESTONE Dec 2021: Groundwater models in use in partner GSAs.

Appendix 7C

USACE Reservoir Regulation Manual for Terminus Dam – Lake Kaweah (excerpts) and KDWCD Updated Tables

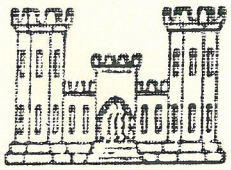

TERMINUS DAM (LAKE KAWEAH)
Kaweah River, California

RESERVOIR REGULATION MANUAL

JUNE 1962

Revised November 1971

DEPARTMENT OF THE ARMY
SACRAMENTO DISTRICT, CORPS OF ENGINEERS
SACRAMENTO, CALIFORNIA

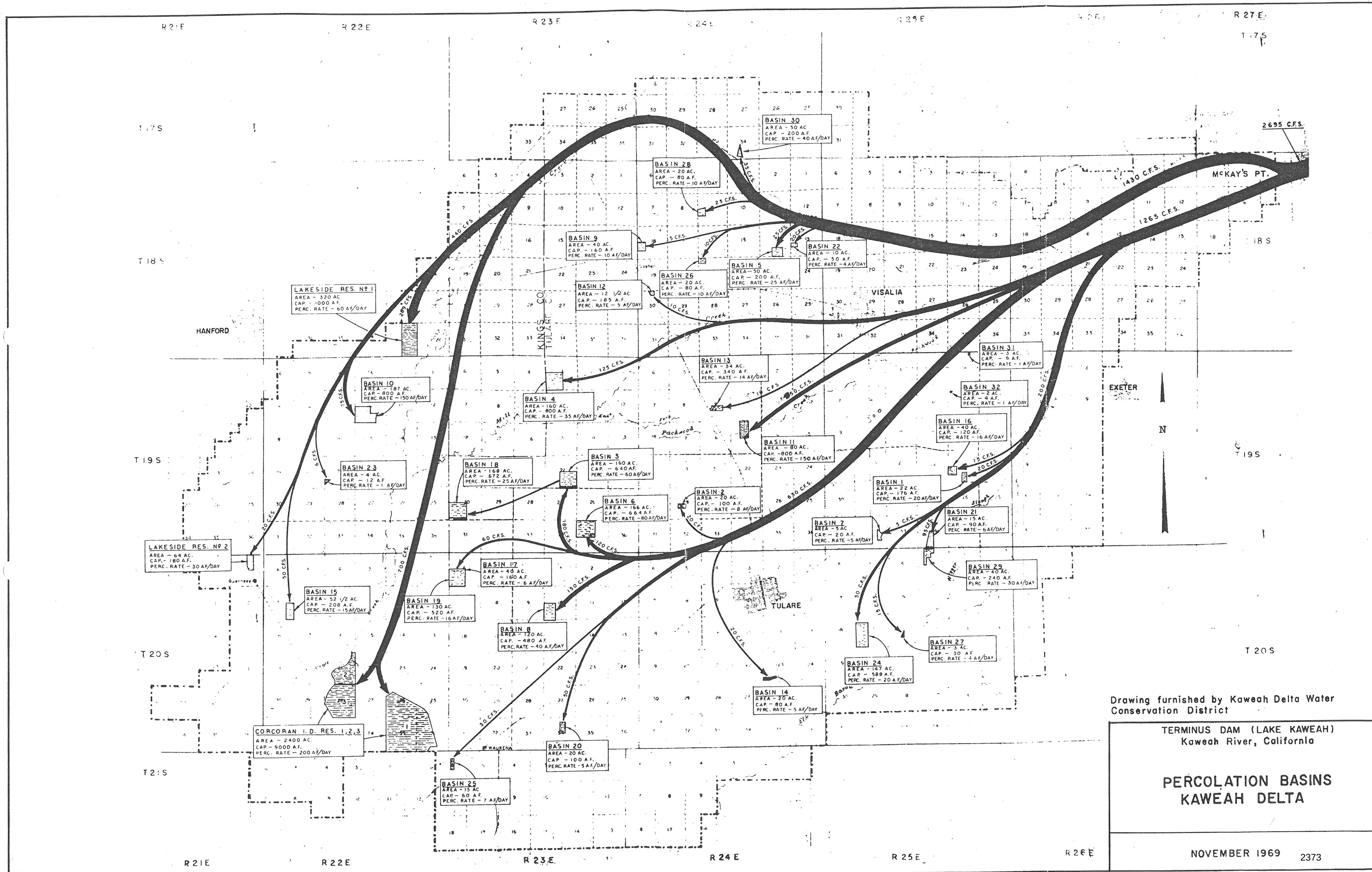

Drawing furnished by Kaweah Delta Water Conservation District

TERMINUS DAM (LAKE KAWEAH)
Kaweah River, California

PERCOLATION BASINS KAWEAH DELTA

NOVEMBER 1969 2373

CHART 16

KAWEAH DELTA WATER CONSERVATION DISTRICT
SPREADING BASINS
AND SPREADING DEMAND USED IN ROUTING STUDIES

NAME	BASIN No.	ACREAGE	CAPACITY AF	INFLOW CAP CSF	DAYS TO FILL	SINKING AF/D	SINKING CSF/D	SUPPLY
Eda Shannon	1	22	176	20	4.4	20	10	Farmers
Enterprise	2	20	100	20	2.5	8	4	Tulare I D
Colpein	3	160	640	180	1.8	60	30	Tulare I D
Packwood	4	160	800	125	3.2	35	18	South Mill
Willow School	5	50	200	25	4.0	25	13	Modoc
Cartmill	6	166	664	120	2.8	80	40	Tulare I D
Gary Shannon	7	5	20	5	2.0	5	3	Farmers
Corcoran Highway	8	120	480	150	9.2	40	20	Tulare I D
Doe	9	40	160	15	5.3	10	5	Modoc
Lakeside	10	187	800	75	5.3	150	75	Lakeside
Tagus	11	80	800	250	1.6	150	75	Tulare I D
Goshen Pit	12	12	185	10	9.3	5	3	North Mill Creek
Nelson Pit	13	34	340	10	17.0	14	7	Evans
Abercrombie	14	20	80	20	2.0	5	3	Tulare I D
Howe	15	52 1/2	208	50	2.1	15	8	Lakeside
Parr	16	40	120	15	4.0	16	8	Farmers
Anderson	17	40	160			6	3	Tulare I D
Franks	19	130	520	60	5.7	16	8	Tulare I D
Guinn	18	168	672	70	4.8	25	13	Tulare I D
Wilbur	20	20	100	50	1.0	5	3	Tulare I D
Shannon	21	15	90	45	1.0	6	3	Farmers
Shannon-Modoc	22	10	50	20	1.3	4	2	Modoc
Green	23	4	12	6	1.0	1	1	Lakeside
Consolidated	24	147	588	50	5.9	20	10	Farmers
Doris	25	15	60	30	1.0	7	4	Tulare I D
Doe-Ritchie	26	20	80	10	4.0	10	5	Modoc
Ellis	27	3	30	15	1.0	4	2	Farmers
Doe-Goshen	28	20	80	25	1.6	10	5	Goshen
Nunes	29	40	240	50	2.4	30	15	Farmers
Harrell	30	50	200	35	2.9	40	20	St Johns River
Hammer	31	3	6	3	1.0	1	1	Peoples
Clark	32	2	4	2	1.0	1	1	Peoples
Lakeside Res. #1		320	1000	289	3.5	60	30	Lakeside
Lakeside Res. #2		64	180	20	4.5	30	15	Lakeside
Corcoran I.D. Resl,2,3		2400	9000	700	6.4	200	100	Corcoran I D
Totals		4640	18845	2695		1114	563	

CHART 17

PLATE 2: Kaweah Delta Water Conservation District

Available Recharge Basin Inventory

Basin Name	No.	River System	Supply Channel	Owner	Acreage	Capacity (A.F.)	Inflow Capacity (CFS)	Percolation A.F. per Day*
Doris	25	(either)	Cameron Creek	KDWCD & TID	15	60	30	7
Hutcheson East	45	(either)	Cameron Creek	Kaweah Delta WCD	4.4	n/a	n/a	n/a
Hutcheson West	44	(either)	Tulare ID Canal	Kaweah Delta WCD	5.5	25	16	2
Enterprise	2	(either)	Tulare ID Canal	Kaweah Delta WCD	20	100	20	8
Colpien	3	(either)	Tulare ID Canal	Kaweah Delta WCD	160	640	180	60
Abercrombie	14	(either)	Tulare ID Canal	Kaweah Delta WCD	20	80	20	5
Creamline	16	(either)	Tulare ID Canal	Kaweah Delta & Tulare ID	153	535	n/a	85
Franks	17	(either)	Tulare ID Canal	Kaweah Delta WCD	40	160	n/a	6
Guinn	18	(either)	Tulare ID Canal	Kaweah Delta WCD	168	672	70	25
Franks	19	(either)	Tulare ID Canal	Kaweah Delta WCD	130	520	60	16
Wilbur	20	(either)	Tulare ID Canal	KDWCD & TID	20	100	50	5
Oakes	43	Kaweah	Lower Kaweah River	Kaweah Delta WCD	40.9	200	40	7
Bill Clark	32	Kaweah	Consolidated PDC	Private Landowner	2	4	2	1
Elk Bayou	106	Kaweah	Elk Bayou Creek	County of Tulare	6	22	n/a	3
Nelson Pit	13	Kaweah	Evans Ditch	Kaweah Delta WCD	34	340	10	14
Art Shannon	1	Kaweah	Farmers Ditch	Kaweah Delta WCD	33.8	270	20	30
Gary Shannon	7	Kaweah	Farmers Ditch	Kaweah Delta WCD	5	20	5	5
Gordon Shannon	21	Kaweah	Farmers Ditch	Kaweah Delta WCD	15	90	45	6
Anderson	24	Kaweah	Farmers Ditch	Kaweah Delta WCD	147	588	50	20
Ellis	27	Kaweah	Farmers Ditch	Private Landowner	3	30	15	4
Nunes	29	Kaweah	Farmers Ditch	Kaweah Delta WCD	40	240	50	30
Sunset	95	Kaweah	Inside Creek	Kaweah Delta WCD	103	320	n/a	60
Creekside (Riverwood)	n/a	Kaweah	Mill Creek	City of Visalia	8	59.7	33	1
Goshen Pit	12	Kaweah	North Mill Creek	City of Visalia	12	185	10	5
Machado	6	Kaweah	Packwood Creek	Kaweah Delta WCD	166	665	120	80
Corcoran Hwy.	8	Kaweah	Packwood Creek	Kaweah Delta WCD	120	480	150	40
Tagus	11	Kaweah	Packwood Creek	Kaweah Delta WCD	80	800	250	150
Packwood	4	Kaweah	South Mill Creek	City of Visalia	160	800	125	35
Corcoran Basins 1,2,3	n/a	St. Johns	Cross Creek	Corcoran DC	2400	9000	700	200
Doe-Goshen	28	St. Johns	Goshen Ditch	Private Landowner	20	80	25	10
Harrell	30	St. Johns	Harrell No. 1	Private Landowner	50	200	35	40
Lakeside	10	St. Johns	Lakeside Ditch	Kaweah Delta WCD	187	800	75	150
Howe	15	St. Johns	Lakeside Ditch	Kaweah Delta WCD	52.5	208	50	15
Green	23	St. Johns	Lakeside Ditch	Kaweah Delta WCD	4	12	6	1
Lakeside Basin No. 1	n/a	St. Johns	Lakeside Ditch	Lakeside DC	320	1000	289	60
Lakeside Basin No. 2	n/a	St. Johns	Lakeside Ditch	Lakeside DC	64	180	20	30
Willow School	5	St. Johns	Modoc Ditch	Modoc Ditch Co.	50	200	25	25
Goshen (Doe)	9	St. Johns	Modoc Ditch	Private Landowner	40	160	15	10
Shannon-Modoc	22	St. Johns	Modoc Ditch	Private Landowner	10	50	20	4
Doe-Ritchie	26	St. Johns	Modoc Ditch	Private Landowner	20	80	10	10
					4929			

Developing Recharge Basin Inventory

Basin Name	No.	River System	Supply Channel	Owner	Acreage	Capacity (A.F.)	Inflow Capacity (CFS)	Perc A.F. per Day*
Paregien	108	Kaweah	Deep Creek	Kaweah Delta WCD	78.5	n/a	n/a	n/a
Hannah Ranch South	n/a	Kaweah	Lower Kaweah	Private Landowner	n/a	n/a	n/a	n/a
Peoples	99	Kaweah	Lower Kaweah River	Kaweah Delta WCD	40	n/a	n/a	n/a
Hannah Ranch North	109	Kaweah	Lower Kaweah River	Kaweah Delta WCD	398	n/a	n/a	n/a
Curtis	107	St. Johns	St. Johns River	Kaweah Delta WCD	95.6	n/a	n/a	n/a
S/K-Vander Stelt	111	St. Johns	St. Johns River	City of Visalia	94.7	n/a	n/a	n/a
Garner (Kit Carson)	n/a	St. Johns	Settlers Ditch	LIWD/KCWD/KDWCD	55	n/a	n/a	n/a

* Estimate only